VALIDATING A CALCIUM TRACER BASED TREE-RING DATING METHOD FOR TROPICAL WOOD

Cheryl Victoria Wood

A Thesis Submitted for the Degree of
at the
University of St Andrews

2014

Validating A Calcium Tracer Based Tree-Ring Dating Method For Tropical Wood

Cheryl Victoria Wood

University of St Andrews

A thesis submitted to the University of St Andrews for the degree of Doctor of Philosophy

Department of Earth and Environmental Sciences

School of Geography and Geosciences

April 2014

Declaration

I, Cheryl Wood, hereby certify that this thesis, which is approximately 63,500 words in length, has been written by me, that it is the record of work carried out by me or principally by myself in collaboration with others as acknowledged, and that it has not been submitted in any previous application for a higher degree.

I was admitted as a research student in October, 2007 and as a candidate for the degree of PhD in October, 2008; the higher study for which this is a record was carried out in the University of St Andrews between 2007 and 2012.

Date Signature of candidate

I hereby certify that the candidate has fulfilled the conditions of the Resolution and Regulations appropriate for the degree of PhD in the University of St Andrews and that the candidate is qualified to submit this thesis in application for that degree.

Date Signature of supervisor

In submitting this thesis to the University of St Andrews I understand that I am giving permission for it to be made available for use in accordance with the regulations of the University Library for the time being in force, subject to any copyright vested in the work not being affected thereby. I also understand that the title and the abstract will be published, and that a copy of the work may be made and supplied to any bona fide library or research worker, that my thesis will be electronically accessible for personal or research use unless exempt by award of an embargo as requested below, and that the library has the right to migrate my thesis into new electronic forms as required to ensure continued access to the thesis. I have obtained any third-party copyright permissions that may be required in order to allow such access and migration, or have requested the appropriate embargo below.

The following is an agreed request by candidate and supervisor regarding the publication of this thesis:

Embargo on all of print copy for a period of 2 years on the following ground(s):

Publication would preclude future publication

Embargo on all of electronic copy for a period of 2 years on the following ground(s):

Publication would preclude future publication

Date Signature of candidate

Signature of supervisor

Abstract

The tropics are a key part of the global biosphere. Specifically, the woodland environments not only moderate large scale climate dynamics, but are also crucial in the global carbon cycle. Despite this, tropical dendrochronological studies are rare due to the uncertainty in annual dating from the minimal seasonality in most tropic environments. Without distinct annual tree rings, dendrochronological dating methods do not work, therefore other dating methods are required before long term forest growth analyses can be made. Alternatives such as radiocarbon and stable isotope measurements can be expensive and require high resolution measurement in order to identify seasonality. This thesis introduces a novel dating method for tropical trees using calcium as a tracer of annual wood formation. Laser Ablation-ICP-MS provides a fast, high resolution method for measuring mineral elements which could potentially provide a solution to the dating of tropical trees.

Initially, Scots pine provided an excellent testing species for the development of both the methodological and analytical dating methods proposed through this thesis. It's well defined, annually dated ring structure formed the basis of seasonal signal detection and the development of an objective analysis for dating. This was achieved by the continuous measurement of calcium, and utilising a threshold detection approach to define annual growth cycles with respect to extreme peaks in the tracer data-series.

The initial success of the calcium dating method using pine allowed for testing the technique on a tropical trees species from Cameroon which lacks distinct rings. Along with radiocarbon dating, the robustness of the calcium dating method for this tropical species was assessed. Promising results were initially found however, these could not be replicated and validation of this method proved problematic.

Finally, radiocarbon dates were used to assess the nature of the oxygen and carbon stable isotopic series from the single tree of the same species from the tropical calcium tests. Results showed that despite the clear cyclic signal present in the oxygen isotope record, this did not represent an annual signal. These results reinforce the problems associated with tropical dendro analysis.

Acknowledgements

I would like to thank my supervisor, Rob Wilson, for his endless enthusiasm, support and encouragement throughout this project, and for always making time to discuss things regardless of how many other students, lectures, proposals or papers he is trying to shuffle at the time. Thanks should also go to SAGES and the University of St Andrews for their financial support as well as the TROBIT group for the organisation and financing of the Cameroon field work. I also thank Yit Arn Teh for support with lab costs.

Thanks to Angus Calder for his help in the lab with useful advice and ideas, for his expertise in maintaining the all of the analytical equipment, and most importantly for the coffee breaks! Thanks must also to Nora Hanson, Gustavo Saiz and Chris Wurster for all their help and advice both in and out of the lab.

I would like to thank Georgina King for all the support she has provided since we met at the start of our postgraduate careers, Amy Tavendale for her continued support and always being there at beer o'clock, and Joanna Fraser for the much needed lunch and cake relief!

Last but not least, thanks to my family for their support, and especially to Dean who has encouraged and supported me throughout, and in particular for his understanding in the last few write-up months when I can only imagine that I was not the most pleasant person to live with!

Table of Contents

Declaration i
Abstract iii
Acknowledgements iv
Table of Contents v
Table of Figures ix
List of Tables xvi
Chapter 1: Introduction and Literature Review 1
1.1. Project Rationale 1
1.2. Dendrochronology 3
1.3. Dendrochronology in the Tropics 6
1.3.1. Measuring Growth Rates in Tropical Trees 11
1.4. Dendrochemistry 12
1.4.1. Stable Isotopes in Tree-Rings 13
1.4.2. Stable Isotopes in Temperate Trees 17
1.4.3. Stable Isotopes in Tropical Trees 18
1.4.4. Mineral Nutrition in Trees 21
1.4.5. Calcium in Trees 34
1.4.6. Applications of Mineral Element Dendrochemistry 39
1.4.7. Mineral Elements in Tropical Trees 40
1.5. Summary 42
1.5.1. Thesis Structure 44
1.5.2. Aims and Objectives 45
Chapter 2: Calcium Tracers and the Dating of Scots Pine 46
2.1. Introduction 46
2.1.1. Mineral Element Measurement 47
2.2. Study Area and Sample Description 49
2.3. Materials and Methods 50
2.3.1. Sample Preparation 50
2.3.2. LA-ICP-MS 51
2.3.3. Method Development 53

2.3.4. Calcium Measurements 63
2.3.5. Data Adjustments 72
2.3.6. Ring Width Measurements 75
2.3.7. Splicing Datasets 76
2.3.8. Method for Ring Detection: Threshold Approach 80
2.4. Results 81
2.4.1. Seasonal Calcium Pattern 81
2.4.2. Ring Identification (Threshold Approach) 83
2.5. Discussion 87
2.5.1. Calcium Seasonality 87
2.5.2. Standard Reference Materials 90
2.5.3. Decreasing Ca signal and Machine Drift 91
2.5.4. Data Adjustments 92
2.6. Refinement of Methods 96
2.6.1. Sample preparation methods 96
2.6.2. Standards Reference Materials 96
2.6.3. LA-ICP-MS equipment and settings 97
2.6.4. Number of replicate tracks 98
2.7. Future Work 98
2.7.1. Spots vs. Tracks 99
2.8. Conclusions 99
Chapter 3: Calcium Tracers and the Dating of Tropical Trees 101
3.1. Introduction 101
3.2. Study Area and Sample Collection 102
3.2.1. Preliminary Radiocarbon Age 106
3.3. Materials and Methods 108
3.3.1. Sample Preparation 108
3.3.2. LA-ICP-MS 110
3.3.3. Data Adjustments 112
3.3.4. Calcium Dating 113
3.3.5. Radiocarbon Sampling 116
3.4. Results and Discussion 119
3.4.1. Wood Structure and Traditional Dendro-dating Methods 119

3.4.2. Calcium Measurements and Seasonal Patterns 121
3.4.3. Calcium Dating 132
3.4.4. Tuning of the Ca Dating Method 142
3.4.5. Validating the "Optimised" Ca Dating Method 151
3.5. Conclusions 159
Chapter 4: Are Stable Isotopes the Answer to Dating Tropical Trees? 161
4.1. Introduction 161
4.1.1. Isotopic Measurement of Trees 162
4.2. Study Area and Sample Description 166
4.2.1. Field Site Characteristics 167
4.2.2. Local Climate 168
4.3. Materials and Methods 169
4.3.1. Sample Preparation 169
4.3.2. Measuring Isotopic Ratios - Isotope Ratio Mass Spectrometry 170
4.3.3. Calendar Dating the Isotopic Series 174
4.3.4. Climate Comparisons 175
4.4. Results 176
4.4.1. Standards 176
4.4.2. Isotope Records 176
4.4.3. Calendar Dating the Isotopic Series 178
4.4.4. Climate Comparisons 180
4.5. Discussion 190
4.5.1. The $\delta^{18}O$ and $\delta^{13}C$ records 190
4.5.2. Climate Comparisons 192
4.6. Conclusions 196
Chapter 5: Discussion and Conclusions 198
5.1. Introduction 198
5.2. Calcium Tracers and the Dating of Scots Pine 199
5.3. Calcium Tracers and the Dating of Tropical Trees 200
5.4. Are Stable Isotopes the Answer to Dating Tropical Trees? 201
5.5. General Overview 202
5.6. An "Ideal" Approach 203
5.6.1. Species Choice 203

5.6.2. Analytical Sampling Strategy 205
5.7. Future Work 206
References 208
Appendices 229
Appendix 1: Additional Data for Chapter 2 230
Appendix 2: Additional Data for Chapter 3 249
Appendix 3: Additional Data for Chapter 4 262
Appendix 4: Additional Data 274
Oxygen Isotope Ratios 274
Carbon Isotope Ratios 276
Comparison of $\delta^{18}O$ and $\delta^{13}C$ Records 279

Table of Figures

Figure 1-1: Schematic of tree stem (DoITPoMS, 2008) showing the main components of a tree stem. The wood tissue (xylem) consists of heartwood and sapwood, surrounded by the cambium layer where cell division takes place. 3

Figure 1-2: Example of annual tree-rings in (a) Scots pine – softwood, (b) Birch – Diffuse porous hardwood, (c) Oak – Ring porous hardwood. Each ring represents one year of growth 4

Figure 1-3: Schematic representation of the principle behind cross-dating (Kaennel and Schweingruber, 1996), illustrating the use of tree-rings from sub-fossil samples, historic buildings and living trees..... 5

Figure 1-4: Visualisation showing the distribution of archived tree-ring chronologies around the world. Few chronologies have been produced in the tropics (highlighted in map) compared to in temperate regions. This map was created in Google Maps using data provided by ITRDB (2012) and map data by Google. 6

Figure 1-5: (a) Example of a false ring occurring in a conifer species (Brown, 2013). (b) Example of a wedging ring in a conifer species (Schweingruber, 2006). 8

Figure 1-6: Visualisations showing the locations of climate stations in Africa. General location of the field site as described in Chapter 3 and Chapter 4 is represented by the red squares. Images were created using Google Maps. Map data was provided by Google, station data from KNMI Climate Explorer (http://climexp.knmi.nl/)..... 9

Figure 1-7: Image illustrating cation exchange on the surface of soil particles. Cations adsorb to the negatively charged surfaces of the soil particle by electrostatic attraction. Bound cations may be displaced into the soil solution by other cations with higher binding affinities, making them available for uptake by the roots. Image adapted from W. H. Freeman & Co. (No Date) and Taiz and Zeiger (2010). 24

Figure 1-8: Illustration representing the symplastic and apoplastic pathway for nutrient movement within the root. Ions are taken up by the epidermal cells, and transferred via the symplast or apoplast through the cortical and endodermal cells into the stele, where they are enter the xylem. In most cases (where present), the Casparian strip interrupts the apoplastic transport. Image adapted from Kimball (2013) 26

Figure 1-9: Schematic illustrating the role of membrane proteins in the transport of cations by primary and secondary active transport, and passive transport (White, 2012). 27

Figure 1-10: Diagram illustrating distribution of calcium in a cell and the transport processes for sustaining low concentrations of cytosolic Ca^{2+}. Figure based on Marschner (1995) and Hindshaw *et al.* (2013). 35

Figure 2-1: Location where Scots Pine samples originated. Approximate location is highlighted with red square.. Images downloaded from Google Earth. (Imagery: Getmapping plc, Map data: Google.)..... 50

Figure 2-2: Example of a sectioned rectangular lath for laser ablation analysis. Each section has been cut at an angle to allow rings to be overlapped on adjacent sections. 51

Figure 2-3: Illustration representing the typical configuration of a Laser Ablation-ICP-MS system. Image from Guillong (2007) 52

Figure 2-4: Plot of the raw data obtained from the continuous measurement of ^{44}Ca by LA-ICP-MS over a 10mm line along the radii of a Scots Pine lath. Two replicate lines were measured (red and blue) in the direction of growth (pith towards bark), with the mean of these represented by the black line. 54

Figure 2-5: Mean ^{44}Ca plot from Figure 2-4 overlaid onto scanned image of the Scots pine wood lath. The two lines measured are represented by the two dark burned lines in the wood. The highlighted peak does not correspond with a ring boundary. 55

Figure 2-6: The above plots show the mean and median raw ^{44}Ca data obtained from the analysis of 10 replicate lines for 3 separate sets of rings (A-C). Each plot has been superimposed onto a scanned image of the corresponding area from which the measurements were obtained. 56

Figure 2-7: Section of Scots pine lath showing the areas measured for the EW and LW tests (highlighted by the red box). 57

Figure 2-8: Plot showing the difference in counts between the earlywood and latewood regions as measured on a Scots pine sample. 58

Figure 2-9: Plots showing the 5 ablated lines plus the median of these for each of the four pelleted standards 61

Figure 2-10: Graph shows the calcium output from the median of three ablated lines of Scots pine and the mean of 3 ablated lines of the NIST pine needles standard. Both y-axis scales are plotted with equal intervals for comparison. 63

Figure 2-11: Example of a sub-sectioned portion of a Scots pine lath showing the three replicated laser ablated tracks across the length of the section. 64

Figure 2-12: Plot of raw data for ^{44}Ca isotope as measured by LA-ICP-MS for one section of tree lath 05147. The Ca intensity is measures in counts per second, and the three lines plotted represent the 3 replicated tracked ablated across the lath section. The graph has been truncated for display purposes. 65

Figure 2-13: A scanned image of a section of analysed tree lath (tree 01547) with the associated raw 44Ca counts plotted and overlaid. The enlarged section highlights (blue circles) two of the resin ducts present on the laser track which corresponds to the calcium spike. 66

Figure 2-14: Figure showing the mean plot (a) and the median plot (b) of the 3 replicated ^{44}Ca tracks as measured by LA-ICP-MS for one section of tree lath 05147 (Figure 2-12). Using the median values opposed to the mean significantly reduced the abundance of calcium spikes. . 67

Figure 2-15: A Typical example of the drift observed over time (distance). (a) Plot showing the median ^{44}Ca (blue) data and the median ^{13}C (red) data obtained from tree 05134 R2 D. (b) Plot showing the ratio of the $^{44}Ca/^{13}C$ values for the same tree 01534 R2 D. 69

Figure 2-16: The median $^{44}Ca/^{13}C$ values (±2 standard error of the mean (SEM))are shown for the four NIST standard measurements carried out on each of the five sections of a single pine tree lath (tree 05129) 69

Figure 2-17: (a) Graph showing the raw median $^{44}Ca/^{13}C$ values for all sections of tree 05135 R1 which had been split into 6 sections for analysis. (b) The same plot with low frequency filters overlaid onto each section illustrating the detrending functions which were applied to the data. These plots clearly illustrate the decreasing trend in calcium counts and the problems associated with section linkage. 73

Figure 2-18: (a) The resultant plot after each section was individually detrended using the filters illustrated in Figure 2-17. (b) The final, fully adjusted, values for tree 05135 R1 are represented here. Data for each section has been detrended as in (a) and converted to z-scores. 74

Figure 2-19: (a) Overlapping regions for two lath sections (tree 05135) after data has been detrended and converted to z-scores. (b) The same graphs have been overlaid onto the scanned image along with RW values for two of these rings. 76

Figure 2-20: The data for the outer section (G) of tree 05135 R1. The increase in Ca values highlighted on the graph represents the outer edge of tree where laser fires into bark. 78

Figure 2-21: The above graph shows the final, fully adjusted, values for tree 05135 R1 after the splicing of data into one single Ca dataset. Data for each section has been detrended as in (a) and converted to z-scores. 79

Figure 2-22: Image illustrating the three threshold values which were used to identify ring boundaries from the $^{44}Ca/^{13}C$ data. Some peaks may only be identified as a boundary at the lower threshold limits. Plot is showing data from tree 05135 R1 81

Figure 2-23: Illustration highlighting the typical seasonal signal in calcium found across a growth ring. The plot represents the median values of 3 replicate lines (ablated lines are visible under the plot) 82

Figure 2-24: Example of the adjusted median $^{44}Ca/^{13}C$ values plotted with the ring widths (green) and Ca years based on the >1 threshold (red) for tree (05134 R1). The data is split into two graphs for easier viewing. 84

Figure 2-25: Illustration of the three threshold values tested for assigning ring status to peaks for 05134 R1. The graph is split into two sections for easier viewing. The red diamonds show the results of designating Ca years based on the >1 threshold. The red oval denotes an area where there is a potential for more than 1 Ca year to be assigned for the 1 true year. 85

Figure 2-26: Enlarged area of the same tree as shown in Figure 2 11. The outer portion of the calcium and RW measurements are shown here along with the lowest threshold value for detecting rings. 95

Figure 3-1: (a) Map showing the general location of Mbam Djerem National Park in central Cameroon. (b) The yellow square in the centre of this map represents the fieldwork location within the park. The blue flags represent the locations of the nearest climate stations; Tibati is north, and Yoko is East of the park. Both maps were downloaded from Google Maps. 103

Figure 3-2: Average monthly rainfall data (±2 SEM) from the Tibati and Yoko weather stations (KNMI Climate Explorer, http://climexp.knmi.nl). Data has been averaged for each month for each year between 1940-1994 (data between 1994-present not available). 104

Figure 3-3: Example of *Terminalia macroptera* growing in the savanna. Most trees were found to grow in this asymmetrical manner. 105

Figure 3-4: (a) Satellite image from 2006 showing the location of the field site within Mbam Djerem National Park (yellow box). The light areas represent savannah regions, darker green areas are forest and the Djerem river is pink. Image downloaded from USGS Global Visualisation (http://glovis.usgs.gov). (b) Shows a representation of the sampling locations (red dots) for the 5 trees in relation to the forest-savanna transition. 105

Figure 3-5: Shows the output radiocarbon plot obtained using the OxCal online calibration software available from https://c14.arch.ox.ac.uk/oxcal using the intcal13atmospheric curve (Reimer *et al.*, 2013)..... 106

Figure 3-6: Graph showing the effect on the ^{14}C levels in the Northern and Southern Hemispheres caused by the weapons testing during the 1950's and 60's. The peak of the bomb spike is slightly lower and later in the southern hemisphere. Image from Earth System Research Laboratory (NOAA, 2012). 108

Figure 3-7: Example of *Terminalia macroptera.* The wood contains ring-like structures, however there are not of a consistent nature. 109

Figure 3-8: Example of sub-sectioned portion of a *T. macroptera* lath showing the three replicated laser ablated tracks across the length of the section. Each track is 0.2mm apart.. 111

Figure 3-9: Example of overlap region between tree 2A-R1 sections B and C as highlighted within the black box. 113

Figure 3-10: Example of applying 4-point smoothing function through the data. 114

Figure 3-11: Image shows the positions of the calcium assigned year comparisons made between each radius for tree 2A. The area where the wood has been removed represents the areas for two of the radiocarbon dates (2A-B and 2A-C), with the location of 2A-A radiocarbon dae indicated by the white arrow. The H/S boundary position is shown by the dashed line. 116

Figure 3-12: Scanned image of tree late 2Y after laser ablation analysis. Black arrows represent show 10 year increments as calculated using the >1.25 SD calcium threshold technique. Red arrows repesent the locations for the ^{14}C sampling based on the >1.25 threshold. The inner sampling location (2Y-Inner) is not shown here..... 119

Figure 3-13: Two problematic areas are highlighted: (a) 3 bands without vessels are present at the right hand side of the box. The middle band fades towards the left hand side and becomes

difficult to follow. (b) Shows an example of wedging, where banding pinches out resulting in incomplete banding around the circumference of the tree. 120

Figure 3-14: The above graphs plot the raw median $^{44}Ca/^{13}C$ values obtained for each of the trees measured. H/S boundary regions (where present) are highlighted within the black rectangles. 122

Figure 3-15: The raw median $^{44}Ca/^{13}C$ data is shown here overlaid onto the section B of tree 2A-R1. An abrupt change in the data intensity is shown here which may be caused by the H/S transition area (highlighted in red). 123

Figure 3-16: Scanned image of *T. macroptera* (tree 2A) with plot showing $^{44}Ca/^{14}C$ signal for this section overlaid on the image. The ring-like structres can be seen clearly. 125

Figure 3-17: (a) Graph showing the raw median $^{44}Ca/^{13}C$ values for all four sections of tree 2A. Each section is plotted with the low frequency part of the Gaussian filter which was used to detrend each section. For section C, the data was detrended by 2 separate functions due to the large change in variance at ~40mm from the bark. (b) Graph showing the result of detrending each section using the detrending functions shown in (a). 128

Figure 3-18: (a) Graph showing the result of converting each lath section to z-scores. The overlapped regions are still present, but have been removed in (b). After data is spliced together (Section 3.3.3) the data is treated as one single dataset. 129

Figure 3-19: Section B of tree 2Y (a) shows the calcium spike in the data caused by the presence of the resinous substance which is highlighted in (b). 130

Figure 3-20: Both plots have been truncated for display purposes. (a) The raw median $44Ca/^{13}C$ values for the 3 sections of tree 2Y are plotted with the low frequency part of the Gaussian filter (detrending function). The effect that the single large calcium spike in section B has can be seen in (b) which shows the detrended data after conversion to z-scores. 131

Figure 3-21: These graphs show the result of removing the spike in data. (a) The raw median $44Ca/^{13}C$ values for the 3 sections of tree 2Y are plotted with the low frequency part of the Gaussian filter (detrending function). (b) results of detrending the data and conversion to z-scores after spike removal. The 3 sections are now in alignment and can be spliced together. 131

Figure 3-22: Plots showing Final calcium data obtained for each of the *T. macroptera* samples. Two radii from sample 2A were analysed. 133

Figure 3-23: The above 3 plots show positions of calcium year assignment for tree 2A-R1, using the threshold >1. The graph is split into 3 sections and truncated for display purposes. The red diamonds represent the start of an annual growth season as determined by the assignment criteria, and the red line represents the threshold position. The arrows show the positions of the 14 tie points used for within tree error assessment. 135

Figure 3-24: The above 2 plots show positions of calcium year assignment for tree 2A-R2, using the threshold >1. The graph is split into 2 sections and truncated for display purposes. The red diamonds represent the start of an annual growth season as determined by the assignment

criteria, and the red line represents the threshold position. The arrows show the positions of the 14 tie points used for within tree error assessment. 136

Figure 3-25: The plots (a-e) were produced using the online CALIBomb software which is available from http://calib.qub.ac.uk/CALIBomb/frameset.html. The calibration was carried out using the intcal13 calibration and Levin datasets, using a smoothing factor of 1.0 year. . 144

Figure 3-26: Graphical explanation of table layout..... 147

Figure 3-27: Graphical explanation of table layout..... 150

Figure 3-28: The plots (a-e) were produced using the online CALIBomb software which is available from http://calib.qub.ac.uk/CALIBomb/frameset.html. The calibration was carried out using the intcal13 calibration and Levin datasets, using a smoothing factor of 1.0 year. . 154

Figure 3-29: Graphical explanation of table layout..... 157

Figure 4-1: Satellite images showing locations of field sampling areas. (a) Positions of the two nearest climate stations to the field area are indicated by white arrows. Image acquired from Google Earth, Image data: Google, Landsat. (b) Shows approximate locations of individual sampling areas. Image acquired from Google Earth, Image data: Google, Cnes/Spot Image. 166

Figure 4-2: Photos representative of the savanna in the field site. (a) Shows trunk of *T. macroptera* tree surrounded by tall grasses. (b) General view with *T. macroptera* trees in the background..... 167

Figure 4-3: Photos show the forest-savanna transitional boundary. (a) Shows the view from the savanna looking towards the forest. (b) shows the view from just inside the forest looking out towards the savanna..... 168

Figure 4-4: Average monthly rainfall data (±2 standard error of the mean (SEM)) from the two closest weather stations to the field site and the gridded CRU TS3.1 ((Mitchell and Jones, 2005, Harris *et al.*, 2014). Precipitation data is shown from the period of 1940-1994 for the two weather stations, and 1901-2009 for CRU dataset. Average monthly temperature data (±2 SEM includes the years 1901-2009 from CRU dataset..... 169

Figure 4-5: Schematic representation of an (a) on-line TC/EA system for $\delta^{18}O$ measurements (b) on-line EA system for $\delta^{13}C$ measurements. Images modified from (Scinco.com)..... 171

Figure 4-6: Schematic representation of an Isotope Ratio Mass Spectrometer..... 171

Figure 4-7: Oxygen isotope series for tree 2A, plotted by distance sampled along the tree's radius..... 177

Figure 4-8: Carbon isotope series for tree 2A, plotted by distance sampled along the tree's radius. Data is uncorrected for Suess effect. 177

Figure 4-9: Oxygen isotope series for tree 2A. Data is plotted on calendar scale using growth rates calculated from the ^{14}C results..... 179

Figure 4-10: Carbon isotope series for tree 2A. Data is plotted on calendar scale using growth rates calculated from the ^{14}C results. $\delta^{13}C$ has been corrected for Suess effect based on (McCarroll and Loader, 2004) 180

Figure 4-11: The five plot show the original $\delta^{18}O$ data for tree 2A, followed by 'seasonal quaterly' $\delta^{18}O$ series generated by the linear interpolation of the orginal series. The correlations between each 'season' are shown as a representation of how this data relates to each other. 181

Figure 4-12: The five plot show the original $\delta^{13}C$ data for tree 2A, followed by the 'seasonal quaterly' $\delta^{13}C$ series generated by the linear interpolation of the orginal series. The correlations between each 'season' are shown as a representation of how this data relates to each other. 182

Figure 4-13: The four plots represent the seasonal precipitation (data from CRU TS 3.1 (Mitchell and Jones, 2005, Harris *et al.*, 2014)) for 4 periods of the year. The correlations between each season show the relationship between the data for each season. 184

Figure 4-14: The four plots represent the seasonal temperature (data from CRU TS 3.1 (Mitchell and Jones, 2005, Harris *et al.*, 2014)) for 4 periods of the year. The correlations between each season show the relationship between the data for each season. 185

Figure 4-15: The plot shows a comparison between the $\delta^{18}O$ season 2 and the temperature season 2 series, with the first differenced versions of the same series (inverted for visual comparison). A significant negative correlation was found only between the 1st diff. series (r=-0.342). 187

Figure 4-16: The plot shows a comparison between the $\delta^{18}O$ season 3 and the precipitation season 3 series, with the first differenced versions of the same series. A significant correlation was found only between the 1st diff. series (r=0.370) 187

Figure 4-17: The plot shows a comparison between the $\delta^{18}O$ season 4 and the precipitation season 3 series, with the first differenced versions of the same series. A significant correlation was found only between the 1st diff. series (r=0.405) 188

Figure 4-18: The plot shows a comparison between the $\delta^{13}C$ season 2 and the precipitation season 4, with the first differenced versions of the same series (series inverted for visual comparison). A significant negative correlation was found only between the 1st diff. series (r=-0.417). 189

Figure 4-19: The plot shows a comparison between the $\delta^{13}C$ season 3 and the precipitation season 1 series, with the first differenced versions of the same series. A significant correlation was found only between the 1st diff. series (r=0.371) 190

List of Tables

Table 1-1: List of essential mineral elements required for growth in higher plants (Fritter and Hay, 2002) 22

Table 2-1: Operating parameters for the LA-ICP-MS system used during initial tests. 54

Table 2-2: Composition of calcium standards. 60

Table 2-3: Final operating conditions which were manually set for LA-ICP-MS. Other parameters which are not listed here were determined by the automatic tuning procedures provided in the software. 60

Table 2-4: Table shows the coeffient of variation for each standard as calculated from the mean values from the 5 replicated lines. 62

Table 2-5: Comparison of the total distance measured from LA-ICP-MS analysis with the distance measured by CooRecorder along the same ablated tracks. The average difference between measurements is 0.19mm with the CooRecorder measurements always being slightly longer. 78

Table 2-6: Actual and estimated rings counts using the > 1 standard deviation threshold..... 86

Table 2-7: Actual and estimated rings counts using the > 1.5 standard deviation threshold ... 86

Table 2-8: Actual and estimated rings counts using the > 2 standard deviation threshold..... 86

Table 3-1: Results from the analysis of a single radiocarbon date obtained from the pith region of a *T. macroptera* tree. Analysis was carried out by the Scottish Universities Environmental Research Centre (SUERC), East Kilbride, Scotland. 106

Table 3-2: Operating parameters used for analysis of *Terminalia macroptera*. The spot size for elemental measurements was reduced to 40µm/s however the preablation spot size was left at 100µm. 110

Table 3-3: The following tables show the results of the calcium assigned year comparisons when using (a) a threshold of > 1 st. dev. above the mean to mark annual increments and (b) a threshold of > 1 st. dev. above the mean to mark annual increments after a smoothing function has been applied to the data. 138

Table 3-4: The following tables show the results of the calcium assigned year comparisons when using (a) a threshold of > 1.25 st. dev. above the mean to mark annual increments and (b) a threshold of > 1.25 st. dev. above the mean o mark annual increments after a smoothing function has been applied to the data. 139

Table 3-5: The following tables show the results of the calcium assigned year comparisons when using (a) a threshold of > 1.5 st. dev. above the mean to mark annual increments and (b) a threshold of > 1.5 st. dev. above the mean o mark annual increments after a smoothing function has been applied to the data. 140

Table 3-6: The following tables show the results of the calcium assigned year comparisons when using (a) a threshold of > 2 st. dev. above the mean to mark annual increments and (b) a threshold of > 2 st. dev. above the mean o mark annual increments after a smoothing function has been applied to the data. 141

Table 3-7: Results from the radiocarbon dates from tree 2A. 143

Table 3-8: Calibrated radiocarbon dates for each of the samples from tree 2A. Radiocarbon age was calculated using the online CALIBomb calibration software (Reimer *et al.*, 2013) available from http://calib.qub.ac.uk/CALIBomb/. The age ranges with the highest probability is highlighted in yellow. 143

Table 3-9: Shows a summary of the possible ^{14}C dates obtained for the samples from tree 2A. The calcium date range for each peak threshold was compared to the ^{14}C ranges, and the difference in years between the two ranges were calculated (Figure 3-26). The calcium ranges which agree, or fall within the ^{14}C date range are highlighted in yellow. 147

Table 3-10: The following table shows a summary of the possible ^{14}C dates obtained for the samples from tree 2A when using the troughs in the calcium data to represent an annual increment. The calcium date range for each threshold was compared to the ^{14}C ranges, and the differences in years between the two ranges were calculated. The calcium ranges which agree, or fall within the ^{14}C date range are highlighted in yellow. 150

Table 3-11: Results from the radiocarbon dates from tree 2Y. 153

Table 3-12: Calibrated radiocarbon dates for each of samples from tree 2Y. Radiocarbon age was calculated using the online CALIBomb calibration software (Reimer *et al.*, 2013) available from http://calib.qub.ac.uk/CALIBomb/. The age ranges with the highest probability is highlighted in yellow. 153

Table 3-13: Shows a summary of the possible ^{14}C dates obtained for four of the samples from tree 2Y. The calcium date each threshold was compared to the ^{14}C ranges, and the difference in years between the two ranges were calculated (Figure 3-26). The calcium ages which agree, or falls within the ^{14}C date range are highlighted in yellow. 157

Table 3-14: Information collected about physical properties of the two radiocarbon dated trees. Height was estimated using a Laser Vertex Hypsometer (Haglöf, Sweden). 158

Table 4-1: Precision is based on the average standard deviations for each standard analysed throughout all runs. 176

Table 4-2: Summary of ^{14}C dates which were obtained for tree 2A (NERC allocation number 1562.0411). The ^{14}C age ranges which have the highested probability are highlighted in yellow. 178

Table 4-3: Growth rates used to date the isotopic series. These were calculated based on ^{14}C dates for the tree 179

Table 4-4: Significant correlations found between the $\delta^{18}O$ data with relevant climate records. 186

Table 4-5: Significant correlations found between the $\delta^{13}C$ data with relevant climate records. 188

Chapter 1: Introduction and Literature Review

1.1. Project Rationale

Dendrochronology is the study of the chronological sequence of annual growth rings in trees (Stokes and Smiley, 1996). Traditional dendrochronological methods do not work well in most tropical ecosystems making it difficult to study past changes in tropical climate, forest productivity and stand dynamics. The principal barriers to using these traditional methods are the lack of an obvious seasonality in many parts of the tropics and the absence of distinct growth rings. Tree growth in many tropical locations is continuous throughout the year (Worbes, 1999, 2002) resulting in trees with either indistinct incremental bands which are generally non-annual in nature, or no ring-like structures at all. This situation means that the dating of trees using traditional dendrochronological methods is almost impossible in most tropical environments resulting in an inability to quantify tree-growth rates. In rare situations distinct annual rings have been found in some species (Indonesia - D'Arrigo *et al.*, 1994, Africa - Trouet *et al.*, 2001, 2006b, Schongart *et al.*, 2006, Therrell *et al.*, 2006). Such studies however are relatively uncommon and tropical dendrochronology remains an elusive "Holy Grail" in forest research and paleoclimatology.

As traditional dendrochronological methods do not work well in the tropics, alternative methods of assessment have been used to determine growth rates in tropical trees. Such methods include cambial wounding (Mariaux, 1967, Sass *et al.*, 1995, Ohashi *et al.*, 2009) and dendrometer measurements, (Worbes, 1999, da Silva *et al.*, 2002, Ohashi *et al.*, 2009) both of which can generally provide continuous growth rate data for the period of measurement. Stable isotope analysis can also be used to develop records of seasonality, leading to the possibility of dating tropical trees. In successful studies, correlations with seasonal rainfall have been established; however the development of tropical chronologies (Evans and Schrag, 2004, Poussart and Schrag, 2005, Anchukaitis *et al.*, 2008b) and climate reconstructions using stable isotopes are still rare and the majority of successful studies in this field have used a combination of stable isotope analysis combined with additional methods for assessing growth rates.

Preliminary research over the last 10 years suggests that elemental analysis may address the problems with dendrochronology in the tropics by helping to overcome the associated dating

issues. Trees undergo many physiological processes during growth which require the uptake, use and storage of many mineral elements. Since growth is affected by seasonality (no matter how slight, whether temperature or precipitation controlled, this seasonality can be represented in the element stores it uses for growth. Patterns of seasonality for some minerals have shown potential for using these archives to develop a novel dating method for tropical trees (Poussart *et al.*, 2006) but little application of the approach has been made.

This thesis explores a novel dendrochemistry method to address the dating of tropical trees using calcium as an indicator of seasonality. Calcium plays an important role in wood formation, providing structure and rigidity to cell walls as well as being required for cell division (Eklund and Eliasson, 1990, Martin *et al.*, 2001, Lautner and Fromm, 2010). The link between calcium and seasonality of tree growth has been investigated in temperate trees (Follet-Gueye *et al.*, 1998, Lautner and Fromm, 2010) as well as some exploratory work in the tropics (Poussart *et al.*, 2006). The severe limitation on dating using traditional based dendrochronological methods in the tropics has led to a need for new approaches to open up these tropical regions. Calcium is utilised in all trees and may provide a means to study growth in trees where traditional methods do not work. Previous studies have investigated the important role calcium plays in tree growth and development, methods for measuring calcium, and have shown seasonal links. These studies have therefore demonstrated the potential for calcium to be used as a seasonal indicator in tropical trees, which will be thoroughly explored in this thesis.

Herein, calcium fluctuations were measured using Laser Ablation-Inductively Coupled Plasma-Mass Spectrometry (LA-ICP-MS); a method that requires minimal preparation time as wholewood cores can be used, and is also a relatively cheap and fast process. The sample size is so small that the process is almost non-destructive and allows replicate measurements to be easily obtained. In order to establish whether this method could be viable for application to tropical trees, the concept was first evaluated using temperate trees with clear annual growth rings as a positive control, as the rings could provide a robust secondary method of dating using traditional dendrochronological methods. *Pinus sylvestris* (Scots pine) collected in the Scottish highlands was chosen as it is a temperate species where growth increments follow a clear annual pattern, therefore any seasonal patterns in the calcium measurements should be easily detectable. An evaluation of the resultant calcium patterns was carried out and, as this

indicated seasonality, the method was further refined for the detection of seasonal patterns from calcium in ringless tropical species.

1.2. Dendrochronology

As a tree grows it increases in circumference due to activity in the vascular cambium (secondary growth) producing the woody part of the tree called the xylem (Figure 1-1). Environmental factors such as seasonal variation, nutrient availability and related changes in temperature and moisture availability influence the speed of growth.

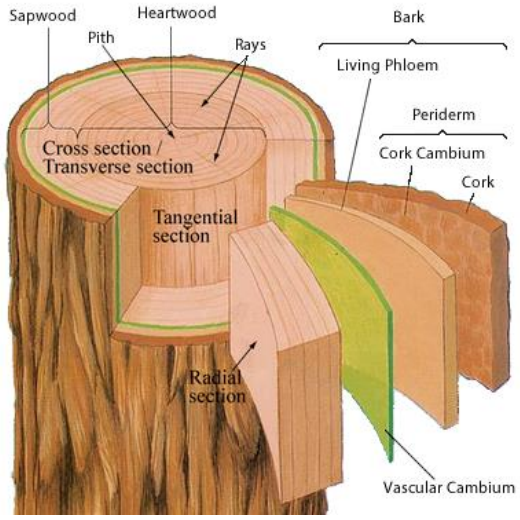

Figure 1-1: Schematic of tree stem (DoITPoMS, 2008) showing the main components of a tree stem. The wood tissue (xylem) consists of heartwood and sapwood, surrounded by the cambium layer where cell division takes place.

Trees can be split into two broad basic types called gymnosperms (softwoods) and angiosperms (hardwoods), with angiosperms further subdivided into monocots and dicots. Monocots do not produce a vascular cambium and are therefore unsuited to dendrochronological studies (Speer, 2010). Most other hardwoods and softwoods, when growing in temperate regions, produce one tree-ring per year which consists of earlywood (produced in spring/early summer) and latewood cells (late summer) which differ in structure. The structural differences between cells can result in an abrupt transition in the xylem and can be seen as a tree or growth ring in many trees; however this transition may take on different forms depending on the tree species and environment (Figure 1-2).

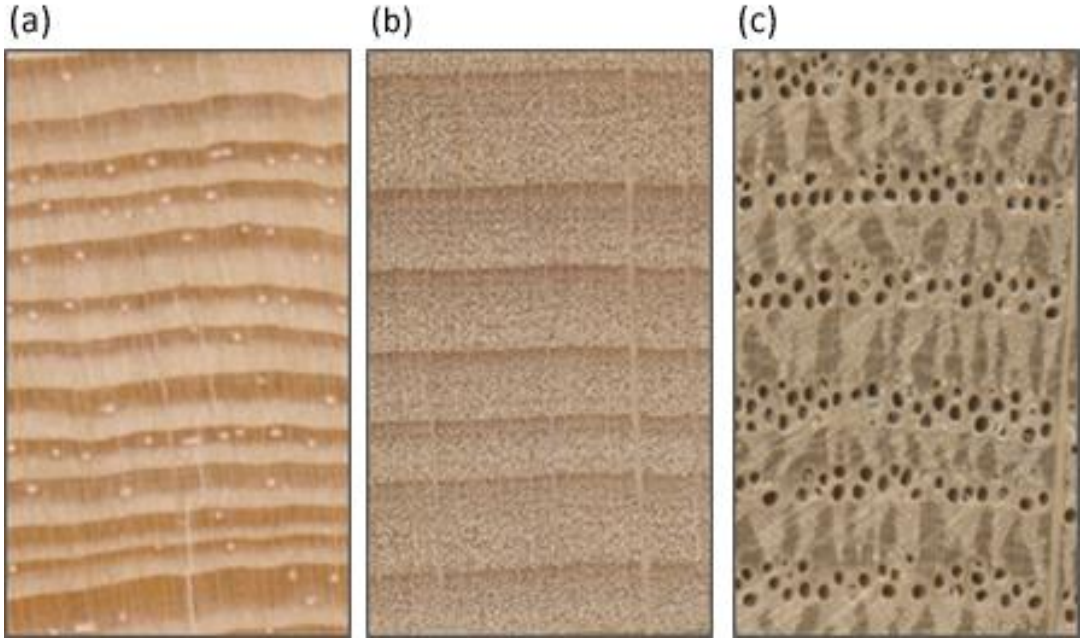

Figure 1-2: Example of annual tree-rings in (a) Scots pine – softwood, (b) Birch – Diffuse porous hardwood, (c) Oak – Ring porous hardwood. Each ring represents one year of growth

Tree growth can be affected by variations in climate which are recorded by patterns of narrow and wide rings depending on the environmental conditions of the local area at that particular time (Baillie, 1995, Stokes and Smiley, 1996). Surrounding trees will respond similarly to these environmental factors thus providing the opportunity to link growth patterns between trees. In regions where growth rings are laid down annually (e.g. temperate zones), the careful measuring of ring widths and the cross-dating of ring width series of the same species can determine the age of a tree. This process forms the basis of dendrochronology. Cross-dating is the art of comparing separate ring width series by matching up patterns and sequences of rings (Figure 1-3) allowing the synchronisation of individual tree-ring series into longer, accurately calendar-dated chronologies (Douglass, 1941, Baillie, 1995). Dendrochronological methods are not restricted only to living trees but can be applied to preserved sub-fossil wood, dead wood and also historical wood such as from beams found in old buildings. In many cases these pieces can be of key importance as living samples can be synchronised with dead material of the same species allowing chronologies to be extended back much further in time to produce very long accurately dated chronologies (Stokes and Smiley, 1996, Eronen *et al.*, 2002, Grudd *et al.*, 2002, Helama *et al.*, 2008).

Dendrochronology has varied uses such as providing a tool for historical dating (Baillie, 1995, Wilson *et al.*, 2004), ecology (Fritts and Swetnam, 1989, Speer *et al.*, 2001, 2010) and climate

reconstructions (Cook *et al.*, 2004, Buntgen *et al.*, 2005, Luckman and Wilson, 2005, D'Arrigo *et al.*, 2006a, Esper *et al.*, 2007, Wilson *et al.*, 2007). Establishing accurately dated chronologies is the basis for all disciplines of dendrochronology. The reconstruction of climate is possible by using available climate data from meteorological stations near to the study sites, evaluating the relationships between the instrumental data and ring widths and applying these relationships to reconstruct climate data for these areas over the length of the chronologies. These methods have been used with great success for assessing the variability in historic climate trends and are very important for late Holocene Palaeoclimate reconstructions, providing spatial patterns of inter-annual climate variability on regional and global scales (Jansen *et al.*, 2007, Jones *et al.*, 2009).

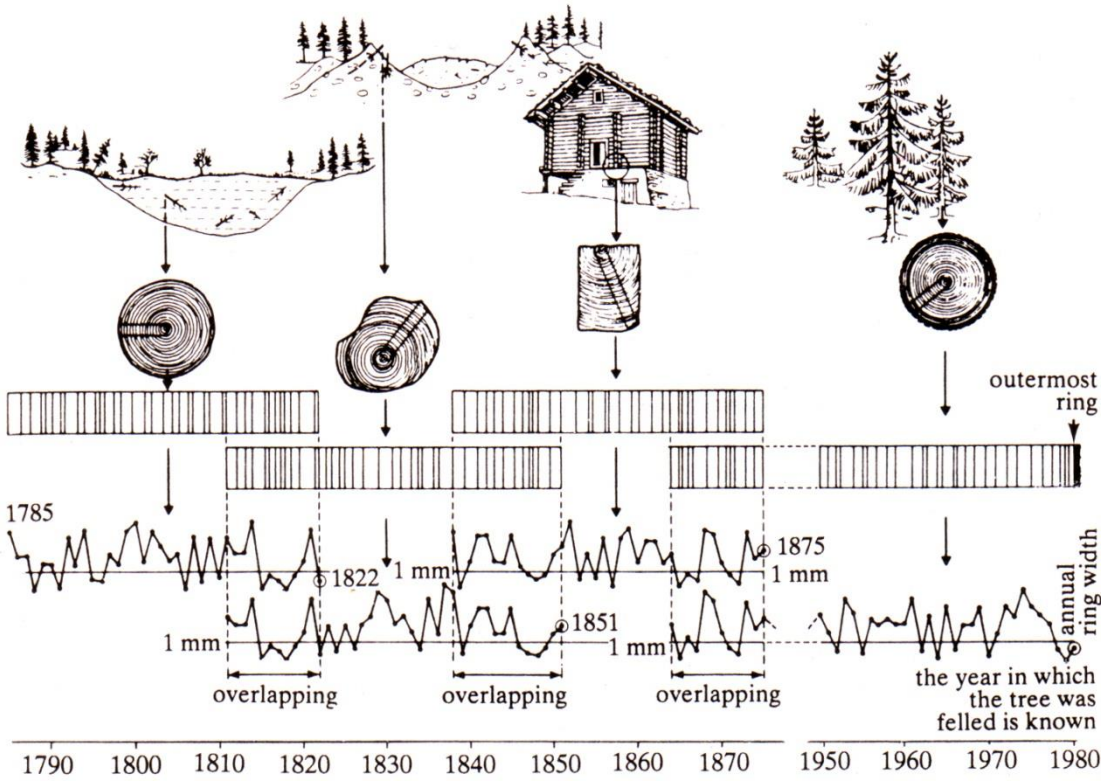

Figure 1-3: Schematic representation of the principle behind cross-dating (Kaennel and Schweingruber, 1996), illustrating the use of tree-rings from sub-fossil samples, historic buildings and living trees.

1.3. Dendrochronology in the Tropics

Thousands of tree-ring chronologies exist in temperate regions (ITRDB, 2012)[1] however this is not the case in the tropics (Figure 1-4). The existence of clearly defined tree-rings in tropical trees has been long debated, despite evidence to the contrary, leading to a general belief that the tropics typically lack sufficient seasonality to produce annual growth rings (Lieberman *et al.*, 1985, Worbes, 1995, Whitmore, 1998, 2002, McCarroll and Loader, 2004). Worbes (2002) reviewed the progress of tropical dendrochronology and highlighted that as far back as 1900, Ursprung (1900) had observed the link between the seasonality of tropical tree growth and its relationship to cambial activity. The first tropical tree-ring chronology was produced by Berlage in 1931 from Indonesian Teak (*Tectona grandis L.f.*) for a period of over 400 years (Berlage, 1931) and demonstrated relationships between dry season precipitation and wet monsoon seasons (D'Arrigo *et al.*, 1994). This chronology was extended over 60 years later by D'Arrigo *et al.* (1994) increasing the chronology length to almost 500 years.

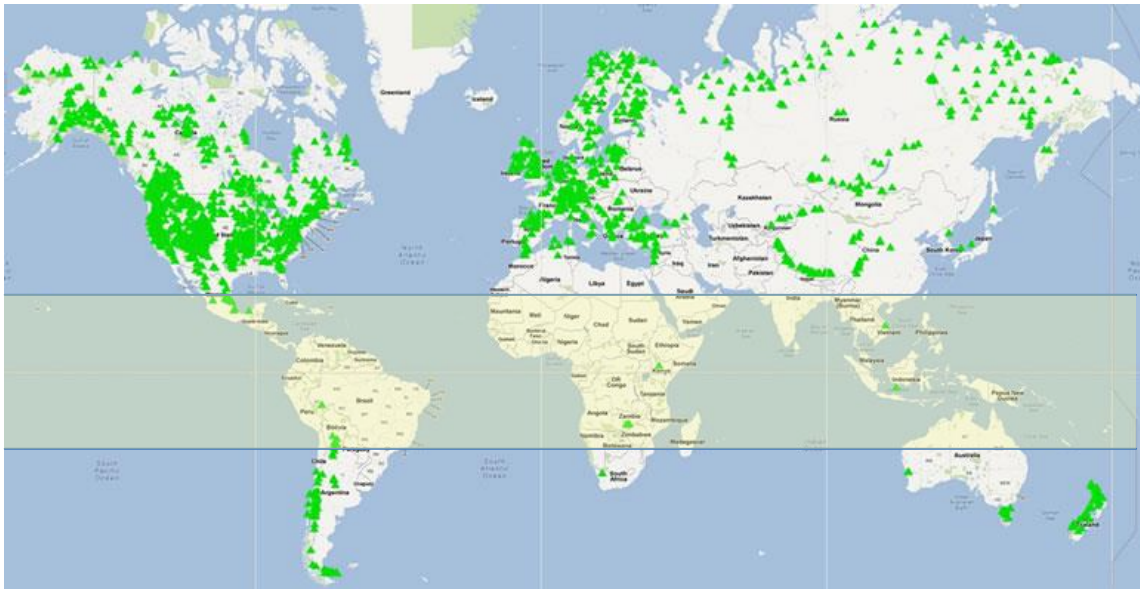

Figure 1-4: Visualisation showing the distribution of archived tree-ring chronologies around the world. Few chronologies have been produced in the tropics (highlighted in map) compared to in temperate regions. This map was created in Google Maps using data provided by ITRDB (2012) and map data by Google.

In an attempt to encourage the expansion of research and chronology development in the tropics, Stahle (1999) produced a strategy guide for the successful development of tropical

[1] The International Tree-Ring Data Bank is a freely available resource allowing access to a vast amount of tree-ring data, contributed by respective authors.

tree-ring chronologies. Where possible, it was suggested to use a species which has been previously identified as suitable for dendrochronological studies or a member of its botanical family, but where this was not possible, to refer to descriptions of wood anatomy to identify a suitable species. Due to the lack of dendrochronological studies in the tropics, knowledge regarding the suitability of different species is limited. Tarhule and Hughes (2002) recognised this lack of information for dendrochronological research and carried out a suitability study in West Africa using 600 trees, from 22 botanical families, 43 genera and over 70 species. Samples were classified into three categories of 'potentially useful', 'problematic' and 'poor' which resulted in 7 species being categorised as potentially useful, 8 as problematic, and the rest as poor. While this study showed the potential for applying traditional dendrochronological methods to several tropical species, it more importantly highlighted the difficulties associated with finding suitable species for such studies. Where information regarding species suitability is available, consideration for the environmental conditions and locality should also be taken into account as the same species found in a one area of the tropics, may respond differently when growing in a different tropical climate.

In temperate trees, an annual ring is produced by the seasonal cycle's influence on cambium activity, where conditions suitable for growth are contrasted against dormancy brought on by stressful conditions such as cold winters. Although many tropical regions do exhibit some seasonality, this is more reflected by changes in precipitation and relative humidity rather than temperature, which may remain relatively constant through the year. Cambial dormancy in the tropics can be induced by prolonged dry periods or by more extreme conditions such as periods of continued flooding (Worbes, 1995), but in many cases, the changes in seasonality may not be large enough to result in distinct annual rings being formed (Poussart and Schrag, 2005). The climate in the inner tropics is often described as everwet, which is based on precipitation records showing rainfall all year round (Worbes, 2002). Such conditions may not provide the stressful environment required by the trees to result in annual or seasonal banding. However, seasonality has been demonstrated in some regions when the recorded monthly precipitation was so low that cambial dormancy was induced. Fichtler *et al.* (2003) studied eight tree species from La Selva, Costa Rica, and observed that all formed visible annual growth rings. La Selva is classified as an everwet region which experiences precipitation all year round, but there are periods (averaging 12 days) without substantial rainfall (<5mm). They reported that the formation of these annual rings could not be due to extreme stress events such as two arid months (Worbes, 1992) or flooding, but rather from

drought stress resulting from these short lived drier periods which caused soil moisture content to drop significantly triggering growth dormancy in the trees. These results indicate that traditional dendrochronological studies can be applied even in areas of the tropics which appear to lack any obvious seasonality.

Although it is clear that distinct annual rings are present in some tropical species, tropical dendrochronology presents further challenges. The occurrence of growth ring irregularities (Figure 1-5) such as false rings, missing rings or wedging rings (where a complete ring has not been formed around the tree) is common (Tarhule and Hughes, 2002). These can be caused by stress events such as drought or physical damage and require care be taken when attempting to cross-date. Such problems aren't unique to tropical trees. However, extreme climatic conditions in tropical regions may make these ring anomalies more frequent, and where ring width variability is low, cross-dating may be difficult or in some cases impossible (Fritts, 1976). To complicate matters further, some tropical tree-ring studies have also reported the occurrence of more than one ring per year (Gourlay, 1995) caused by more than one stress event such as a second dry season, and also irregular ring formations (Sass *et al.*, 1995).

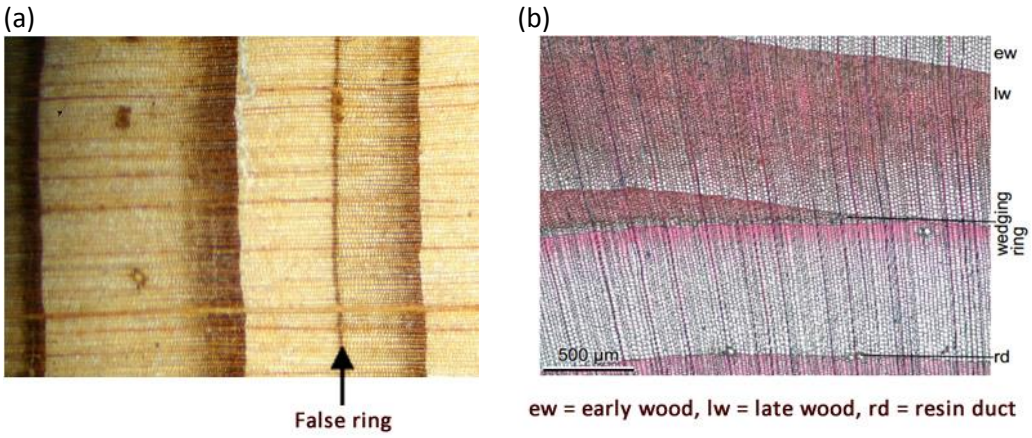

Figure 1-5: (a) Example of a false ring occurring in a conifer species (Brown, 2013). (b) Example of a wedging ring in a conifer species (Schweingruber, 2006).

Long tree-ring chronologies are needed to study past climatic variability of regions in the tropics. Over Africa, the network of climate stations is sparse and in most cases the data is relatively short (around 100 years) and spatially incomplete (Figure 1-6); therefore an alternative solution is needed for understanding past climates and to expand on the available instrumental data. Tree-ring chronologies could provide valuable inter-annual information for extending the sparse instrumental data in the tropics and when conditions are amenable for

trees producing annual rings and tropical dendrochronology could offer this solution. Although the strong potential for applying traditional dendrochronological methods in the tropics has been demonstrated with the successful construction of tree-ring chronologies, in reality the application of these methods are still rare and success has been limited.

(a) Stations with at least 100 years of historical observations of monthly temperature data

(b) Stations with at least 100 years of historical observations of monthly precipitation data

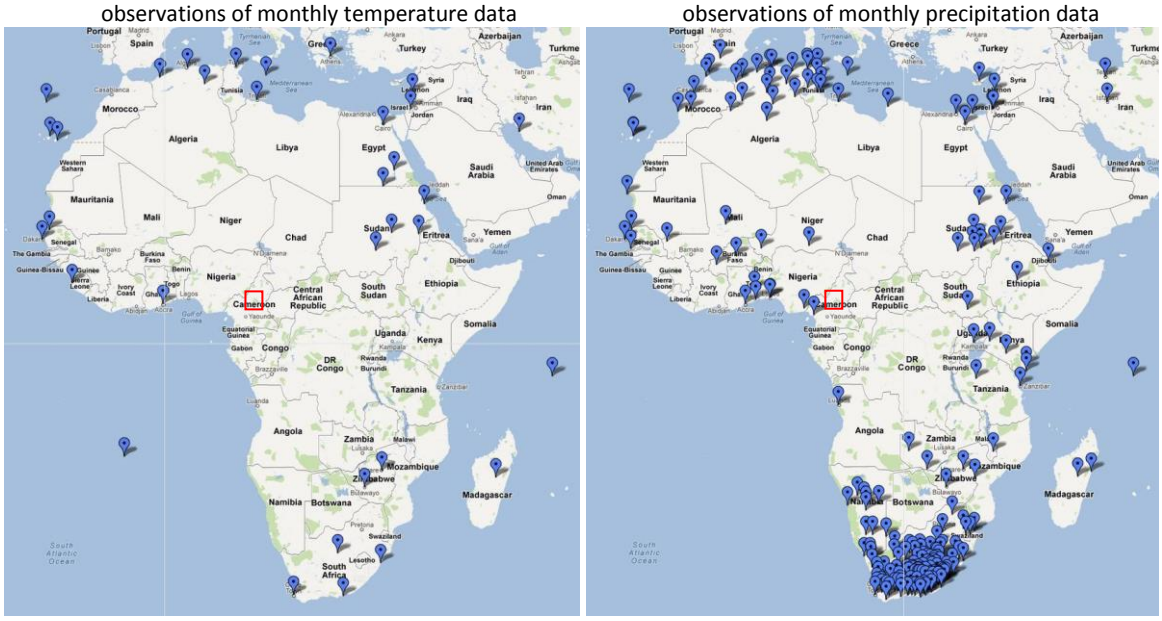

(c) Stations with at least 50 years of historical observations of monthly temperature data

(d) Stations with at least 50 years of historical observations of monthly precipitation data

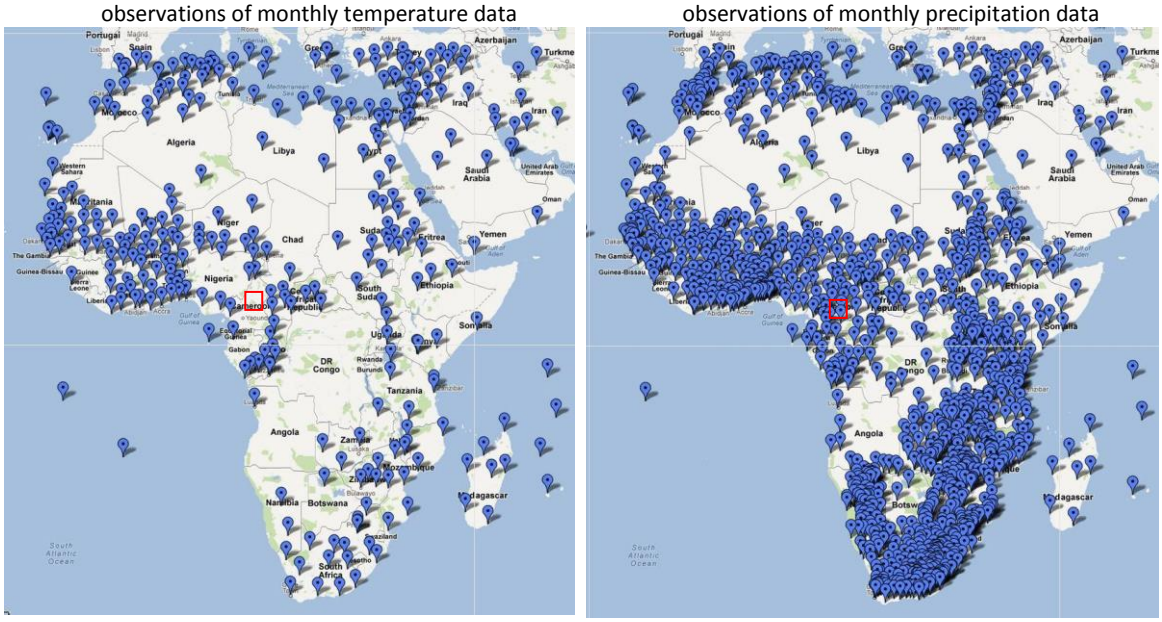

Figure 1-6: Visualisations showing the locations of climate stations in Africa. General location of the field site as described in Chapter 3 and Chapter 4 is represented by the red squares. Images were created using Google Maps. Map data was provided by Google, station data from KNMI Climate Explorer (http://climexp.knmi.nl/)

Some tree ring chronologies have been developed in the tropics but far fewer than in temperate regions and the time span covered is also shorter. Stahle *et al.* (1999) analysed *Pterocarpus angolensis* in Zimbabwe and found that the ring anatomy showed distinct boundaries and the ring width was highly correlated with wet season precipitation. This work was extended by Therrell *et al.* (2006), where they developed a 200 year long regional chronology and the first tree ring based precipitation reconstruction in tropical Africa. Fichtler *et al.* (2004) used *Pterocarpus angolensis* and *Burkea africana* to develop short, site specific chronologies (between 60 and 100 years) for two separate dry forests (900Km apart) in Namibia. Correlations between ring width and precipitation were observed for both species at both sites, as well as strong correlations with temperature and relative humidity for *Pterocarpus angolensis* at one of the sites.

In South America, Schongart *et al.* (2004) developed the first ENSO[2]-sensitive dendroclimatic proxy of the Amazon basin for *Piranhea trifoliata.* This 200 year chronology allows the dating of El Nino events which happened prior to instrumental records, and indicated that the severity of these events has significantly increased over time. In a different study, Schongart *et al.* (2005) developed chronologies in Central Amazonia of *Macrolobium acaiifolium* from two different floodplain types. From the nutrient-poor floodplain, an almost 400 year chronology was produced, and from nutrient-rich floodplains, a 146 year chronology was developed. Trees growing in the nutrient-poor floodplain were found to have significantly more rings than similar sized (DBH[3]) trees growing in the nutrient-rich floodplain with the nutrient poor trees also living longer. Both chronologies were significantly correlated with the non-flooing period and increased wood growth was found to occur during El Nino events, however the climate-growth relationship between this species and ENSO were less distinct than found in the previously mentioned study. Success in the North American tropics has seen the production of a 400 year chronology for Mexican mountain pine, *Pinus hartwegii,* in Nevado de Colima, Mexico (Biondi, 2001). This study included trees of up to 500 years old, despite past logging events in the area. The strongest correlated climate signal was for summer monsoon precipitation which occurs in June, which is also when the transition from the dry to the wet season occurs.

[2] El Niño–Southern Oscillation
[3] Diameter at Breast Height

The above successes in tropical dendroclimatology illustrate the potential for such studies. However this requires either prior knowledge of suitable species, a willingness to carry out pilot studies or a wider sampling approach which in either case does not guarantee success. With the complications that can arise from using traditional dendrochronological methods in the tropics, other methods have been explored to assist in establishing growth rates and seasonality on tropical trees, or as alternatives to traditional dendrochronological methods where these may not be possible due to complications such as indistinct rings.

1.3.1. Measuring Growth Rates in Tropical Trees

Measuring the growth rates of tropical trees could provide a method of establishing dating control for tropical species which lack visible annual rings. Annual incremental growth can be measured by cambial wounding (Mariaux, 1967) which, as the name suggests, involves physically wounding the tree stem at specific dates creating scarring on the xylem as the tree continues growing around the wound. Sass *et al.* (1995) used this method, with mixed success, to study the growth of two Malaysian tree species, *Dryobalanops sumatrensis* and *Shorea leprosula* , over a period of four years by wounding the tree stems every two months. In both species, relatively large areas of callus tissue formed around the wounded areas, which was complicated further with them having particularly slow growth rates as well as highly variable cambial activity across the tree stems. Despite these issues, it was shown for *D. sumatrensis* that wood formation was continuous throughout the year. It is clear however that this method presents many challenges that require consideration prior to use in the tropics but the major concern for using this method to establish growth rates is that ultimately the tree needs to be felled in order to visualise all the scars and to assess the rate of growth. This may make it unsuitable in areas where felling trees would not be permitted and also effectively ends that particular chronology.

Cambial wounding results in scarring around the wounded area as the tree recovers, which would not be desirable if further analysis were to be performed on the tree, especially as the tree needs to be cut to view the growth around the scars. Dendrometer bands (Drew and Downes, 2009) offer an alternative non-destructive method to measure growth rates *in situ*. Measurements can be taken by attaching metal dendrometer bands around tree stems which allows the continuous measurement of the tree circumference for the period of time they are

in place. Worbes (1999) used dendrometer measurements on different tropical species from Venezuela to determine growth rates and seasonality, and showed that cambial activity stops at the start of the dry season, and recommences during the wet season. This approach was also implemented by da Silva *et al.* (2002) to assess the growth patterns of trees in relation to rainfall growing over two sites in Central Amazon. Dendrometer measurements spanning 12 months, from 272 trees, were used to assess their growth patterns and calculate mean annual diameter increment for the Brazilian Amazon region. While they reported that this provided an accurate way to monitor and assess individual tree growth, it was noted that the particular bands used could only monitor a 20mm expansion in diameter growth before requiring to be changed which then required a lengthy adjustment period. This expansion size may vary depending on the construction of the bands, however all bands do require a period of adjustment to minimise any source of errors once the band has been set in place. Dendrometer bands allow non-destructive measurement of tree growth over the period of time they are in place. Advances in these measurement techniques have allowed variations of dendrometers to be developed including bands that use data loggers to remotely take accurate measurements at specific times (Drew and Downes, 2009).

Cambial wounding and dendrometer bands both provide methods of monitoring the growth rates of trees which could assist in the dating of trees in the tropics. However each have limitations as discussed, with the biggest one being that these methods can only assess growth rates and trends over the period of measurement which covers only a very small percentage of a tree's life. Cambial wounding also requires the tree to be felled to view the resultant scarring, but does provide a very cheap way to monitor growth. Such methods would be ideally used in species suitability studies when little information is available about the trees in a certain area.

1.4. Dendrochemistry

Dendrochemistry is the study and interpretation of the different elements in tree-rings. This can include measurements of stable isotopes and other elements which can be taken up into a tree and stored within the woody tissue. The basic premise is that these stores of chemicals can be accessed from tree-rings and may be indicators of past chemical fluctuations in the environment (Cutter and Guyette, 1993, Speer, 2010). This could offer an alternative solution

to building tree-ring chronologies and reconstructing past climates, as well as offering a wealth of additional information regarding the environmental conditions affecting the tree's growth. Dendrochemistry should not be thought of as a replacement for traditional dendrochronological methods as ring width measurements still provide the 'best' solution for dating trees and climate reconstructions with the added advantage of being a relatively cheap and fast solution, but as not all trees are amenable to ring width measurements (Section 1.3), such as in the tropics, additional methods are required to extract potential information stored within trees.

1.4.1. Stable Isotopes in Tree-Rings

The three main elements in wood are carbon, oxygen and hydrogen. Each of these contains isotopes which are forms of the same element differing only by mass (due to having a different number of neutrons). Carbon has two stable isotopes (^{12}C and ^{13}C) and one radioactive isotope (^{14}C), oxygen has three stable isotopes (^{16}O, ^{17}O and ^{18}O), and hydrogen has two stable isotopes (^{1}H and ^{2}H, also called H and D) and one radioactive isotope (^{3}H). The stable isotopes of an element have almost identical chemical properties. However the slight differences in masses between them can cause chemical, biological and physical processes to discriminate against one of them thereby altering the proportions in which they are present.

Carbon enters the tree as CO_2 from the air and both oxygen and hydrogen enter via the tree's roots from soil water. The elements aren't simply stored in these states, but undergo changes from physiological processes resulting from the tree's response to the climatic conditions at that particular time. An understanding of these fractionation factors presents us with the potential to use these natural stores to develop records of environmental change.

1.4.1.1. Stable Isotope Notation

Stable isotopes are reported as a ratio, relative to a standard. The ratio (*R*) of carbon, oxygen and hydrogen isotopes are measured as the abundance of the rare isotope to that of the common isotope and reported relative to the isotope ratio of a standard as follows (Farquhar *et al.*, 1982):

$$\delta^a E = \left(\frac{R_{sample}}{R_{standard}} - 1\right) \times 1000$$

where E is the element, a is the atomic mass of its heaviest isotope. The δ value is multiplied by 1000 and reported in parts per thousand (‰ or per mil).

1.4.1.2. Carbon Isotopes

Carbon isotopes are expressed as $\delta^{13}C$ which represents the observed $^{13}C/^{12}C$ ratio relative to a standard. The standard for carbon isotope ratios was originally a fossil belemnite from the Pee Dee formation of south Carolina (PDB) but has since been replaced by Vienna-PDB (VPDB) due to the supply of the original PDB being exhausted (Coplen, 1995).

Trees take in carbon dioxide (CO_2) from the air by diffusion through the stomata in the leaves. During the intake, CO_2 is fractionated in preference to the lighter carbon isotope ($^{12}CO_2$) by ~-4.4‰ making the internal air depleted in ^{13}C relative to the external air. Photosynthesis causes the internal CO_2 to be further fractionated by ~-27‰ during carboxylation where the lighter $^{12}CO_2$ molecules are preferentially used to produce sugars (Loader *et al.*, 2007). The discrimination against the heavier carbon isotope (^{13}C) during these processes can be expressed as:

$$\Delta‰ = a + (b - a)(c_i/c_a)$$

where a is the discrimination against the heavier isotope through the stomata, b is the discrimination from carboxylation and c_i and c_a are the internal and external CO_2 concentrations (Farquhar *et al.*, 1982).

The dominant environmental conditions that affect carbon isotopic fractionation are those that affect the rates of photosynthesis (light and leaf temperature) and stomatal conductance (relative humidity and soil moisture) (McCarroll and Loader, 2004).

1.4.1.3. Oxygen Isotopes

Oxygen isotopes are expressed as $\delta^{18}O$ which represents the observed $^{18}O/^{16}O$ ratio relative to a standard. The standard for oxygen isotope ratios when measuring carbonates is usually the same as used for carbon, Vienna-PDB (VPDB), however for the measurement of waters, ice and plant material, the standard is Vienna Standard Mean Ocean Water (Vienna-SMOW or VSMOW), which replaced the original Standard Mean Ocean Water (SMOW).

Trees get their water from soil moisture. The isotopic signatures of precipitation will therefore play a part in the water isotopes stored in the wood, however fractionation by evaporation (loss of lighter isotope ^{16}O) in the soil can occur before water has entered the tree. Roots take in soil water and transport it up to the leaves through the xylem. No fractionation occurs during the transport (Evans and Schrag, 2004); the critical site of fractionation is in the leaf (McCarroll and Loader, 2004). The loss of the lighter oxygen isotope, at the first fractionation step, is caused by transpiration (Barbour *et al.*, 2001). This occurs when the stomata open either to allow in CO_2 for photosynthesis or in response to climatic variables such as wind speed or atmospheric humidity and H_2O diffuses out. The first fractionation step of oxygen means that since the leaf has a higher $\delta^{18}O$ than the surrounding environment, it is not simply a matter of the tree giving a "snapshot" of the isotopic ratio of soil water but rather a means by which we can deduce the temporal conditions from the given ratio. This can be achieved by:

$$\Delta^{18}O_e = \varepsilon^* + \varepsilon_k + (\Delta^{18}O_v - \varepsilon_k)e_a/e_i$$

where ε^* is the resulting water vapour pressure caused by the heavy $H_2{}^{18}O$, ε_k represents the fractionation caused by transpiration, $\Delta^{18}O_v$ is atmospheric isotope ratio of water vapour relative to source water and e_a & e_i is the ambient intercellular vapour pressure (Barbour *et al.*, 2001, McCarroll and Loader, 2004). Atmospheric conditions, mainly temperature, affect ε^* however the main factors affecting the $\delta^{18}O$ are the variations in the isotopic content of the source water (soil water) and the vapour pressure differences between the internal and external leaf.

Sucrose is formed within the leaf resulting in an enrichment in ^{18}O by 27‰ due to the exchange of carbonyl oxygen in organic molecules with water (Sternberg *et al.*, 1986). During the formation of cellulose from sucrose, fractionation may occur if oxygen molecules exchange

with xylem water (Roden *et al.*, 2000). Sternberg *et al.* (2006) demonstrated further fractionation during cellulose synthesis related to the location of oxygen in the carbohydrate moiety and showed that the biosynthetic pathway towards cellulose affects oxygen isotope partitioning. More recently, Sternberg and Ellsworth (2011) demonstrated that biochemical oxygen isotope fractionation during cellulose synthesis is affected by temperature showing an increase of up to 5 ‰ at lower temperatures.

1.4.1.4. Hydrogen Isotopes

Hydrogen isotope ratios are expressed as δD which represents the observed D/H ratio relative to a standard (Vienna Standard Mean Ocean Water (Vienna-SMOW or VSMOW)). Since both hydrogen and oxygen uptake into the tree is via the roots as source water, the processes of fractionation are very similar. The heavy isotope of hydrogen (deuterium) is less able to pass through the stomata, therefore increasing the δD concentration of the internal leaf relative to the source water. The next fractionation step takes place in photosynthesis where again, light hydrogen is favoured over heavy, thereby increasing the internal leaf δD in relation to the heavy isotopic content of the created sugars (laid down as tree-rings). Interaction between the internal leaf hydrogen content and the water content from the xylem occurs as it does with oxygen thereby creating an equilibrium that is closer to that of the source water (McCarroll and Loader, 2004), although environmental factors such as atmospheric $\delta D/^{18}O$ and factors that increase transpiration will affect the outcome. Hydrogen is least studied in regards to stable isotopes in tree-rings and it has been suggested that the model for fractionation may be lacking an understanding of the processes as it does not take into account differences in the kinetic isotope effects of chemical reactions involved in the synthesis of glucose (Waterhouse *et al.*, 2002). This affects the distribution and intramolecular positions of hydrogen isotopes and therefore the isotopic composition of hydrogen within the tree-ring.

1.4.2. Stable Isotopes in Temperate Trees

The use of stable isotopes in trees rings has allowed the production of palaeoclimate reconstructions in temperate regions. Treydte *et al.* (2006) reconstructed a millennium long record of precipitation variability from the $\delta^{18}O$ of Juniper trees in northern Pakistan. Centennial scale variations showed that the late 19th and the 20th centuries were the wettest over the past 1000 years. In a related study, Treydte *et al.* (2009) produced a millennium long $\delta^{13}C$ record from Juniper trees in the same region of northern Pakistan. Results suggested that the trees responded to both climate and elevated atmospheric CO_2 levels with the high frequency $\delta^{13}C$ variations showing a response to summer temperature. The low frequency variations from this record deviated from long term temperature trends and statistical tests suggested that increasing atmospheric CO_2 concentrations impact the carbon isotope fixation.

In traditional dendrochronology it is common practice to statistically detrend individual series to remove biological based age trends, in particular the juvenile growth trends, which results in retaining climate information at frequencies relating to the mean segment length (Cook *et al.*, 1995). Gagen *et al.* (2007) illustrated that it is possible to construct a stable isotope tree-ring chronology which retains all climate related information recorded in the low temporal frequencies which is normally lost due via detrending. Individual $\delta^{13}C$ series for pine trees in northern Finland were produced, the juvenile portion of every series was removed, followed by a correction for anthropogenic atmospheric CO_2 changes. The resultant non-detrended 362 year $\delta^{13}C$ chronology showed a high correlation with summer temperature, and the reconstructed summer temperatures suggested that AD 1660 and 1760 experienced a higher summer temperature than found during the late 20th century. This chronology was later extended to AD 886 using sub-fossil trees preserved in lakes where the authors reported that the significant relationship is actually linked to cloud cover as opposed to the original hypothesised summer temperatures (Gagen *et al.*, 2011).

Stable isotope studies in temperate regions can offer the production of long chronologies and the opportunity for climate reconstructions. The constant improvements of isotope ratio mass spectrometers and their associated peripherals can reduce the throughput time and increase the accuracy of results. However, measurements are costly and sample preparation can be labour intensive. In many regions, the use of stable isotopes as a potential climate proxy may not be appropriate as stable isotopes may not be able to contribute more than traditional tree-

ring proxies already do, however in some cases stable isotopes can provide additional climate information or can be used as an alternative where ring width signals are weak (Loader *et al.*, 2008). In regions such as the tropics where tree rings are often indistinct or irregular, stable isotope analysis may provide a solution.

1.4.3. Stable Isotopes in Tropical Trees

With the problems associated with traditional dendrochronological methods in the tropics, stable isotope analysis (and in particular $\delta^{13}C$ and $\delta^{18}O$) could potentially provide an alternative tool in the development of proxy climate records by reconstructing the physiological responses of trees to climate. Carbon isotope values are mainly influenced by stomatal conductance and photosynthetic rate, whereas influences on oxygen isotope values include the isotope signature of source water, the evaporation enrichment in the leaf and fractionation during cellulose synthesis (Sections 1.4.1.2 and 0). The driving influence may be dependent on the environmental conditions at the time of growth which may result in multiple factors controlling the variability of $\delta^{13}C$.

As discussed earlier, it has been shown that some tropical trees have annual growth rings (D'Arrigo *et al.*, 1994, Gourlay, 1995, Stahle *et al.*, 1999, Worbes, 1999, 2002, Therrell *et al.*, 2006, Touchan *et al.*, 2011), however the likelihood of encountering ring anomalies are high (Gourlay, 1995, Sass *et al.*, 1995, Worbes, 2002, Wils *et al.*, 2009). The application of stable isotopes to tropical trees could provide a way of overcoming these issues by identifying seasonal trends which can lead to the detection of growth increments. However, ring anomalies such as wedging or missing rings will still complicate matters. Stable isotopes may not only assist with dating issues in the tropics, but could further open up opportunities for climate reconstructions in both ringed and ringless species.

Tarhule and Leavitt (2004) developed an approach using the stable carbon isotope series of tropical trees which exhibit growth rings to identify missing or false rings in wood segments with indistinct growth. The $\delta^{13}C$ ratios were obtained from 9 West African trees of 3 different species, previously identified as having distinct rings but with many problematic areas (ring pinching, missing rings (Tarhule and Hughes, 2002)). Samples were cut from stumps of an unknown felling date and an estimated date was calculated based on the stump condition and

the size of sprouting offshoots. The oppositional relationship normally observed between seasonal rainfall and $\delta^{13}C$ was used to identify missing rings within the isotopic series, significantly increasing the correlations between them. Applying such a technique to tropical trees with known outer dates, could further potentially overcome some of the issues associated with ring anomalies.

Poussart *et al.* (2004) were the first to successfully apply stable isotope methods to ringless trees in the tropics. A species with well-defined rings, *Tectona grandis* (from Java), was first used to demonstrate the reproducibility of the isotopic signal, and the method then applied to 2 ringless species. Tree discs from 2 *Samanea saman* trees, a ringless species found in Bali, and a single wedge section from a ringless *Podocarpus neriifolius* tree found in Northern Thailand, were analysed for $\delta^{18}O$ and $\delta^{13}C$. The seasonal nature of the isotopic signals for *S. saman* were established using end point radiocarbon age estimates for each sample, which showed close agreement with the number of isotopic cycles obtained for that period. The cutting date of the *P. neriifolius* sample, along with the date of a coring scar which was visible in the sample was used to determine seasonality and annual cyclicity of the isotopic signals. The number of $\delta^{18}O$ and $\delta^{13}C$ cycles matched the number of years between the two dates implying the tree exhibited strong seasonal growth.

In a related study, Poussart and Schrag (2005) assessed the application of stable isotope dendroclimatology in northern Thailand for 11 trees, consisting of 9 species, 6 of which were ringless. All trees were analysed for $\delta^{18}O$ and $\delta^{13}C$, with 2 of the species (*Miliusa velutina* and *Quercus kerrii*) selected for additional radiocarbon measurements to test the seasonal timescale of observed stable isotope cycles. Radiocarbon sampling for one of the trees consisted of 9 dates between 1957 and 2001 which encompassed the atmospheric bomb peak, and the other had 6 dates extending back to 1979. Age-growth models for these trees were constructed using the $\delta^{18}O$ series, where it was assumed that peaks and troughs were related to maxima and minima in relative humidity and when compared to the radiocarbon dating, showed an agreement of age estimates within 3 years. Of the remaining 9 trees that were measured, 5 produced cyclic isotopic patterns indicating seasonality, but the remaining 4 were deemed unsuitable for tropical dendroclimatology as the resultant isotopic signals lacked any cyclic patterns. These results may not provide as much accuracy as traditional ring width measurements; however they do provide reasonable age estimates for ringless tropical trees where no alternative methods are available.

Evans and Schrag (2004) also used stable oxygen isotope records to explore the potential for chronology development using rainfall reconstructions in tropical species. They tested this approach by examining the $\delta^{18}O$ records on a selection of tropical tree types; tropical trees with annual rings, without distinct rings but dated via radiocarbon, and without distinct rings but of known age from a plantation. They found evidence of strong cyclicity in the $\delta^{18}O$ records which, when compared to model predictions suggested these cycles represented the annual cycles or rainfall and relative humidity.

More recent studies have had success identifying and assessing climate signals from trees with non-distinct rings using stable isotopes. Anchukaitis *et al.* (2008b) produced an annual chronology from *Ocotea tenera* trees, a species with non-distinct rings, from monitored plots in a montane cloud forest in Costa Rica. High resolution $\delta^{18}O$ measurements identified seasonal cyclic patterns which were associated with precipitation and moisture sources, and were used to calculate growth rates. These growth rates matched those detected from basal growth measurements, confirming annual growth. Ohashi *et al.* (2009) combined cambial wounding and dendrometer growth rate measurements (Section 1.3.1) with $\delta^{13}C$ measurements to identify seasonality and annual growth within several tropical species from northern Thailand, which either lacked distinct rings or showed irregular growth rings. Dendrometer bands were used to monitor the growth of all trees and during this time cambial wounding was used to measure one year's growth. Results from the dendrometer studies concluded that growth was seasonal and suspended during the dry season. A stable carbon isotope ($\delta^{13}C$) chronology was developed for all species showing annual cyclic patterns confirmed by the cambial wounded areas, and a strong negative correlation with precipitation records was found from the region.

More recently Loader *et al.* (2011) developed a stable carbon isotope series from four ringless Malaysian trees. The $\delta^{13}C$ series was developed from the analysis of sequential 1mm sections. Radiocarbon dating was used to develop age-growth relationships resulting in an age estimate of the inner pith of 759 ±40 years for the oldest tree. Stable isotope analysis was only however performed on samples dating back to 1850AD. While the ±40 year error may seem large compared with traditional dendrochronological methods, the identification of these old trees would not be possible using traditional methods due to the lack of identifiable annual rings.

Although stable isotope analysis has proved successful for some tropical species which lack distinct growth rings (Evans and Schrag, 2004, Poussart *et al.*, 2004, Poussart and Schrag, 2005,

Anchukaitis *et al.*, 2008b, Ohashi *et al.*, 2009, Loader *et al.*, 2011), this approach requires high resolution sampling in order to attempt to show seasonality, which is not only expensive, but very time consuming in terms of sample preparation and analysis time. Poussart and Schrag (2005) illustrated that success with ringless species is not always guaranteed, finding that a third of the trees did not produce usable isotopic patterns. A combination of growth assessment studies and stable isotope measurements may help avoid expensive analyses if these methods suggest growth is constant rather than seasonal, but success is again not guaranteed and this may be a rather time consuming process. Due to these constraints, it is clear that another approach for identifying seasonality in ringless tropical species is required to open up these crucial tropical regions for research such as climate reconstruction, assessment of forest dynamics and carbon cycling.

1.4.4. Mineral Nutrition in Trees

Most higher plants require the same set of essential mineral nutrients in order to grow (Table 1-1). In order for an element to qualify as 'essential' it should fulfil the following criteria; (1) without the element, the plant would be unable to survive; (2) no other element can act as a replacement; (3) the element is required for plant metabolism (Marschner, 1995, Kirkby, 2012). Other elements which are not deemed to be essential, such as aluminium, selenium and cobalt, can still be taken into the plant and accumulate in plant tissues (Taiz and Zeiger, 2010).

A common assumption has been that these elements may represent the environment at the time the woody tissue was formed (Cutter and Guyette, 1993), however a greater understanding of the physiological processes involved is required in order to gain a better understanding of what these elemental archives represent.

Table 1-1: List of essential mineral elements required for growth in higher plants (Fritter and Hay, 2002)

Element	Symbol	Form
Nitrogen	N	NO_3^-, NH_4^+
Potassium	K	K^+
Phosphorus	P	$H_2PO_4^-$, $H2PO4^{2-}$
Calcium	Ca	Ca^{2+}
Magnesium	Mg	Mg^{2+}
Sulphur	S	SO_4^{2-}
Iron	Fe	Fe^{3+}
Manganese	Mn	Mn^{2+}
Zinc	Zn	Zn^{2+}
Boron	B	$B(OH)_3$
Copper	Cu	Cu^{2+}
Nickel	Ni	Ni^{2+}
Chlorine	Cl	Cl^-
Sodium	Na	Na^+
Cobalt	Co	Co^{2+}
Silicon	Si	$Si(OH)_4$

1.4.4.1. Nutrient Uptake

The main path of nutrient uptake is from the soil into the tree via the root system, although alternative absorption via the bark into the cambium layer and through the leaves after direct deposition is also possible. Nutrients are mostly transported from the soil solution in ionic form (Table 1-1) with mechanisms for uptake, transport and distribution varying between elements (Maathuis, 2009). Soil contains a solid, liquid and gaseous phase, all of which interact with mineral elements. The solid phase acts as a nutrient reservoir for cations[4] which bind to the negatively charged surfaces on the soil particles (Figure 1-7), and the liquid phase provides a means for ion movement to the root surface. Cations which are adsorbed to the soil particles are not easily lost through leaching. The binding affinity of the different cations influence which cations form electrostatic attractions with the negative soil surfaces. Generally, polyvalent cations have a higher binding affinity than divalent cations, which have higher binding affinities than monovalent cations, with the exception of H^+ (Alloway, 2013).

[4] Ions are charged atoms (or group of atoms). Positively charged ions are known as cations, and negatively charged ions are anions.

Hydrogen ions have a higher affinity than the divalent cations due to their small size allowing them to move much more closely to the negatively charged surfaces (Hopkins, 1995).:

$$Al^{3+} > H^{+} > Ca^{2+} > Mg^{2+} > K^{+} \text{ and } NH_4^{+} > Na^{+}$$

Cations adsorbed at the soil particle surface may be displaced and dissolved into the soil solution (liquid phase) by a cation of higher binding activity, making it available for uptake into the root. Cations of a lower binding affinity may also exchange with higher affinity cations when concentrations of the lower affinity cation are high in the soil. The cation exchange capacity (CEC) of soil is the ability of the soil to hold exchangeable cations. This may be dependent on soil type, and soil pH influences the amount of nutrients available in the soil.

The gaseous phase of soil consists of air-filled spaces which supplies oxygen for root respiration resulting in the release of CO_2 from the root into the soil solution (Figure 1-7). The dissociation products of respiratory CO_2 when equilibrated with soil water (H^+ and HCO_3^-) promotes ion exchange at the soil particle surfaces (Larcher, 2003). The decomposition of organic matter in the soil also produces CO_2 which equilibrates with soil water producing bicarbonate (HCO_3^-) and hydrogen ions (H^+) (Taiz and Zeiger, 2010):

$$CO_2 + H_2O \leftrightarrow HCO_3^- + H^+$$

The production of hydrogen lowers the pH of the soil around the roots. More H^+ becomes available in the soil solution, displacing cations from the soil particles into the soil solution. The same result occurs from the release of CO_2 from the root into the soil (Figure 1-7). Ions which are dissolved in the soil solution may be transported to the root, reducing their concentration in the soil solution, which can be replaced by the release of cations from the soil particle nutrient stores. Further cations are released into the soil via the weathering of rocks which relies on the soil acidity from the release of hydrogen ions (Taiz and Zeiger, 2010).

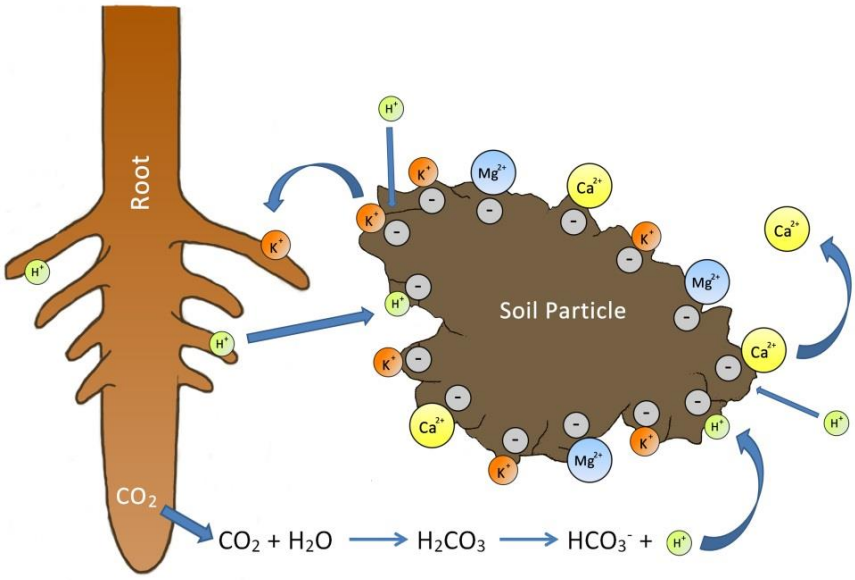

Figure 1-7: Image illustrating cation exchange on the surface of soil particles. Cations adsorb to the negatively charged surfaces of the soil particle by electrostatic attraction. Bound cations may be displaced into the soil solution by other cations with higher binding affinities, making them available for uptake by the roots. Image adapted from W. H. Freeman & Co. (No Date) and Taiz and Zeiger (2010).

Minerals move to the root surface via diffusion or bulk flow[5]. Cell walls in the root (and other plant tissues) contain free carboxyl groups ($R{\cdot}COO^-$) which act as cation exchangers allowing the movement of ions by electrostatic interactions into the apoplast[6]. The negative charges on the carboxyl groups attract and bind cations, allowing more cations to diffuse in, until equilibrium is reached with the soil solution. This results in the accumulation of bound cations in the apparent free space (AFS)[7] of the apoplast. At the same time, anions are repelled by the negative carboxyl groups therefore the concentration of total cations is usually much higher than that of anions in the apoplast. The AFS is often described as containing an area of restricted ion movement area called the Donnan free space (DFS) where the cation exchange/anion repulsion takes place, and the water free space (WFS) which is the area where the free diffusion of ions occur (Sattelmacher, 2001). The binding affinity of the cations influence which are preferentially bound at the cation exchange sites in the DFS, while they are passing through the pores from the extracellular solution. Polyvalent and divalent cations bind

[5] Diffusion is the movement from regions of high concentration to low concentration. Bulk flow is the movement of nutrients carried by water from the soil towards the root.
[6] The apoplast is the area external to the plasma membrane in a plant cell, containing the extracellular space surrounding the symplast, the cell walls and the space between cells. The symplast is the compartment of the plant cell on the inner side of the plasma membrane.
[7] The AFS is essentially the apoplastic space, however it is referred to as the apparent free space to emphasise that ion movement is dependent on their interaction with anions present in the cell wall (Sattelmacher, 2001).

more strongly and are therefore preferentially selected for than monovalent cations, leading to a greater concentration of charged ions which are available for the binding sites located on the plasma membrane. The root CEC can affect the rate and selectivity of entry to the cell proper at the active uptake sites of the plasma membrane (Sattelmacher, 2001, White, 2012). As well as competition between ions with the same electrical charge, competition also occurs between ions with similar physiochemical properties. This competition may occur at both specific and non-specific binding sites. For example, potassium (K^+) and rubidium (Rb^+) are similar in radii and compete for the same binding sites; however Rb^+ does not perform the same metabolic function as K^+. Mg^{2+} can be successfully out-competed at cell wall binding sites by both Ca^{2+} and K^+, due to its weaker binding strength, and blocked at specific plasma membrane binding sites by Mn^{2+} (Marschner, 1995).

Ion movement through the root is by active transport, either apoplastically (e.g. calcium (Lautner and Fromm, 2010)) or symplastically (e.g. potassium (Karley and White, 2009)) into the xylem (Figure 1-8). Apoplastic transport is the movement between cells via the extracellular space external to the plasma membrane, whereas symplastic transport is the movement from cell to cell in the cytoplasm through the plasmodesmata channels. The symplast is the compartment of the plant cell on the inner side of the plasma membrane.

Ions and water which travel through the roots via the apoplast may be restricted by the Casparian strip (or band), which is a lignified barrier of cell wall material in the endodermis cells (Larcher, 2003). The Casparian strip potentially ends their transport or forces some movement through the plasma membrane into the symplast. Transport via the apoplast however is particularly important to some ions such as calcium where Ca^{2+} concentration in the cytoplasm of the cell must be strictly regulated. Certain sites on the root axis, such as the very root tip, lack a fully developed Casparian band allowing apoplastic transport to continue into the stele (Figure 1-8) and ion release into the xylem (White and Broadley, 2003). Although the main route of transport for calcium is via the apoplast, some calcium may enter the symplast, however this is strictly controlled.

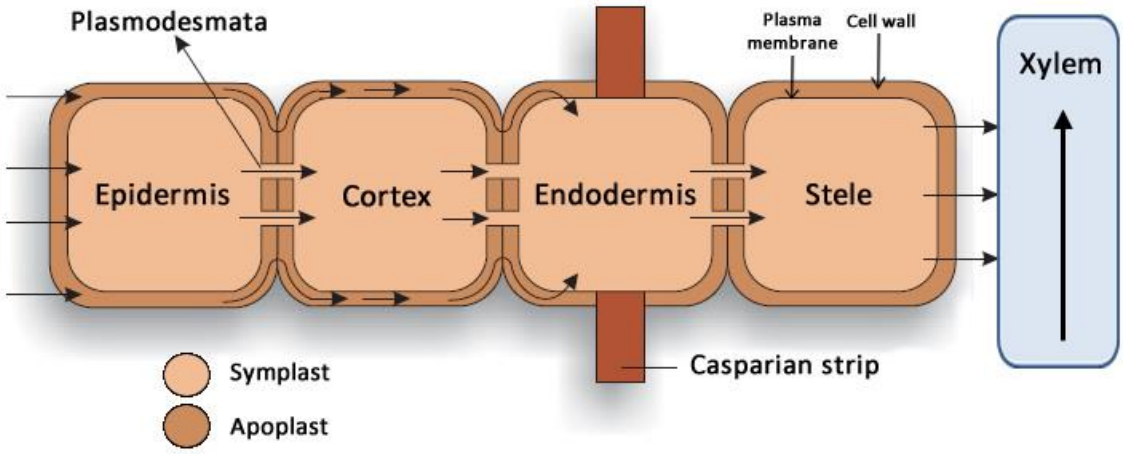

Figure 1-8: Illustration representing the symplastic and apoplastic pathway for nutrient movement within the root. Ions are taken up by the epidermal cells, and transferred via the symplast or apoplast through the cortical and endodermal cells into the stele, where they are enter the xylem. In most cases (where present), the Casparian strip interrupts the apoplastic transport. Image adapted from Kimball (2013)

Most mineral ions are transported through the root system via symplastic transport. The plasma membrane is the main site of ion uptake selectivity, acting as an effective barrier to restrict entry from the apoplast into the symplast or vice versa. The tonoplast (vacuolar membrane) within the cell behaves in a similar way to the plasma membrane, controlling entry into and out of the vacuole[8]. Entry into the symplast (Figure 1-9) is either down an electrochemical potential gradient by diffusion, assisted by transport proteins and ion channels, or against an electrochemical potential gradient by active transport (Lambers *et al.*, 1998). Active transport processes require additional energy and hydrolysing proteins in the membrane act as proton pumps to establish electrochemical gradients across membranes (Larcher, 2003). Secondary active transporters move ions either in the same direction (symport) or opposite direction (antiport) using the electrochemical gradient of H^+ (White, 2012).

[8] The vacuole is a large storage compartment within the cell for ions, sugars and other solutes.

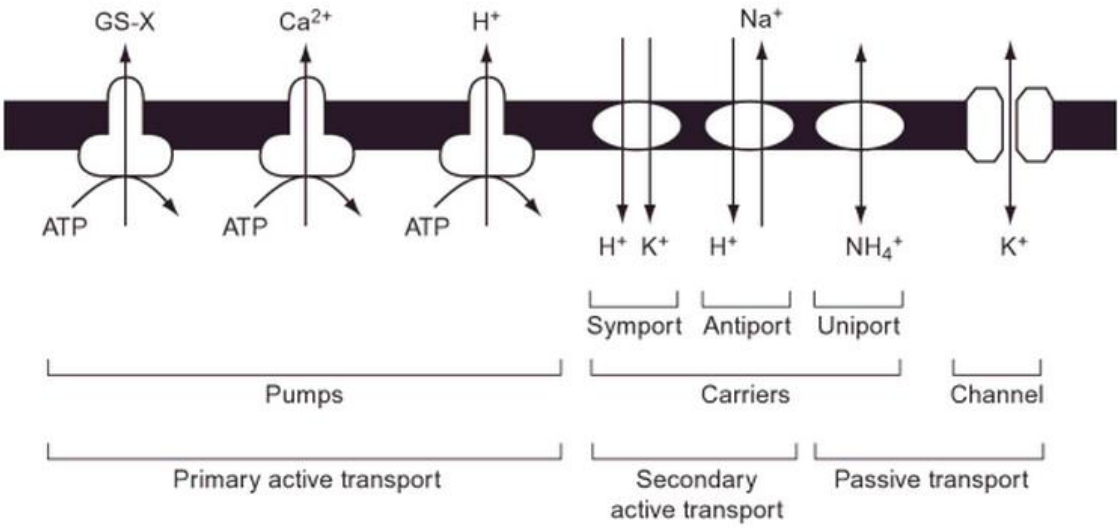

Figure 1-9: Schematic illustrating the role of membrane proteins in the transport of cations by primary and secondary active transport, and passive transport (White, 2012).

Figure 1-8 shows the pathway for symplastic transport. Ions enter the root by means of the epidermal cells and move cell to cell through the cytoplasm, via the plasmodesmata[9] to the stele. The transport of minerals in this manner is mainly by diffusion, assisted by radial water flux (Larcher, 2003). Ions are released (loaded) into the xylem (and in some cases also into the phloem) from the stele across the plasma membrane of parenchyma cells. In a similar manner to the initial entry into the symplast, protein transporters and channels facilitate this movement out into the xylem, where rapid ion distribution by water flow through the xylem. Reabsorption of ions from the xylem sap can occur at various locations by xylem tissues, enabled by xylem parenchyma cells.

1.4.4.2. Considerations for Mineral Measurement

For dendrochemical studies, several factors should be taken into consideration. Although mineral uptake for most tree species follows the same general pathways (as described above), the actual nutrient requirements may vary depending of the tree type, gymnosperm or angiosperm (ring porous, semi-ring porous or diffuse porous) (Section 1.2), and tree species. Within species variation may also occur as a result of the tree location. It should not be

[9] Narrow channel passing through the cell walls of adjacent plant cells

assumed that the same species of tree will behave in the same way in two separate environments or that different species growing in the same place will exhibit the same elemental characteristics.

The size and structure of the heartwood and sapwood may also influence nutrient allocation (Cutter and Guyette, 1993, Speer, 2010). Many trees contain an area of apparently dead or physiologically inactive heartwood surrounded by living sapwood (Figure 1-1). The size of the heartwood and sapwood can vary within the same species and between species, and in some cases a distinct heartwood may not be present at all (Watmough, 1999, Penninckx *et al.*, 2001). Cutter and Guyette (1993) suggested that trees most suitable for dendrochemical analysis would be long lived species with a distinct heartwood, a low moisture content, and a low number of sapwood rings, which should minimise the radial mobility of minerals. In practise however, a major influence for species selection may be the simple use of the most dominant species in the region of interest.

It is important for successful analysis that any elemental trends observed are distinguished from naturally occurring age related trends and not misinterpreted as environmental indicators. To address this, many investigations into the radial distributions of elements in a variety of species have been undertaken (detailed below) as well as consideration of the potential of element mobility across the stem.

Element Mobility

If dendrochemical studies are to be successful then the elements in question should remain immobile within the wood. Ideally, elements entering a tree should be deposited and stored within in the outermost ring representing that year of growth with no further movement across tree-rings in subsequent years. The mobility or radial translocation of elements is therefore perhaps the most important factor to be considered in these dendrochemical studies as any movement between rings reduces the usefulness of such an approach. Cutter and Guyette (1993) suggested that the physiological processes affecting an element's mobility and storage could differ between species and also environments. This was supported by Hagemeyer and Schäfer's (1995) findings for *Fagus sylvatica* L. (European beech) when they observed different lead (Pb) distributions between two separate sites in Germany for the same species. This suggestion was also supported by Penninckx *et al.* (2001) who found

differences in concentration profiles between two separate species, *Quercus robur* L. (Pendunculate oak) and *F. sylvatica* L. from the same site in Belgium. They compared the mineral element concentrations between the two species and concluded that the differences between elemental profiles were consistent with the contrasting wood structures of these species. Penninckx *et al.* (2001) also noted that in the oak samples, many of the metals showed a steep jump in concentration at the heartwood-sapwood boundary which may be a result from the reabsorption of nutrients from the adjacent sapwood rings. Other studies have also reported a steep jump or a peak in concentration around this boundary point for various species (Hagemeyer and Schäfer, 1995, Nabais *et al.*, 1999, Watmough and Hutchinson, 2002).

The sapwood contains active cells which are part of the transpiration stream and therefore usually has a higher moisture content than the heartwood (Shigo and Hillis, 1973). Sapwood cells also act as a reserve for starch (Smith and Shortle, 1996, Taylor *et al.*, 2002). During the transition from sapwood to heartwood, several biochemical and physical changes occur which can result in an increase in density, colour change due to deposition of extractives from cells, and a decrease in moisture content and permeability (Cutter and Guyette, 1993). The resultant heartwood cells are basically inactive and therefore no longer part of the transpiration stream or acting as starch reserves. It is for this reason that Cutter and Guyette (1993) recommended the use of species containing a distinct heartwood, with a low number of sapwood rings relative to the heartwood, as this increases the likelihood of minerals staying 'fixed' within a ring. The heartwood-sapwood boundary can include a transition zone which contains living cells, although they may lack starch and have a lower moisture content than the sapwood but higher than the heartwood cells (Taylor *et al.*, 2002). Such a transition zone may account for a sharp increase or decrease in elemental concentrations across the heartwood-sapwood boundary.

Since the mobility of minerals across ring boundaries is such a significant issue, potentially affecting the usefulness of subsequent studies, several authors have focussed on determining the movements of elements for various species after uptake into the tree stem. Hoffmann *et al.* (1996) modelled the migration of elements in oak, using autocorrelation functions to calculate the correlation time of a suite of metals, which in turn gave an indication of element transport within the tree. They concluded that most of the elements analysed (Pb, Sr, Mn, Al, Ba, Zn, Cu, Ni, Mg) exhibited short correlation times indicating minimal migration with the exception of Ca, Fe and Cr which had correlation times of over 10 years suggesting radial

migration. Prohaska *et al.* (1998) investigated element variability of young (12-15 years old) *Pinea abies* L. (Norway spruce) trees from Austria. They grouped elements according to their horizontal mobility in the tree stem, based on factors outlined by Cutter and Guyette (1993) and reported Mg to have the highest mobility; Ca, Sr, Ba, Zn, Co, Cr and Mn to be of moderate mobility; Al, Pb, Fe, and Cd to be of low mobility. These classifications disagree with those described above for several elements (Mg, Sr, Ba and Zn), particularly for Mg which is reported to be of high mobility, whereas Hoffmann *et al.* (1996) reported Mg to have minimal migration potential. A radial mobility study by Martin *et al.* (2003) observed yet another different scenario during their investigation into metal distributions of *Picea mariana* (black spruce), when they reported that the mobility of Ca was much less than that of Zn. This contrasted with results from both the above studies, where Zn was one of the metals which Hoffmann *et al.* (1996) found to be least mobile, with Ca exhibiting higher movement potential between rings. Prohaska *et al.* (1998) reported both Zn and Ca to be moderately mobile. These inconsistent findings could partly be attributed to the different methods used to measure and assess mobility of these elements, however it is more likely that these conflicting results reiterate the importance of the appropriate species selection as outlined by Cutter and Guyette (1993).

As well as influencing the mobility of elements after they have entered a tree, the species, and in particular its physical characteristics, can play a major part in how elements are utilised across the tree stem. In the same study as touched on above, Penninckx *et al.* (2001) compared the radial variations in element concentrations in two, structurally different, dominant species from the Belgium Ardennes. They analysed *Quercus robur L.* (Pedunculate oak), a ring porous species containing a typical heartwood, and *Fagus sylvatica L.* (European beech), a diffuse to semi-ring porous species which lacks typical heartwood[10]. It was assumed that any differences found in the mineral element profiles would be primarily due to the structural differences between the species, and any common trends may have been caused by an environmental influence. The only similarity in profiles observed between the two species was for the distribution of Al which showed an increase in concentration over the last 15 years. For all of the metals measured in the oak, higher concentrations were observed in the sapwood. This contrasted with the profiles found for some of the metals in the beech trees,

[10] European beech is usually a whitish colour; however older beech may develop "red heartwood" which reduces timber quality (mainly for aesthetic reasons). This red heartwood can be highly variable in colour and form (Knoke, T. (2003). Predicting red heartwood formation in beech trees (*Fagus sylvatica* L.). *Ecological Modelling*, 169 (2–3), 295-312.).

where a general decline from pith towards bark for Ca, Mg, K and Mn was seen. They concluded that the differences observed in the elemental concentration profiles between species were a direct result of the contrasting wood structures. It was suggested that the similarities could be explained as an effect from acid rain or possibly related to similarly decreasing cation binding capacity of wood with ageing however further investigation would be needed to confirm this.

It is clear that careful consideration should be given when carrying out this type of dendrochemical study since wood type, species, and location can all influence the storage and mobility of elements within a tree.

Observed Radial Trends

Despite the concerns about the stability of metals over time, encouraging results have been reported illustrating consistency in radial patterns for several elements over large geographical areas. Penninckx *et al.* (2001) observed an overall decreasing trend in the direction of pith to bark for Ca, K, Mg, Mn and P in European beech trees in Belgium. Very similar, almost identical trends for these elements were produced in a more recent study by Hristovski and Melovski (2010) who investigated the radial patterns of 13 elements in European beech from an area in Macedonia. Comparing the results from these two independent studies shows that despite the differences in locations, the trees behaved in a physiologically similar manner.

The decreasing trend observed in concentration from the pith towards the cambium for Ca, Mg and Mn observed by (Penninckx *et al.*, 2001, Hristovski and Melovski, 2010) in European beech has been replicated in other species such as in Norway Spruce trees in Austria (Prohaska *et al.*, 1998, Berger *et al.*, 2004) and Scots Pine trees in Estonia (Parn, 2001). Although these particular elements have shown a consistent pattern over several species and study sites, this is not applicable to all species. In a Canadian multi-elemental study of *Acer rubrum* L. (red maple), neither Ca nor Mn demonstrated any obvious trend over the life of the trees (Watmough *et al.*, 1998)), and Ca also lacked any trend in the heartwood of Pendunculate oak trees in France, but did show a steady increase throughout the sapwood for this species (Lévy *et al.*, 1996). The similarities observed in these metal distributions may partly be attributed to the type of trees analysed. Both Scots pine and Norway spruce are gymnosperms while maple and oak are angiosperms. The European beech is also an angiosperm, however it does not

develop the typical dark heartwood as can be found in the oak and maple, which may explain why the more consistent results were found for this species compared to other angiosperms. A strong decreasing trend from pith to cambium has also been reported for strontium in European beech (Drouet *et al.*, 2005), oak (Aberg, 1995, Drouet *et al.*, 2005), Scots pine (Aberg, 1995) and Norway spruce (Poszwa *et al.*, 2003). The reproducible trends shown for these elements across a variety of species would indicate that these are mostly age-growth trends rather than climatic trends. Such long term trends could be removed by detrending.

Meerts (2002) reviewed the available literature data to explore patterns in concentrations found in the heartwood and sapwood for of N, P, K, Ca and Mg. Their study consisted of 93 different tree species, 22 of which were gymnosperms and 71 were angiosperms. It was found that in general, gymnosperms have overall lower concentrations of all analysed metals in both the heartwood and sapwood compared with angiosperms which they suggested could be attributed to the environments in which each type of tree grow in; gymnosperms are often found in nutrient-poorer sites then angiosperms.

Seasonal Patterns

The seasonal nature of growth in temperate, and in some cases tropical, trees can be observed and measured in the annual growth rings (Section 1.3). Each ring consists of cells which change in structure as the growing season comes to an end resulting in an abrupt transition between each year's growth. This seasonality therefore affects the distribution of elements stored in the tree rings throughout the growth cycle and such inter-annual variability may provide additional climate related information not accessible using traditional dendrochronological methods.

Inter-annual seasonal patterns were detected when Hagemeyer and Schäfer (1995) investigated the radial distribution patterns of Cd, Pb and Zn in beech. Peaks in concentrations of these metals were found either during winter dormancy in December or just before bud break in April. They suggested these fluctuations were due to changes in the amount and the composition of xylem sap over the year with the December peak caused by reduced sap flow during cambium dormancy allowing storage pools of minerals to accumulate, and the April peak caused by the increased sap mobility and higher capacity to transport minerals during the spring mobilisation period. Martin *et al.* (2001) found seasonal variations and a strong

indication of seasonal uptake for Ca, Mn, Zn and Ni during their examinations of metal distributions of *Pinus resinosa* (red pine). Calcium was found to have the highest overall concentration in the stem wood which they suggested was due to its role as a major structural element in cell walls where it strengthens them by binding to functional groups. The observed distribution patterns for Ca and Mn were very similar, indicating that Mn also acted as a structural element and it competed with Ca for cation-exchange sites in the cell walls (Section 1.4.4.1). Seasonal uptake was also indicated for Zn and Ni, however the physiological roles of these metals were unclear from this study. St George *et al.* (2006) conducted a dendrochemical study to investigate whether elemental analysis could be used as a method to identify past flood events. They analysed metals in both the early and latewood of *Quercus macrocarpa* (Bur Oak) and found higher concentrations of Mg, Mn and Sr in the earlywood compared with latewood, indicating that seasonal uptake in metals may reflect in the inter-annual variability rates. It was concluded however that elemental analysis does not provide a method to identify past flooding events.

Martin *et al.* (2001) suggested that the similar seasonal patterns observed for Ca and Mn linked to their similar structural roles. Drouet *et al*. (2005) took advantage of structural and physiological similarities of Sr and Ca, when they analysed Sr isotopes to assess the origin of calcium sources in oak and beech trees. Calcium has been the main focus of several other studies which also reported a strong seasonal cycle in calcium fluctuations in trees (Follet-Gueye *et al.*, 1998, Arend and Fromm, 2000, Poussart *et al.*, 2006, Lautner and Fromm, 2010) linking this to the physiological roles calcium plays in wood formation and structure.

An assessment of the literature in this field strongly indicates that Ca is a good candidate for identifying seasonal patterns, hence showing potential for dating purposes in ringless tropical trees. Various studies have demonstrated reproducible negative trends in calcium concentrations over the life of the tree, and strong inter annual signals making it an ideal candidate for possible climate studies. Other potential candidates, including Sr, Mg and Mn, have also shown reproducible signals in a variety of species.

1.4.5. Calcium in Trees

Calcium has the highest concentration of all the metals present in stemwood (Martin *et al.*, 2001), it has been shown to be an important element in the regulation of many of the tree's physiological functions and plays a significant structural role in cell stability (Lautner and Fromm, 2010). It's main target is the carboxyl groups of pectin, which is the main structural component in the middle lamella and cell walls providing rigidity to the cells (Martin *et al.*, 2001). Once calcium is bound in cell wall compartments, it is no longer available for further processes (Lautner and Fromm, 2010). As well as providing structural support, it is a fundamental component of cell signalling events which are critical for cellular activity and responses (White and Broadley, 2003, Hirschi, 2004).

1.4.5.1. Ca^{2+} Distribution and Transport

Calcium is taken up from the soil solution by the roots as described in Section 1.4.4.1. It is a divalent cation which, unlike other cations, is mainly deposited in the apoplast (Lautner and Fromm, 2010) where movement into the symplast is strictly controlled. Figure 1-10 illustrates the distribution and main transport processes of Ca^{2+} within the cell. High concentrations of Ca^{2+} are found within the apoplast with a portion of the Ca^{2+} firmly bound in cell wall structures, some is exchangeable at the cell walls (Section 1.4.4.1), and some remains free and exchangeable at the plasma membrane (Marschner, 1995, Hirschi, 2004). In the symplast, concentrations of cytosolic free Ca^{2+} are very low and are tightly regulated. Excess Ca^{2+} is removed from the cytoplasm by Ca^{2+} ATPase and Ca^{2+}/H^{+} antiporters into intercellular organelles or through the plasma membrane into the apoplast (Hirschi, 2001, White and Broadley, 2003). High concentrations of calcium can be found in the vacuole and the endoplasmic reticulum within cells as a result of the removal of this excess cytosolic-free Ca^{2+} into these endomembranes (Marschner, 1995, Hirschi, 2004).

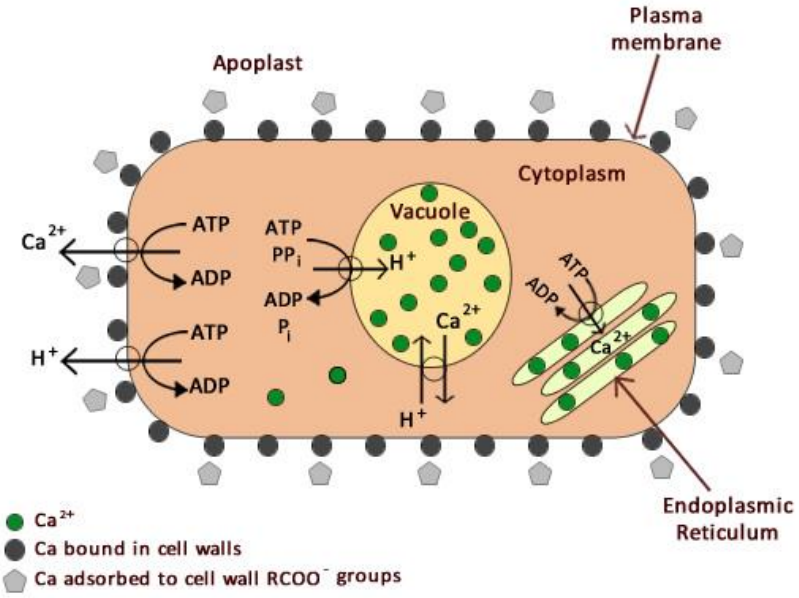

Figure 1-10: Diagram illustrating distribution of calcium in a cell and the transport processes for sustaining low concentrations of cytosolic Ca^{2+}. Figure based on Marschner (1995) and Hindshaw *et al.* (2013).

Due to the stringent regulation of Ca^{2+} entering the cytoplasm, calcium is mainly transported apoplastically. However, the presence of the Casparian strip (Figure 1-8) limits the apoplastic movement of Ca^{2+} (and other ions) across the endodermal cells of the root into the stele. Previously, it was presumed that in order to circumvent the Casparian strip, Ca^{2+} would complete its journey to the xylem via the symplast, entering the endodermal cells via ion channels (Marschner, 1995). This theory was found, at least in part, to be implausible. White (2001) outlined several problems suggesting that in the first instance, the endodermal cells could not contain enough Ca^{2+}-ATPase proteins to catalyse the vast amount of Ca^{2+} which is transported into the xylem. Secondly, transport solely by the symplastic pathway would result in selectivity due to cation competition at Ca^{2+} channels and transporters, whereas the apoplastic flux is relatively non-selective in comparison (White and Broadley, 2003, Gilliham *et al.*, 2011). If Ca^{2+} was transported exclusively via the symplast, discrimination between cations would be expected, however this is not observed in their transport from the root to the shoot (White, 2001, White and Broadley, 2003). Movement of Ca^{2+} to the xylem therefore appears to follow both the apoplastic and symplastic pathways. However, the contribution of each pathway in not clear, but may be species dependant (White, 2001, Gilliham *et al.*, 2011). Passage via the apoplast is constrained to the extreme root tip where the Casparian strip is absent, or to regions where the Casparian strip has not fully formed or has been disrupted

such as emerging lateral roots (White, 2001). Calcium is transported through the xylem where the transpiration rate and the root CEC determine the accumulation of calcium (White and Broadley, 2003, Hindshaw *et al.*, 2013).

1.4.5.2. Function of Calcium

Cell Wall and Membrane Stability

Calcium plays a vital role in the stability and strengthening of cell walls and plasma membranes (Lautner and Fromm, 2010). In the middle lamella[11], calcium forms stabilising cross-linkages by binding to the carboxyl groups ($R{\cdot}COO^-$) of opposing pectins (polygalacturonic acids) providing rigidity to the cells. Cell walls are further strengthened with the cross-linking of cellulose micro-fibrils by Ca^{2+} interactions with negatively charged groups of glycans and pectins (McLaughlin and Wimmer, 1999, Maathuis, 2009). At the plasma membrane, Ca^{2+} binds with the negatively charged groups within the membrane phospholipids, providing stability. Cell wall and plasma membrane integrity becomes compromised with low Ca^{2+} concentrations or during stress responses (salinity stress, aluminium toxicity etc.) which can result in Ca^{2+} being replaced by other cations (Marschner, 1995, Hirschi, 2004, Hepler, 2005, Maathuis, 2009). Eklund and Eliasson (1990) assessed the importance of calcium on wood formation by growing cuttings of Norway spruce trees in media containing varying concentrations of Ca^{2+}. In the absence of Ca^{2+} cell wall yield and stability was substantially reduced and when cuttings were exposed to very high levels of Ca^{2+} cell wall yield was increased, however major disturbances in patterns of cell wall synthesis was observed. Lautner *et al.* (2007) carried out similar investigations using young Poplar clones, grown in hydroponic nutrient solutions with different calcium concentrations for 6 weeks. Saplings exposed to the low calcium solutions showed reduced shoot and root development and reduced wood increments resulting from fewer cambium cells. The calcium deficient poplars also developed cells containing peculiar vacuole constructions; several small vacuoles rather than one large one, concluding that calcium plays an important role in cell structure, cell chemistry and wood formation.

Seasonal changes affect the structure of cambium cells, where the cells changes from an active to a resting state. In preparation of cambial dormancy, the cell walls thicken and are stabilised

[11] The middle lamella is the pectin rich layer which 'cements' adjoining cells together.

by the cross-linked calcium to pectin bridges. In spring when growth resumes, the calcium bridges are degraded, loosening the cambium cell walls ready for extension growth (Marschner, 1995, Lautner and Fromm, 2010).

Cell Signalling

As well as providing structural support, calcium functions as a second messenger during cell signalling events which are critical for cellular activity and responses (Marschner, 1995, White and Broadley, 2003, Hirschi, 2004). As outlined above (Section 1.4.5.1), Ca^{2+} is present in the cytoplasm at very low levels which are stringently controlled. Calcium is transported into the cytoplasm through Ca^{2+} permeable channels in the plasma membrane (from the apoplast) or through channels in the intracellular stores (such as the endoplasmic reticulum, vacuole, etc.). These channels allow the controlled influx of Ca^{2+} into or efflux from the cytoplasm, changing the cytosolic Ca^{2+} concentrations in response to signalling events. Different signalling events utilise the different calcium stores within the cell, and it is thought that each environmental stimulus invokes a specific change to the cytosolic Ca^{2+} concentration to produce the required physiological response (White and Broadley, 2003). The specific physiological response may be encoded in the resulting temporal and spatial changes as well as the Ca^{2+} concentration increase (White, 2000). Examples of processes which requires a Ca^{2+} cytosolic response include cell division, heat shock, cold shock, salinity, hypo-osmotic stress, aluminium stress etc. (White and Broadley, 2003). During cell extension, pectate bound calcium is released allowing the free Ca^{2+} to pass though the activated plasma membrane calcium channels, increasing the concentration of cytosolic Ca^{2+} and stimulating the synthesis of cell wall precursors (Marschner, 1995). Similarly, the physiological response of aluminium toxicity is triggered by elevated cytosolic Ca^{2+}. As a result, callose is produced in replacement to normal cellulose production (Hirano *et al.*, 2004, Hirano and Brunner, 2006). This switch from cellulose to callose also occurs in a response to other injury, both physical and infection (Marschner, 1995). Although most of these environmental stimuli require an increase in cytosolic Ca^{2+}, prolonged increases are harmful to cells.

Wood Formation

Ca^{2+} in the xylem sap is transported upward in the transpiration system, but once deposited in the cell wall layers, it is almost immobile and is no longer available for metabolic processes in the symplast (Hirschi, 2004, Lautner and Fromm, 2010). Cambium functioning follows a cyclic seasonal pattern and its cell divisions allow the production of xylem cells which in turn make up an annual ring (Follet-Gueye *et al.*, 1998). Since calcium binds to every cell wall (Martin *et al.*, 2001), a seasonal pattern should be detected across the width of a ring, with concentrations depending on the density and type of cells present. The evidence supporting the suggestion that calcium follows the cyclic nature of cambium activity in the tree has been demonstrated through the tropical dendrochemistry study by Poussart *et al.* (2006) outlined below (Section 1.4.7) for *Miliusa velutina* trees in Thailand. Further evidence to support this comes from an early study into calcium oxalate crystals in trees where Gourlay (1995) reported a line of calcium oxalate crystals in marginal parenchyma of African *Acacia* species.

Several studies have indicated the importance of calcium during the cambium pre-activation phase in early spring, and its involvement in the regulation of wood formation. Follet-Gueye *et al.* (1998) imaged cambium cells of beech trees at various phases of cambium functioning, and observed a strong temporary increase in calcium concentration in the cells during the pre-activation phase. A similar imaging approach was taken by Arend and Fromm (2000) and Lautner and Fromm (2010) to detect changes in calcium concentration in poplar trees. Arend and Fromm (2000) also observed a sharp, temporary increase in Ca^{2+} concentration within the symplast of cambium by up to 40% at the onset of cambial reactivation. Lautner and Fromm (2010) suggested calcium was required in promoting cell division when they observed concentration levels rising in the apical meristem during swelling and budbreak.

The radial distribution and mobility of calcium in tree rings have been investigated in many studies (Hoffmann *et al.*, 1996, Prohaska *et al.*, 1998, Watmough *et al.*, 1998, Penninckx *et al.*, 1999, 2001, Watmough and Hutchinson, 2002, Martin *et al.*, 2003, Poussart *et al.*, 2006, Hristovski and Melovski, 2010). Many of these studies have reported a general decrease in calcium concentration from the pith towards the cambium (Prohaska *et al.*, 1998, Parn, 2001, Penninckx *et al.*, 2001, Berger *et al.*, 2004, Hristovski and Melovski, 2010) which has been attributed to a decrease of cation binding capacity from pith to bark, due to the reduced amount of pectins (Bondietti *et al.*, 1990, Momoshima and Bondietti, 1990, Meerts, 2002).

The seasonal nature of tree growth and calcium's close relationship with wood formation makes this element an ideal candidate for dendrochemical analysis.

1.4.6. Applications of Mineral Element Dendrochemistry

Most dendrochemical studies have focussed on using the analysis of metal distributions in tree-rings to investigate environmental pollutants (Garbe-Schonberg *et al.*, 1997, Prohaska *et al.*, 1998, Nabais *et al.*, 1999, Parn, 2001, Ferretti *et al.*, 2002, de Vives *et al.*, 2006, Yu *et al.*, 2007, Mihaljevič *et al.*, 2008, Kwak *et al.*, 2009, Saint-Laurent *et al.*, 2011) or environmental events such as volcanic eruptions (Pearson *et al.*, 2005, Watt *et al.*, 2007, Pearson *et al.*, 2009).

An early study by Baes and McLaughlin (1984) found evidence linking metal concentrations in tree-rings with records of air pollution for *Pinus echinata* trees in Tennessee, U.S.A.. Relationships between reduced tree growth and increased Fe xylem accumulation rates were observed in trees affected by smelting emissions from an ore smelting plant. Since then others have investigated the effects of pollution from smelters in tree-rings; Watmough *et al.* (1996) found cadmium in a tree situated at a Cu-Cd refinery and not in trees 6Km away; Prohaska *et al.* (1998) observed significant increases in Al, Fe, Cu, Ba and Sr profiles in Norway spruce linked to a nearby Al smelter; Mihaljevič *et al.* (2008) analysed Norway spruce trees growing near a Pb smelter and found peak Pb levels corresponded to highest smelter emissions. They also related peak Mn and Ca levels to changes in soil chemistry caused by acid deposition. Lead contaminants in polluted air from leaded gasoline have been traced in trees from Sao Paulo State, where a reduction in Pb levels was observed in the years after it was no longer permitted for use in gasoline (de Vives *et al.*, 2006). Yu *et al.* (2007) observed an overall declining trend in elemental concentrations for most trace metals analysed (including Pb, Sn, Ba, Cu, Cd) in mangrove trees in Southern China which correlated with ring width indicating this general decline as a growth related trend. In most cases however, these declining elemental profiles were interrupted with several large peaks in concentration which was reported to coincide with local environmental events such sediment stirring by typhoons or localised pollution.

Others have used mineral element dendrochemistry to investigate environmental events, Pearson *et al.* (2005) investigated the use of tree-ring chemistry (10 elements) to date past

volcanic eruptions using Scots pine trees from Turkey. Pearson *et al.* (2009) followed this up when they analysed the elemental content of Juniper trees to attempt to date the eruption of the Thera volcano around 3600 years ago. Monticelli *et al.* (2009) tested the reliability and potential of using metals as an alternative environmental proxy by comparing the concentration profiles for Zn, Cd, Cu, Pb and U of tree rings with profiles obtained from lake sediments, in northern Italy finding significant correlations between the two archives for Zn, Cd and Cu.

The majority of the work has focussed on using calendar dated temperate trees with annual rings which allows the date of elemental 'events' to be established and compared to other records. Although the seasonal nature of some metals in trees has been observed (Hagemeyer *et al.*, 1992, Hagemeyer and Schäfer, 1995, Martin *et al.*, 2001, St George *et al.*, 2006), this was not the main focus the investigations until Poussart *et al.* (2006). Since it is known that some elements play a central role in tree growth, such as the physiological roles that calcium plays in wood formation and structure, it is surprising that so little work has been carried out in exploring this seasonal relationships.

1.4.7. Mineral Elements in Tropical Trees

Although many studies have looked at mineral elements in temperate trees, there has been little work undertaken on tropical trees. One study assessed the use of metal levels in relation to pollution, and another group applied the analysis of mineral elements to dating tropical trees.

Mihaljevic *et al.* (2011) measured the levels of Co, Cu, Mn and Pb in several young tropical pine species in Zambia which contained annual rings, to study their relationship to pollution sources. Trees from four sites were examined; one site near to an ore smelter, two site by a busy roadway, and one remote site. The trees by the smelter were found to be directly affected from the smelter emissions since these trees contained the highest levels of Cu and Co compared with the other sites, the maximum Mn was found in the trees on the roadway, and the Pb levels in all trees were too inconsistent to associate any relationship to a pollution source. This study was of a similar nature to those carried out in pollution studies in

temperate regions (Watmough *et al.*, 1996, Prohaska *et al.*, 1998, Mihaljevič *et al.*, 2008) highlighting the potential for future tropical studies.

Another area of investigation carried out is the potential to use these dendrochemical methods to detect seasonality in ringless tropical trees and applying this as a potential dating method. It has been demonstrated that the elemental fluctuations across tree rings can be seasonally regulated (Hagemeyer *et al.*, 1992, Hagemeyer and Schäfer, 1995, Martin *et al.*, 2001, St George *et al.*, 2006), and also that seasonality can exist in the tropics, resulting in annually resolved rings. Seasonal variation has even been shown in tropical ringless species using stable isotopes (Evans and Schrag, 2004, Poussart *et al.*, 2004, Poussart and Schrag, 2005, Anchukaitis *et al.*, 2008a, Ohashi *et al.*, 2009, Loader *et al.*, 2011). Applying dendrochemistry in regards to metal distributions in tropical trees would be the next logical step for explorative research.

Poussart *et al.* (2006) realised this potential and demonstrated that variations in calcium concentration could be used to date a ringless tropical tree (*Miliusa velutina)* from northern Thailand. They used synchrotron x-ray microanalysis to scan two high resolution replicate lines (~15cm each) to determine the radial concentrations in the wood for Ca, Cu, Fe, K, Mn, Ni and Zn, however only results for Ca were reported in the paper. The resultant calcium records showed distinct cycles from the cambium to the pith across the wood. In a previous study (see Section 1.4.3), Poussart and Schrag (2005) analysed the $\delta^{18}O$ of the same tree along with nine ^{14}C dates. The cyclicity of the $\delta^{18}O$ allowed an age-growth model to be developed which on comparison agreed within ≤3 years of the radiocarbon age. For this calcium study Poussart *et al.* (2006) constructed an age model based on the Ca record, using the assumption that each Ca cycle represented a single year's growth. When this record was compared with the radiocarbon estimates, not only was the annual nature of the Ca cycles confirmed, but the record agreed within ≤ 2 years of the radiocarbon age, which was a slight improvement on the age model created from the $\delta^{18}O$ measurements. Furthermore, a correlation was found between maximum Ca intensities with dry season rainfall, showing the potential of dendrochemical studies for palaeoclimate application. This study also highlighted some other interesting features in terms of the radial distribution and mobility of calcium and other elements analysed. They found calcium to be the least mobile of all the analysed elements (Zn, Cu, Fe, K, Mn and Ni) and noted that the calcium distribution showed a sharp increase at the heartwood/sapwood boundary, similar to that discussed earlier (Section 1.4.4.2).

Although data was not shown for the other elements, they reported that Zn also had a cyclic pattern from pith towards cambium. Despite these promising preliminary results, no further work has been published using calcium or any other mineral element as a means of dating tropical trees.

The work of Poussart *et al.* (2006) demonstrated the potential for opening up the tropics to dendrochronological studies. Calcium has been shown in this study to be a promising candidate for future mineral element analysis due to the seasonal nature of its uptake and storage. Traditional dendrochronological methods only yield success in dating tropical trees where rings are distinct and then the overall success rate is low compared to that of temperate regions. Other dendrochemical methods such as stable isotope measurements can be successful in both ringed and ringless trees, however reported successes in ringless species are limited, and the process is expensive with potentially time consuming sample preparation. The ability to date trees is the limiting factor in the tropics. Mineral element dendrochemical techniques, and in particular calcium analysis, may be able to overcome these issues, providing a method of dating ringless species as well as allowing the potential for climate or ecological studies in these crucial areas.

1.5. Summary

The nature of tree growth in the tropics is much more complicated than that in temperate regions resulting in limited dating success by conventional dendrochronological methods. Growth can be continuous throughout the year (Worbes, 1999, 2002) resulting in either trees with indistinct incremental bands that may not be annual in nature or trees that have no ring-like structures at all. Without the presence of annually formed rings, dating tropical trees by traditional dendrochronological methods is almost impossible, and without robust dating, ecological or climatological analyses are not really possible. As the tropics play a critical role in modulating climate, it is important that other methods are sought to open them up to environmental research.

Quantifying growth rates by other methods such as cambial wounding and dendrometer bands provide an insight into growth patterns but only over short periods of analysis, which may be limited to funding or site access restrictions, or by the tree 'out-growing' the bands. These

methods may be suited to pilot studies as they provide a cheap and easy way of accurately monitoring tree growth. Stable isotope analysis has also proved successful in demonstrating seasonality within tropical trees resulting in the possibly of an alternative dating method, however this approach has the disadvantage of requiring very high resolution sampling to be used which can be an expensive option that does not guarantee success.

Novel methods of tree-ring analysis are required to overcome these dating issues in the tropics. If tree growth could be measured in the tropics, this would open the field for chronology development, climate reconstructions and ecological studies. Mineral element analysis through dendrochemical methods could provide an alternative to traditional dendrochronology. Such an approach may not only assist with the dating problems of the tropics but some elemental profiles may act as a historical record of pollution, soil chemistry and other local, regional or global events that can affect tree chemistry.

Previous studies have indicated calcium is an ideal candidate for such studies due to its responsibilities in cell structure and wood formation. The seasonal nature of the calcium stores in trees provides a potentially excellent opportunity to exploit this as a dating method in the tropics and will be the main focus of this thesis.

1.5.1. Thesis Structure

This thesis is structured into a series of chapters based around three overall themes as laid out in the objectives.

Chapter 1: Introduction and Literature Review

This chapter provides a general introduction outlining the project rationale as well as an introduction to dendrochemistry, and its related applications with respect to both temperate and tropical regions.

Chapter 2: Calcium Tracers and the Dating of Scots Pine

This chapter outlines the development of a calcium based dating method. The nature of the calcium distributions and fluctuations in trees through the year are assessed using a well-dated temperate species using LA-ICP-MS. A statistical empirical approach to dating the trees by the identification of seasonal (annual) cycles in the calcium record is tested.

Chapter 3: Calcium Tracers and the Dating of Tropical trees

The Laser Ablation-ICP-MS method for measuring calcium in trees developed in Chapter 2 is applied and tested on a tropical species with indistinct growth rings. The statistical approach for identification of annual increments is optimised to radiocarbon dates for a single tree. Validation of the optimal method is made through an independent test on a second tree.

Chapter 4: Are stable isotopes the answer to dating tropical trees?

Using the same tropical tree species examined in Chapter 3, this chapter explores whether stable isotopes could be used to date the wood. Exploration of the climatic controls on isotopic variability is also made.

Chapter 5: Discussion and Conclusions

Summary and overall discussion of the previous three chapters. Conclusions and recommendations for future work

1.5.2. Aims and Objectives

- Develop a LA-ICP-MS method to assess the nature of calcium fluctuations within a temperate species with well-defined and datable annual rings.
- Develop a statistical approach to identify annual cycles within the calcium data measured form a temperature species and test how well such data could be used to date the wood.
- Apply and tune (using radiocarbon dating) this method to a tropical species, lacking distinct annual tree rings, to obtain age estimates from the calcium fluctuations.
- Validate the method with further radiocarbon dates on an independent sample.
- Measure oxygen and carbon isotopes to ascertain whether these data could be used to date the wood as well as investigate climatic controls.

Chapter 2: Calcium Tracers and the Dating of Scots Pine

2.1. Introduction

Trees can live for hundreds of years, taking in and using the available nutrients, water and carbon dioxide from their surroundings in order to survive. Although tree ring studies usually focus on so-called standard parameters such a ring-width or density, many studies have shown elemental seasonal patterns across tree rings that could prove useful for environmental research (Hagemeyer and Schäfer, 1995, Martin *et al.*, 2001, Poussart *et al.*, 2006, St George *et al.*, 2006). The detection of a seasonal signal can, however, depend on the sampling strategy and type of analytical technique used as well as the tree species. For most trees, growth is seasonal. Even most tropical regions experience a period of unfavourable growing conditions for trees resulting in cambial dormancy (Worbes, 1995), this does not always result in the formation of distinct annual tree rings (Section 1.3). Without distinct annual growth rings, dating trees by traditional dendrochronological methods is not possible. Therefore an alternative approaches are required to overcome these dating problems in the tropics.

In tropical regions, where traditional dendrochronological methods have limited applicability, other methods for establishing dating controls of trees have been sought resulting in some, though still limited, success using dendrometer bands, cambial wounding and stable isotope analysis (Section 1.3). The potential for using trace metals to establish dating control was highlighted by Poussart *et al.* (2006) when they demonstrated the existence of annual cyclic seasonal fluctuations in the calcium record from a ringless tropical species (*Miliusa velutina*). However this concept has not been further developed (or at least published).

In this thesis, a method for dating tropical trees is hypothesised and investigated using trace element analysis to measure the seasonal cycles of calcium stores within trees. This approach is first developed and tested in this chapter using well dated temperate trees as proof of concept by the continuous measurement of calcium profiles along the tree's radii. Previous studies have shown laser ablation-inductively coupled plasma-mass spectrometry (LA-ICP-MS) to be a suitable method for analysis, however continuous measurements across rings does not appear to have been previously reported. The development of this continuous method is imperative if the technique is to be successfully applied to ringless tropical species.

2.1.1. Mineral Element Measurement

There are a number of analytical methods available, many of which have been used to analyse trace elements in tree rings. Penninckx *et al.* (1999, 2001) and Hristovski and Melovski (2010) used Atomic Absorption Spectrometry (AAS) to investigate radial distribution patterns of various metals in European beech (Section 1.4.4.2). Groups of 5-10 rings were measured, which allowed the detection of general elemental trends across the tree, but their approach was not capable of determining any seasonal trends. Many others have used Inductively Coupled Plasma-Mass Spectrometry (ICP-MS) (Padilla and Anderson, 2002, Pearson *et al.*, 2005, Watt *et al.*, 2007, Kirchner *et al.*, 2008, Liu *et al.*, 2009, 2009) which allows the analysis of individual rings. However, due to the sample preparation methods it may be difficult to detect inter-annual seasonal signals. Both AAS and ICP-MS require a destructive pre-treatment of the wood samples such as acid digestion or ashing before analysis. There are non-destructive methods available such as X-ray based analysis, however, a bench-top X-ray system can generally only measure elemental concentrations of larger areas such as groups of rings. Synchrotron x-ray analysis provides an attractive non-destructive analytical method providing good spatial resolution (~1μm) and low detection limits with minimal sample preparation. Martin *et al.* (2001) used synchrotron radiation induced X-ray emission and secondary ion mass spectrometry (SIMS) to examine the distribution and seasonal variations of metals in the growth rings of red pine (Section 1.4.4.2) and Poussart *et al.* (2006) applied the same method to establish a seasonal pattern in a ringless tropical species (Section 1.4.7). Martin *et al.* (2003) applied a slightly different method of analysis, synchrotron induced x-ray fluorescence (SXFRA), to investigate element mobility within black spruce trees. Although both of these synchrotron x-ray analysis techniques provide good resolution and detection limits, access to such instruments is limited, with the UK currently having only one synchrotron facility, (Diamond Light Source) with access via a competitive application process.

Another increasingly popular method of analysis in dendrochemistry is laser ablation-inductively coupled plasma-mass spectrometry (LA-ICP-MS). Such systems are usually bench top systems which are capable of multi-element analysis providing high sensitivity measurements with high sample throughput. Most laser systems are equipped with a mounted camera; therefore the operator can set up ablation points with ease and accuracy. The first use of LA-ICP-MS for dendrochemical analysis was by Hoffman *et al.* (1994) who investigated the possibilities of using this method by analysing an array of metals in single pine

and poplar trees from Germany (Leipzig and Berlin respectively). For each ring, they analysed 17 metals from a total of 12 equally sized ablated craters and results indicated the presence of seasonal cycles for some elements. Other investigations quickly followed with many focussing on using this method to assess elemental variability (Section 1.4.4.2) over the life of a tree, (Hoffmann *et al.*, 1996, Prohaska *et al.*, 1998) external environmental factors (Section 1.4.6) such as pollution (Garbe-Schonberg *et al.*, 1997, Watmough, 1997, 1999, St George *et al.*, 2006, Mihaljevič *et al.*, 2008, Monticelli *et al.*, 2009, 2011) or as an historical record of past volcanic activity (Pearson *et al.*, 2005, Watt *et al.*, 2007, 2009). LA-ICP-MS systems provide an almost non-destructive method for producing rapid, high resolution multi-element analysis of tree rings. This process requires minimal sample preparation and the amount of sample actually used destroyed by the ablation process is very small, therefore the prepared tree laths are available for further analysis after the ablation process is completed.

As with other types of tree-ring based studies, most mineral element analysis in this field has been in temperate areas, where trees have well defined, and dated, annual rings. Dendrochronology is such a well-established method for dating trees and reconstructing past climates, that there has been little need for consideration on using dendrochemical methods in tree rings as proxy records (Monticelli *et al.*, 2009) or for dating, despite the acknowledgment of the seasonal nature of elemental uptake and storage (Hagemeyer and Schäfer, 1995, Martin *et al.*, 2001, Poussart *et al.*, 2006).

The focus of this study was to build upon the results of Poussart *et al.* (2006) as a basis for developing a calcium based method for dating tropical trees using a LA-ICP-MS. Most of the previous dendrochemical studies which used LA-ICP-MS to measure metals aimed to assess either the suitability of the method itself (Hoffmann *et al.*, 1994, Watmough *et al.*, 1996, 1998, 2002), the mobility of particular metals within the wood (Hoffmann *et al.*, 1996, Prohaska *et al.*, 1998) or studying environmental influences or events (Garbe-Schonberg *et al.*, 1997, Padilla and Anderson, 2002, Pearson *et al.*, 2005, Monticelli *et al.*, 2009). However, none of the above mentioned studies set out to specifically assess the seasonal trends (see Section 1.4.5.2) and not all measured calcium in their analyses. In addition, most previous work using LA-ICP-MS have analysed individual spots rather than undertaking continuous measurement across whole rings.

The main aim of this PhD was to develop a method using LA-ICP-MS to detect a seasonal signal from the calcium fluctuations along a tree lath which could be applied to dating ringless

tropical trees. This chapter focuses on the development of this method using a clearly annual ringed temperate tree species, *Pinus sylvestris* L. (Scots pine). The seasonal nature of the calcium in well-defined annual rings was assessed, and a method developed to produce anindependant age estimate using the calcium output which could then be compared to actual ring width based cross-dated ages. In the next chapter, this method is applied to tropical trees.

The objectives were to:

- Determine that calcium fluctuations could be detected using LA-ICP-MS in a species with well-defined annual rings and that any resultant Ca pattern was annual in nature
- Develop a statistical method for calculating objective age/ring count estimates
- Test this method of dating using Scots pine samples of known age

2.2. Study Area and Sample Description

Scot pine (*Pinus sylvestris* L.) is a coniferous species, native to Scotland but is well established throughout Europe and Asia. It contains regular, well defined annual growth rings featuring clear areas of earlywood and latewood cells making it a good candidate for assessing seasonal growth. This species has been the subject of many traditional dendrochronological studies (Eronen *et al.*, 2002, Grudd *et al.*, 2002, Helama *et al.*, 2002, 2008, Young *et al.*, 2011) and stable isotope based studies (Gagen *et al.*, 2007, 2011, Young *et al.*, 2012), with many based in Scotland (Fish *et al.*, 2010, Wilson *et al.*, 2012, Loader *et al.*, 2013),. Previous dendrochemical studies have also used Scots Pine (Garbe-Schonberg *et al.*, 1997, Parn, 2001, Watmough and Hutchinson, 2002, Pearson *et al.*, 2005) however none of these were based in Scotland.

Loch Garten is a large fresh water loch which is situated within Abernethy Forest in the Cairngorms National Park, Scottish Highlands (Figure 2-1). Abernethy Forest is a remnant of the Great Caledonian Forest, and is the largest native Scots pinewood in Great Britain (Visit Scotland, 2012). Today the forest it is largely managed in an attempt to restructure the region to resemble the 'Old Caledonian Forest'. Pines trees of over 200 years old can be found here (mostly at higher >400m elevations), and palynological evidence suggests that the pine woodland has been continuous in this region since this species first colonised the region 8-

9000 years ago (Bennett, 1984). Discs were collected from Scots pine trees that were felled in 1999 during the building of the RSPB Osprey centre which is located at the north-west end of Loch Garten (Figure 2-1 (b)). Although there are many more pine samples within the broader Scottish Pine Project (http://www.st-andrews.ac.uk/~rjsw/ScottishPine/), the Loch Garten site represents the only location in Scotland where whole tree disks have been collected by St. Andrews Tree-Ring Laboratory and collaborators, therefore allowing abundant material for analysis.

(a) Loch Garten is located within the north of the Cairngorms National Park, in the Scottish highlands.

(b) Scots pine samples were collected in the at the north-east end of Loch Garten (57°14'40.85"N, 3°41'42.23"W)

Figure 2-1: Location where Scots Pine samples originated. Approximate location is highlighted with red square.. Images downloaded from Google Earth. (Imagery: Getmapping plc, Map data: Google.)

2.3. Materials and Methods

2.3.1. Sample Preparation

In this study, a total of nine Scots pine tree laths were analysed, which included five trees with a single radius and two trees with two radii. For each tree, thin rectangular sections were cut from the tree sections using a band saw, producing laths that were approximately 1cm wide x 0.5cm thick. It was noted when cutting that some of the trees contained high resin content. To minimise any possibe interference, steps were taken to extract this excess resin using an acetone extraction technique. Each lath was securely attached to a rod to prevent bending or

twisting during the extraction process, and then submerged into a sealed cylinder of acetone for a maximum of 7 days. After this time, the laths were then removed and air dried.

Due to size limitations of the laser ablation system sample chamber, the laths had to be split into smaller sections of approximately 4cm in length. Each lath was initially sanded using a 120 grade abrasive paper to produce a flat surface to allow the rings to be seen clearly, and then cut, using a clean blade, into smaller sections by marking a groove through the required area before snapping the lath along this line. Where possible the laths were cut in such a way as to allow at least one ring to be overlapped on either side of the cut (Figure 2-2) which was crucial to allow the accurate linking of individual lath datasets after measurement.

Figure 2-2: Example of a sectioned rectangular lath for laser ablation analysis. Each section has been cut at an angle to allow rings to be overlapped on adjacent sections.

Laser ablation requires samples to have as flat and smooth a surface as possible in order for the laser to be focussed onto the sample surface. Producing such a surface was also necessary to visualise the rings for ring width measurements, as well as visualisation of the ring structures through the camera and software attached to the laser system. Each sectioned lath was sanded using progressively finer grade sand paper up to maximum of 2500, producing a smooth flat surface for laser ablation. The sanding process produces fine wood dust which could be a source of contamination. Sawdust may travel across rings as the sample is sanded and into the resin ducts within the wood. To minimise this contamination, excess wood dust was removed from each lath section using compressed air.

Before analytical measurements, each lath section was observed under a light microscope to determine the track to follow during the laser ablation. A light line was made using a sterile scalpel blade across each section as a visual guide to assist when the setting up scans in the laser software. These lines aimed to cover as many rings as possible per section, but at the same time ensure that the growth direction of the wood was followed.

2.3.2. LA-ICP-MS

The elemental analysis of the wood samples was carried out using a NewWave Research 213 Laser Ablation System which features a high performance Nd:YAG deep UV (213nm) laser,

coupled to a Thermo X-Series 2 Quadrupole Inductively Coupled Plasma Mass Spectrometer (ICP-MS) located in the Department of Earth and Environmental Sciences, University of St Andrews. Figure 2-3 shows a representation of such a system. For analysis, a sample is secured inside the laser ablation cell and ablated material is transported via the helium carrier gas to the ICP-MS where it is directed to the plasma. The sample is atomised and ionised within the plasma then passed through the sampler and skimmer cones into the ion lenses where only the positive ions are selected (neutral and negative species are rejected). While positively charged ions are steered into the quadrupole mass filter, photons which were generated by the intense light of the plasma are lost. As the ion beam passes through the quadrupole mass analyser, the ions are filtered by specific mass-to-charge ratio, allowing the required ions to be accelerated through the quadrupole to the detector. The voltages of the quadrupole rods are very quickly changed to allow other desired ions to pass to the detector in a sequential manner.

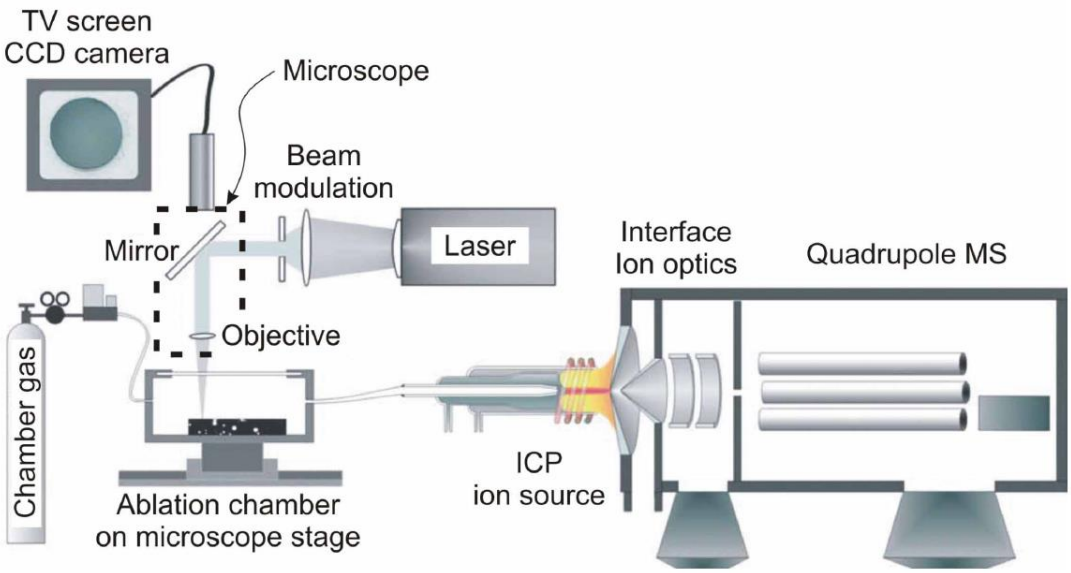

Figure 2-3: Illustration representing the typical configuration of a Laser Ablation-ICP-MS system. Image from Guillong (2007)

It was necessary to perform instrument set up and tuning procedures before analysis. Daily auto-tuning procedures were carried out to optimise the ion path, and further tuning procedures were performed if instrumental maintenance had been carried out between the last auto-tune. The tuning procedures are specific to the ICP-MS system and were therefore carried out following the procedures used for nebuliser sampling of liquids. Parameters that were adjusted included the nebuliser gas flow, torch position and lens voltage. After tuning,

the laser system was reconnected to the ICP-MS, the plasma re-lit, and left to settle for 30 minutes prior to any measurements were being carried out.

2.3.3. Method Development

2.3.3.1. Determination of the Calcium Signal

The application of LA-ICP-MS to perform continuous measurements across tree rings does not appear to have been previously reported. It was therefore necessary to develop a method for this analysis and also for the interpretation of the results. The first stage in the method development was to ensure a calcium signal could be detected successfully using the LA-ICP-MS system, and to determine whether a seasonal cycle could be identified from continuous calcium measurements.

A segment of untreated Scots pine lath was sanded as described in section 2.3.1, and mounted in the laser chamber. A line of approximately 1cm in length, crossing 4 rings, was marked out using the NewWave laser software and set up with the parameters detailed in Table 2-1. These initial parameters were chosen on advice of the laboratory manager, based on previous laser ablation experiments.

Before measurement, a pre-ablation pass was carried out in order to remove any surface contamination from the sample preparation procedure. After ablation, the raw data (measured in counts per second) was exported from the PlasmaLab software into Microsoft Excel where the pre-ablation portion of the data was removed. The ^{44}Ca counts were plotted against distance (Figure 2-4) which showed peaks in the data which appeared to be consistent with ring boundaries. A duplicate line was measured using the same settings. Both lines, along with the mean, are shown in Figure 2-4. Comparison of line 1 and 2 shows that each contains large distinct peaks in almost identical physical positions along the lath, although the overall intensity of the ^{44}Ca counts were lower in line 2. Line 2 was measured two hours later than line 1 which may be partly accountable for this difference.

Table 2-1: Operating parameters for the LA-ICP-MS system used during initial tests.

LA-ICP-MS Operating Parameters	
Carrier gas flow (He)	0.76 L/min
Laser Power	60%
Pulse frequency	20 Hz
Laser warm-up time	10s
Pre-ablation	70µm/s transit, 40% power
Spot diameter	80µm
Laser transit time	5µm/s

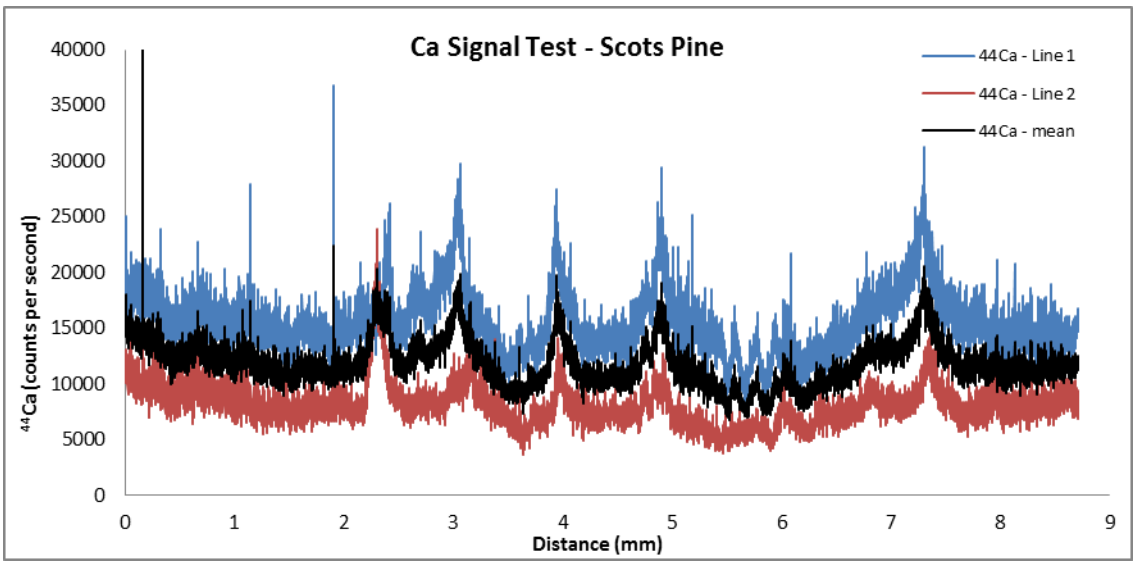

Figure 2-4: Plot of the raw data obtained from the continuous measurement of ^{44}Ca by LA-ICP-MS over a 10mm line along the radii of a Scots Pine lath. Two replicate lines were measured (red and blue) in the direction of growth (pith towards bark), with the mean of these represented by the black line.

The process of continuous laser ablation resulted in a visible 'groove' in the wood along the line which was ablated. A scanned image of the wood section was obtained using a flatbed scanner which allowed a visual comparison of the resultant mean calcium plot with the ablated lines (Figure 2-5). This visual comparison illustrated that the peaks coincided with ring boundaries, with the exception of one anomalous peak which occurred in the first full ring (highlighted in Figure 2-5). The cause of this extra peak was not determined at this stage, however this initial test indicated that it may be possible to detect a seasonal calcium signal

from this tree species. This experiment was repeated several times (results not shown here) which produced similar calcium patterns over the measured rings.

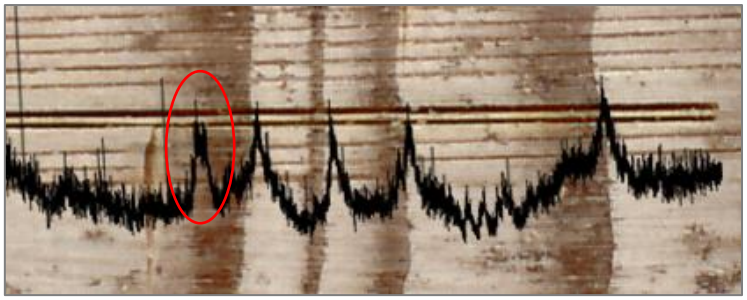

Figure 2-5: Mean ^{44}Ca plot from Figure 2-4 overlaid onto scanned image of the Scots pine wood lath. The two lines measured are represented by the two dark burned lines in the wood. The highlighted peak does not correspond with a ring boundary.

The data obtained above (Figure 2-4) was obtained using a very slow transit speed of 5µm/second which generated many data values for a small area of measurement. This also resulted in noisy data due to the amount of data points produced. To address this, similar experiments were set up where the transit time was increased and with more replicated lines. Figure 2-6 shows the calcium signal (mean and median values) obtained from the analysis of three sets of rings using the same operating parameters as outlined in Table 2-1, with the exception of an increased transit speed of 50µm/second. Each set consisted of 10 equally spaced ablated lines to assess the reproducibility of the calcium signal. Set A incorporated 3 annual rings, and sets B and C incorporated 2 annual rings each. All were approximately 5mm in length.

Figure 2-6 shows the plots overlaid onto scanned images of the equivalent ablated areas of the lath. The ring boundaries appeared to coincide with a change in calcium signal, similar to that observed in Figure 2-5. A sharp increase in ^{44}Ca counts occurs at the ring boundary where the earlywood begin, with "troughs" in the signal occurring in the latewood. Each set however contained at least one additional calcium peak not coincide with a ring boundary. Examination of the individual plots for each of 10 lines per set (data not shown) highlighted that these extra peaks were usually the result of one very large spike present in only one of replicate lines. This often single spike was large enough to influence the mean values even when there were as many as 10 lines averaged. Calculating the median values for each set reduced the occurrence of these extra peaks as shown by the red lines in Figure 2-6, with the exception of the

additional peak in set C at approximately 2.2mm. In this case several of the lines which were adjacent to each other produced a peak at this point, which therefore influenced the median value as well as the mean. For the rest of this thesis, the median values of multiple tracks would be used to minimise "peak" biases.

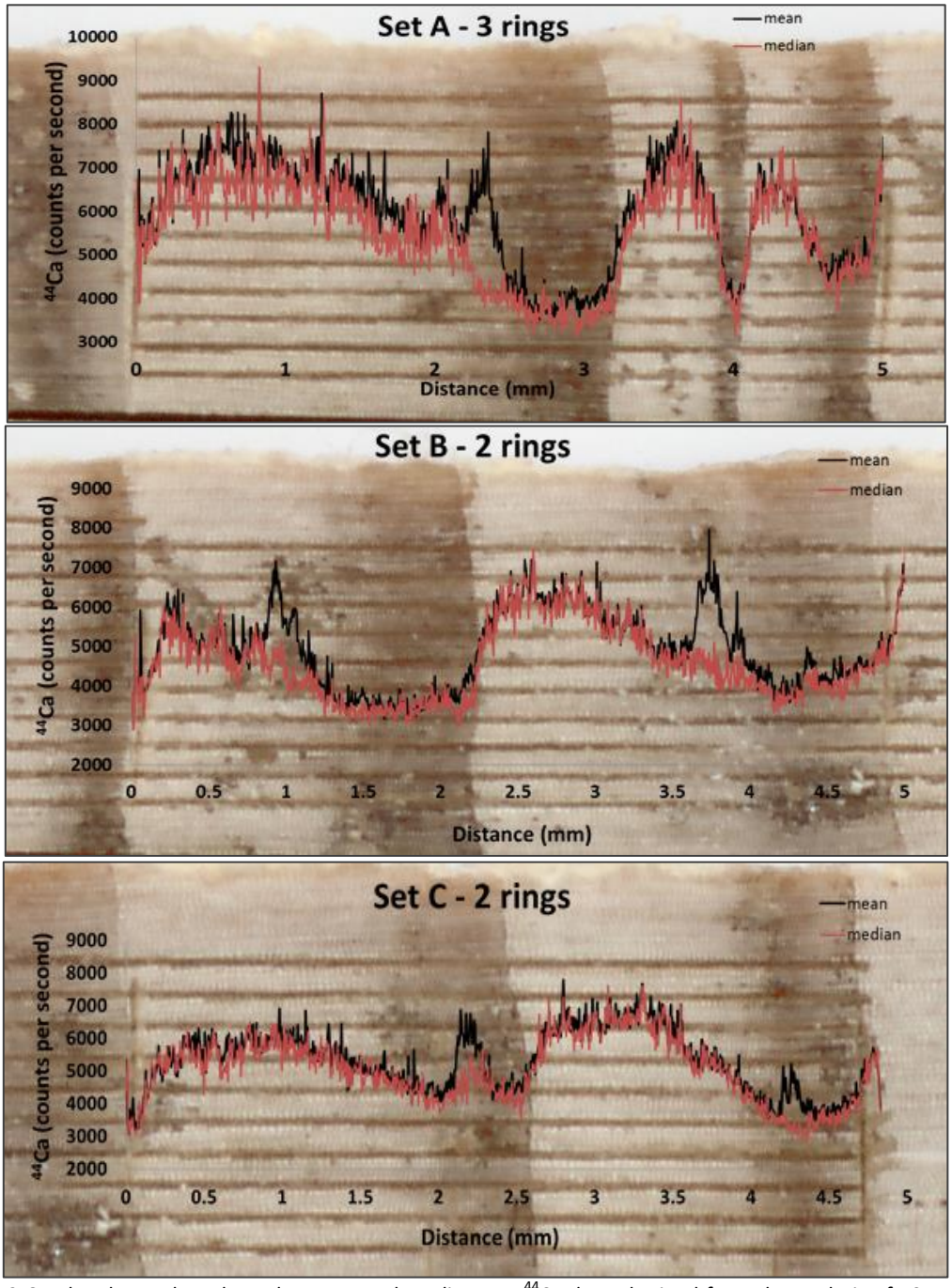

Figure 2-6: The above plots show the mean and median raw ^{44}Ca data obtained from the analysis of 10 replicate lines for 3 separate sets of rings (A-C). Each plot has been superimposed onto a scanned image of the corresponding area from which the measurements were obtained.

Increasing the transit speed of the laser reduced the noise in the data as predicted. This also resulted in large drop in the measured average calcium counts from approximately 20000 (Figure 2-4) to around 5000 (Figure 2-6). At slower transit speeds (and larger spot sizes), more material is ablated creating deeper and potentially wider tracks in the wood. Although the average counts were around 5000, some latewood regions had as few as 2500 counts which was only slightly higher than background levels. To account for the reduction in signal intensity using higher transit speeds, the ICP-MS interface cone was changed from the Xt (high tolerance) interface to the Xs (high sensitivity) interface. The Xs interface offers higher levels of sensitivity than the Xt interface (Thermo Electron Corporation, 2005).

Earlywood and Latewood Signal

The three median time-series shown in Figure 2-6 show that a minimum calcium signal is found in the latewood (LW) region of each ring and the maximum calcium occurring in the earlywood (EW) regions. This was confirmed by ablating areas of earlywood and latewood separately. Three lines were ablated in the EW and three in the LW, with each line between 6-9mm in length (Figure 2-7). The results for each line are shown in Figure 2-8. There is a distinct difference in signal intensity between the EW and LW, with the EW being consistently higher, as in the tests above. The EW signal is also less variable than that of the LW, which may be influenced due to the presence of resin ducts in latewood.

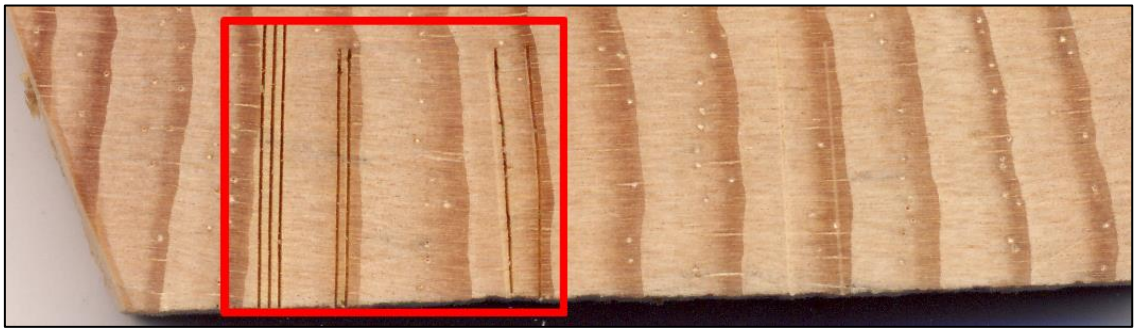

Figure 2-7: Section of Scots pine lath showing the areas measured for the EW and LW tests (highlighted by the red box).

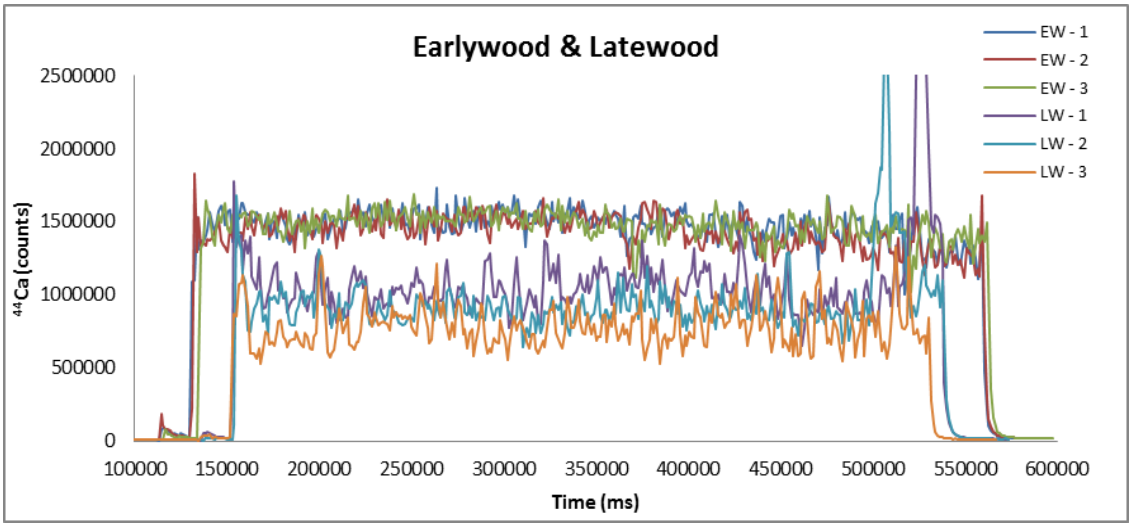

Figure 2-8: Plot showing the difference in counts between the earlywood and latewood regions as measured on a Scots pine sample.

Additional adjustments were made to the final operating parameters for analysis to optimise the calcium signal. The transit speed was reduced from 50µm/second to 20µm/second and the spot size was increased slightly to 100µm as this appeared to optimise the signal. The speed was reduced to account for narrower rings where less wood is present. A slightly slower speed ensured that enough material was ablated to produce the seasonal signal, while minimising extraneous noise generated from the vast amount of additional data point generated at lower speeds.

2.3.3.2. Standard Reference Materials

LA-ICP-MS has not been widely used for wood analysis, therefore there are currently no available certified solid matrix-matched standards available. Other certified standards are available for use with a laser ablation system such as the various NIST standard glass reference materials (SRM), however this was deemed unsuitable due to the differences in construction between the standard and the wood samples. Ideally a standard should be of a similar construction and concentration to the samples analysed so that it abates the material in a similar manner. The use of a standard is required to check the stability of the instrument and allow the output signal (measured in counts) to be converted to concentrations. Other dendrochemical studies using LA-ICP-MS faced the same issues with standards and several

approaches were taken. Some studies created their own standard by doping cellulose powder with a multi-element Standard Reference Material (SRM) (Hoffmann *et al.*, 1994, Hoffmann *et al.*, 1996, Prohaska *et al.*, 1998). Others used a homemade standard from a different tree species (Watmough *et al.*, 1998, St George *et al.*, 2006), and Pearson *et al.* (Pearson *et al.*, 2005) used NIST glass SRM 610 despite the differences in structure.

To assist with the creation of a suitable solid standard, the approximate calcium content of Scots Pine was determined by X-Ray Fluorescence (XRF)[12]. Two 32mm discs, which had been cut from different areas of a Scots pine sample were analysed by XRF to determine approximate calcium content for this species. Results showed that the samples contain approximately 0.05 and 0.07% calcium respectively. The difference in calcium content may be accounted for by the variation in ring size and structure between the 2 discs. XRF is not an ideal method for elemental analysis in tree rings due to the heterogeneous nature of wood; however for the purposes of this study it provided a useful estimate of %Ca for construction of standards.

Cellulose is the main component of wood (Plomion *et al.*, 2001) and was therefore chosen as the main constituent of the standard. A similar method to that employed by Hoffmann *et al.* (1994, 1996) and Prohaska *et al.* (1998) was attempted here to create a suitable standard. In these studies, cellulose powder was doped with a standard element solution, followed by pelleting the power to produce a solid standard. Three cellulose based pellets were prepared by thoroughly mixing cellulose powder with the appropriate amount of calcium source material (Table 2-2) and pressing into a pellet. In addition, a forth pellet was prepared from NIST Standard Reference Material 1575a (Pine Needles). This is a certified powdered standard containing 0.25% calcium (as well as a suite of other elements).

Five lines were marked out and ablated on each of the four standards using the finalised settings (Table 2-3). All analyses were completed in one sitting, after initial auto-tuning of the instrument (Section 2.3.2).

[12] X-ray fluorescence (XRF) is an analytical technique which determines the elemental composition of a material by non-destructive interaction of x-rays with the target material (Sampling Technologies Pty Ltd (2013) What is XRF Technology. Available at: http://www.sampletech.com.au/content/what-xrf-technology [Accessed11 November 2013].)

Table 2-2: Composition of calcium standards.

Standard	Bulk Material	Source of Ca	Final Ca concentration
$CaCO_3$ Pellet	Cellulose	$CaCO_3$	0.1%
CaC_2O_4 Pellet	Cellulose	CaC_2O_4	0.1%
Ca Std. Solution Pellet	Cellulose	Single Standard Element Solution	1%
Pine Needle Pellet	N/A	NIST 1575a SRM	0.25%

Table 2-3: Final operating conditions which were manually set for LA-ICP-MS. Other parameters which are not listed here were determined by the automatic tuning procedures provided in the software.

LA-ICP-MS Operating Parameters	
Carrier gas flow (He)	0.76 L/min
Laser Power	80%
Pulse frequency	20 Hz
Laser warm-up time	10s
Pre-ablation	70µm/s transit, 40% power
Spot diameter	100µm
Laser transit time	20µm/s

Figure 2-9 shows the results for each standard test along with the mean of each the 5 lines. In each case there appears to be quite a lot of variation in calcium counts in each ablated line. The Ca Std Solution Pellet (Figure 2-9 (c)) expressed greatest variance between the 5 lines. The $CaCO_3$ pellet contained several higher peaks in the individual lines which may have been caused by insufficient mixing of the cellulose and $CaCO_3$, or as a result of ablating a compressed powder (uneven burning). As expected, taking the median of the 5 lines produced a smoother signal for all standards.

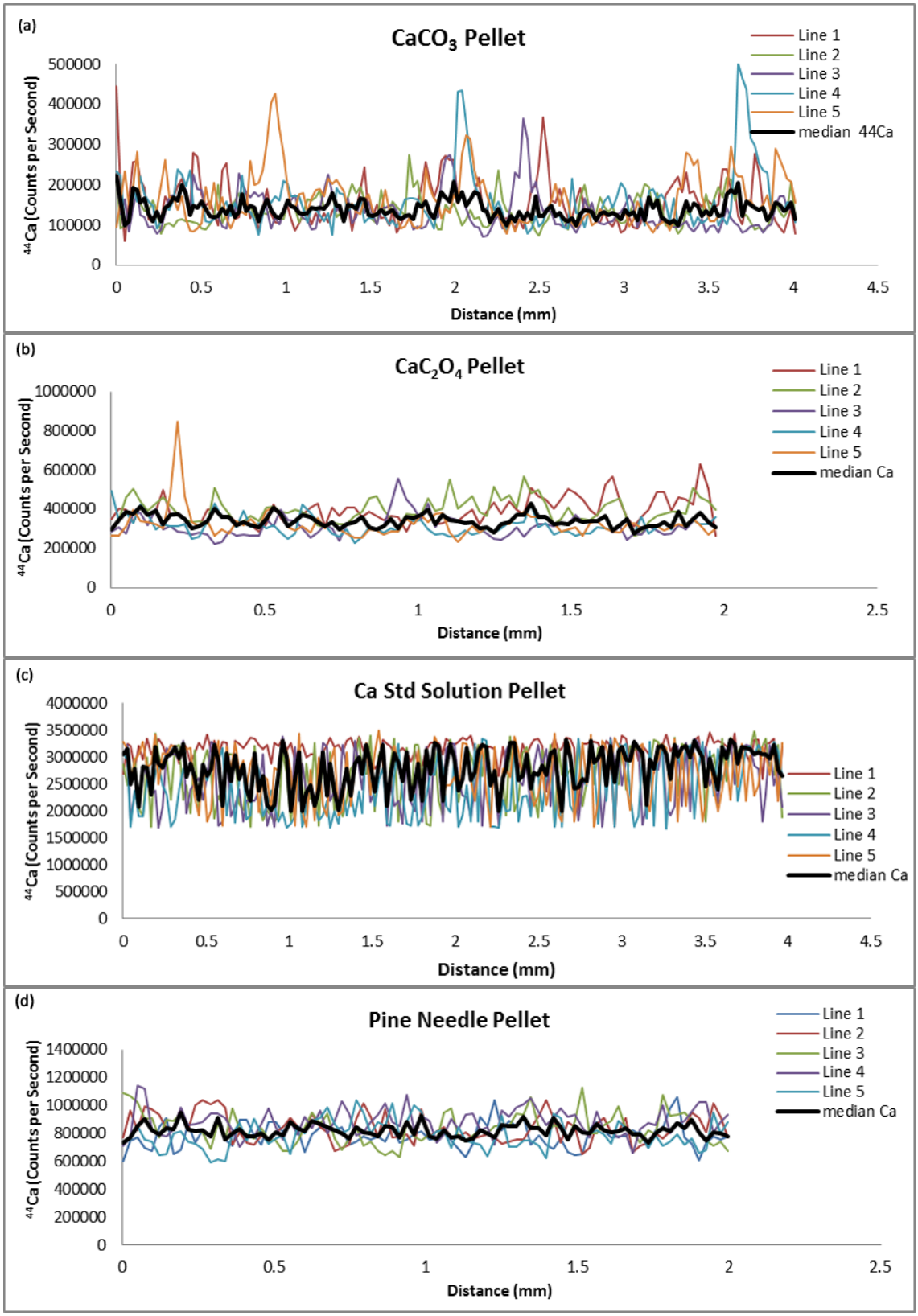

Figure 2-9: Plots showing the 5 ablated lines plus the median of these for each of the four pelleted standards.

The coefficient of variation was calculated (Table 2-4) using the different runs for each set of standards to allow a comparison. The pine needle standard had the lowest variance of approximately 5.6%. Additional tests of these standards produced similar results (data not shown) resulting in the decision to use this standard for further analyses.

Table 2-4: Table shows the coeffient of variation for each standard as calculated from the mean values from the 5 replicated lines.

Standard	Coefficient of Variation (CV)
$CaCO_3$ Pellet	0.1659
CaC_2O_4 Pellet	0.0937
Ca Std. Solution Pellet	0.1320
NIST Pine Needles	0.0564

The prepared standard pellets were also tested in the same run sequence as a sample of Scots pine to assess how the variation in counts compared to that of the seasonal signal in the wood. In all cases, the difference between the variations in counts occurring in the standards was similar to that found in the Scots pine. Figure 2-10 shows an example of the comparison of the calcium signal from a section of Scots pine with the calcium signal from the pine needle pellet. In both cases, the plot represents the mean of 3 replicated lines. The range in actual calcium values between EW and LW is slightly greater than the range (or variance) in the standard NIST pine needle data. Laser ablation of the NIST pine needle pellets did however produce a noisy signal which is most likely caused by the ablation procedure itself, resulting in an inconsistent burn from the pelleted powder. It was therefore not possible to use the pine needle standard (or the cellulose standards) in a quantitative manner to calculate calcium concentrations. This limitation luckily did not affect the main aim of the project which was to develop a statistical method of assigning annual tree-growth to the calcium fluctuations and to establish a robust dating control. It was therefore not necessary to determine the actual concentrations to achieve this goal. The pine needle standard would be used only to monitor the stability of the machine.

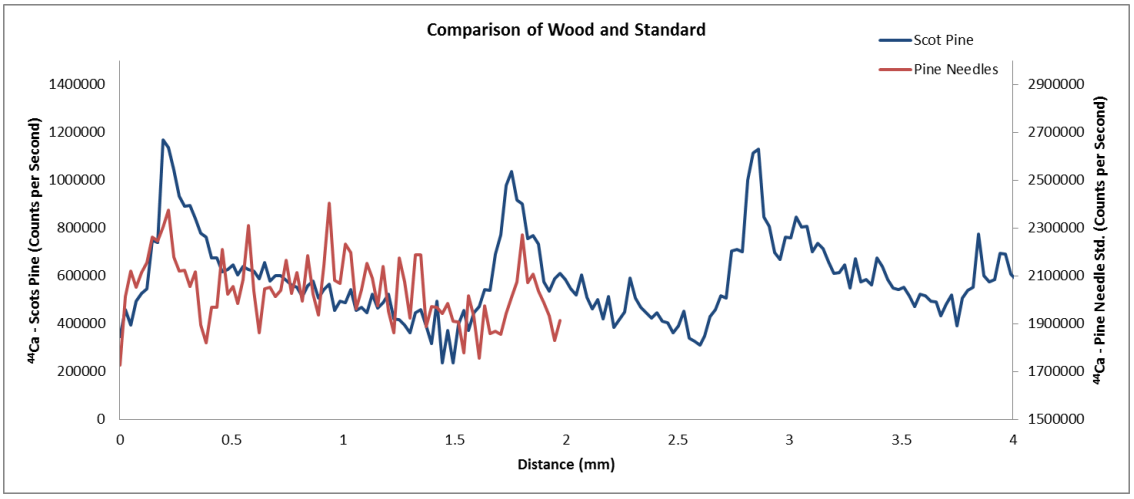

Figure 2-10: Graph shows the calcium output from the median of three ablated lines of Scots pine and the mean of 3 ablated lines of the NIST pine needles standard. Both y-axis scales are plotted with equal intervals for comparison.

2.3.4. Calcium Measurements

2.3.4.1. Laser Ablation Sampling Procedure

The powdered NIST pine needle standard was measured intermittently throughout analyses to monitor the stability of the output measurements. These measurements consisted of short 2mm laser scans usually performed before, after and between the wood scans. Each wood section was levelled and individually secured onto the sample holder along with the NIST pine needle standard pellet. The laser system is fitted with an on board camera which allows the user to view the position of the laser beam. The sample was brought into focus and the starting position selected. The laser ablation software (NewWave Research) allowed the length and shape of the line to be altered therefore each was drawn following the path marked out during sample preparation under the microscope. For each sub section of lath, this line crossed the rings in the direction of pith towards bark, following the trachea – i.e. the direction of growth. Care was taken to make sure that the laser path was not directly on the bladed line ensuring this lightly marked area did not interfere with the ablation process. Each line was pre-ablated before measurement which involved the laser 'lightly' ablating the area of analysis immediately before measurement using a lower laser power and faster transit speed resulting in the top layer being 'skimmed' off. This was done to remove any surface

contaminants and to prepare the surface for analysis. Two replicate lines were drawn at ~0.25mm above and below the original line (Figure 2-11).

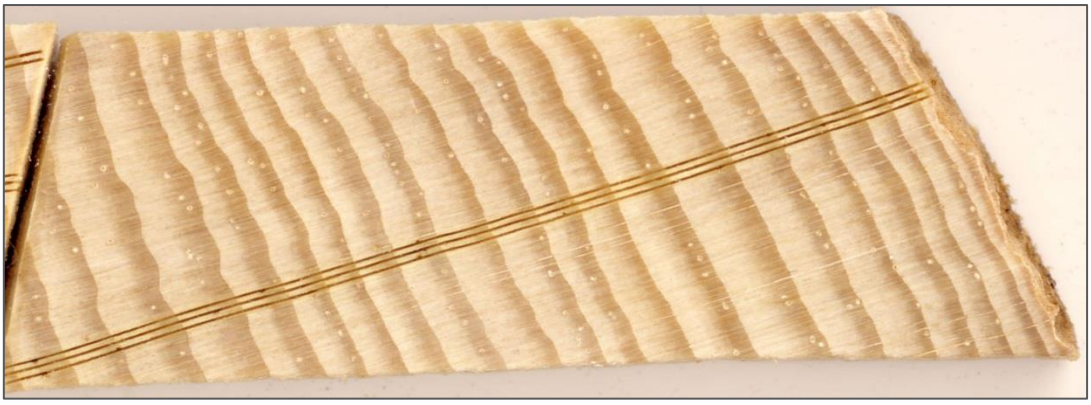

Figure 2-11: Example of a sub-sectioned portion of a Scots pine lath showing the three replicated laser ablated tracks across the length of the section.

The ICP-MS software (PlasmaLab) was used to set up and control the laser ablation run sequence. Before each run, the laser was allocated a 10s warm-up period as well as a short uptake delay where the gas blank[13] was measured. At the end of the run, a 40s wash-out time was added to ensure all of the ablated material was removed before the next run sequence began. Laser sampling was carried out in a continuous manner following the pattern drawn in the software rather than ablating individual spots. Data was collected in peak jumping mode for a several different elements, however only data for ^{44}Ca and ^{13}C was used for this study. The gas blank values were calculated and subtracted for each value. To account for any variations in laser energy output, sample matrix effects, mass differences in ablation or variations in transported material, ^{13}C was used as an internal standard (Durrant, 1999, Austin *et al.*, 2011) which has been used in previously in dendrochemical studies (Hoffmann *et al.*, 1996, Prohaska *et al.*, 1998, Pearson *et al.*, 2005).

An internal standard would ideally be one that behaves in a similar manner to the analyte during the ablation process (Austin *et al.*, 2011) and has a signal intensity which is in the same order of magnitude as the analyte (Hoffmann *et al.*, 1994, Prohaska *et al.*, 1998). De Ridder *et al.* (2002) reported that the use of one internal standard does not take into account the complete drift pattern, however it was decided due to the added complications of ablating a

[13] The gas blank value is acquired when the laser is firing but the shutter is closed. This is recorded directly before the sample analysis begins. Wills, J*., et al.* (2007) Improved time resolved analysis (TRA) Software for LA-ICP-MS. Available at: http://www.analiticaweb.com.br/newsletter/06/AN30114-XSERIES_2_TRA_Analysis.pdf [Accessed 12 October 2013].

soft, heterogeneous material that one only one internal standard should be considered. Most LA-ICP-MS analyses are based around geological material which ablates in a more uniform manner.

Analysis time for the tree lath sections varied depending on the length of the lines to be measured. Generally, ablation time was between 60-90 minutes per line, therefore a single lath section sequence was between 3-5 hours. During one day, several sections could be analysed amounting to as much as 12 hours of ablation time over the course of one day.

2.3.4.2. The Calcium Signal

The raw data (measured in counts per second) was exported into Microsoft Excel. The mean gas blank value was subtracted and the pre-ablation portion of the data was removed. The remaining ^{44}Ca counts were plotted against distance and immediately the cyclic pattern was clear. Occasional large peaks, similar to that found described in Section 2.3.3.1, were observed which did not coincide with a ring boundary (Figure 2-12). When compared with the section of wood which had been ablated, it was noted that these spikes occurred mostly in the latewood section of a ring where the laser had ablated over a resin duct in the wood (Figure 2-13).

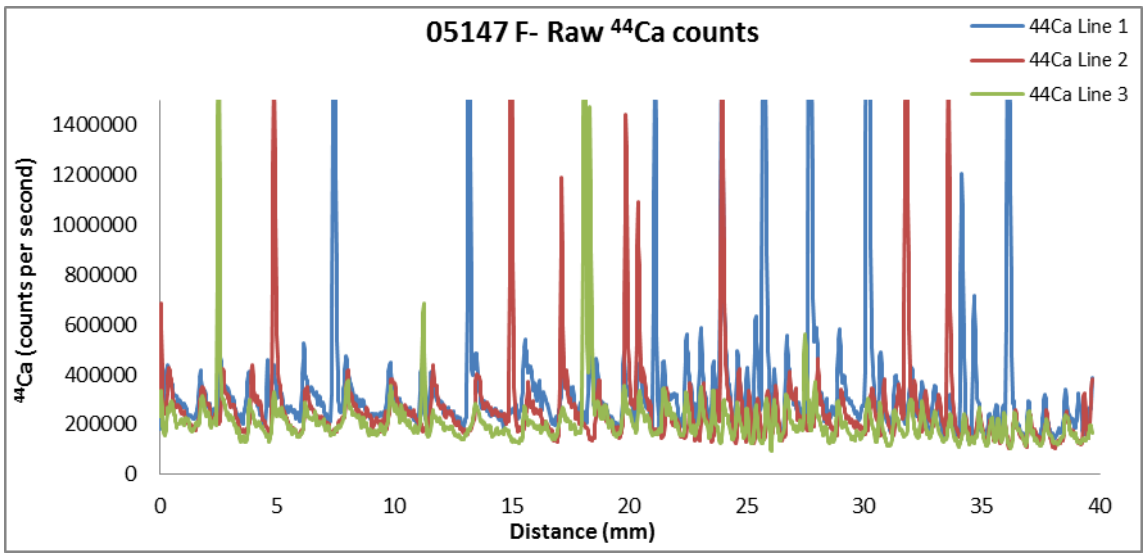

Figure 2-12: Plot of raw data for ^{44}Ca isotope as measured by LA-ICP-MS for one section of tree lath 05147. The Ca intensity is measures in counts per second, and the three lines plotted represent the 3 replicated tracked ablated across the lath section. The graph has been truncated for display purposes.

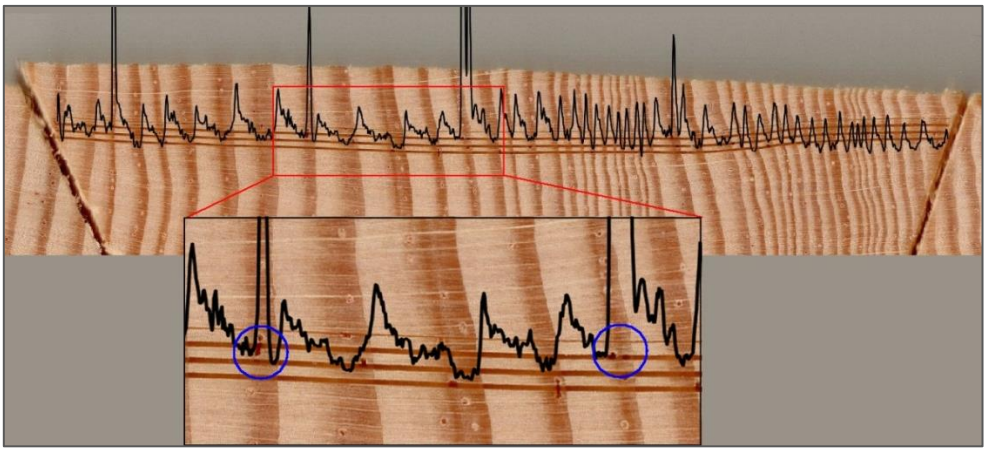

Figure 2-13: A scanned image of a section of analysed tree lath (tree 01547) with the associated raw 44Ca counts plotted and overlaid. The enlarged section highlights (blue circles) two of the resin ducts present on the laser track which corresponds to the calcium spike.

The calcium spikes usually only occurred in one of these three tracks. However the latewood areas contained a reasonable amount of resin ducts therefore duplicate spikes did occur if resin ducts occurred in the equivalent place on another ablated track. Figure 2-13 shows the graph for ^{44}Ca Line 3 for the same lath section as in Figure 2-12 (green line), but overlaid onto a scanned image for that section. The seasonal cycles can be observed very clearly on this figure, and ablated tracks from the laser are visible below the plot. Line 3 represents the top ablated line, and the enlarged area of the figure highlight (blue circles) where two of the resin ducts are present on the ablated track coinciding with the large calcium spikes.

During the initial testing phases, it was noted that the use of the median of the 3 values for each distance unit provided a better measure of the data than the mean (Figure 2-6). This frequency of the calcium spikes in the raw data confirmed the need to move away from using the mean (Figure 2-14). The use of the median to minimise the influence of the calcium spikes was in the main beneficial as it was unusual to find resin ducts in more than one of the ablated lines. In areas where resin ducts did occur in the same area on more than one line, taking the median values did not remove the calcium spikes. The example plots in Figure 2-14 shows the mean and median values of three replicate tracks for one lath section. Calculating the mean values in this case resulted in the appearance of 19 calcium spikes in the dataset, in comparison to only 2 spikes when the median values were calculated. It is clear therefore that the use of the median vastly reduces the influence these spikes will have on further analyses, however does not completely eradicate the problem.

Another possible way to discount the calcium spikes would be to use a trimmed or truncated mean. This would be implemented by excluding a proportion of the data (e.g. upper and lower 10%) and taking the mean value of the remaining portion. With only three replicate line however, this was not an option. Ablating more replicated tracks would help overcome this problem and will be considered for future analyses.

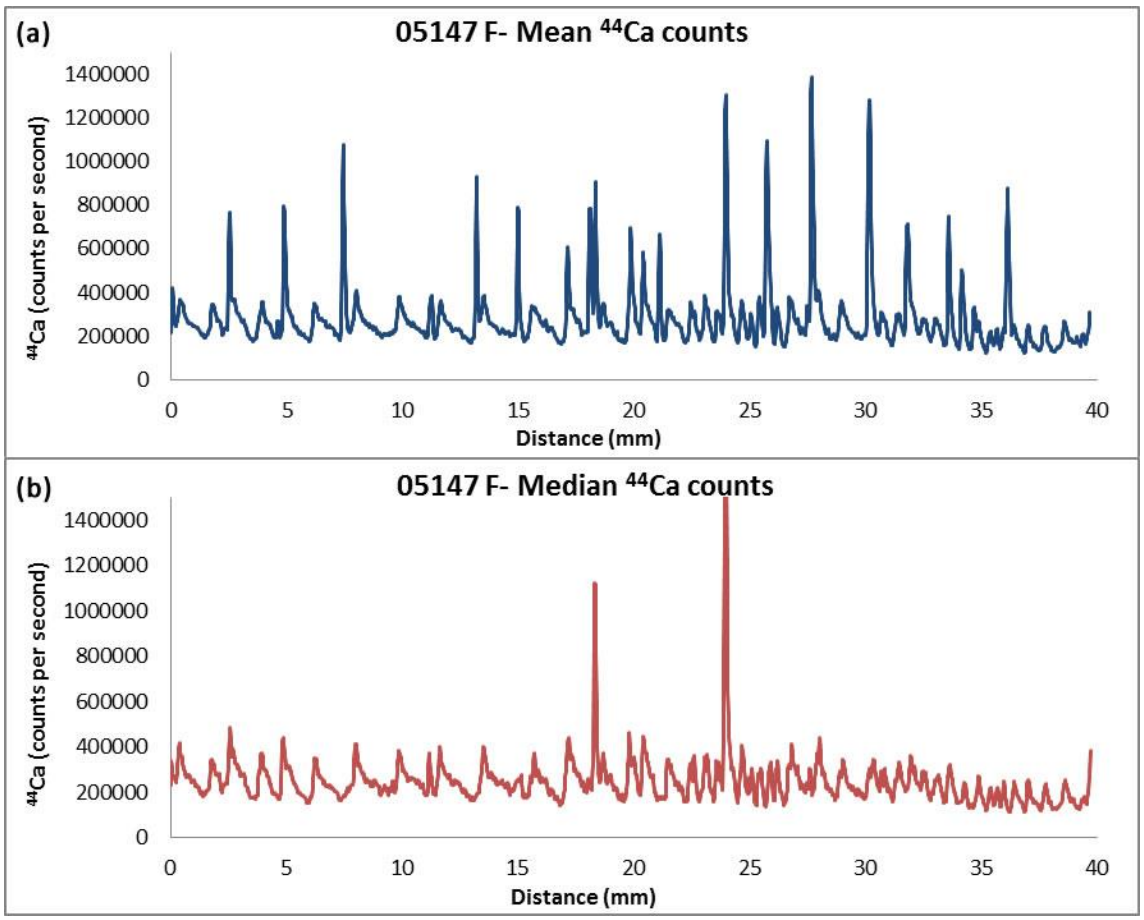

Figure 2-14: Figure showing the mean plot (a) and the median plot (b) of the 3 replicated ^{44}Ca tracks as measured by LA-ICP-MS for one section of tree lath 05147 (Figure 2-12). Using the median values opposed to the mean significantly reduced the abundance of calcium spikes.

The output from the LA-ICP-MS gives the values for each element in counts per seconds with 416 measurements recorded per 1cm (when using the settings in Table 2-3). For all lath sections, the ratios of the ^{44}Ca counts to ^{13}C (internal standard) was calculated to account for small differences caused during the ablation process (Pearson *et al.*, 2005).

Since at least one ring was overlapped on adjacent lath sections, the data from the laser scans could theoretically be easily linked together. However this process highlighted two issues which had to be addressed:

- Decrease in counts over time
- Variations in signal intensity after optimisation

2.3.4.3. Decrease in Counts Over Time (Drift)

Initial inspection of the data for each ablated track of a lath section showed that the $^{44}Ca/^{13}C$ signal decreased over time. Figure 2-15 shows the (a) median ^{44}Ca and ^{13}C data which clearly shows a decreasing trend in the calcium measurements for the lath section. There is a perhaps a very slight downward slope in the trend line for the ^{13}C data however it is not nearly as pronounced as that of the calcium. Figure 2-15 (b) shows the plot for the $^{44}Ca/^{13}C$ data for this lath section which again shows a decreasing trend over the lath section which is highly influenced by the decreasing ^{44}Ca values over the period of measurement. A decreasing trend in calcium distribution across a tree stem has been reported for various species, in the direction of pith to bark, (Prohaska *et al.*, 1998, Parn, 2001, Penninckx *et al.*, 2001, Berger *et al.*, 2004, Hristovski and Melovski, 2010) including Scots pine and it is likely that the same decreasing trend was present here. It is likely however, that in addition to such an age related trend, there is also a loss of counts over time from instrumental error. Since the NIST standard pellet was ablated before and after each individual Scots pine lath line, it was possible to identify that this decrease over time was, in the main, caused by drift in the signal from the LA-ICP-MS system. This is illustrated in Figure 2-16 where the median counts obtained from the NIST standard pellet reduce over each set of run sequences for each tree lath. In each sequence run for a lath section, the following measurements of the NIST standard were made:

- At the start of the laser sequence (before Line 1 of wood)
- Between Line 1 and Line 2
- Between Line 2 and Line 3
- At the end of the laser sequence (after Line 3)

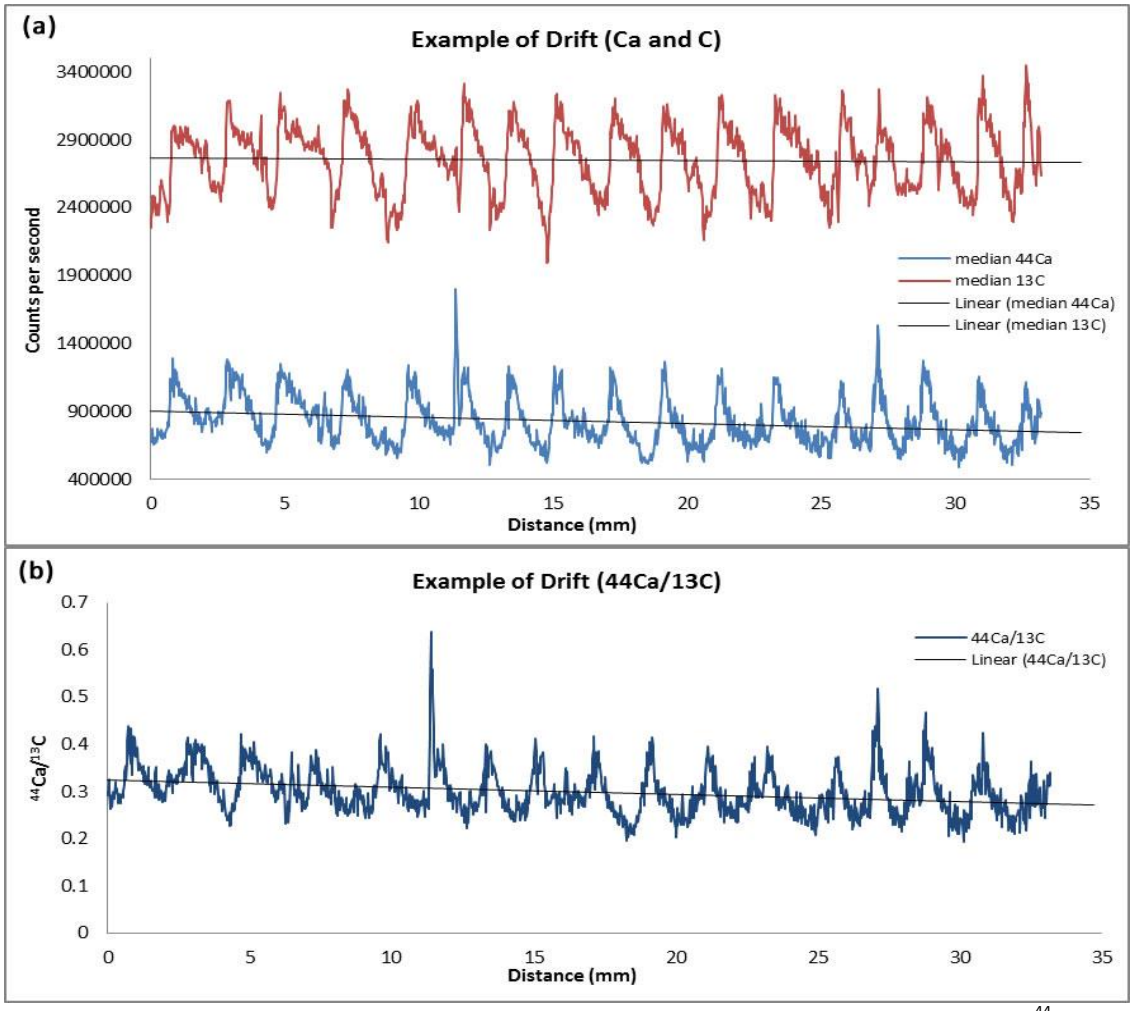

Figure 2-15: A Typical example of the drift observed over time (distance). (a) Plot showing the median ^{44}Ca (blue) data and the median ^{13}C (red) data obtained from tree 05134 R2 D. (b) Plot showing the ratio of the $^{44}Ca/^{13}C$ values for the same tree 01534 R2 D.

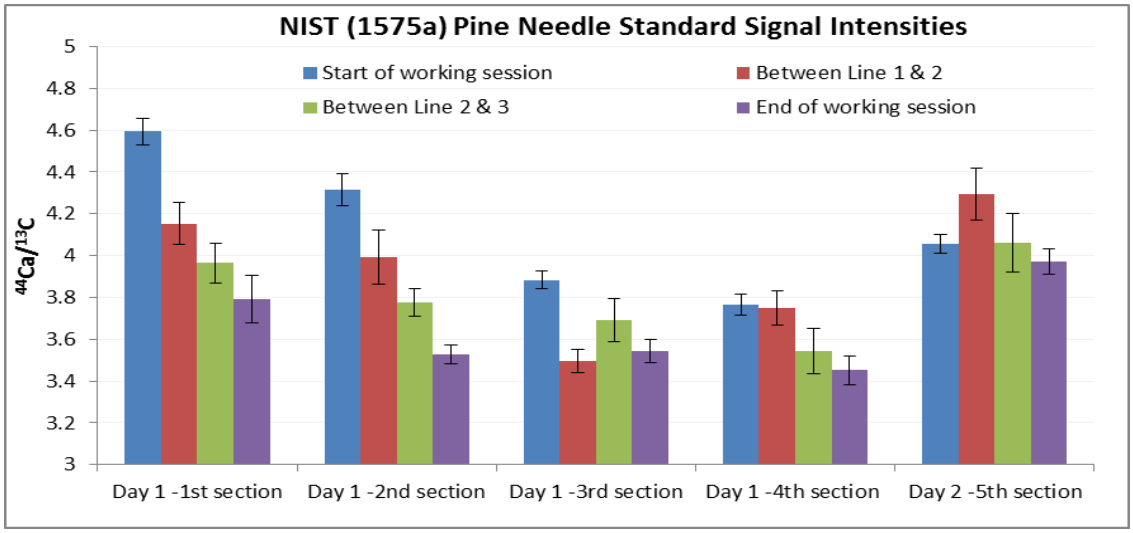

Figure 2-16: The median $^{44}Ca/^{13}C$ values (±2 standard error of the mean (SEM))are shown for the four NIST standard measurements carried out on each of the five sections of a single pine tree lath (tree 05129)

Comparison of the median $^{44}Ca/^{13}C$ values for the NIST standard from before and after the ablation of an individual track from the lath section showed a decrease in values for the standard output. If the decreasing trend observed in the $^{44}Ca/^{13}C$ for the lath section was simply an age related or climatic trend, then the measurements on the standards ran before and after each track would not have consistently decreased. The chart in Figure 2-16 includes the mean $^{44}Ca/^{13}C$ NIST standard values measured with all sections of a single pine tree lath. Four parts of this lath were analysed in the same day, with the fifth part analysed on the following day. Each of the five sections included four sets of the NIST standard measurements as described above. For each individual section, the mean $^{44}Ca/^{13}C$ NIST standard values decreased over time. At the start of "Day 1" (first day of analysis for that particular tree lath), the mean $^{44}Ca/^{13}C$ NIST value was at its highest. Subsequent measurements taken between the lath section measurements decreased over time. During the ablation sequence for the next lath sections, the initial mean $^{44}Ca/^{13}C$ NIST value measured increase slightly, but not to the full original amount, and the subsequent values decreased in a similar manner as before.

When more than one section was analysed in a day, there was a period of around 30 minutes where the new section was loaded, the sample chamber purged of air, and the system was allowed to settle after the change. This may have accounted for the initial increase in counts after a sample change, but an explanation as to why this occurred is currently unknown. This pattern however was typical for every sample change throughout a day. The fifth section of the lath was measured the following day after signal optimisation procedures had been carried out (Section 2.3.3). This signal intensity for this section increased in comparison with the values recorded at the end of the previous day's analysis, but not to the same starting value as was witnessed in day 1. This is discussed further in the next section. Figure 2-16 illustrates how the average values for each set of standard measurements decreases throughout a day's analysis. This decrease is caused by reduction in both the ^{44}Ca and the ^{13}C counts over the measurement period.

The signal loss observed over the long periods of analysis shows that at least some of this declining trend is the direct result of machine drift. De Ridder *et al.* (2002) describes drift in LA-ICP-MS as "an artificial and common pattern appearing in the raw data of all nuclides, even those of the internal standard". This can be complicated as some elements can be measured more precisely than others and in some cases drift observed in the measurements can cause

fluctuations that may be larger than the differences in the chemical behaviour between elements (De Ridder *et al.*, 2002).

2.3.4.4. Variations in signal intensity after optimisation

Auto-tuning sequences were performed on a daily basis to optimise the ICP-MS signal intensities before measurements were carried out. These sequences were controlled by the PlasmaLab software and adjustments to the instrument's parameters were automatically made to acquire the optimised value in counts. Figure 2-16 shows the mean $^{44}Ca/^{13}C$ values for the measurements made on the NIST standard after optimisation on two separate days. Comparison of these show that the initial $^{44}Ca/^{13}C$ values after optimisation are lower in Day 2 than in Day 1 suggesting that the auto-tune procedures optimised the signal but did not result in it returning the signal back to the same "switch on" values. These differences in values were not restricted to this particular example, but were present between all daily measurements. This resulted in an offset of the $^{44}Ca/^{13}C$ values recorded in some of the lath sections and different tree laths. In normal circumstances, these discrepancies would be corrected using the certified standards however as no consistent standard was identified (see Section 2.3.3.2), the counts measured from ablating the tree laths could not be converted into concentrations. Even though the NIST 1575a Pine Needles standard reference material was ablated intermittently between wood scans, the consistency in counts for the pelleted standard was not sufficiently low, due to the high variance of measurements, to allow concentrations to be calculated. If it had been possible to convert the signals to concentrations, then these discrepancies between counts could have been accounted for. A similar issue was reported in a LA-ICP-MS based dendrochemical study by Pearson *et al.* (2005) who created a calibration factor based on the averages of the standard material measurements to account for the variation observed between analysis days. A similar approach was taken herein by using the mean values for the NIST Pine needle standard to calculate an adjustment factor which was applied to each measurement for the wood sections.

Despite these problems, the main focus of this study is to develop a statistical method for dating trees using calcium as a tracer. For that reason the observed trends, whether these are climatic, age related, or a systematic machine bias are not of great importance in this instance ad can essentially be detrended for the purposes of this thesis. The datasets from each section

of a lath needed to be linked using the overlapping regions measured in adjacent sections and the data aligned on a similar scale in order to achieve this goal. Therefore systematic adjustments to the data were necessary to maximise the dating potential.

2.3.5. Data Adjustments

Plotting the raw median $^{44}Ca/^{13}C$ data for all of the sections in a single tree lath, which were analysed across three separate days, illustrates the need for a systematic adjustment to the data. Figure 2-17 (a) shows an example of the raw median $^{44}Ca/^{13}C$ counts from all six sections for tree 05135 R1. Each section demonstrates the result of the decrease in counts over time and the offsets between each section. This has resulted from a combination of drift effects and age related decreasing trends, plus variations in signal intensity between days. Regions of overlap in the data are present on each lath section which represents the overlapped rings measured in the adjacent lath section. For parts B and C, and parts E and F the overlapping datasets were reasonably well aligned in these unadjusted values, however the remaining adjoining sections are offset with each other preventing data linkage in this raw form. Since the overall goal is to apply these methods to a ringless tropical species, it was important that any adjustments made were based on an objective method which could be applied to other species.

The data was adjusted in a two-step process, and during each of these steps, each lath section data was treated separately. The first step was to detrend each section to remove the decreasing calcium trend. This step would also remove any potential age-related growth or longer term climatic signal which may have been present. The $^{44}Ca/^{13}C$ values were detrended by fitting a low pass Gaussian filter to each individual dataset with the wavelength dependant on the number of measured data points present in each section. Figure 2-17 (b) illustrates the detrending function applied to each of the individual datasets plotted over the original raw values with the high pass detrended data as showing in Figure 2-18 (a). The decreasing slopes in the datasets for each lath section have been completely removed, however the offsets in values between each section is clearly highlighted and in this form prevents the linking of sections.

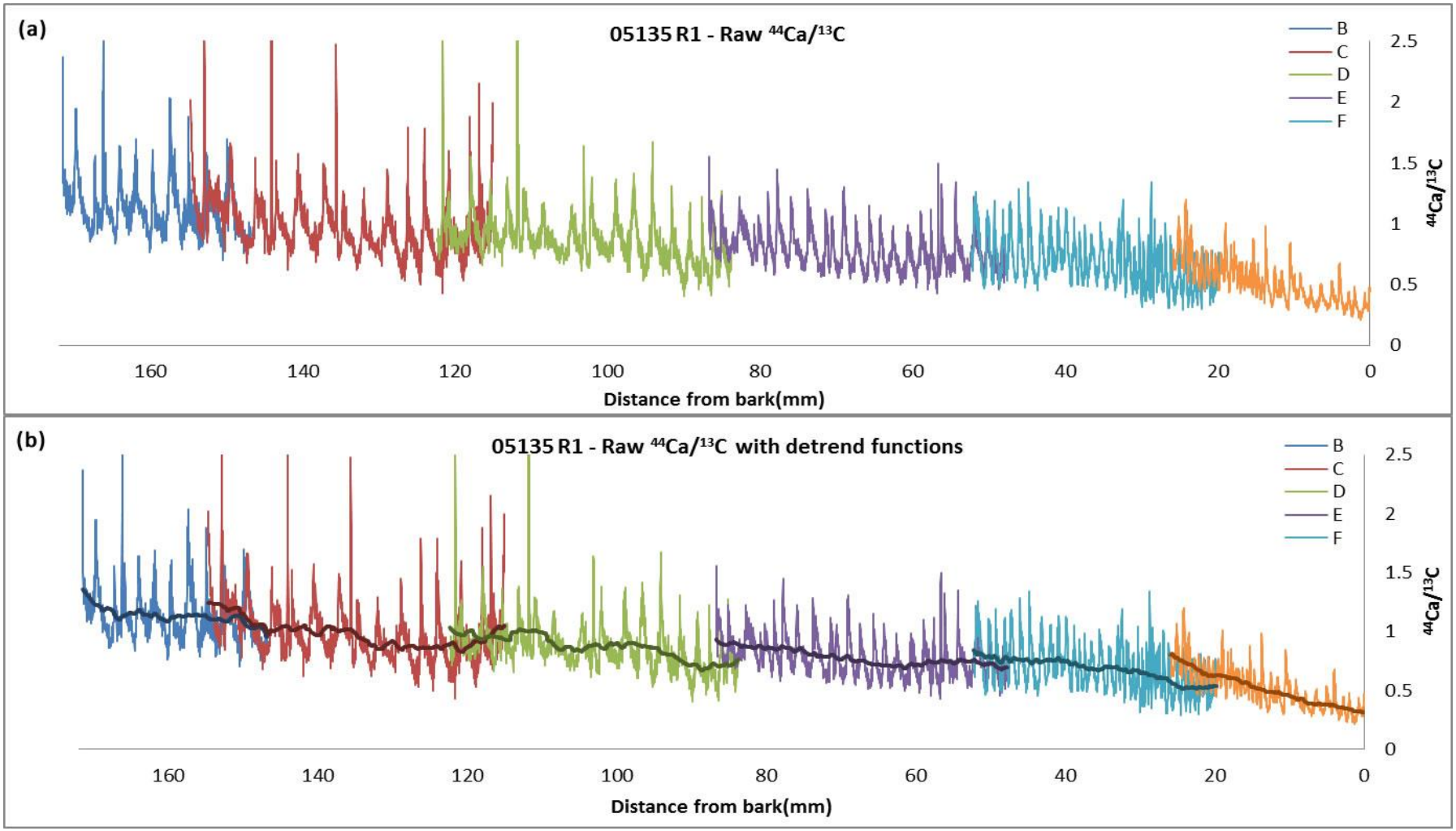

Figure 2-17: (a) Graph showing the raw median $^{44}Ca/^{13}C$ values for all sections of tree 05135 R1 which had been split into 6 sections for analysis. (b) The same plot with low frequency filters overlaid onto each section illustrating the detrending functions which were applied to the data. These plots clearly illustrate the decreasing trend in calcium counts and the problems associated with section linkage.

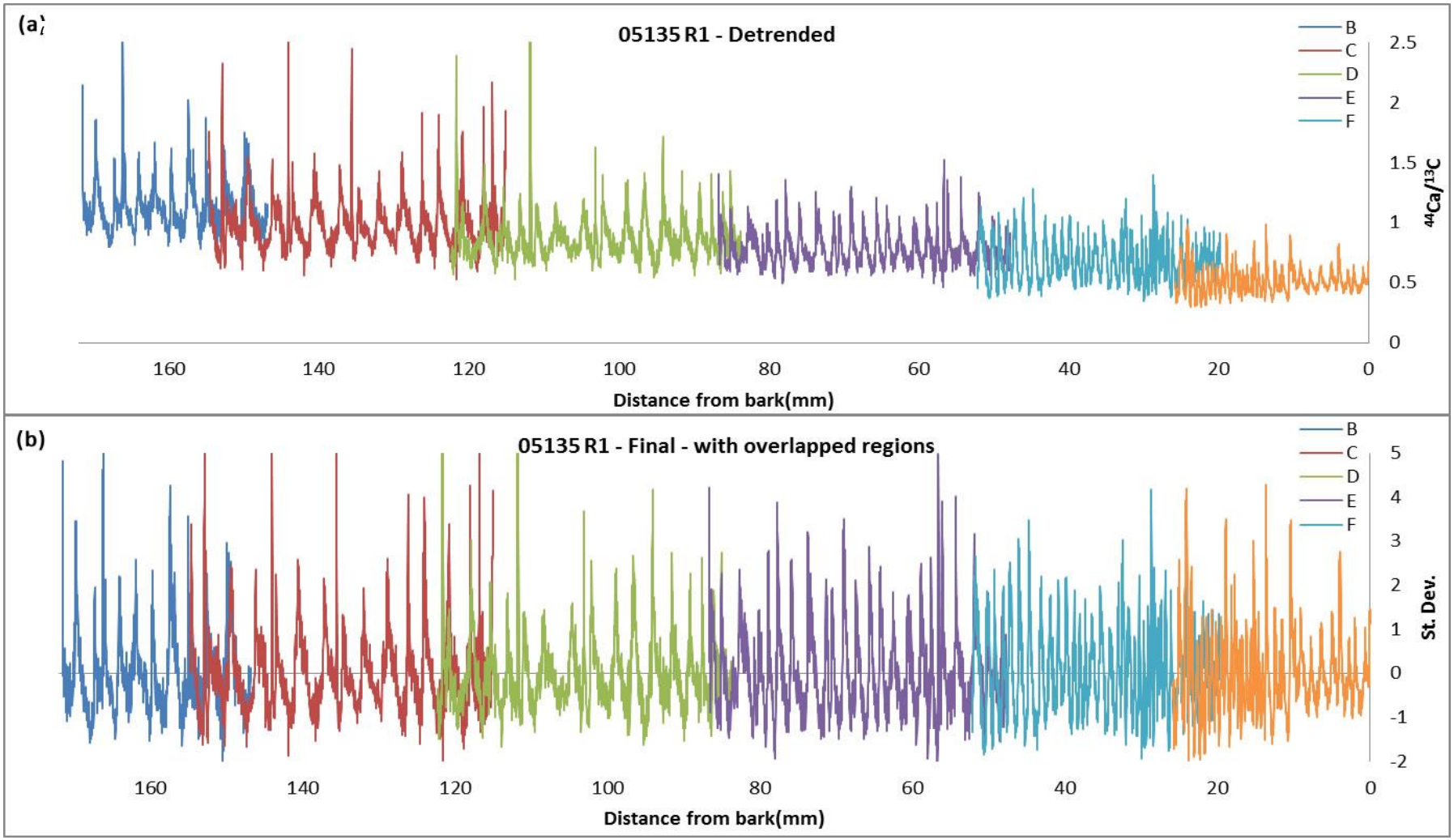

Figure 2-18: (a) The resultant plot after each section was individually detrended using the filters illustrated in Figure 2-17. (b) The final, fully adjusted, values for tree 05135 R1 are represented here. Data for each section has been detrended as in (a) and converted to z-scores.

A second step was applied to address this linkage issue by transforming the data on to a standardised scale by converting the detrended $^{44}Ca/^{13}C$ values for each section into z-scores using the following equation:

$$z = \frac{x - \overline{x}}{s}$$

where $\overline{x}$ is the mean of the measured lath section and s is the standard deviation of the measured lath section.

Converting the values to z-scores provided a means to align the data on common scale but also provided a method for statistically determining what represents a ring (using the peaks) since a z-score indicates how many standard deviations an observation is above or below the mean. This is discussed later in 2.3.8. The results of converting the individual datasets to z-scores are shown in Figure 2-18 (b) for 05135 R1. Each section is now aligned as they have a mean of zero (and standard deviation of 1.0) and none of the individual sections or the overall tree show any apartment trends longer than the annual cycle.

2.3.6. Ring Width Measurements

In order to determine if the seasonal nature of the calcium data obtained from the LA-ICP-MS could be used to determine ring boundaries and in turn as a dating tool, traditional dendrochronological methods were used to date the analysed tree laths. This was carried out to allow a direct comparison with the ring width (RW) measurements with the measured laser ablation data.

After all sections of a lath had been measured using LA-ICP-MS, the laths were re-assembled and scanned using a Canon CanoScan 9000F flatbed scanner at 2400 dots per inch resolution. Each lath image was imported into CooRecorder v. 7.3 (Cybis Elektronik & Data AB, 2010) image analysing software which was used to measure the annual ring increments to the nearest 0.001mm. The measurements were taken following the tracks created by the laser to ensure the ring-width measurements could be easily related to the distance measures from the laser ablation data. Where overlaps in ring occurred at either side of the lath splits, it was noted which part of the lath was used for that particular ring.

2.3.7. Splicing Datasets

As outlined in Section 2.3.1, the size restrictions of the LA-ICP-MS system required the laths to be analysed in sections. Each section was cut at an angle resulting in the same ring being present on each of the adjoining sections. The scanned images of the laser ablated pine samples were used to determine how many rings on each section overlapped with the adjacent sections. The width of a ring is not constant around the circumference of a tree (Figure 2-19 (b)) and the continuous nature of the calcium measurements meant that when the same ring on each lath section was measured, small difference in ring width would be present, hence the distance measured by the calcium would vary slightly. It was therefore decided to retain the $^{44}Ca/^{13}C$ data from one of the laths, allowing the splicing of datasets.

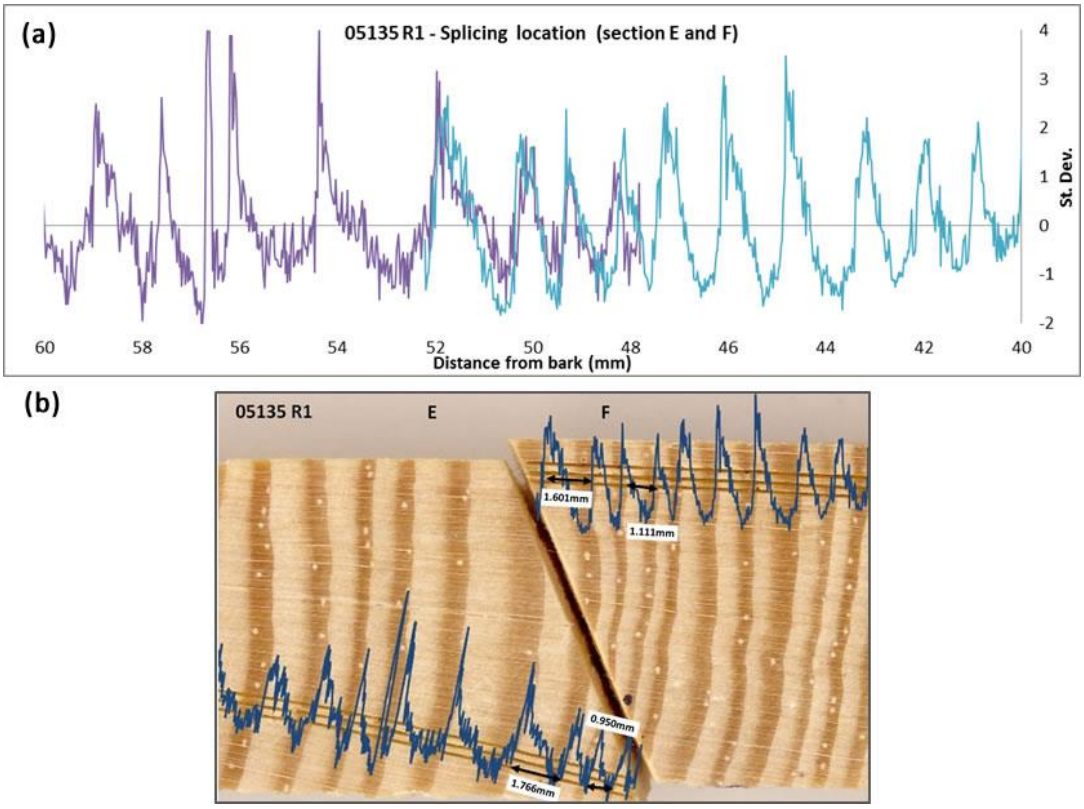

Figure 2-19: (a) Overlapping regions for two lath sections (tree 05135) after data has been detrended and converted to z-scores. (b) The same graphs have been overlaid onto the scanned image along with RW values for two of these rings.

The data adjustments bring all the lath section measurements for a single radius onto the same scale (Figure 2-18) which aids the splicing of the data. Figure 2-19 features the same tree lath as found in Figure 2-18, but highlights the overlapping region between sections E and F. Figure 2-19 (a) shows the alignment of the four rings which have been analysed on both

adjacent lath sections. The rings generally overlap well with only minor differences. However by the end of the third ring, the overlapping graphs are slightly mis-matched due to the factors mentioned above. The variation in ring width is more pronounced in situations such as when a tree grows on a slope. However, small variations can be found in trees that appear to grow in ideal locations. Figure 2-19 (b) contains the scanned image of the same adjacent sections as in Figure 2-19 (a) with the graphs overlaid on the image. The overlapping rings have been ablated at opposite sides of the lath (lath approximately 1cm wide) and for two of the overlapped rings, the ring widths are displayed (as measured by CooRecorder). Both rings had slightly different widths when each was measured in the areas represented by the arrows. The other overlapping rings also had slight differences in ring width but the values are not shown here. These differences account for the small variations between ring widths in the overlapped sections. Since the laser ablation datasets correspond directly to ring width, transformation of the data would be required to 'squeeze' or 'stretch' the values to compensate for the mis-matched rings.. As dating is the focus of the project there was no need to normalise the ring widths as all that was required was a count, therefore, this additional step was deemed unnecessary and data were taken from only one of the sections, determined using CooRecorder (Section 2.3.6).

As an additional check to make sure the overlapped regions had been spliced successfully (without the loss of data), the total length of the lath from the laser ablation data was compared with the full length as measured by CooRecorder (Table 2-5). In every case the measured ring width from CooRecorder was slightly longer than the total ablated length with an average difference of 0.19mm. The cause of this discrepancy was most likely related to an inaccuracy in the removal of excess data points from the outer edge (bark) of the tree. In the outer section, the laser ablated past the last ring into the bark area, and resulted in a sharp increase in counts as it reached the very end of the lath. An example of this region is shown in Figure 2-20. It is unlikely that that source of error has occurred when linking the data sections since the rings on either side of the overlap were very clear and easy to align (Figure 2-19). Figure 2-21 shows the dataset (for the same tree as shown in Figure 2-17 and Figure 2-18) in its final form after each lath section has been sliced together. Datasets for the other tree cores, showing each stage of the data adjustments, can be found in Appendix 1.

Table 2-5: Comparison of the total distance measured from LA-ICP-MS analysis with the distance measured by CooRecorder along the same ablated tracks. The average difference between measurements is 0.19mm with the CooRecorder measurements always being slightly longer.

Tree Code	Total distance measured (mm) (LA-ICP-MS)	Total distance measured (mm) (CooRecorder)	Difference between Distance (mm)
05129	138.791	138.880	0.089
05130	111.109	111.207	0.098
05134 R1*	71.687	71.828	0.141
05134 R2	168.985	169.082	0.097
05135 R1	171.534	171.640	0.106
05135 R2	170.294	170.833	0.539
05142	105.378	105.583	0.205
05144	169.995	170.383	0.388
05147	102.713	102.757	0.044
		Mean difference	0.19

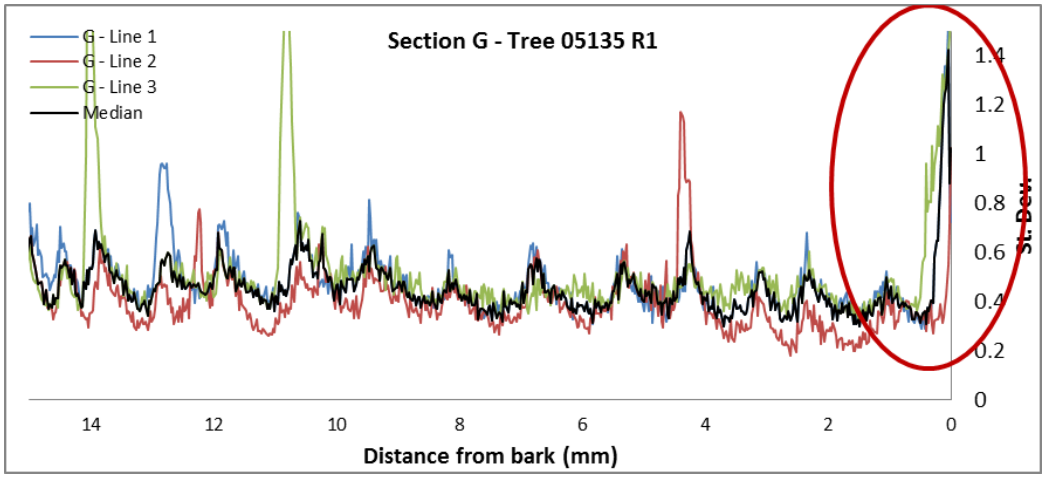

Figure 2-20: The data for the outer section (G) of tree 05135 R1. The increase in Ca values highlighted on the graph represents the outer edge of tree where laser fires into bark.

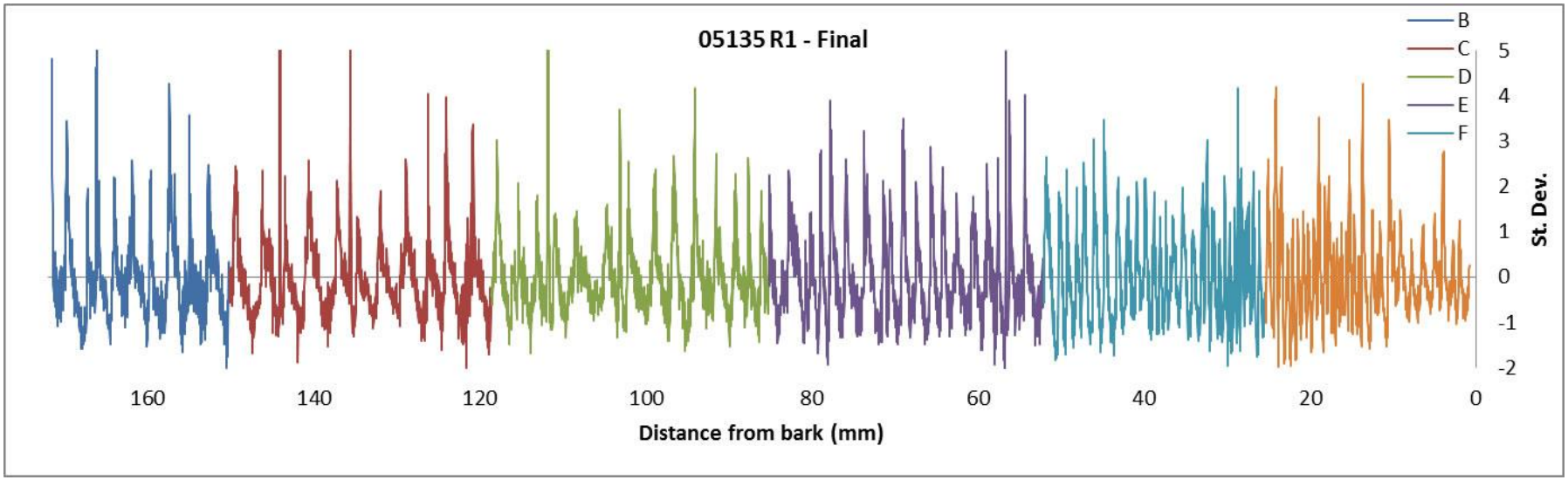

Figure 2-21: The above graph shows the final, fully adjusted, values for tree 05135 R1 after the splicing of data into one single Ca dataset. Data for each section has been detrended as in (a) and converted to z-scores.

2.3.8. Method for Ring Detection: Threshold Approach

The seasonal and annual nature of the calcium signal in the pine trees were very clear (Figure 2-21). The main objective of this study was to develop a method for detecting and measuring seasonality using Scots pine thereby dating the trees, which could be applied to other species including ringless tropical trees. As a result of the data adjustments, the data for each of the laths were linked together into one continuous series and plotted on the same standard scale. This allowed an objective threshold approach to be used to determine a ring count for each lath using only the LA-ICP-MS data.

For each lath, three different threshold values (Figure 2-22) were tested for peak detection:

- Values > 1 standard deviation above the mean
- Values > 1.5 standard deviation above the mean
- Values > 2 standard deviation above the mean

For each of the above threshold values, the first $^{44}Ca/^{13}C$ value to meet the condition was marked as a ring. Any subsequent points immediately after, which also met this condition, were not marked as they were assumed to be part of the same ring. A further condition was therefore required due to the spot size and distance between each measured data point. Each single data point was recorded at ~24µm apart using the spot size of 100µm therefore to ensure there was no overlap between measurements and to reduce the possibility of the same peaks being measured twice due to noise in the data, a minimum distance of 200µm was set as a requirement between the threshold values before being designated as a Ca year.

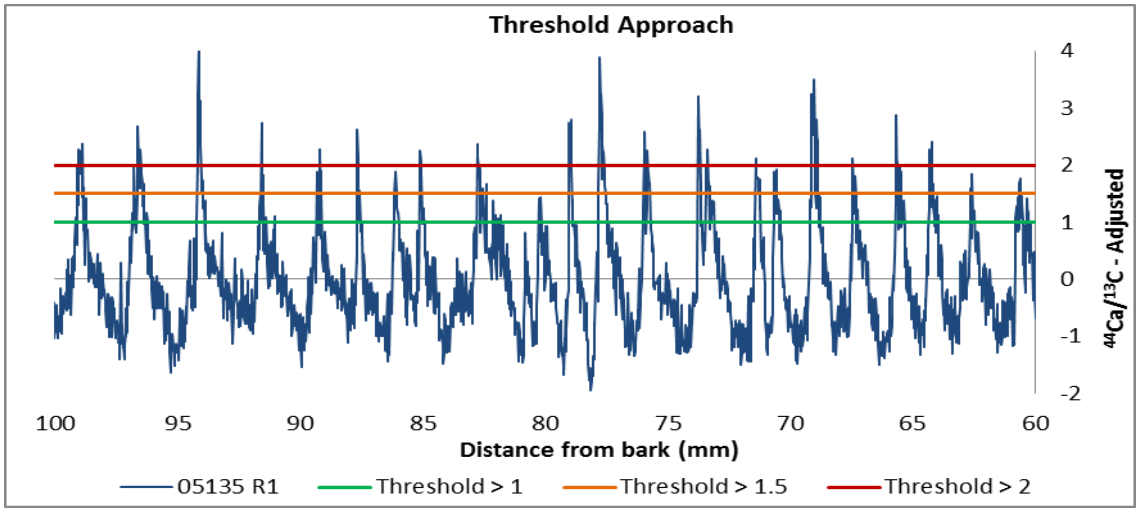

Figure 2-22: Image illustrating the three threshold values which were used to identify ring boundaries from the $^{44}Ca/^{13}C$ data. Some peaks may only be identified as a boundary at the lower threshold limits. Plot is showing data from tree 05135 R1

2.4. Results

2.4.1. Seasonal Calcium Pattern

During the early trials (Section 2.3.3.1), it was shown that the calcium signal obtained from ablating across a tree ring represented a clear seasonal cycle in Scots pine (Figure 2-6). This typical pattern was replicated across each ring analysed. Figure 2-23 shows an example of this seasonal pattern. The calcium sharply increases to its peak at the start of the growth ring in the earlywood, followed by a decrease in calcium over the remaining earlywood. The calcium reaches its lowest concentrations in the latewood portion of the ring before the cycle starts over for the next growth year.

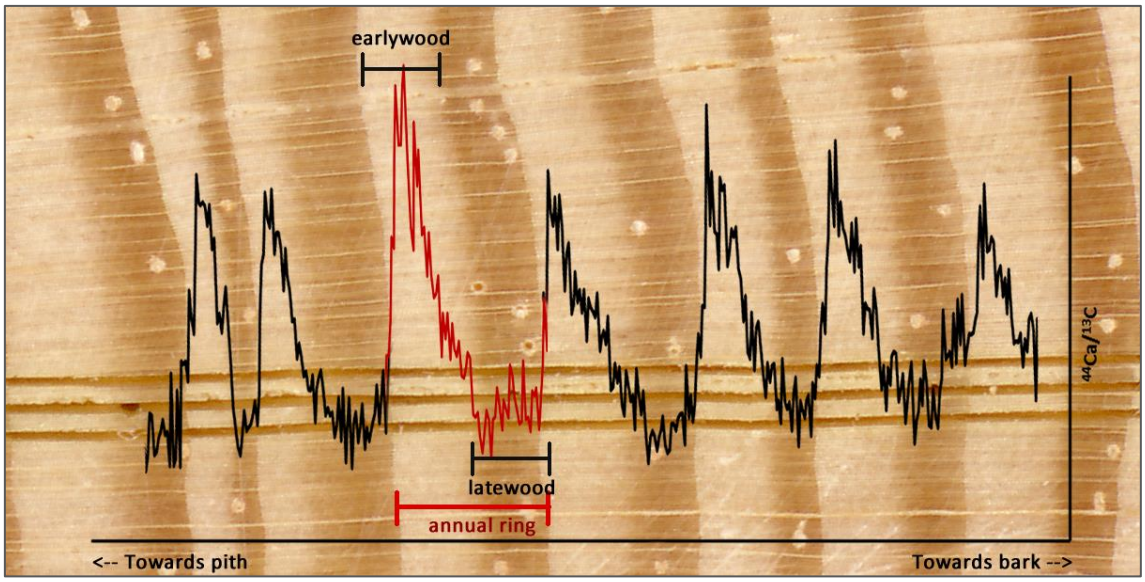

Figure 2-23: Illustration highlighting the typical seasonal signal in calcium found across a growth ring. The plot represents the median values of 3 replicate lines (ablated lines are visible under the plot)

2.4.1.1. Comparison to Ring Width

A further confirmation that calcium cycles are representative of an annual signal can be found in comparisons of the distances between the Ca cycles and the RW (ring width). The RW data that was measured using CooRecorder followed the laser ablation tracks where the Ca measurements were made and could therefore be directly compared with the $^{44}Ca/^{13}C$ values for each tree. Figure 2-24 shows an example comparison between the Ca years (>1 SD threshold) plotted with the measured ring widths (RW) from CooRecorder for tree 05134 R1 (chosen here as it was the shortest measured tree). The data for 05134 has been adjusted following the steps outlined above (Section 2.3.5). The graph shown here is split into two sections for easier viewing and shows the CooRecorder RW boundaries plotted as green markers (total of 78 rings). The seasonal nature of the calcium fluctuations is further highlighted here showing the RW boundaries coincide well with the abrupt increase in $^{44}Ca/^{13}C$ values. As would be expected for a conifer, the ring size typically decreases along the lath and towards the end. Where the rings are particularly thin, the laser ablation data appears to lose sensitivity and Ca years using the >1 threshold are missed. This is particularly clear in the 0-5mm distance from the bark. Similarly, it can be observed that occasionally the threshold approach has assigned 'extra' years when compared to the RW. An example of this happened

at 66mm from bark. The cause of the extra Ca defined year is related to calcium spikes in the data (see Section 2.3.4.2)

2.4.2. Ring Identification (Threshold Approach)

Figure 2-25 shows the Ca data for tree 05134 R1 with the thresholds marked plus the Ca years as assigned by the >1 SD threshold. The three thresholds are shown on the graph which gives an indication of the success of each threshold to designate an annual cycle as a Ca year. An area is highlighted (red circle) showing erroneous ring identification using this method. The peak at the left of the highlighted area has only one Ca year assigned, which is due to the additional condition of 2xspot size between allocates years, however the peak to the right has been counted as 2 years due to a noise in the data

The results from the threshold Ca based ring counts compared to actual ring counts are shown in Table 2-6 (>1 SD), Table 2-7 (>1.5 SD) and Table 2-8 (>2 SD). Best results were obtained using the >1 SD threshold as this produced the lowest error (±5.9 rings) on comparison with the ring counts, although overall, there was still a slight over count. This is likely related to the calcium spikes in the data. The error increased by a factor of three (±18.1) when the threshold value was increased to >1.5 standard deviations above the mean (Table 2-7) and to around seven times (±40.56) higher when the >2 threshold was applied (Table 2-8).

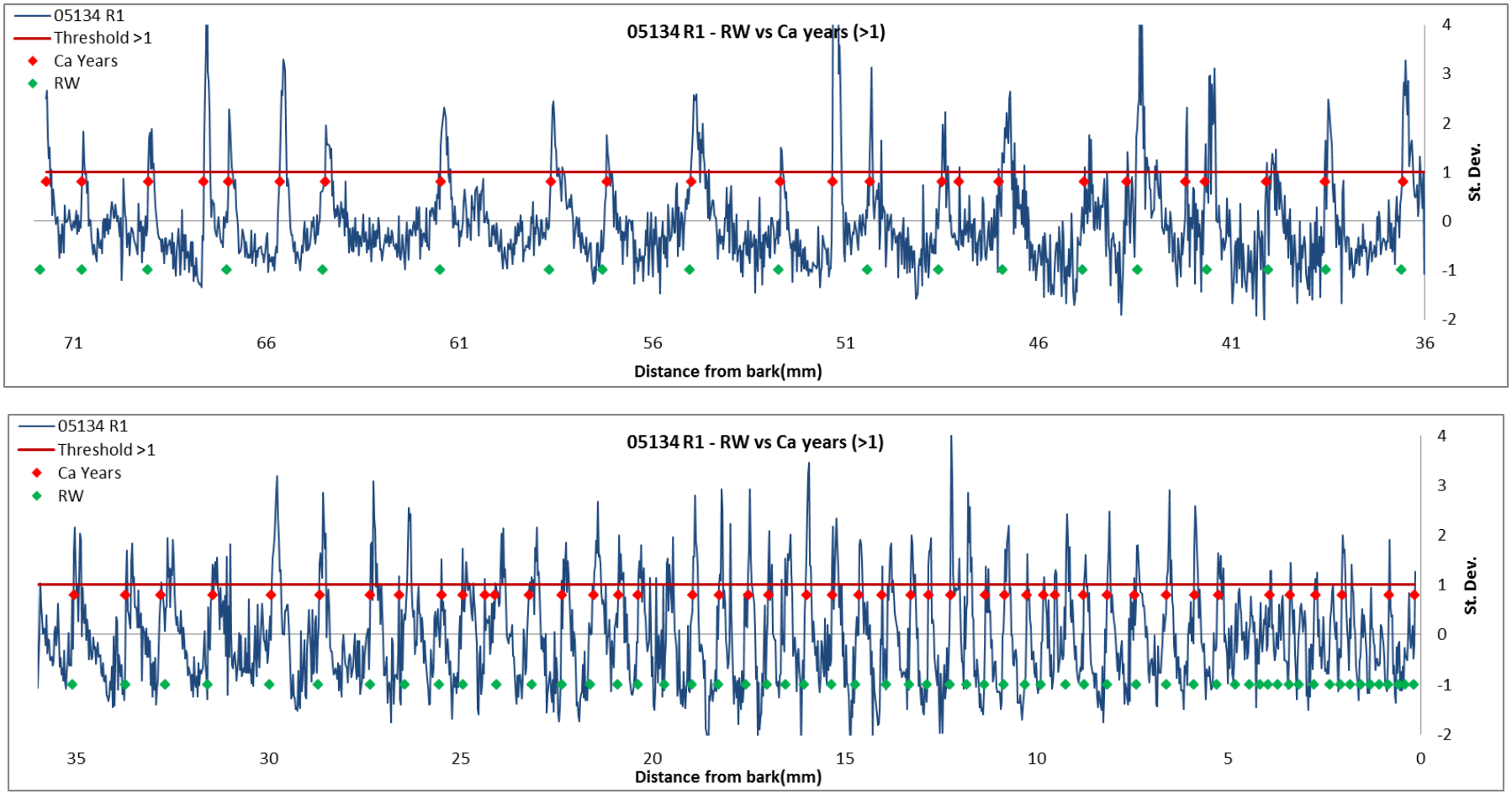

Figure 2-24: Example of the adjusted median $^{44}Ca/^{13}C$ values plotted with the ring widths (green) and Ca years based on the >1 threshold (red) for tree (05134 R1). The data is split into two graphs for easier viewing.

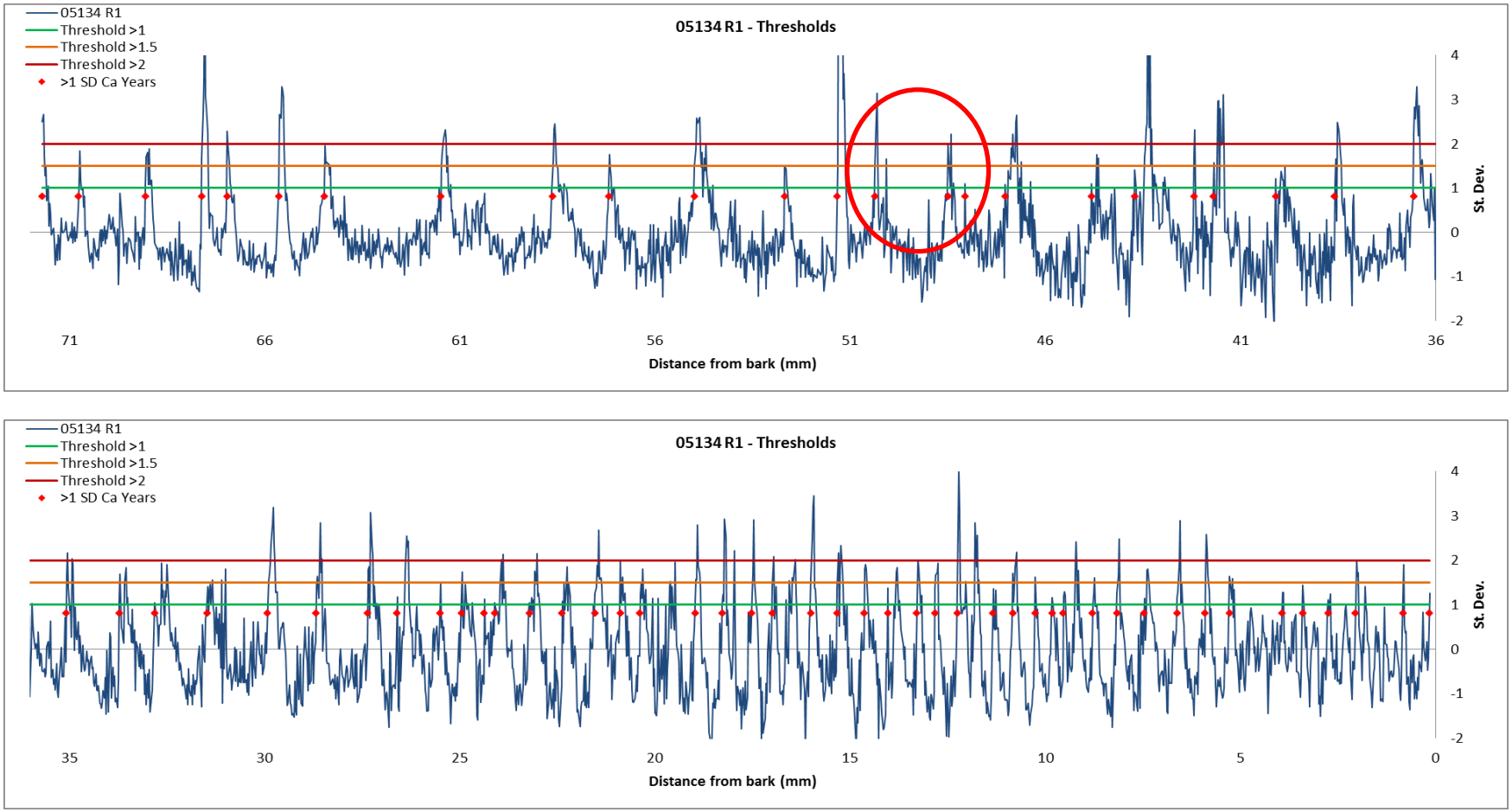

Figure 2-25: Illustration of the three threshold values tested for assigning ring status to peaks for 05134 R1. The graph is split into two sections for easier viewing. The red diamonds show the results of designating Ca years based on the >1 threshold. The red oval denotes an area where there is a potential for more than 1 Ca year to be assigned for the 1 true year.

Table 2-6: Actual and estimated rings counts using the > 1 standard deviation threshold

Tree	No. of rings (CooRecorder)	Threshold >1 Ring count	Difference between no. of rings
05129	81	87	6
05130	79	81	2
05134 R1	78	76	-2
05134 R2	98	114	16
05135 R1	114	120	6
05135 R2	131	133	2
05142	76	80	4
05144	95	94	1
05147	72	59	-13
	Mean difference in no. of rings		±5.89

Table 2-7: Actual and estimated rings counts using the > 1.5 standard deviation threshold

Tree	No. of rings (CooRecorder)	Threshold >1.5 Ring count	Difference between no. of rings
05129	81	66	-14
05130	79	60	-19
05134 R1	78	64	-14
05134 R2	98	100	2
05135 R1	114	91	-23
05135 R2	131	105	-26
05142	76	74	-2
05144	95	65	-30
05147	72	40	-32
	Mean difference in no. of rings		±18.11

Table 2-8: Actual and estimated rings counts using the > 2 standard deviation threshold

Tree	No. of rings (CooRecorder)	Threshold >2 Ring count	Difference between no. of rings
05129	81	47	-34
05130	79	32	-47
05134 R1	78	38	-40
05134 R2	98	74	-24
05135 R1	114	73	-41
05135 R2	131	68	-63
05142	76	66	-10
05144	95	35	-60
05147	72	26	-46
	Mean difference in no. of rings		±40.56

The results from the comparisons of the threshold tests clearly indicate that for the Scots pine, using the >1 standard deviation threshold provides the best estimate of tree age. The mean difference between the Ca year count and the actual year count provides an error for this Ca method, as well as an objective method for assessing and identifying the seasonality in the recorded calcium fluctuation of trees.

Graphical representations of the results from applying the >1 SD threshold to all of the Scots pine samples is shown in Appendix 1.

2.5. Discussion

2.5.1. Calcium Seasonality

The calcium distribution found in the Scots pine laths followed a consistent pattern across the tree rings. This seasonal pattern consisted of a sharp increase of calcium at the start of the growth ring, followed by a steady decrease in values where the minimum calcium values are observed in the latewood (Figure 2-17). The cyclic pattern was shown to represent the annual tree ring by comparison between the distance travelled with ring with measurements as well as visual analysis. Since the LA-ICP-MS system obtained calcium measurements in a continuous manner, it may conceivably be possible that the peak in calcium which appeared to coincide with the start of the growing season could have been carried over from the latewood of the previous year. Separate analysis of the earlywood and latewood (Figure 2-8) however confirmed that the latewood contained an overall lesser amount of calcium than the earlywood regions.

As outlined in Chapter 1 (1.4.5), calcium is required for a variety of physiological functions (structural cell support, cell signalling and division etc.) therefore the observed calcium cycles may be influenced by a combination of factors. In order to attempt to understand what the calcium signal may represent, it is worth considering the calcium's involvement at various stages of tree growth.

An annual tree ring is formed by the division and differentiation of cambium cells, into xylem cells. In early spring, cambium cells resume metabolic processes in preparation for cell division (Sitbon *et al.*, 1993). Both Follet-Gueye *et al*. (1998) and Arend and Fromm (2000) suggested that calcium plays a prominent role in cambium reactivation when they observed a large, but temporary increase, in calcium concentrations within cambium cells (of beech and poplar trees respectively) during the pre-activation phase. However, only small changes in the in cytosolic Ca^{2+} concentrations are required in cell signalling events such as to trigger the start of cell division (Section 1.4.5.2), therefore this dramatic rise in calcium concentration must be

required for additional reasons. The cambium Ca^{2+} increase reported by these authors is unlikely however to be a direct representation of the sharp increase observed herein for the Scots pine samples. In both cases, the increased calcium concentrations described by the authors were observed prior to cell division and therefore before the differentiation of any new xylem cells. This increased Ca^{2+} ions however must be reallocated elsewhere since it has been shown to only be a temporary phenomenon. In conifers, the physical size of the cambium zone increases with cambium reactivation, often doubling the cell count (Vaganov *et al.*, 2006), which could, at least in part, account for a rise in cambium calcium.

As cell division begins, the cells swell, breaking the stabilising cross-linked calcium-pectin bridges (Section 1.4.5.2), and releasing Ca^{2+} (Funada and Catesson, 1991, Lautner and Fromm, 2010). The released Ca^{2+} ions, perhaps along with the Ca^{2+} from the cambium reactivation or from a seasonally related uptake from the soil, are potentially free to compete for binding sites in newly differentiated xylem cells. As discussed in the previous chapter (Section 1.4.4.1), the binding affinities of cations influence the uptake and movement of cations within cells. Calcium has a strong binding affinity which could be amplified in situations when Ca^{2+} ions are in excess. The first few layer of new xylem cells may be richer in calcium partly due to the vast amount of recently acquired, and the newly available Ca^{2+} which had been 'left over' after cambium reactivation.

The annual calcium signal in the Scots pine shows a gradual decrease over the earlywood until it reaches a minimum in the latewood portion of the ring. Earlywood cells are generally large, often expanding up to 8 times in size (after cambium cell division) and contain a large lumen relative to the cell wall (Vaganov *et al.*, 2006, Speer, 2010). Latewood cells are commonly smaller and flatter in appearance, with a small lumen relative to the cell walls. Latewood cells are much denser than which is due to the smaller cell size and thicker cell wall (Plomion *et al.*, 2001). Since the main target for calcium ions are the carbonyl groups of pectins in the middle lamella and cell wall sites (Section 1.4.5), it may have been expected that the latewood calcium concentration would be higher. The profile found in the Scots pine laths appears to suggest that calcium may be inversely related to the wood density, however further work is needed to explore this.

There are very few studies which have focussed on identifying a detailed seasonal cycle of any mineral element within the annual tree rings of a species. Martin *et al.* (2001) identified a

seasonal calcium cycle from a *Pinus resinosa* tree in Canada, with a maximum present in the middle of the growing season. The timing of the calcium maxima differs from what was found in this study which may be related to species, location or other factors. The Martin *et al.* (2001) study was only based around three individual years from one a single tree, which was situated in a highly polluted area. Poussart *et al.* (2006) also identified a seasonal (annual) calcium pattern, in a ringless tropical species (details outlined in Section 1.4.7) in which they used radiocarbon dating to validate the method. The exact timing of the Ca maximum peak is not as clear due to the lack of identifiable ring boundaries, but is suggested that it occurs at the start of the growing season. This study was also only based around 1 individual tree, but covered approximately 40 years of growth, in which the apparent annual calcium cycle was clearly replicated. Both of these studies show similarities with the seasonal calcium pattern found in Scots pine, containing a cyclic calcium profile over a single growing season. Growth dynamics can vary between species and locality, including the timing of the initiation and cessation of cell divisions therefore it is likely that elemental profiles would reflect this. Scots pine has been shown as having a distinct growth maximum period during the first half of the growing season (Vaganov *et al.*, 2006). Since calcium is required for growth, this may be linked to the higher calcium concentrations found throughout the earlywood found here. Poussart *et al.* (2006) proposed the the calcium maximum may be linked to an increased presence of pectin in the early cells, or from a pulsed uptake of calcium via the tranpiration stream from the soil. They suggest that this uptake results from the accumulation of calcium from the decomposition of plant litter during the dry (dormant) season. Although tropical and temperate environments are vastly different, a similar situation may be possible as the spring reactivation occurs in temperate Scotland.

The only interruption to the consistent cyclic pattern in the Scots pine calcium record occurred when the laser ablated through a resin duct as highlighted in Figure 2-13. Resin ducts are hollow vessels surrounded by guard cells which control the resin flow through the duct (Speer, 2010), and although steps were taken to remove extractives from the tree laths, it is possible that resin or other material (e.g. calcium oxalate (CaOx) crystals) remained in the ducts potentially causing these high values.

Calcium oxalate crystals are reported to have two main functions in plants. CaOx is produced in conifers as a defence mechanism against bark-boring insects and fungal infections and also as a mechanism for regulating high levels of calcium ions (Hudgins *et al.*, 2003, Franceschi and

Nakata, 2005, Nagy *et al.*, 2006). Hudgins *et al.* (2003) examined 46 species of conifer and found CaOx crystals present in each. They suggested that conifers produce CaOx primarily as a defence mechanism. The calcium spikes only occurred when the ablation track passed through a resin duct therefore it may be likely to contain CaOx crystals which may have been produced for this purpose. Calcium ions enter the apoplast where they bind to cell wall sites which have a high exchange capacity for Ca^{2+}. When excess Ca^{2+} ions are present, they accumulate in the apoplast which can interfere with cell division and expansion. In response to this, CaOx is produced which precipitates in the intracellular space in gymnosperms (Fink, 1991, Franceschi and Nakata, 2005). It was not possible in this study to conclusively identify whether calcium oxalate crystals were present in the resin ducts or in the apoplast of surrounding cells, however this would be something to consider in future work.

An alternative theory with regards to a cause of the spikes could be contamination from wood dust. The most obvious source of contamination would be from the sample preparation procedures (Section 2.3.1) where each lath section was sanded using progressively finer graded paper to produce the required finish for laser ablation. Compressed air was used remove excess wood dust from the samples, however no further treatments or inspections were carried out to ensure all traces were removed. It is possible that some wood dust collected in the resin ducts and was partly responsible for the calcium spikes. The spikes contained significantly higher concentrations of calcium then what was measured in the highest levels of the earlywood therefore this theory seems somewhat unrealistic.

2.5.2. Standard Reference Materials

In most types of analysis, it is essential to use standard reference materials for quality and calibration purposes. The lack of available suitable standards for the laser ablation of wood resulted in the inability to quantify the actual amount of calcium across the profile of the Scots pine laths. The ability to calculate and evaluate the absolute calcium concentrations was not however the focus of this study, and will be an area for further investigation in future research.

The attempts to create a standard from powered materials (Section 2.3.3.2) was problematic and in each case produced noisy calcium signals, which were unsuitable even when using the mean of 5 replicate ablation lines. The importance of using as close to a matrix matched

standard as possible ruled out the option of using a NIST glass standard which was what was adopted by Pearson *et al.* (2005). As well as the differences in the ablation of such different materials, the NIST glass standards all contain much higher calcium concentrations than wood. Using an alternative standard which is not suited to this type of analysis may provide a method to convert these values to concentrations and resolve the drift problems, however such a standard would not ablate in a similar manner to the wood laths and would likely increase error further in the datasets. The pelleted NIST 1575a (pine needles) provided the most stable and reproducible calcium signal. Since it is a certified standard (albeit not in a pelleted version intended for this purpose), it provided the added assurance of a homogenous standard pellet for ensuring instrument stability.

2.5.3. Decreasing Ca signal and Machine Drift

During of the laser ablation of each lath section, the calcium counts decreased over time (Figure 2-15). The reason for this decrease is likely to be a combination of a real age-related decreasing trend in the calcium profile from pith to cambium, and from instrumental drift over the measurement period. Many analytical instruments experience a drift in signal sensitivity over time requiring data corrections to compensate for this systematic error and LA-ICP-MS is no exception (De Ridder *et al.*, 2002). Possible causes for drift in ICP-MS systems include the changes in the sample composition, deposition of sample matrix on the cones or changes in laboratory conditions (Thermo Electron Corporation, 2002). Internal standards are used to monitor any drift in signal sensitivity. During the analysis of the wood lath sections and the NIST SRM pellet, a substantial amount of machine drift was experienced. A drop in average counts from the ablation of the standard immediately prior to a lath section, and the mean of the standard ablated immediately after the lath section, shows that there is a significant reduction in the measured calcium signal. Such drifts in the signal sensitivity with time are not unexpected and it is recommended by the instrument manufacturer to monitor changes in the signal with standards and apply appropriate corrections where necessary (Thermo Electron Corporation, 2002). Corrections in this manner were not possible due to the lack of appropriate standard materials, although an internal standard (^{13}C) was used during analysis and the ratio of $^{4}Ca/^{13}C$ was calculated to account for minor differences during ablation (such as during material transport). As discussed in Section 2.3.4.3, this did not resolve the issue of

the variations in signal intensities between lath sections and trees measured on separate days. It is important to note that this issue is not limited to this study but is a universal problem associated with LA-ICP-MS. Converting the signal intensities to concentration would have eliminated the need for further data corrections but requires suitable standards.

Any natural calcium trends which may have been present within the calcium signal could not be determined as it was not possible to separate it out and correct for any drift effects. However, a general decreasing trend would be expected and was most likely present within the calcium profile. Momoshima and Bondietti (1990) reported a decline in the cation binding capacity of calcium in red spruce trees as a function of a tree's radius rather than directly linked to age. Several other authors reported general decreasing calcium trends in various species including Scots pine (Parn, 2001), Norway spruce (Prohaska *et al.*, 1998, Berger *et al.*, 2004) and Beech (Penninckx *et al.*, 2001, Hristovski and Melovski, 2010). These trends are only relevant if the focus is to understand longer term trends in the calcium fluctuations. This is not the case in this study which concentrates on the dating of tree rings. The relationship between the peaks and their intensity are central for establishing a robust dating control, however it is the relative differences that are of importance, rather than the actual calcium concentration, in determining whether each peak represents a ring.

2.5.4. Data Adjustments

Since the data could not be corrected relative to a standard, it was necessary to make systematic corrections or adjustments to the raw data to remove any artificial patterns in the calcium profiles. It was important to carry out all data management in a way that could be applied to datasets for any species. Adjustments were required to compensate for the machine drift and to bring the datasets for each tree into alignment on a common scale.

It was decided to use the median values of the three replicate lines as a measure of central tendency. This had the advantage over the mean as it minimised the influence of the calcium spikes in the data. The intensity of many of the spikes was so great that using the mean values expressed large spikes in the averaged data even when the spike was only originally present in 1 of the lines. Retaining these spikes would impact heavily on the ring identifications threshold approaches (Section 2.4.2. The occasional calcium spike did however remain in some datasets.

This occurred when more than one resin duct was present in a ring which resulted in the extra 'rings' being counted by the threshold approach. The analysis of additional replicate tracks may have improved ring count estimates further by the omission of the remaining spikes when calculating the median value. Even if the additional tracks ablated over additional resin ducts present in the same latewood areas other tracks, then the use of median values would still reduce the inclusion of these for ring identifications. The analysis of additional tracks would also present the opportunity to investigate a trimmed mean approach to exclude the additional peaks. This would be a useful consideration for future work.

2.5.4.1. Detrending the Datasets

The final data adjustments were carried out on each individual lath section dataset, before splicing the data for each section together to represent the whole tree. The datasets for each section contained a different number of data points which was dependant of the length of the ablated line. The number of data points present in each lath section was used to define the wavelength for the Gaussian filter which ensured that each sub section was detrended in a standard and consistent manner. This method of filtering could then be directly applied to ringless tropical species (see Chapter 3). It was necessary to treat the lath sections as separate datasets due to the possible variations in measurement intensity caused by changes to the system such as after tuning sequences between different days. Figure 2-17 (b) shows the raw data plotted for each lath section with the low frequency Gaussian filters for each overlaid on top. This illustrates the detrending function which was applied to the individual section and highlights the decreasing Ca trend present in each lath section. The result of detrending each section is shown in Figure 2-18 (a). The Gaussian smoother removed the decreasing calcium trends within the calcium data for each lath section. This process would remove potential secular scale changes in calcium that could be a product of age related trends or longer term environmental influences. If it had been possible to remove the machine error without affecting any longer term climatic or age related signal, the data would still need to be detrended in order to apply a method for detecting seasonality and dating the trees. For the purposes of this study, secular calcium trends whether age related or climatic would not assist in dating the trees.

It is clear from Figure 2-18 (a) that another step is required to adjust the data before any statistical method for identifying rings can be applied. Although each individual section had been detrended, these separate datasets were slightly offset from each other. In addition, the variance of the peaks in some of the sections is lower, such as in the outer section of the tree (G). This may be due to this area of the tree having narrower rings, as would be expected from the outer regions, and therefore there is physically less cells and in turn less calcium. It could also be related to differences in measurement intensity after daily auto-tuning procedures (Section 2.3.2), which would be accounted for in normal circumstances where data corrections could be made relative to a standard. Since the purpose of developing this method of dating is to apply it to ringless tropical species, it is necessary to assess the relative differences between peaks rather than the absolute differences. After detrending, the individual datasets were normalised then spliced together to derive a single time-series from which a threshold approach could be used to identify ring boundaries.

2.5.4.2. Ring Detection

The clear cyclic calcium signal obtained from the Scots pine laths allowed simple visual comparisons to be carried out between the $^{44}Ca/^{13}C$ data series for each tree's calcium profile and scanned images of lath itself to confirm its annual cyclicity. Visual comparisons were also made between the adjusted $^{44}Ca/^{13}C$ data series with the associated ring widths measured using the Ca threshold method and using CooRecorder (Figure 2-24). Although this was simply a visual analysis at this stage, it provided an indication of how well the LA-ICP-MS measurements were representing the annual rings. A potential problem, highlighted for the analysis of narrow rings which mainly affected the outer region of the tree, is discussed later.

The threshold method tested for assigning 'ring' status to the LA-ICP-MS adjusted tree series calcium data produced promising results. Since the data for each series was converted to z-scores, this provided an obvious method for assigning and testing different threshold values for ring detection. The extra condition added was necessary due to the limitation of the spot size as outlined in 2.3.8. For the three thresholds tested, the results indicated that using values >1 standard deviation (Table 2-6) as a basis for assigning a ring status was a viable method for detecting the seasonal calcium cycles in the Scots Pine samples. This method

produced an average error of just under 6 rings, however there was no directional control on this error. The high thresholds of 1.5 and 2 significantly increased the error and were deemed too high.

The main source of errors associated with this threshold method include falsely identifying values as rings which may result from the presence of a calcium spike in the data (Section 2.3.4.2). Missing rings are most likely to be a problem in the outer regions of a tree lath where rings are thinner. Figure 2-26 shows the adjusted $^{44}Ca/^{13}Ca$ series for the outer area of tree 05134 R1, plotted with the RW as measured by CooRecorder. The Ca fluctuations from ~67mm are not as well defined as in the inner portion of samples and have lower values for the corrected $^{44}Ca/^{13}Ca$ measurements showing the potential of 'missing' rings out when estimating a ring count using a threshold value. Even the lower threshold (>1) missed some rings in these outer regions of the samples. This highlights a limitation of the settings chosen for LA-ICP-MS measurements. The spot size selected for all the pine analysis was 100µm (0.1mm) with a transit speed of 20µm/second (0.02mm/second). The combination of this spot size and transit speed may not provide enough sensitivity to measure these narrower regions. This is a critical factor which should be considered for future analysis and when applying the method to ringless tropical trees (this is taken into consideration in Chapter 3). Despite, these limitations, if the calcium base tracer method is similarly applicable to tropical trees, then even a dating error of ~6 years would be a huge improvement on the current situation where robust dating is almost impossible for most tropical tree species.

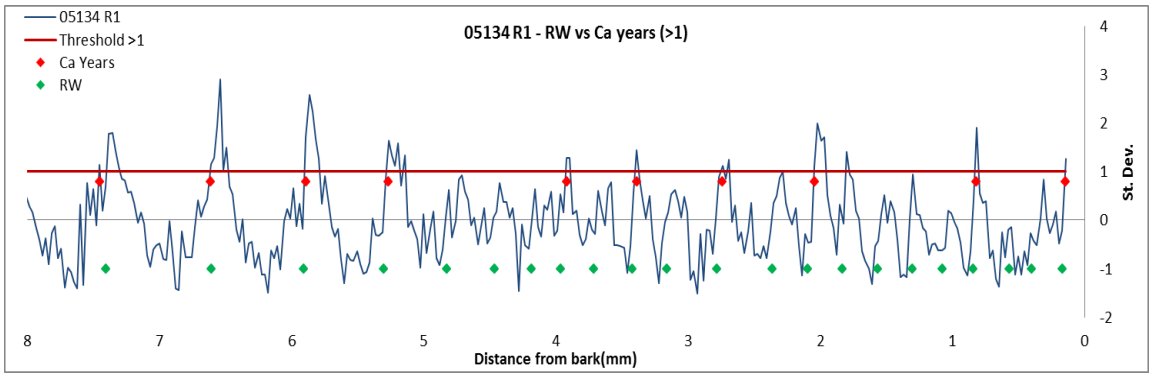

Figure 2-26: Enlarged area of the same tree as shown in Figure 2 11. The outer portion of the calcium and RW measurements are shown here along with the lowest threshold value for detecting rings.

2.6. Refinement of Methods

Despite the promising results using clear ringed Scots pine samples, there are several areas where refinements could be made to improve on the methods used in this study. These are outlined below.

2.6.1. Sample preparation methods

The spikes in the calcium measurements highlighted the sample preparation method as a potential source of contamination from wood dust build up in the resin ducts from the sanding process. Steps were taken to remove excess wood dust from the laths using compressed air, however closer examination of the laths would be recommended before analysis to ensure this was sufficient to remove the contamination risk. Alternative methods to sanding could be tested such as using a microtome or similar to leave smooth cut edge for lasering. Pearson *et al.* (2005) used an acid washed microtome blade to produce a fresh surface prior to analysis to avoid contamination from sanding procedures.

It is more likely however that the calcium spikes are caused due another source of calcium such as oxalate crystals within the resin ducts. If the presence of calcium oxalate was established, then additional washes could be considered to remove these from the wood before analysis. This would minimise error associated with the identification of 'false' rings as determined by the threshold approach.

2.6.2. Standards Reference Materials

The lack of a suitable matrix-matched standard was potentially the biggest problem highlighted in this study. A suitable standard would have allowed the calcium concentrations to be calculated, which although not necessarily required for the purposes of this study, would have allowed data to be corrected to the standard. This would also speed up the correction process and potentially reduce the issues associated with variations on counts between

samples. This would have resulted in less adjustment of the data, although detrending the presumed longer term trends in age related trends may still needed to have been performed.

As outlined in Section 2.5.2, several authors have used a variety of in house standards or alternative non-matrix-matched, which have served the purpose of their investigations but have not proved to be of good enough quality for fully quantitative analysis. Further investigation and testing is required to help resolve this problem.

2.6.3. LA-ICP-MS equipment and settings

The laser ablation system has many parameters which can be changed such as spot size, transit time, power and more. Initial investigations trialling various laser settings determined the settings used in this study, however further improvements could be made. The spot size used in this study was chosen as it provided a reasonably high level of counts with minimal noise; however results from this study suggest that a smaller spot size would have improved the sensitivity for detecting narrower rings (see Section 2.5.4.2) in the outer portions of the samples. Simply reducing spot size may however result in inadequate counts, therefore further investigation is recommended. For trees where the rings are clear, it might be possible to have an adjustment factor of spot size as a function of mean RW. A reduced transit speed could be implemented for narrow ringed sections to overcome the count issue.

Similarly the ICP-MS also has a vast amount of parameters which could be tweaked potentially improving the signal. Many of these are automatically set during auto-tuning sequences but others can be manually chosen. Again, further trials would be needed to assess the effect of altering these parameters.

To complicate matters further, the type of wood to be analysed may influence the settings chosen for the LA-ICP-MS system. The settings chosen in this study were based on analysing Scots pine which is a soft wood conifer, however they may not be applicable for different species and wood types.

This also highlights the need for developing a suitable standard, as adjustments to the settings or ablating different types of wood may make it difficult to compare results across species.

The ability to translate the output to concentrations would make cross species comparisons more robust.

2.6.4. Number of replicate tracks

Due to Ca spike outliers, the median was found to be the more robust measure of central tendency for each measured radii when using multiple tracks. As outlined earlier (Section 2.3.4.2), future studies could increase the amount of replicates run which would effectively smooth out the data. Five lines would be the recommended minimum, however, this would increase the cost and time taken for analysis but may provide a more robust approach for deriving a non-biased estimate of Ca change through the samples.

2.7. Future Work

Traditional dendrochronological methods work very well with clear ringed trees in temperate and high latitude regions. Calcium tracers were only used on Scots pine to test the potential of using calcium as an objective method for dating ringless tropical trees. However, one thing that was not explored in this thesis was what the calcium actually represents with regards to environmental forcing.

As the peak of calcium is in the earlywood it may offer new environmental information in addition to what can already be gleaned from ring-width, density or stables isotopes.

Traditional dendrochronology is a well-established method for dating trees and developing tree-ring proxies for climate reconstructions (Section 1.2). However, in some cases RW signals can be weak (Loader *et al.*, 2010) and although additional climate information can be gleaned from density and isotopes, wood chemistry properties may provide a new swath of potential environmental proxies. It is possible that the relationship between the seasonal calcium cycles in trees could provide such additional information. Before such data could be extracted, refinements to the method should be considered.

2.7.1. Spots vs. Tracks

Due to the focus of this study and its utilisation (next chapter) on ring-less tropical trees, continuous tracks were measured across the tree radii. The downside to this approach was biases were induced with the laser running over resin ducts resulting in abnormally high Ca values. These calcium spikes, although minimised using the median values, did still have an impact of the resultant signal. To test the possibility of using the seasonal calcium signals as a potential source of climate or other environmental information, individual spots in the earlywood and latewood could be measured across a selection of rings of many, established cross-dated, temperate trees. Analysing individual spots is a very fast process and since the laser ablation system has a mounted camera, it would be a straight forward task to set up multiple replicate spots across the rings. Such a method may be more suited to determining whether a climate signal is present within the calcium signal, however this approach would not have been appropriate for the objectives of this study and would not be possible at all on ringless tropical trees.

2.8. Conclusions

Analysis of Scots pine samples using LA-ICP-MS has demonstrated that calcium fluctuations are easily detectable and that they are seasonal in nature forming reproducible cyclic patterns across the annual tree rings, which are in agreement with previous observations made for calcium in tree rings (Follet-Gueye *et al.*, 1998, Arend and Fromm, 2000). The use of Scots pine to test the nature of the calcium fluctuations was beneficial since the tree rings in this species are well defined and can be calendar dated through cross-dating. The continuous manner of the measurements across the tree rings allowed the direct comparison of the calcium data from the ablated tracks against the cross-dated ring width data which verified the annual cyclic patterns as age. It was also beneficial as this direct comparison showed the cause of the calcium spikes in the data and other sources of potential error.

LA-ICP-MS provided a method to analyse wood laths, requiring minimal sample preparation, in an almost non-destructive manner as so little of the wood is actually ablated during analysis. This in itself is huge advantage over other methods of analysis since it leaves the remaining

wood available for other analyses. The tracks formed from the laser ablation process were easily visible which allows the exact areas analysed to be visualised. Although not considered here, this method can analyse multiple elements in the same sequence which reduces analytical costs that multi-element analysis of this nature often requires.

An objective statistical approach was taken to develop and test a method using the calcium data to estimate the age of the samples which could be applied to other species, including tropical ringless species, without major refinements. The results, using a >1SD threshold for the Scot pine samples had an average error of ±6 years which would be a vast improvement for dating tropical ringless trees which is not possible through traditional dendrochronological methods. Previous attempts of dating such ringless trees has had minimal success using stable isotopes (Section 1.4.3) which can be expensive, in terms of preparation time as well as analytical costs, and does not guarantee success. The methods developed here for Scots pine will be applied to a ringless tropical species from Cameroon in the following chapter.

Chapter 3: Calcium Tracers and the Dating of Tropical Trees

3.1. Introduction

The problems associated with dating tropical trees were discussed in Chapter 1 (Section 1.3). Traditional dendrochronological dating is possible only where distinct annual rings are present (Berlage, 1931, D'Arrigo *et al.*, 1994, Stahle, 1999, Fichtler *et al.*, 2004, Schongart *et al.*, 2004, Therrell *et al.*, 2006), however many tropical species do not develop distinct rings and therefore other methods of dating are required. Cambial wounding and dendrometer bands have been used to measure growth rates on ringless trees (Sass *et al.*, 1995, da Silva *et al.*, 2002, Ohashi *et al.*, 2009) but these methods are limited as they can only assess growth trends over a very small percentage of a tree's life. The use of stable isotopes in ringless tropical trees (Section 1.4.3) has had some success in dating (Evans and Schrag, 2004, Poussart *et al.*, 2004, Poussart and Schrag, 2005, Anchukaitis *et al.*, 2008b, Ohashi *et al.*, 2009, Loader *et al.*, 2011) but can be an expensive and time consuming analytical method that does not guarantee success. Poussart and Schrag (2005) found that one third of the tree species they analysed did not produce a useable isotopic series.

A possible alternative dendrochemical method was introduced by Poussart *et al.* (2006) using calcium as a tracer for observing seasonal patterns in the tropical species. However no further work was carried out in this area. This concept was evaluated in Chapter 2 where a method for analysing the calcium signal in trees using Laser Ablation-Inductively Coupled-Mass Spectrometry (LA-ICP-MS) was developed and tested using Scots pine, a temperate species with well-defined annual rings. A clear seasonal calcium pattern was found in the Scots pine and an objective statistical threshold method was developed for providing an age estimate, within ±6 years of the actual age. Using LA-ICP-MS and the analytical method had the added advantages of (1) requiring little sample preparation, (2) utilising an on board camera which allows the visualisation of the sample and the selection of the exact area for analysis, and (3) destroying minimal amount of the wood allowing the possibility of further analysis.

The objectives of this study revolve around validating the potential of the calcium method for dating tropical trees:

- Apply the methods detailed in Chapter 2 to a ringless tropical species (*Terminalia macroptera*) to produce an age estimate based on calcium measurements
- Validate the annual calendar date estimates produced using the calcium tracers from tropical wood samples using ^{14}C dating
- Apply this dating method to other samples of the same species

Validation of this method could prove vital in providing a new method in which tropical ringless trees can be accurately dated. Instrumental data in the tropics is sparse and limited in length, therefore alternative proxy records are required to gain an understanding of past climates and to expand on the available instrumental data. Without dating control, interpretation of dendrochemical studies such as isotopic analysis is not possible.

3.2. Study Area and Sample Collection

The study area was situated within the Mbam Djerem National Park (5°50'12.80" N; 12°42'47.31" E) in Central Cameroon (Figure 3-1). This area was chosen as an opportunity arose to accompany the Tropical Biomes in Transition (TROBIT) project research group. TROBIT is a NERC-funded consortium (www.geog.leeds.ac.uk/research/trobit) involving researchers from many UK universities and international partners from Africa, South America and Australia. The central objective of TROBIT is to obtain new and better predictions of the state of the future Earth System by examining the role of tropical biome transitions in affecting the magnitude and rate of future climate change and the response of these transitions to climate change. Focusing on the historical, current and future dynamics of forest-savanna transitions could assist in developing an improved ability to predict tropical biome distributions.

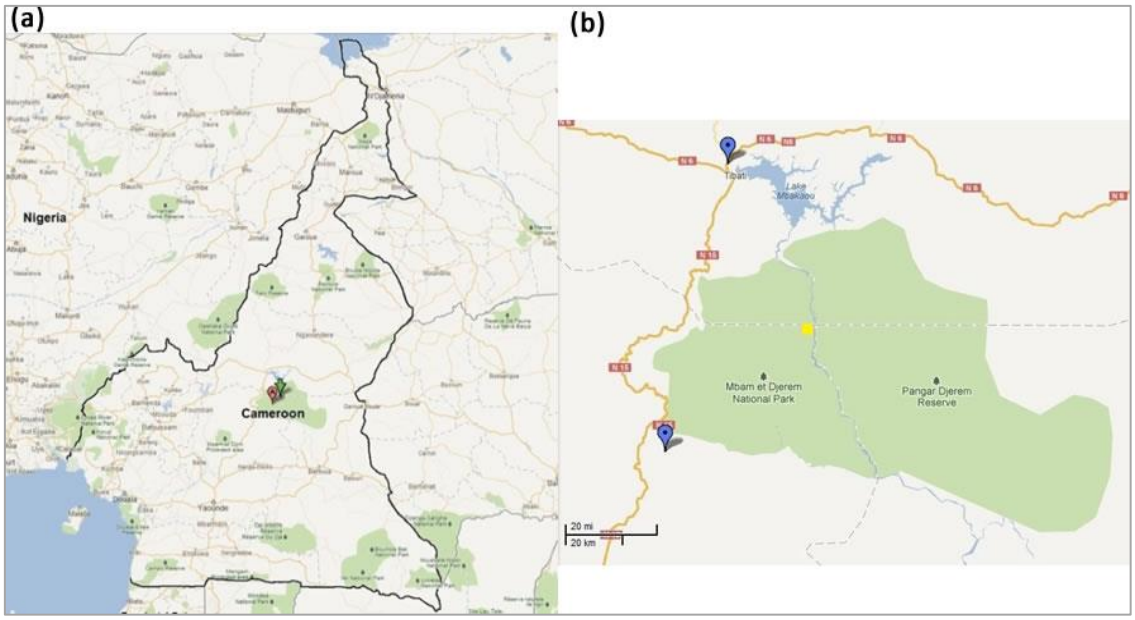

Figure 3-1: (a) Map showing the general location of Mbam Djerem National Park in central Cameroon. (b) The yellow square in the centre of this map represents the fieldwork location within the park. The blue flags represent the locations of the nearest climate stations; Tibati is north, and Yoko is East of the park. Both maps were downloaded from Google Maps.

Mbam Djerem National Park was declared a national park in 2000 and covers 4165Km^2 including areas of lowland rainforest, woodland gallery forests and savannah. It has been managed by the Wildlife Conservation Society since 2003 who confirmed the presence of more than 360 species of birds, 60 species of mammals, 65 species of reptiles, 21 species of fish and a high diversity of plant species making this the most biologically diverse protected area in Cameroon (Pouomegne, 2008). The area experiences an average annual rainfall of 1650mm and has a pronounced dry season beginning in November and ending in March, with an average monthly rainfall of 30mm during these months (Figure 3-2). The driest three months are December, January and February with an average rainfall of < 10mm month^{-1}. The data presented in Figure 3-2 shows the average monthly rainfall from the two nearest stations and their relative locations to the field site are illustrated in Figure 3-1.

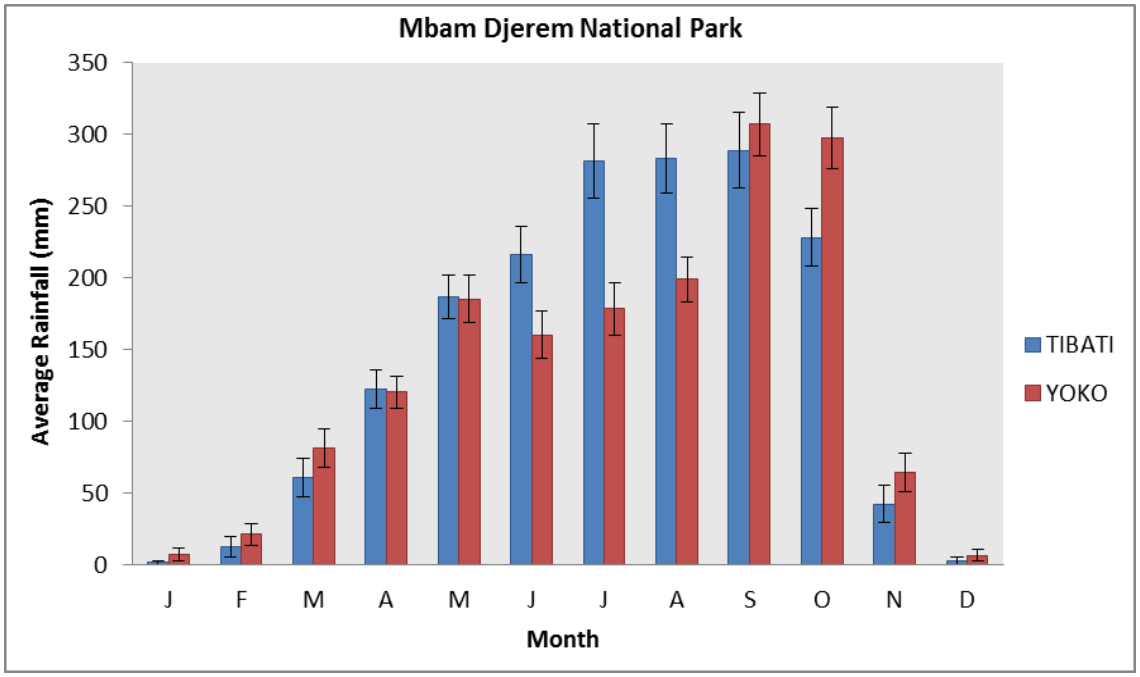

Figure 3-2: Average monthly rainfall data (±2 SEM) from the Tibati and Yoko weather stations (KNMI Climate Explorer, http://climexp.knmi.nl). Data has been averaged for each month for each year between 1940-1994 (data between 1994-present not available).

Tree samples were collected from the field site (located 5°59'08.33" N; 12°52'12.86" E) which lies within Mbam Djerem National Park (Figure 3-1) in Nov/Dec 2007. Wedges were cut from *Terminalia macroptera* Guill. & Perr. (Combretaceae) trees, dominant species found in the savannah region in the area represented by the light regions in Figure 3-4 (b). The savannah frequently experiences fires during the dry season and evidence of fire could be seen on the bark of some of the trees in the field area.

Terminalia macroptera (Figure 3-3) is a deciduous, hardwood tree which is mainly distributed in Western Africa (Pham *et al.*, 2011) and is usually found in savannah sites. It is a common, sometimes dominant species between 10-20m high with a fire resistant deeply fissured corky bark (Arbonnier, 2004). It has a hard, dense, yellowish brown wood which is used for a broad range of purposes including carpentry, beehives, firewood and charcoal. The leaves, bark and roots are used to treat a vast range of diseases and ailments including depression, jaundice, epilepsy, snakebites, tooth decay and tuberculosis (Arbonnier, 2004, Pham *et al.*, 2011). Previous studies using this species have focussed on analysing the components of the roots, bark and leaves of this species to assess their medical properties (Silva *et al.*, 1997, Silva *et al.*, 2010, Pham *et al.*, 2011) and no studies could be found which attempted to date trees of this species, therefore it was difficult to establish what age these trees could reach.

Figure 3-3: Example of *Terminalia macroptera* growing in the savanna. Most trees were found to grow in this asymmetrical manner.

Five *T. macroptera* trees were analysed in in this study. Samples 2A and 2T were collected from trees found growing in the transitional zone between the forest and savannah boundary, where the forest had expanded into the savannah. Sample 2Y was collected from a tree growing in the savannah, and samples 4P and 4Q were from trees which were situated in a younger forest. In this region, only a few savannah trees were remaining since the forest expansion. Figure 3-4 (b) illustrates the locations of the trees in relation to the forest-savanna boundary. After sample collection, each tree wedge was allowed to air dry before transportation.

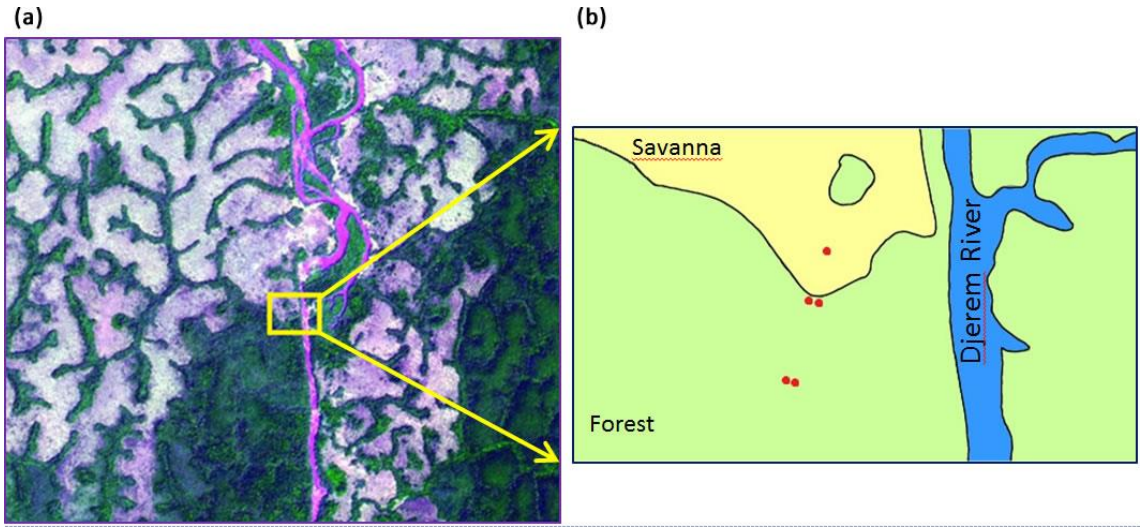

Figure 3-4: (a) Satellite image from 2006 showing the location of the field site within Mbam Djerem National Park (yellow box). The light areas represent savannah regions, darker green areas are forest and the Djerem river is pink. Image downloaded from USGS Global Visualisation (http://glovis.usgs.gov). (b) Shows a representation of the sampling locations (red dots) for the 5 trees in relation to the forest-savanna transition.

3.2.1. Preliminary Radiocarbon Age

Shortly after collection of the wood samples from Cameroon, an explorative radiocarbon date (SUERC-21124 (GU-17822)) was obtained for one sample of *T. macroptera* to ascertain a rough potential age of the trees sampled. The results are given in Table 3-1 and Figure 3-5 below.

Table 3-1: Results from the analysis of a single radiocarbon date obtained from the pith region of a *T. macroptera* tree. Analysis was carried out by the Scottish Universities Environmental Research Centre (SUERC), East Kilbride, Scotland.

Laboratory Code	**SUERC-21124 (GU-17822)**
$\delta^{13}C_{VPDB}$‰	-25.5 ‰
Radiocarbon Age BP	105 ± 30
Fraction Modern Carbon	0.9868 ± 0.0031
Calibrated age ranges (2σ)	AD 1682 – AD 1736 (27.5%)
	AD 1805 – AD 1933 (67.9%)

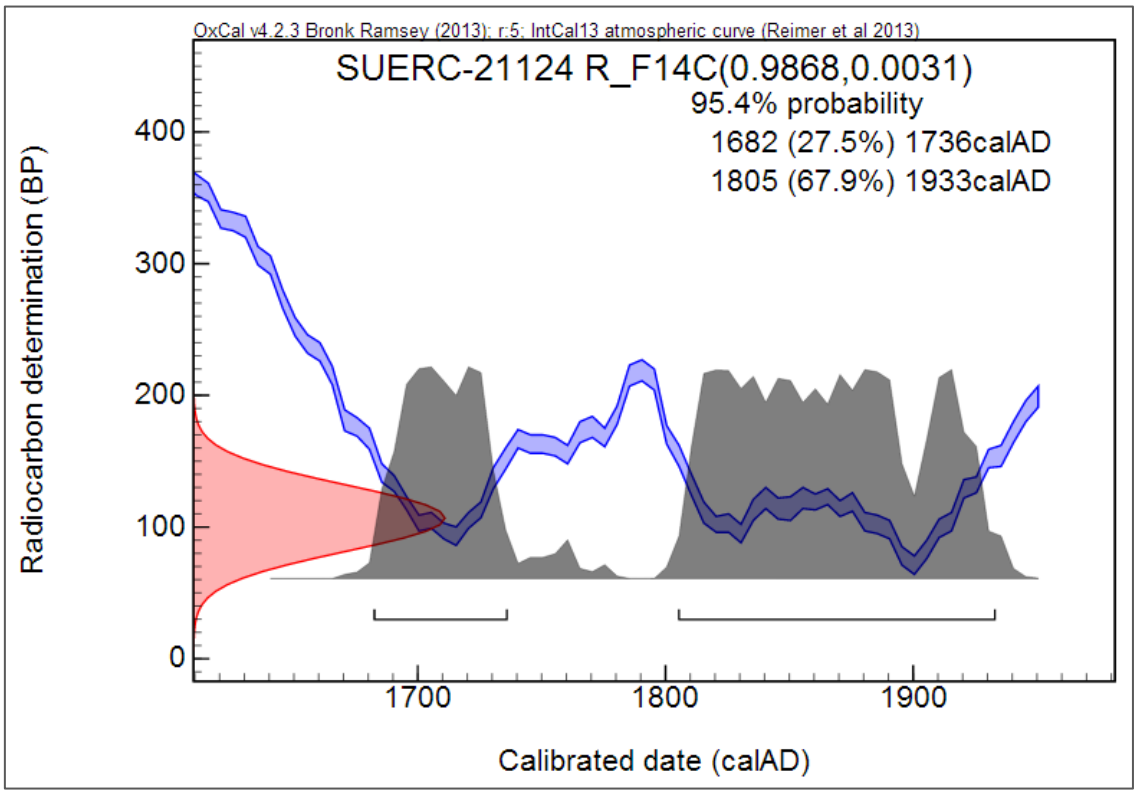

Figure 3-5: Shows the output radiocarbon plot obtained using the OxCal online calibration software available from https://c14.arch.ox.ac.uk/oxcal using the intcal13atmospheric curve (Reimer *et al.*, 2013)

A calibrated date range was obtained using the OxCal online software (Figure 3-5). The red curve indicates the radiocarbon age of the sample, the blue lines represent the radiocarbon measurements of a known age material, and the likelihood of the different possible ages is represented by the grey shaded areas. At the 95% confidence level the sample "dates" to the period of AD 1682-1736 or 1805-1933 with the relative likelihood for these individual ranges provided in brackets on Figure 3-5. This gives a very large range of potential ages for this sample and clearly highlights the difficulty of dating ringless tropical trees over the recent centuries. Consideration of this age range which has the highest likelihood within the 95% probability (1805-1933), still puts the tree's age within a 128 year bracket giving it an age anywhere between 73-202 years old.

It is unfortunate that this sample fell within this particular period of the radiocarbon curve since this has not provided an age for the sample with an acceptable error for any relevant environmental analysis. The problem is not limited to this particular sample, as it is associated with most living trees which rarely gain ages > 300 years. Radiocarbon dating is an expensive process which, as seen here, may not necessarily narrow down a tree's age if only one date per tree if obtained. This would not be an adequate approach to provide an exact age of a sample and would result in difficulties for environmental research.

A preferred method for radiocarbon dating would be to acquire several dates for each tree and to obtain a dating profile along the tree's radius. Several dates around the 'bomb peak' period would help constrain the dating of tropical species and allow the development of growth rate estimates for the periods between the radiocarbon dates. Nuclear weapons testing carried out during the 1950's and 1960's substantially influenced the amount of ^{14}C in the atmosphere resulting in a significant peak occurring in the 1960's (Levin and Kromer, 2004). The weapons testing was carried out in the northern hemisphere where the timing of the bomb peak is in 1963 (Goslar *et al.*, 2005). The bomb peak is observed slightly later in 1965 in the southern hemisphere (Currie *et al.*, 2006) due to the time taken for the northern and southern hemisphere air to mix, and as a result is slightly lower (Figure 3-6). Due to the high costs involved with radiocarbon dating, such approaches are not always feasible on multiple trees. This emphasises the need for alternative tree dating solutions in the tropics.

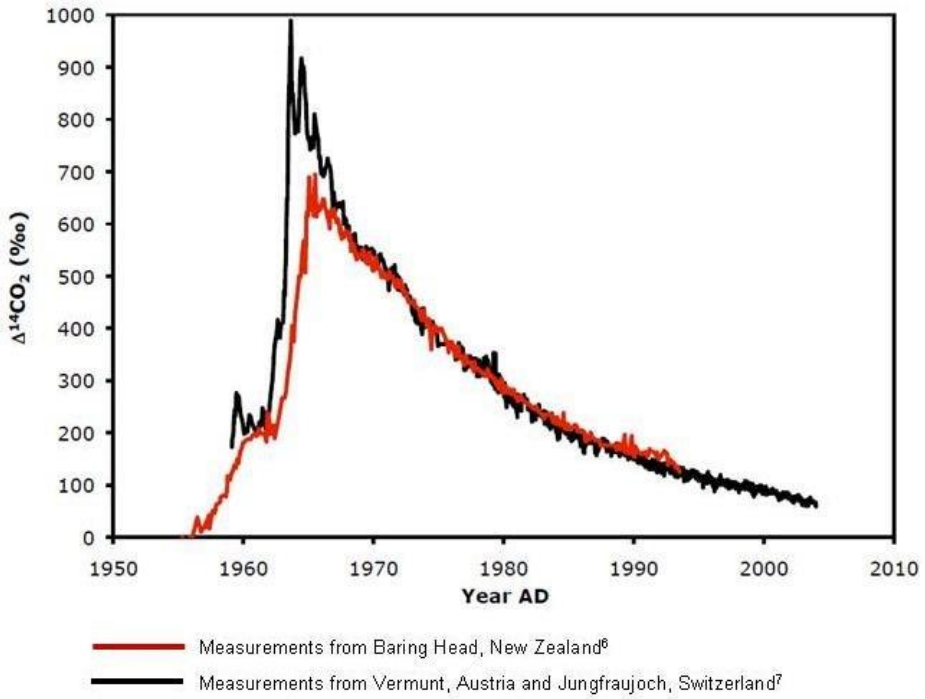

Figure 3-6: Graph showing the effect on the ^{14}C levels in the Northern and Southern Hemispheres caused by the weapons testing during the 1950's and 60's. The peak of the bomb spike is slightly lower and later in the southern hemisphere. Image from Earth System Research Laboratory (NOAA, 2012).

3.3. Materials and Methods

3.3.1. Sample Preparation

Before elemental analysis was performed, a sample of *T. macroptera* was inspected under a light microscope to examine the nature of the wood structure and to determine if ring width measurement was possible. A section from a tree wedge was sanded using fine abrasive papers ranging from 400 to 1200 grit to allow the structure of the wood to be visualised more clearly. Traditional dendro methods were attempted using scanned images of the wood and measuring ring-like structures using CooRecorder v. 7.3 (Cybis Elektronik & Data AB, 2010) software.

The sample preparation for LA-ICP-MS analysis was performed in a similar way to the method detailed in Chapter 2 (Section 2.3.1) and is summarised here. Laths, approximately 1cm wide x 0.5cm thick, were cut from the tree wedge sections using a band saw. Due to the size limitations of the laser ablation sample chamber, the laths were split into smaller sections (up

to 4cm length) and prepared in the following manner. Each lath was initially sanded using a 120 grade abrasive paper to produce a flat surface and to allow the nature of the wood to be visualised. Although annual growth increments were not apparent in this species, the direction of growth and some ring like structures (Figure 3-7) were clear, allowing the laths to be cut diagonally over these structures ensuring overlap on each section (Section 2.3.1). The cuts were made by etching a groove into the wood with a clean blade and snapping the lath along this line. Each section was then sanded using progressively finer grade abrasive paper up to a maximum of 2500 producing a flat, smooth surface. Excess wood dust was removed using compressed air. The proposed laser ablation paths were lightly marked using a scalpel blade following the direction of growth on each section, ensuring that measurements from each section would overlap with the next.

Figure 3-7: Example of *Terminalia macroptera.* The wood contains ring-like structures, however there are not of a consistent nature.

3.3.2. LA-ICP-MS

The elemental analysis was carried out using a NewWave Research 213 Laser Ablation System coupled to a Thermo X-series 2 ICP-MS (Section 2.3.2). Daily auto-tuning procedures for the ICP-MS were carried out to optimise the ion path and then afterwards, the plasma was allowed to settle for 30 minutes before analysis.

The operating conditions used for the Scots Pine samples in Section 2.3.3.2 (Table 2-3) included a 100µm laser spot size with a transit speed of 20µm/s. Although the growth rates were unknown for this species, the single explorative radiocarbon date (Section 3.2.1) indicated a possible age range. The error from this single date was large, but suggested that growth rates could be relatively low which would result in a small amount of wood being laid down per annual increment. It was found when analysing calcium in the pine samples that the settings used may not have provided enough sensitivity to allow the detection of particularly narrow rings. The laser operating conditions were therefore modified to account for potential small incremental growth. The laser spot size was reduced from 100µm to 40µm which reduced the amount of material ablated and therefore the overall intensity of the calcium counts. Although the counts were still within the detection limits of the machine, this may have proved problematic if counts were lost over time as observed in the Scots pine measurements (Section 2.3.4.3). The transit speed of the laser was therefore reduced to 10µm/s which increased the count intensity. The operating parameters used for the calcium measurements of *T. macroptera* are summarised below tin Table 3-2.

Table 3-2: Operating parameters used for analysis of *Terminalia macroptera*. The spot size for elemental measurements was reduced to 40µm/s however the preablation spot size was left at 100µm.

LA-ICP-MS Operating Parameters	
Carrier gas flow (He)	0.76 L/min
Laser Power	80%
Pulse frequency	20 Hz
Laser warm-up time	10s
Pre-ablation	100µm spot, 70µm/s transit, 40% power
Spot diameter	40µm
Laser transit time	10µm/s

3.3.2.1. Laser Ablation Sampling

Each sample was measured alongside a pellet of NIST Standard Reference Material 1575a (Pine Needles), which was used to monitor the stability of the output measurements. As previously discussed (Section 2.3.3.2), no suitable matrix matched standards are currently available for the laser ablation of wood, therefore element concentration data could not be obtained for these measurements. Each wood section was mounted onto the sample holder and levelled alongside the NIST standard pellet. The camera was focussed onto the loaded samples, and the ablation tracks were marked out along the length of the tree lath (following the previously lightly marked line) in the direction of pith towards bark. 2mm lines of the NIST standard were ablated before, after and between each measurement of the wood sections. For each wood section, a total of three replicated tracks were measured at a distance of 0.2mm apart (Figure 3-8). Immediately before laser ablation began, elemental analysis of the background gas which passed through the sample chamber was recorded to be used for gas blank subtraction. Each line was pre-ablated before the measurements to prepare the wood surface for ablation. Laser sampling was carried out in a continuous manner and data was collected in peak jumping mode for both the ^{44}Ca and ^{13}C isotopes.

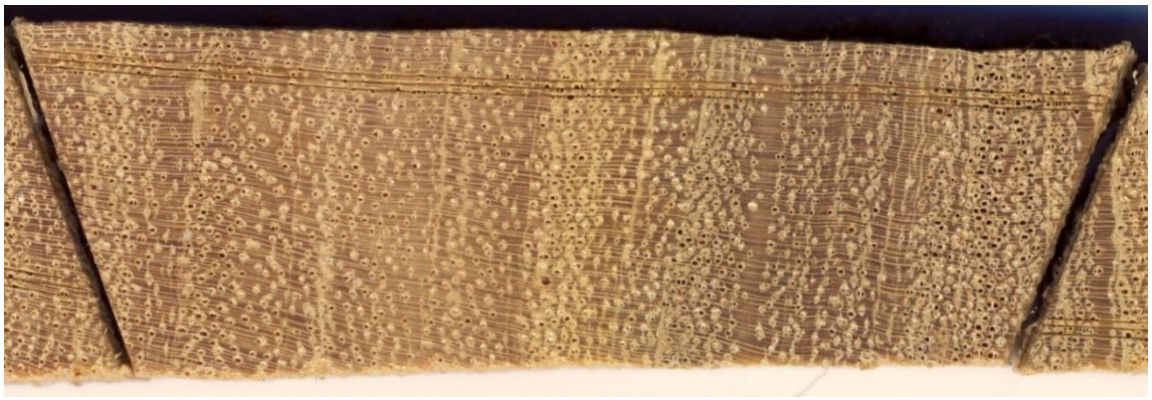

Figure 3-8: Example of sub-sectioned portion of a *T. macroptera* lath showing the three replicated laser ablated tracks across the length of the section. Each track is 0.2mm apart

3.3.3. Data Adjustments

As discussed in Chapter 2 (Section 2.5.4), the raw data was adjusted in a systematic manner to allow the splicing of tree lath sections. The data was exported from the LA-ICP-MS computer and treated in a similar manner to the data from the Scots pine analysis (Section 2.3.4.1). The mean gas blank values for each element was calculated and subtracted from each run of each sample and the data from each run was normalised to ^{13}C which was used as an internal standard. The median of the three replicated data tracks for each section were calculated and the resultant median data detrended using a high pass Gaussian filter. Each individual section dataset was finally converted to z-scores (mean of zero and standard deviation of 1) which were required to stabilise the variance through the full spliced time series for each tree, allowing the linkage of datasets from different days of analysis. Converting the data into z-scores aligned all the data onto a common scale allowing identification of potential seasonal calcium cycles using the threshold approach discussed in the previous chapter (Section 2.5.4.2).

Once in z-score format, the data for each individual section was spliced into a single dataset for each tree. To ensure sections were joined correctly, the distance was measured on each part of the core relating the position of linkage, and the data for each section was spliced together (Figure 3-9). The full length of the ablated tracks on all sections was measured (minus the overlapped sections) and compared with the resultant length of the laser dataset to ensure that the splicing of data was successful and data was not lost. Tree growth can vary around the circumference of a tree resulting in uneven amounts of wood being laid down around the tree. This can be more pronounced in situations such as when a tree grows on a slope or in cases where the trunk is bent such as can be seen in Figure 3-3.

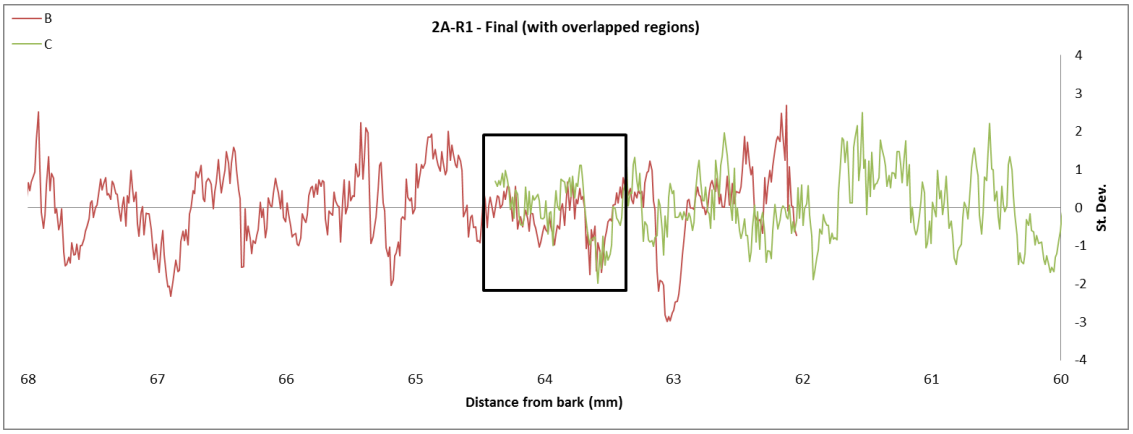

Figure 3-9: Example of overlap region between tree 2A-R1 sections B and C as highlighted within the black box.

3.3.4. Calcium Dating

Qualitatively, the data for this tropical species appeared to be noisier than for the Scots pine samples (Figure 3-9) which may have been a result of the reduced spot size and slower speed used for the analysis or due to the physical differences between wood types and species. This additional noise in the data could lead to potential problems and misidentification of annual cycles.

The same threshold approach, as detailed in Chapter 2 (Section 2.5.4.2), was applied to the tropical tree data. Peaks in the data points would be marked as a boundary for an annual growth phase if the peak met certain conditions. As the samples were taken in 2007, each radius was assigned yearly values with 2007 as the outer date using the assumption that each point meeting the threshold value represented one year. For example using the >1 standard deviation threshold, data points were marked as an annual growth boundary if the first data point with a value > 1 standard deviation above the mean. Any sequential points immediately after, which also met this condition, were not marked as an additional growth boundary as they were assumed to be part of the same growth year. A further condition was required due to the spot size and distance between each measured data point. Each point was recorded at ~13µm apart with a spot size of 40µm therefore to ensure there was no overlap between measurements and to reduce the possibility of the same peaks being measured twice, a minimum distance of 80µm (2x spot size) was required between the threshold values before being marked as an annual growth boundary. Any data point which was > 1 and did not

immediately follow an already marked point (i.e. had data points < 1 between this and the previous assigned annual cycle) was marked if there was at least 80µm distance between this and the last marked boundary. Each calcium cycle was assigned a date based on the assumption that each cycle was annual. Several different thresholds were tested (details below).

In addition to testing various thresholds, the effect of a smoothing function was also tested. Due to the apparent noisiness of the calcium data for this species and to avoid spuriously identifying too many peaks as annual cycles, a smoothing function was applied to the data to assess the differences between assigned years (Figure 3-10). A 4-point moving average was chosen to smooth the data as 4 points was approximately equal to the spot size used in analysis.

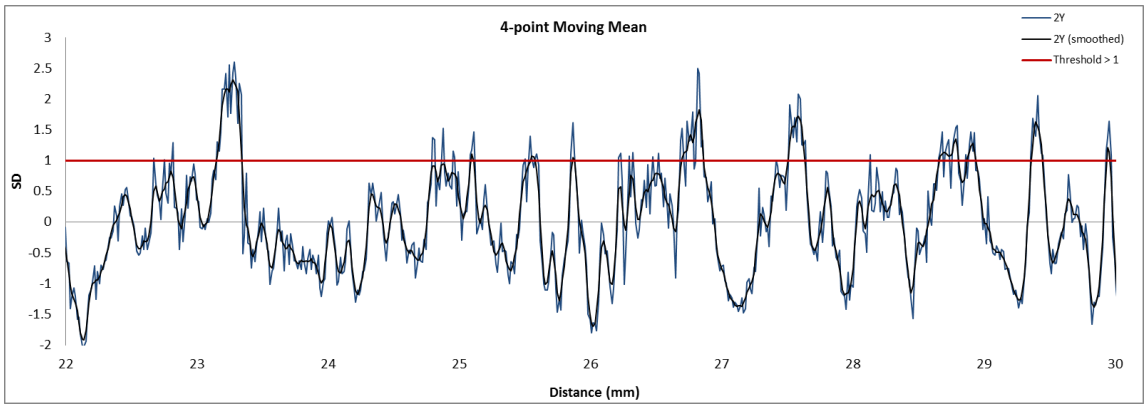

Figure 3-10: Example of applying 4-point smoothing function through the data.

The remaining methodical procedures in this Chapter initially focussed on tuning and defining an error estimate for the optimal calcium threshold. This was first made on a single sample and was facilitated using ^{14}C dating to constrain the dating of the tree. Once identified, the "optimal" calcium threshold which provided the best agreements with the ^{14}C dates was then tested on an independent second sample of the same species (located <100 metres away) where it was assumed growth rates would be similar. Radiocarbon dates were acquire for this second sample to validate the calcium threshold dating method.

3.3.4.1. Within Tree Calcium Threshold Error

The calcium record for tree 2A was measured along 2 radii. Comparisons could therefore be made between these records to give an indication of the within tree dating error. Anatomical features common to both radii (i.e. consistent around the tree) were used as fixed age tie points where it was hypothesised that they should have the same relative age. Fourteen common physiological features were chosen as reference tie points (Figure 3-11) and allowed detailed analysis of the within tree error by continuing assessment of the differences between the threshold assigned annual peaks over the length of the measured radii. The numbered areas on the image represent the equivalent positions for comparison on each radius. For each comparison point, the distance that they fell along the laser ablated tracks was measured for each radii. This distance measurement was then compared with the adjusted calcium data (for each radii), providing an equivalent calcium year as assigned by each of the tested threshold conditions. Two of the points compared covered the locations where two radiocarbon dates were taken (see 3.3.5). Results were obtained for each radius, using both the smoothed and non-smoothed data, for the following iterations:

- Calcium years using threshold > 1
- Calcium years using threshold > 1.25
- Calcium years using threshold > 1.5
- Calcium years using threshold > 2

It is clear from Figure 3-11 that growth is not equal around the circumference of the tree. This is particularly clear when comparing the positions of points #7 and #8 where there is a clear wedging of the wood resulting in potentially different increment counts between both radii. This is a known common problem in many tropical species (Tarhule and Hughes, 2002)

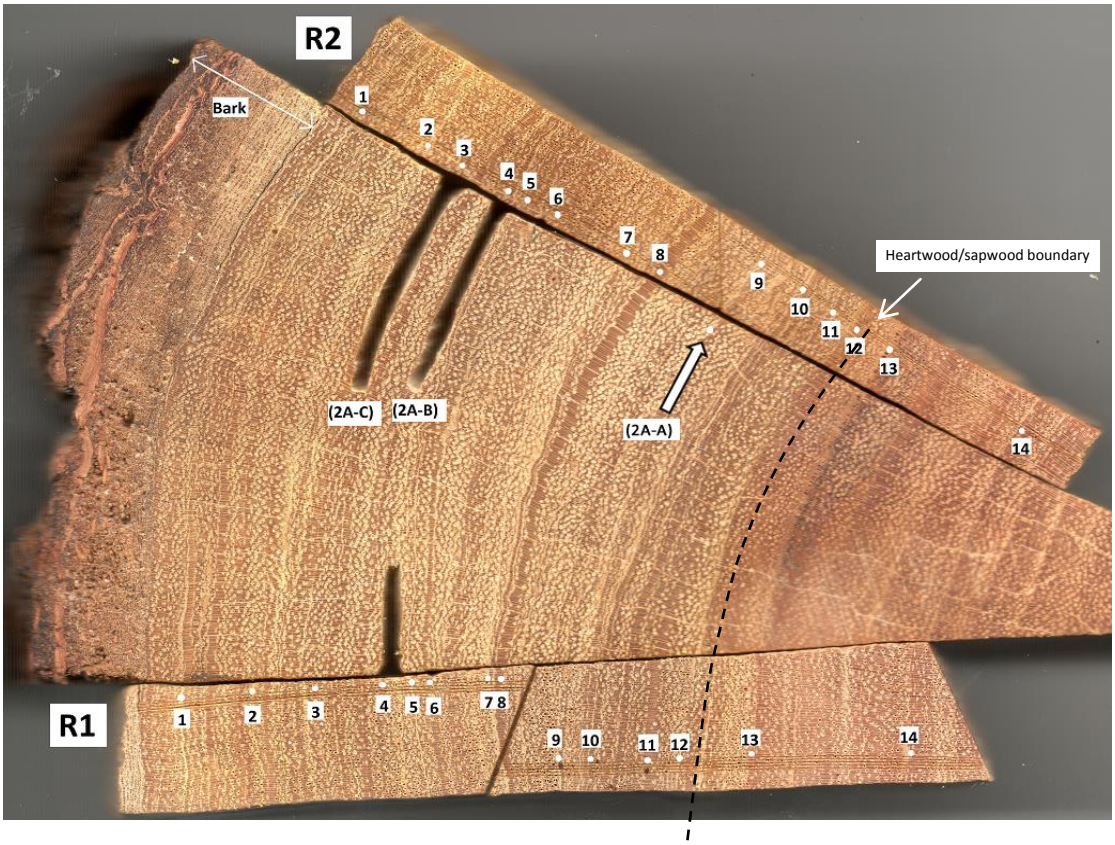

Figure 3-11: Image shows the positions of the calcium assigned year comparisons made between each radius for tree 2A. The area where the wood has been removed represents the areas for two of the radiocarbon dates (2A-B and 2A-C), with the location of 2A-A radiocarbon dae indicated by the white arrow. The H/S boundary position is shown by the dashed line.

3.3.5. Radiocarbon Sampling

Funding was sought for radiocarbon dates in a two-step process with the initial step focussing on using ^{14}C dates to initially "optimise" the calcium dating by testing the threshold approach of assigning years. The second step aimed at validating the consistency of the calcium dating "optimal" methodology for this tree species using an independent tree.

3.3.5.1. Tuning of Ca Dating Method

The funding application for radiocarbon dates to validate the calcium dating method had initially requested 9 AMS dates from each of two *T. macroptera* trees. This proposed 'ideal'

approach would have included the pith dates to constrain the overall tree ages, the bark dates, and 7 further dates per tree to provide high resolution AMS dates around the bomb peak and therefore allow validation of the calcium counts. Although the application for dates was successful (NERC allocation number 1562.0411), only funding for 5 dates was provided. Unfortunately, due to the timing of receiving the radiocarbon funding, sampling and submission of the tropical tree samples was required to be done before the Ca data analysis method and ring detection methods had been finalised. Due to this low number of samples, and the preliminary nature of the Ca method at the time, the three samples were likely not located in an ideal location with regard to the bomb peak.

The five analyses comprised of:

- One sample from the pith of the tree to help constrain the age of the tree
- One sample from just beneath the bark to confirm the ^{14}C levels for the recent period
- Three samples on either side of, or at relative points on the declining limb of the bomb peak

The Ca track data were processed in a similar way to that described in Section 3.3.3, but as it was during the early stages of development some differences between procedures are summarised here. During this processing, the data were not normalised to the internal standard, the mean was calculated rather than the median, and the high pass Gaussian filter used an arbitrary wavelength. The peaks were counted using a >1 threshold approach and samples taken at years that were estimated as 1965 and 1975.

Shavings of wood were cut from tree 2A using clean scalpel blades, packaged in tinfoil, and sent to the NERC Radiocarbon Facility (East Kilbride) for processing and analysis. Accelerator mass spectrometry (AMS) ^{14}C dating was performed at the Scottish Universities Environment Research Centre (SUERC) AMS Facility, East Kilbride, with the sample preparation carried out at the NERC Radiocarbon Laboratory. The following pre-treatment process was carried out for each of the four wood samples by this facility prior to ^{14}C determination (method provided by NERC Radiocarbon Facility).

Each sample was digested in 4M HCl at 80^{o}C for 8hrs, then washed free of mineral acid with deionised water and digested in 2M KOH. The digestion was repeated using deionised water until no further humics were extracted. The residue was washed with deionised water to remove alkali traces, digested in 1M HCl at 80^{o}C for a further 5 hours, and then rinsed free of

acid with deionised water. The de-humified wood was digested at 70°C in acidified sodium chlorite solution (13g $NaClO_2$ + 2ml conc. HCl in 500ml deionised water) until the entire sample had been oxidised to cellulose, i.e. a white flocculent precipitate. The cellulose was filtered through glass fibre filter paper (Whatman GF/A), washed acid free with hot deionised water and dried in a box oven. The total carbon in a known weight of the pre-treated sample was recovered as CO_2 following combustion in an elemental analyser. The gas was converted to graphite by Fe/Zn reduction, ready for AMS analysis.

3.3.5.2. Validating the "Optimised" Ca Dating Method

A follow up application was submitted to NERC for phase 2 of this validation process. Funding was allocated for a five additional ^{14}C dates (NERC allocation number 1720.0413) to test the Ca dating method on an independent sample of the same species (tree 2Y). The optimal approach identified for the first tree (2A) was applied to the second tree (2Y) and the calcium dated based date ranges were compared to the radiocarbon dates.

As with tree 2A, one sample was taken from just under the bark to confirm the ^{14}C levels for the recent period and one sample from the inner portion of the tree (pith was not available) to help constrain the age of the tree. For the remaining three samples, two were taken from positions on which were estimated (using calcium method) to be at either side of the bomb peak record so that one would be on the ascending limb, and the other on the descending limb. The fifth sample was intended to lie in the mid 1980's. Figure 3-12 illustrates the locations of these sampling locations on a scanned image of the tree lath.

After the locations had been determined, shavings of wood were cut from each location using clean scalpel blades, packaged in tinfoil, and sent to the NERC Radiocarbon Facility (East Kilbride) for processing and analysis. Sample pre-treatment and AMS analysis were carried out at the NERC Radiocarbon Facility as described above (Section 3.3.5.1).

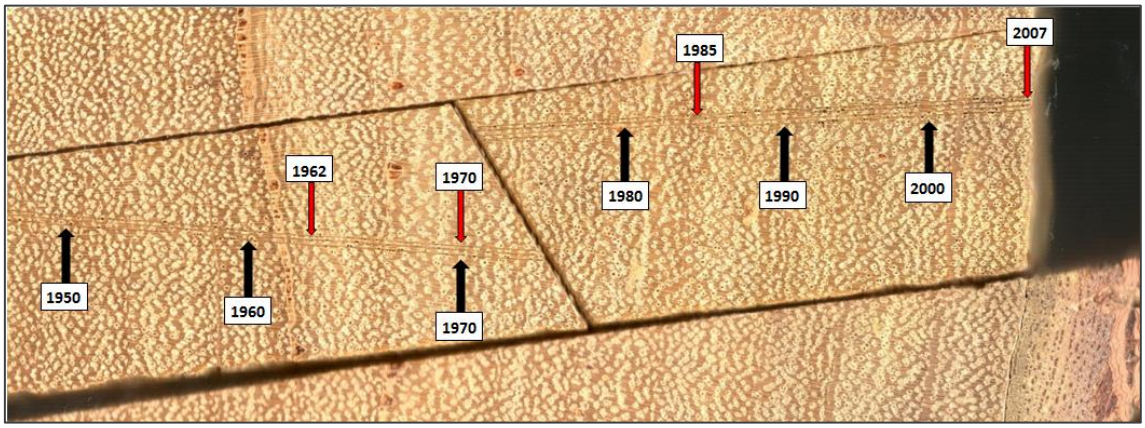

Figure 3-12: Scanned image of tree late 2Y after laser ablation analysis. Black arrows represent show 10 year increments as calculated using the >1.25 SD calcium threshold technique. Red arrows repesent the locations for the ^{14}C sampling based on the >1.25 threshold. The inner sampling location (2Y-Inner) is not shown here.

3.4. Results and Discussion

3.4.1. Wood Structure and Traditional Dendro-dating Methods

T. macroptera is a diffuse porous hardwood species, which is typical of many tropical species (Gourlay, 1995), and features many pores (vessels) throughout the wood. The visual examination of the wood identified some ring-like structures around the sample. The nature of these structures varied (Figure 3-13); some of the banding around the sample appeared as areas which were free from vessels, whereas other bands appeared as a thin line. Dating attempts were made between the 2 radii of tree 2A using Coo Recorder to measure the ring-like structures to attempt within tree cross-dating, however this did not yield reliable results due to the inconsistency of these bands. Identifying possible ring boundaries was difficult as often a feature which appeared to be a ring-like would fade further around the tree (Figure 3-13 (a)). Wedging was also found which made measurements inconsistent (Figure 3-13 (b)) between radii. These types of ring anomalies are not unique to tropical trees, however they can occur more frequently in tropical conditions (Tarhule and Hughes, 2002).

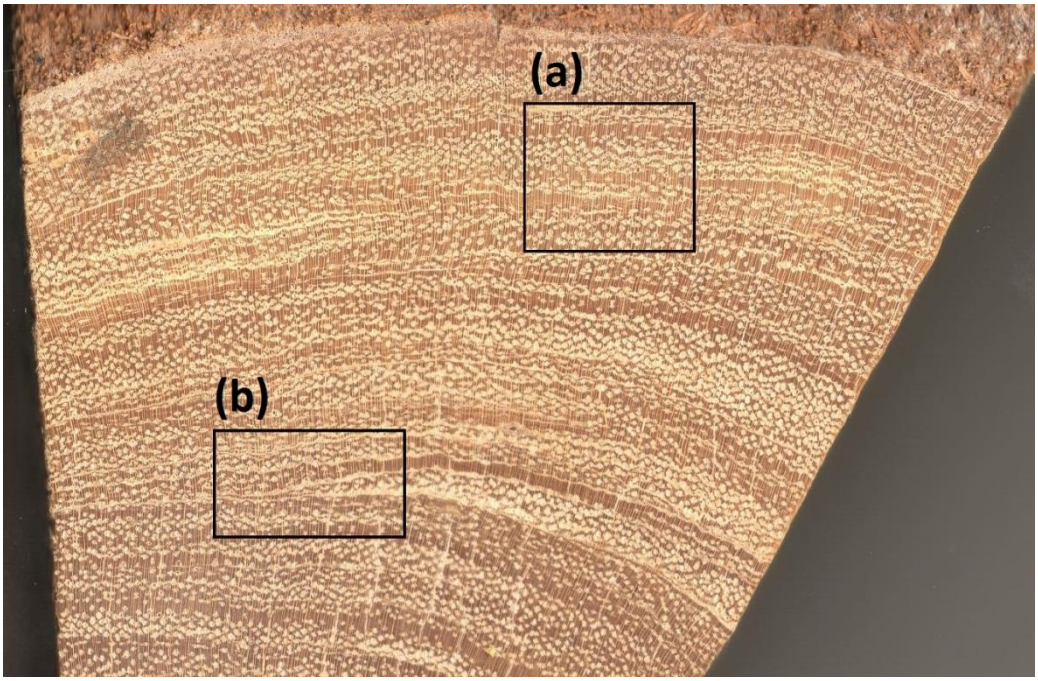

Figure 3-13: Two problematic areas are highlighted: (a) 3 bands without vessels are present at the right hand side of the box. The middle band fades towards the left hand side and becomes difficult to follow. (b) Shows an example of wedging, where banding pinches out resulting in incomplete banding around the circumference of the tree.

As a result of these growth anomalies, traditional dendrochronological dating attempts were quickly abandoned. It was possible to follow some of the ring-like features around the circumference of the sample, which although not allowing successful dating in this case, they were used as common dating tie-points of reference to assist with comparisons between calcium measurements. These problems highlight the need for alternative dating methods in tropical species. The *T. macroptera* considered here grows in an environment which experiences a distinct dry season covering at least 3 months of the year where almost no rainfall occurs (Figure 3-2) which should result in some degree of cambium dormancy. Banding is clearly visible on the wood; however it does not appear to correspond to seasonality and therefore does not allow a means to date these trees using normal tree-ring methods. As outlined in Chapter 1 (Section 1.3), this is not an uncommon problem in the tropics, and currently restricts opportunities for further tree-ring based research in these regions. A study in West Africa by Tarhule and Hughes (2002) also classified *T. macroptera* as having a 'poor' potential for dendrochronology. They studied and categorised over 70 species during this study, and only found 7 which were classed as 'potentially useful'.

3.4.2. Calcium Measurements and Seasonal Patterns

The calcium patterns observed in the Scots pine samples in Chapter 2 (Section 2.4.1) showed a clear cyclic pattern relating to the tree rings which, in the raw data, showed an overall decline in the counts over the life of the tree. This decline appeared to be a combination of an age related trend along with a loss of signal intensity over time caused by machine drift. The raw data for the *T. macroptera* trees was plotted and assessed for any features or trends across the tree radii and to ascertain if a cyclic pattern was present. Figure 3-14 shows the raw median $^{44}Ca/^{13}C$ plots for each tree (and lath sections). Each graph is plotted with the distance from bark (mm) on the x-axis against the $^{44}Ca/^{13}C$ ratio on the y-axis. No further adjustments to the data have been made at this stage therefore the sections are not aligned on a common scale. The overall intensity of the peaks can vary between sections and trees when measured on separate days. As discussed in Chapter 2 (Section 2.5.4), the lack of matrix matched standards prevents the translation of the raw calcium counts into concentrations, which would account for these differences.

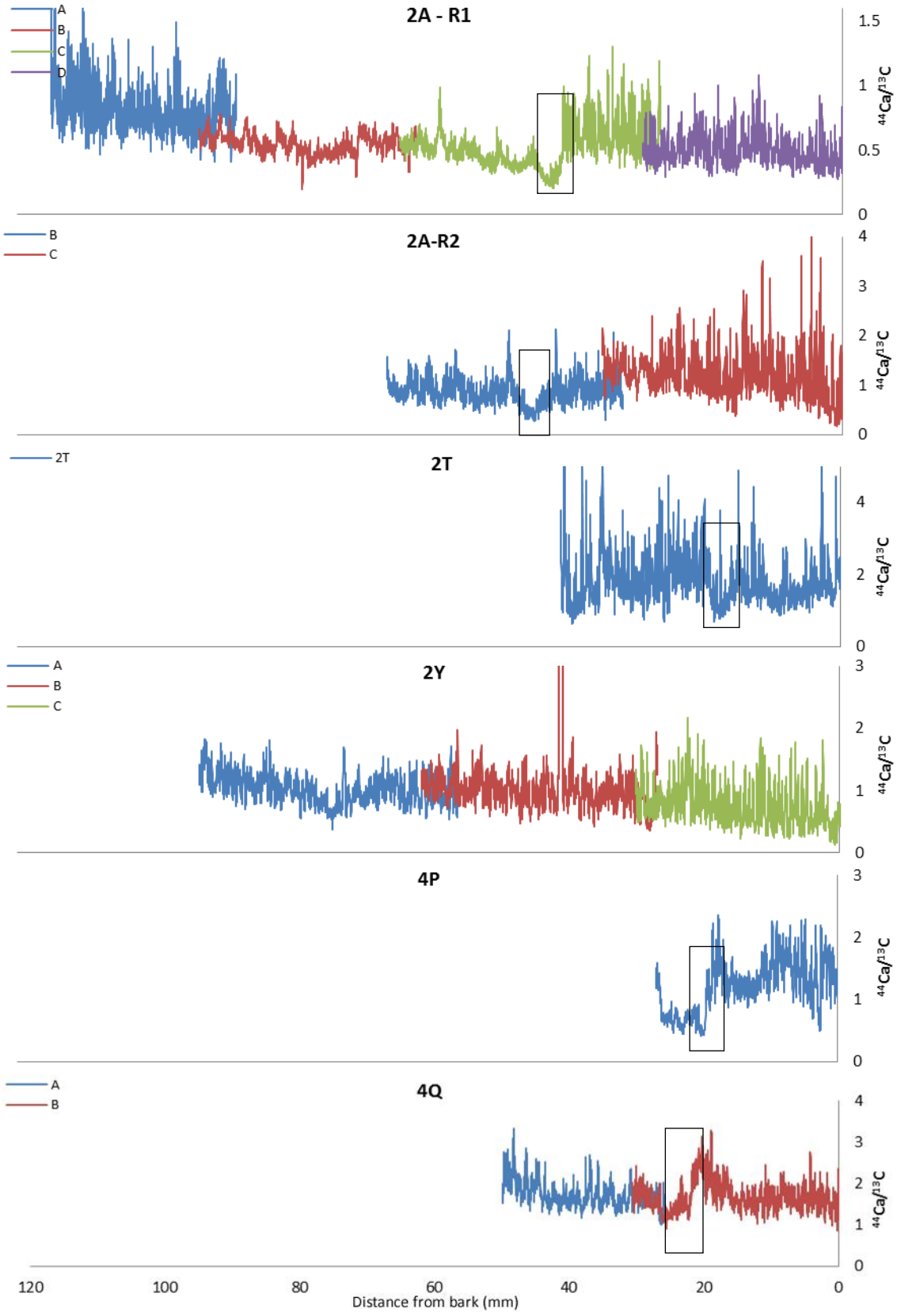

Figure 3-14: The above graphs plot the raw median $^{44}Ca/^{13}C$ values obtained for each of the trees measured. H/S boundary regions (where present) are highlighted within the black rectangles.

3.4.2.1. Heartwood/Sapwood Boundary

All of the trees except for 2Y appeared to express a clear heartwood/sapwood (H/S) boundary which resulted in a change in the raw counts. These areas are highlighted with black rectangles in Figure 3-14. In sample 2A-R1, the H/S boundary zone coincides with a dip in the counts followed with a sharp variance transition in the calcium record, observed midway through a section of the tree lath. A similar dip can be seen in the calcium record for the second radius for tree 2A (2A-R2) around the H/S transition area but there is no sharp change in signal intensity. Samples 2T, 4P and 4Q also feature a dip in signal around the H/S transition zone, but do not show any major variance change in the raw median values.

The variance change that was observed in tree 2A-R1 was not replicated in other samples, although it could be argued that the variance after the transition for tree 4P increased in a similar manner. However, there is not enough data prior to the change to confirm that. This variance change was replicated in all 3 tracks ablated across the wood, therefore a machine error or disturbance in the signal can be ruled out as a cause. It is more likely that this change relates to a physiolo gical change in the wood at the heartwood/sapwood (H/S) boundary. Figure 3-15 illustrates this change showing the plotted raw $^{44}Ca/^{13}C$ (median) data overlaid onto the scanned section of tree 2A-R1.

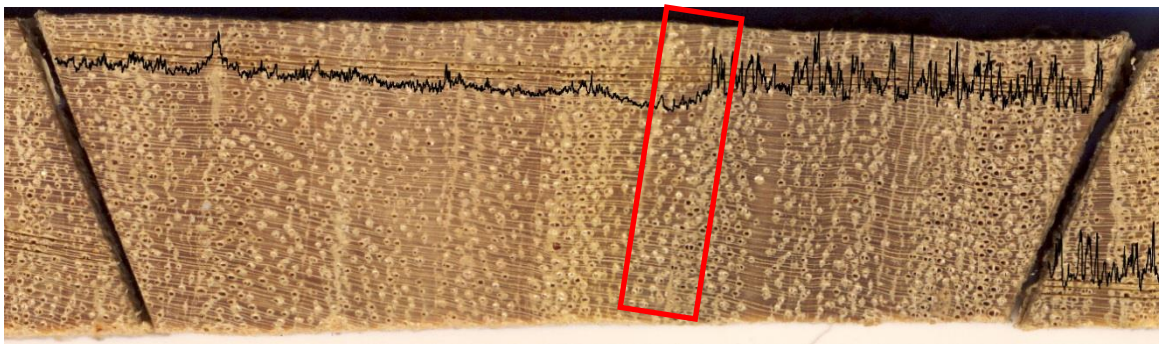

Figure 3-15: The raw median $^{44}Ca/^{13}C$ data is shown here overlaid onto the section B of tree 2A-R1. An abrupt change in the data intensity is shown here which may be caused by the H/S transition area (highlighted in red).

The change in calcium signal in 2A-R1 raises a few questions. If it was due to the differences between the storage properties of heartwood compared with sapwood as the three replicated tracks would suggest, then it would be expected for this feature to be present in the second radius of this sample (2A-R2) as well as in the other samples which crossed a heartwood/sapwood boundary. Other samples which contained heartwood did not appear to

experience the same variance change. Since the raw values cannot be corrected to a standard in this case, any such changes which may occur between lath sections may be missed. Until a suitable standard has been found, further comparisons between physical features of the wood are not possible. An alternative suggestion for the cause could be contamination. This however seems highly unlikely due to the care taken in handling and storing the samples. If contamination was the cause then this would have been surface contamination which would be removed during the sanding (sample preparation) and pre-ablation processes.

The raw $^{44}Ca/^{13}C$ records shown in Figure 3-14 for the *T. macroptera* trees generally appeared to show an overall similar response in the $^{44}Ca/^{13}C$ record over the H/S transition area which, where present, included a dip in intensity around this period. Changes in the signal and concentration of calcium and other elements have been previously reported across H/S boundaries although the response appears to vary between species (Hagemeyer and Schäfer, 1995, Nabais *et al.*, 1999, Penninckx *et al.*, 2001, Watmough and Hutchinson, 2002, Poussart *et al.*, 2006). Penninckx *et al.* (2001) found that the concentrations of Ca, Mg, K, Mn, N and P were all higher in the sapwood region of *Quercus robus* L. (temperate oak species) and Poussart *et al.* (2006) found a two fold increase in calcium intensity at the H/S boundary for *Miliusa velutina* in the same study mentioned earlier (Section 3.4.2.2). The increase in intensity at the H/S boundary found by Poussart *et al.* (2006) was a large, yet a temporary increase, marking the transition of heartwood into sapwood. The mean amplitude of the calcium cycles after the transition (i.e. of the cambium/bark side) was found to be 1.5 greater than the mean amplitude prior to the transition (pith side). It is important to note that the reported pattern of calcium concentrations for *M. velutina* (Poussart *et al.*, 2006) was based on one individual tree where two replicated lines of measurements were performed. This low sample number is not unusual in dendrochemical studies and therefore care should be taken when comparing reported trends based on such small sample numbers as results may not be truly representative.

The heartwood is often thought of as dead or physiologically inactive compared with the living active sapwood. Some studies have argued that nutrients may translocate during the transformation from heartwood into sapwood (Cutter and Guyette, 1993, Andrews *et al.*, 1999) which if this happened for calcium, may explain the reduced signal in the heartwood region for section B. However, if calcium was to translocate in this manner then the change in intensity observed in 2A-R1 would certainly have been present in the second radius of this tree

(2A-R2) and would be clear in the other samples analysed. Several early dendrochemical studies assessed the mobility and translocation potential of elements which were discussed in Chapter 1 (Section 1.4.4.2) with mixed results. However, calcium has proven to behave in a consistent manner with many studies reporting an overall decreasing trend from bark to pith (Prohaska *et al.*, 1998, Parn, 2001, Penninckx *et al.*, 2001, Berger *et al.*, 2004, Hristovski and Melovski, 2010). Such a trend did not appear to present itself for the tropical trees analysed in this study (Figure 3-14).

3.4.2.2. Seasonal Calcium Pattern

Figure 3-16 shows an example median plot for tree 2A overlaid onto the scanned image of the wood. As was found with the Scots pine samples in Chapter 2 (section 2.4.1), the calcium data appear to show a cyclic pattern that herein is hypothesised to represent the annual cycle. These cycles are not as pronounced as those shown for the Scots pine trees where the tree rings are clearly defined into early and latewood, however this may be due to the type of wood. Scots pine is a softwood conifer species, whereas *T. macroptera* is a diffuse porous hardwood species. differences in the nature of the calcium cycles would therefore be expected regardless of whether the species is tropical or not.

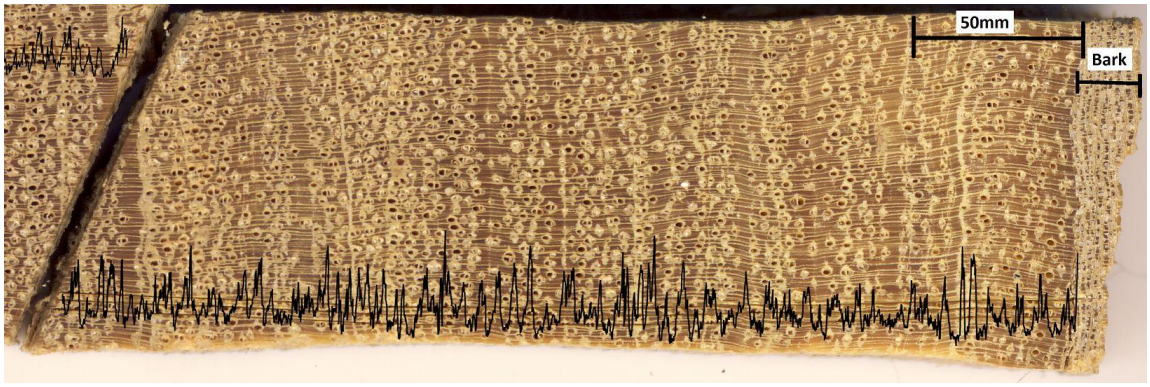

Figure 3-16: Scanned image of *T. macroptera* (tree 2A) with plot showing $^{44}Ca/^{14}C$ signal for this section overlaid on the image. The ring-like structres can be seen clearly.

The nature of the calcium signal observed for *T. macroptera* is more similar in nature to that reported by Poussart *et al.* (2006) for *M. velutina,* a deciduous tropical species from Northern Thailand. Both records show apparent cyclic patterns from the pith towards the bark of the

tree. Details of their study have been described in Chapter 1 (Section 1.3) however it is worth noting that their results indicated that the calcium cycles to be annual in nature.

The Scots pine samples analysed in Chapter 2 (Section 2.5.1) contained resin ducts which, when ablated by the laser, caused very large spikes in the calcium record. Hardwood species may contain vessels in the wood which are used mainly for water transport throughout the tree (Speer, 2010). Figure 3-16 clearly shows the large amount of vessels present in *T. macroptera*. These vessels do not appear to cause extra spikes in the data, but likely do contribute to the noisiness of the records produced.

3.4.2.3. Data Adjustments

The plotted raw $^{44}Ca/^{13}C$ data shown in Figure 3-14 illustrates the need for some degree of data adjustments with respect to detrending and normalisation. In this raw form, it was not possible to accurately link the adjoining datasets for each lath section into a single series accurately due to the differences in the signal intensity between sections. For example, in tree 2A-R1 there is a clear and very large difference in the intensity of the calcium signal variance between the lath section A and B. This difference in the calcium signal results in offsets and abrupt variance changes between the sections. Due to this, it is not possible to join the datasets while it is in the raw, unadjusted form. These issues are fully outlined in Chapter 2 (Section 2.3.5) but result mainly from the lack of appropriate matrix matched standard.

For most of the samples, the data adjustments as detailed in the method (Section 2.5.4) were carried out successfully, however trees 2A-R1 and 2Y required additional attention. Due to the abrupt change in variance which occurred at the H/S boundary in section C of tree 2A-R1 (Figure 3-14 and Figure 3-15), the data for that portion was split into two smaller datasets for detrending and normalising the data to z-scores. If the data was not split in this manner, the overall mean of the lath section would have been compromised causing additional problems with the data linkage to adjacent sections as well as the process for assigning calcium peak based dates.

Figure 3-17 (a) shows the raw values for tree 2A-R1 plotted along with the appropriate detrending functions for each section, including the 2 separate functions for section C. A

decrease in calcium counts for each lath section can be observed in this figure. This decreasing trend is similar to that found in chapter 2 (Section 2.3.4.3) for the Scots pine samples and is similarly most likely to be due to from a combination of signal drift from the instrument over time and a 'real' age related trend. Figure 3-17 (b) shows the effect of applying these detrending functions to each lath section. The decreasing calcium trend has been completely removed, but the data for each lath section is still offset from the adjacent laths as well as being of vastly different intensities in places. The second data adjustment step converted the data for each lath section to z-scores (Figure 3-18 (a)). After this transformation, each lath section has been aligned onto a common scale and the overlapping regions which were analysed on adjacent sections lined up allowing the splicing together of the time-series (Figure 3-9). The final, fully adjusted and spliced plot, for tree 2A-R1, is shown in Figure 3-18 (b). Similar plots for the other trees can be found in Appendix 2.

(a)

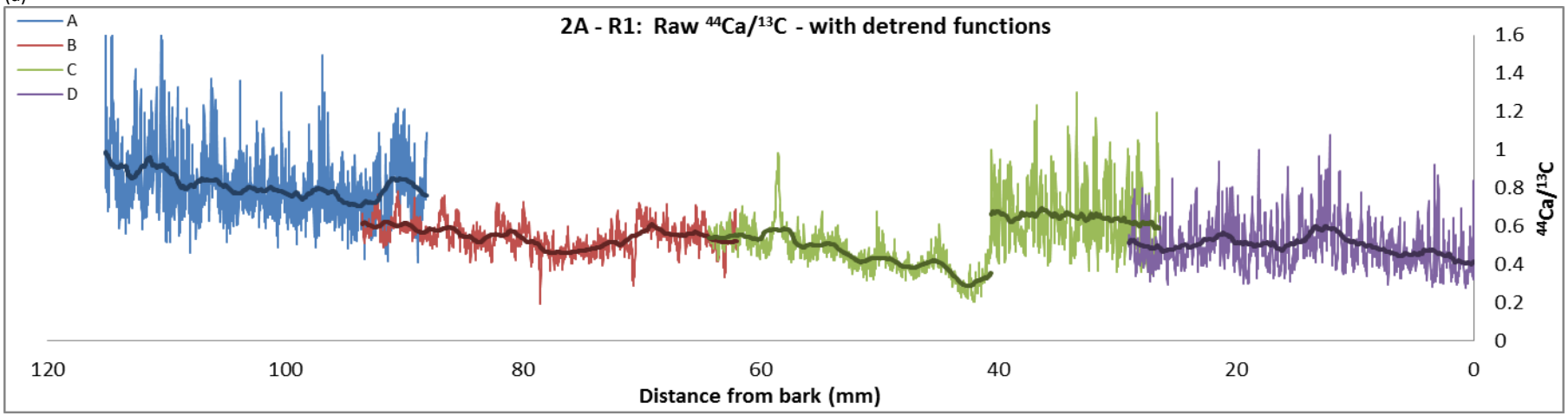

(b)

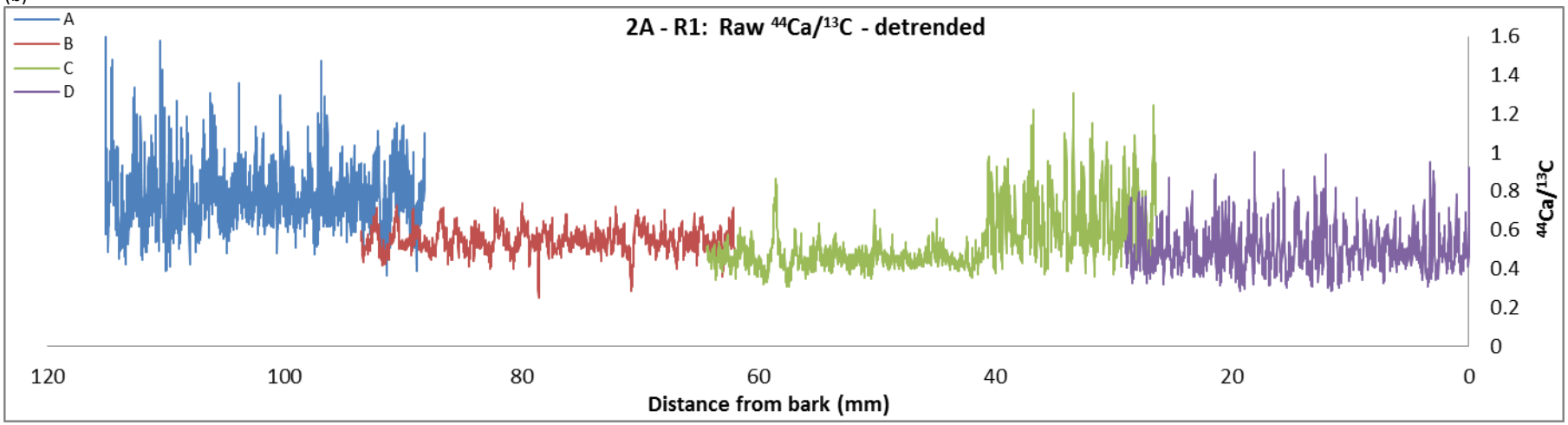

Figure 3-17: (a) Graph showing the raw median $^{44}Ca/^{13}C$ values for all four sections of tree 2A. Each section is plotted with the low frequency part of the Gaussian filter which was used to detrend each section. For section C, the data was detrended by 2 separate functions due to the large change in variance at ~40mm from the bark. (b) Graph showing the result of detrending each section using the detrending functions shown in (a).

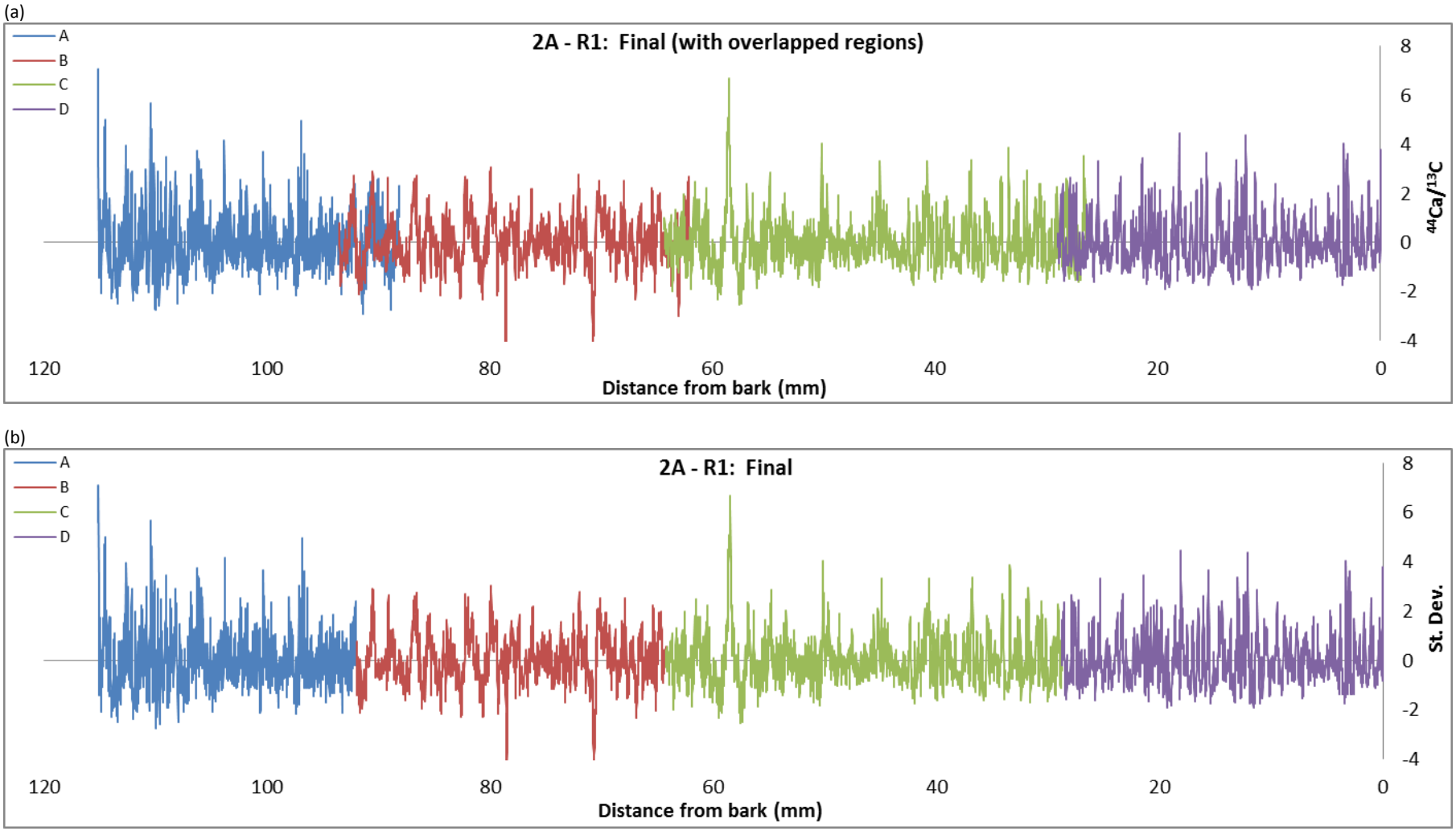

Figure 3-18: (a) Graph showing the result of converting each lath section to z-scores. The overlapped regions are still present, but have been removed in (b). After data is spliced together (Section 3.3.3) the data is treated as one single dataset.

The second tree requiring additional attention was 2Y. It can be seen that within the raw data for section B of this tree (Figure 3-14), a single irregular spike in the calcium data is present at approximately 40mm from the bark. When comparing the raw plot with the ablated tracks on the wood, this spike was shown to occur where tree 2Y contained an unusual band containing an orange/brown coloured resin-like material (Figure 3-19). The cause of this feature is unknown but is likely related to some sort of trauma experienced by the tree resulting in the production of resin as a defence mechanism. Since this line appeared perpendicular to the laser ablation tracks, all three ablation lines were affected and the spike remained present in the data after the median values were calculated. This singular spike increased the calcium signal, in this region, by a factor of ten.

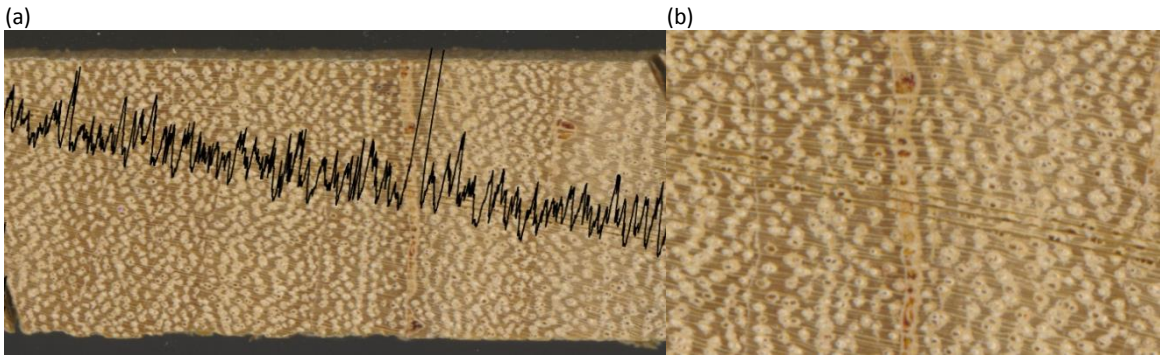

Figure 3-19: Section B of tree 2Y (a) shows the calcium spike in the data caused by the presence of the resinous substance which is highlighted in (b).

The intensity of this singular peak had a profound effect on the detrending and z-score adjustments (Figure 3-20), which prevented the splicing of datasets and subsequent ring counts. Figure 3-20 (a) shows the raw data containing this anomaly plotted with the detrending function when the spike is still present and (b) demonstrates the affect leaving it in the dataset has when converting the values to z-scores (b). When the spike is present in the data which is converted into z-scores, the resulting data loses amplitude making it no longer possible to splice the data series from different sections and almost the whole of that section would be under any of the threshold limits when it came to annual counts. With the spike removed, the amplitude of the peaks are in line with each other and the resulting datasets for each part can be spliced together (Figure 3-21).

(a)

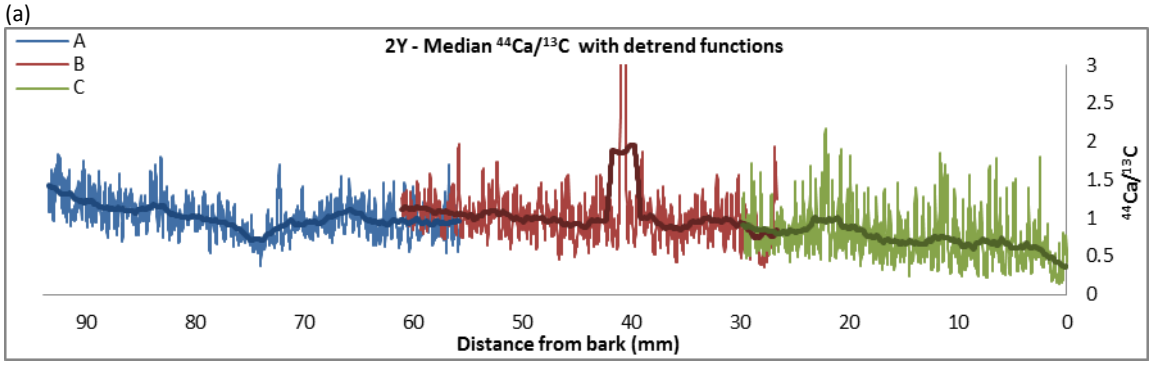

(b)

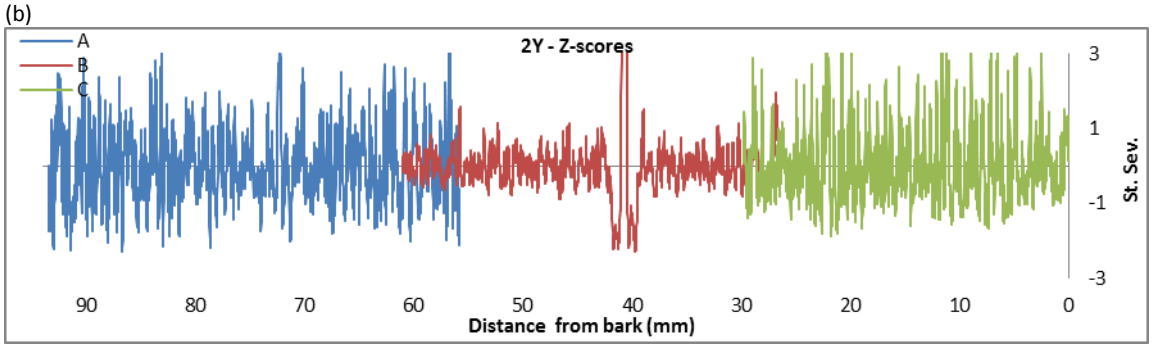

Figure 3-20: Both plots have been truncated for display purposes. (a) The raw median 44Ca/^{13}C values for the 3 sections of tree 2Y are plotted with the low frequency part of the Gaussian filter (detrending function). The effect that the single large calcium spike in section B has can be seen in (b) which shows the detrended data after conversion to z-scores.

(a)

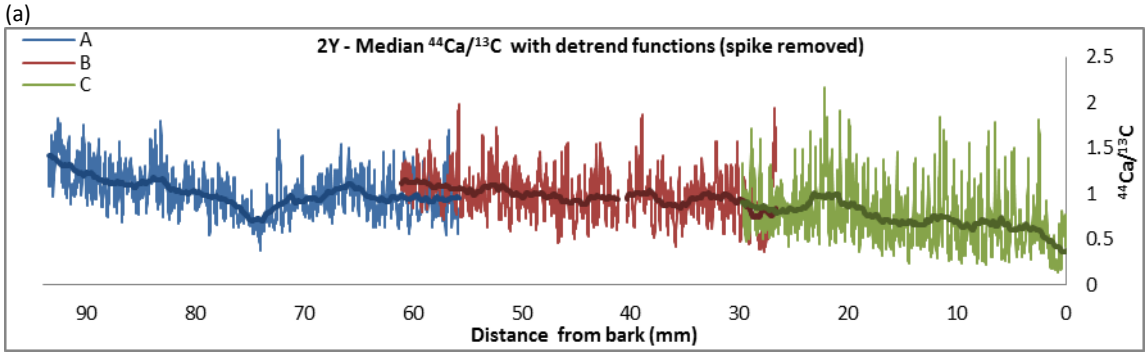

(b)

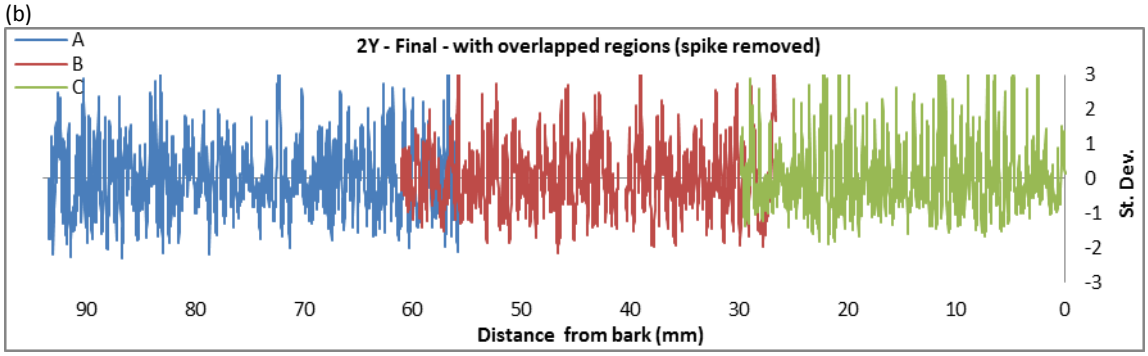

Figure 3-21: These graphs show the result of removing the spike in data. (a) The raw median 44Ca/^{13}C values for the 3 sections of tree 2Y are plotted with the low frequency part of the Gaussian filter (detrending function). (b) results of detrending the data and conversion to z-scores after spike removal. The 3 sections are now in alignment and can be spliced together.

The final adjusted spliced data series for all of the trees are shown in Figure 3-22. The data for each section of a tree lath have been spliced together into one dataset per tree, with all trees now presented on a standard scale allowing direct comparisons between trees. Any age or climatic related trends which may have existed have been removed from the data leaving only the variance between calcium cycles across the tree laths.

3.4.3. Calcium Dating

Chapter 2 (Section 2.3.8) detailed the development of an objective statistical approach for the identification of annual growth increments from calcium masurements. This approach was based around detrending the data, normalising to z-scores and thresholding the data according to standard deviations above the mean. Since Scots pine contains well-defined annual tree rings, the effectiveness of this approach could be accurately and easily tested. For tropical species such as *T. macroptera* (Figure 3-13), which does not contain distinct annual rings, two approaches were taken to validate the dating using the calcium peaks as annual increments. Detailed analysis was first carried out using 1 tree (2A) with 2 radii to optimise the threshold method and derive estimate of dating error. The "optimal" method was then tested on an independent second sample. Radiocarbon dates proved invaluable in this two-step exercise.

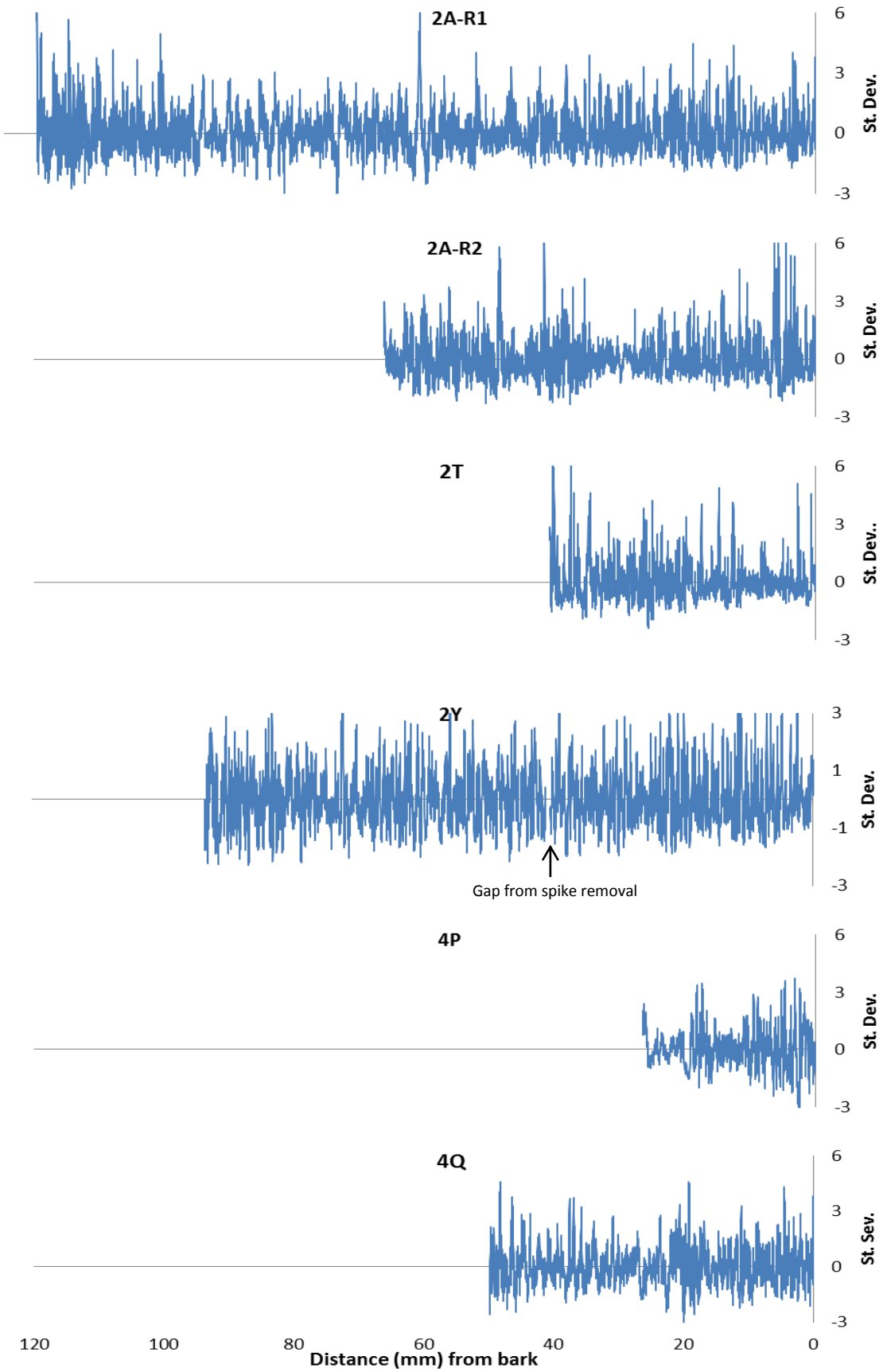

Figure 3-22: Plots showing Final calcium data obtained for each of the *T. macroptera* samples. Two radii from sample 2A were analysed.

3.4.3.1. Within Tree Calcium Threshold Error

For the assessment of Scots Pine in chapter 2, a threshold of >1 standard deviations above the mean was found to be the most appropriate threshold to identify the annual tree rings via the calcium peaks. This resulted in an average error between the calcium age and ring width crossdated age of ±5.9 years (Section 2.4.2). To assess the error encountered for this tropical species, the calcium threshold peak counts between the two radii (R1 and R2) of tree 2A were compared to provide a measure of within tree error.

As outlined in Section 3.3.4.1, the fourteen tie points (Figure 3-11) were chosen as the anatomical features in these positions could be identified on both radii. It is apparent from this image however, that growth rate is not equal around the circumference of the tree.

The results of assigning an annual "calcium" year using the threshold > 1 standard deviation (SD) above the mean, are illustrated in Figure 3-23 for tree 2A-R1 and Figure 3-24 for 2A-R2. These graphs show each tree radii as a single dataset plotted with the resultant starting positions of the annual cycle. For both radii, the assigned annual increments generally coincide with the calcium peaks; however occasional smaller peaks appear to be missed. It is not possible at this stage, without further investigation, to determine whether these potentially missed peaks are in fact annual cycles or simply noise in the data. Similarly, in areas where the calcium data for this species becomes noisier (for example between 115mm and 95mm from bark) potentially "extra" peaks may have been counted. Due to the apparent noisier nature of these tropical samples, the effect of smoothing the data was tested as well as different standard deviation thresholds. Figure 3-23 illustrates defined "annual" peaks which were greater than the threshold value (dark red horizontal line). The same principal applied when the threshold limit was increased resulting in a decrease of the number of identified peaks.

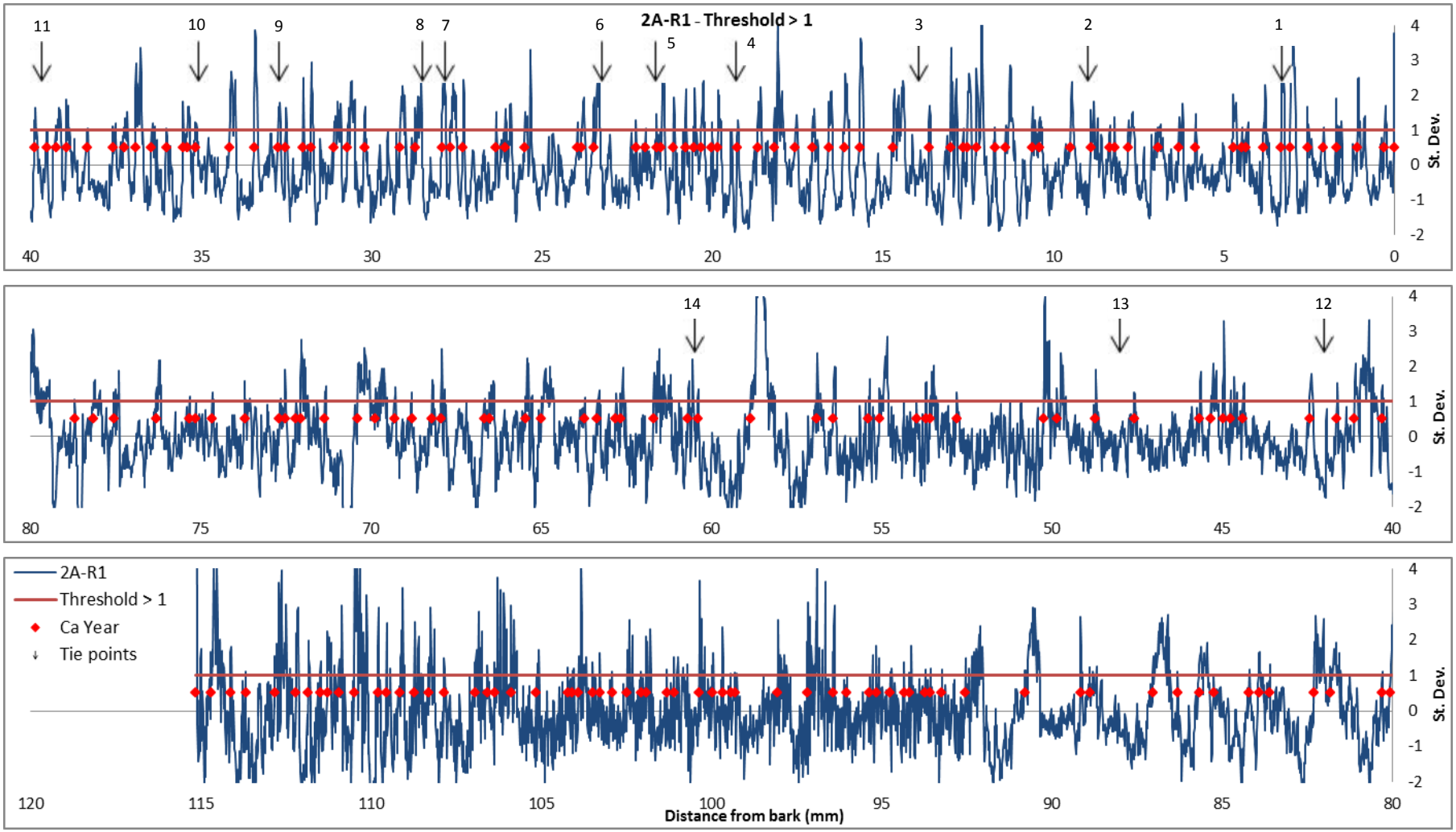

Figure 3-23: The above 3 plots show positions of calcium year assignment for tree 2A-R1, using the threshold >1. The graph is split into 3 sections and truncated for display purposes. The red diamonds represent the start of an annual growth season as determined by the assignment criteria, and the red line represents the threshold position. The arrows show the positions of the 14 tie points used for within tree error assessment.

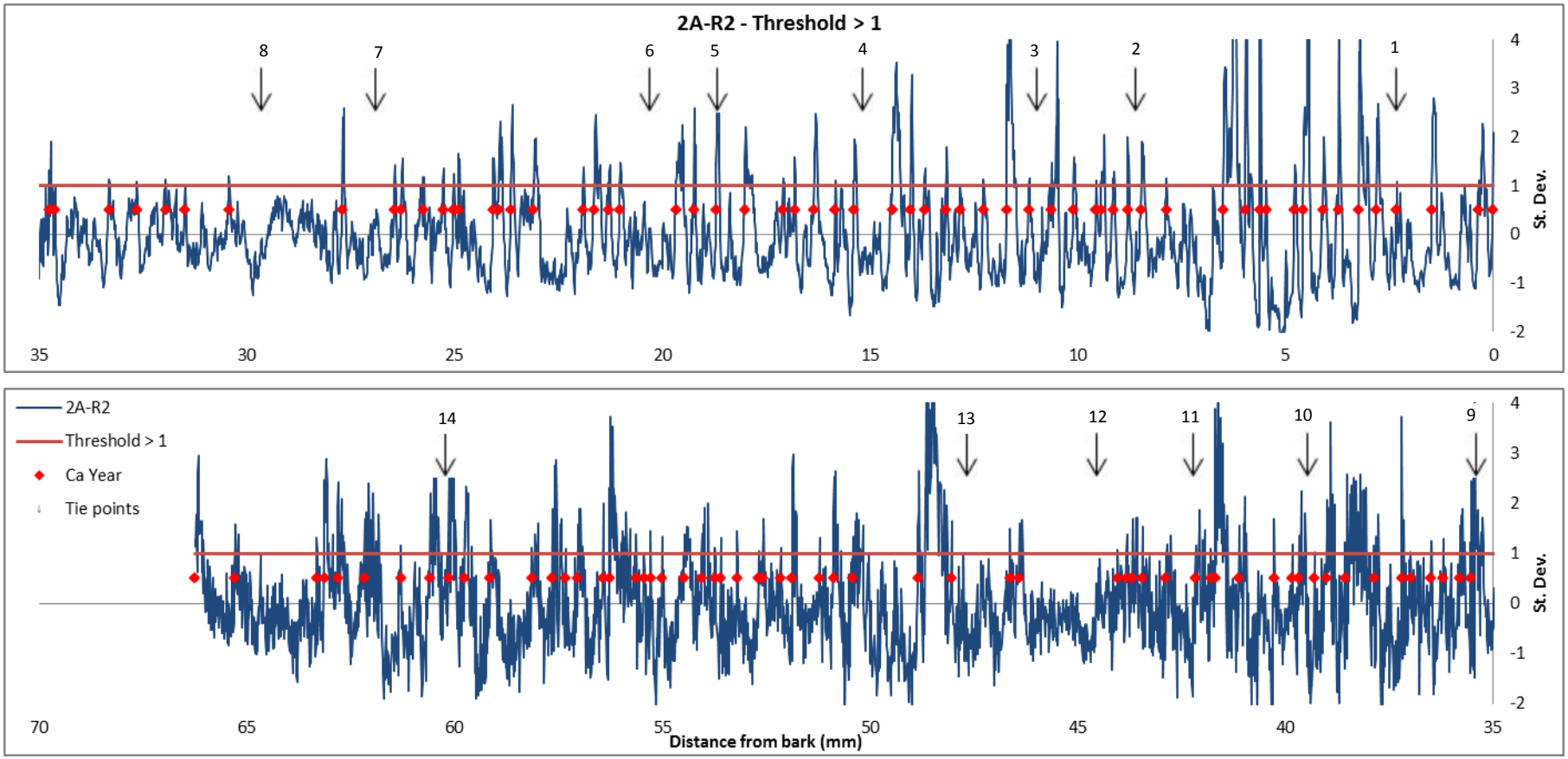

Figure 3-24: The above 2 plots show positions of calcium year assignment for tree 2A-R2, using the threshold >1. The graph is split into 2 sections and truncated for display purposes. The red diamonds represent the start of an annual growth season as determined by the assignment criteria, and the red line represents the threshold position. The arrows show the positions of the 14 tie points used for within tree error assessment.

A total of 8 iterations of the threshold approach were tested. The results of the comparisons between the fixed tie points for the two radii are shown in Table 3-3 for the threshold >1 SD, >1.25 SD (Table 3-4), >1.5 SD (Table 3-5) and Table 3-6 for the threshold >2 SD. The within tree error (average difference in years between radii) appears to decrease with higher thresholds. Although this may at first glance appear to improve the error, the reduction in differences between radii as the threshold increases is not unexpected since higher thresholds result in much less peaks being identified. For example, when considering each threshold iteration for the unsmoothed data, an average of 101 years were identified between the comparison points #1 and #14 using the >1 threshold This is compared with only 86 years for the >1.25 , 70 when using >1.5 and 42 years for >2. The difference between the numbers of years identified for each threshold is very large and therefore choosing the wrong threshold value would have a huge impact on the resulting age estimate of the tree. As would be expected, for all thresholds, smoothing the data by applying a moving average function resulted in a reduction of years identified for that threshold.

In most cases the differences in the assigned calcium year between radii increased with distance from the bark edge of the tree. As noted above, this growth rates do not appear to be consistent around the circumference of the tree. Figure 3-11 highlights such a problematic area in tree 2A where it can be seen that the anatomical features of the wood pinch out which could account for this increase between radii error found in the inner areas of the tree.

Comparison of the two radii for this tree addresses the within tree error associated with using a threshold method to determine age estimates for the calcium record. The errors associated with these different thresholds do not however provide a better estimation of which threshold is best suited, but rather just changes the potential dates. Different thresholds however result in vastly different age estimates therefore another method of dating, such as ^{14}C dating, is required to determine the most appropriate threshold for this species.

Table 3-3: The following tables show the results of the calcium assigned year comparisons when using (a) a threshold of > 1 st. dev. above the mean to mark annual increments and (b) a threshold of > 1 st. dev. above the mean to mark annual increments after a smoothing function has been applied to the data.

(a) Results for Threshold > 1 (No smoothing)

Comparison No.	2A-R1 Distance from bark (mm)	2A-R2 Distance from bark (mm)	2A-R1 Assigned Ca Year	2A-R2 Assigned Ca Year	Difference between year counts
1	3.291	2.328	2000	2004	4
2	8.976	8.604	1987	1992	5
3 (14C – C)	13.940	10.996	1977	1986	9
4 (14C – B)	19.317	15.176	1968	1978	10
5	21.680	18.679	1960	1972	12
6	23.226	20.309	1958	1969	11
7	27.843	26.898	1949	1956	7
8	28.500	29.644	1948	1955	7
9	32.705	35.397	1940	1949	9
10	35.088	39.474	1937	1940	3
11	39.662	42.215	1925	1934	9
12	42.002	44.552	1921	1929	8
13	48.003	47.679	1913	1927	14
14	60.490	60.210	1899	1903	4
			Average difference in years between radii		**8**

(b) Results for Threshold > 1 (Smoothed - Moving average)

Comparison No.	2A-R1 Distance from bark (mm)	2A-R2 Distance from bark (mm)	2A-R1 Assigned Ca Year	2A-R2 Assigned Ca Year	Difference between year counts
1	3.291	2.328	2002	2005	3
2	8.976	8.604	1995	1995	0
3 (14C – C)	13.940	10.996	1987	1990	3
4 (14C – B)	19.317	15.176	1979	1985	6
5	21.680	18.679	1973	1982	9
6	23.226	20.309	1973	1979	6
7	27.843	26.898	1966	1969	3
8	28.500	29.644	1965	1968	3
9	32.705	35.397	1957	1967	10
10	35.088	39.474	1954	1963	9
11	39.662	42.215	1948	1960	12
12	42.002	44.552	1945	1959	14
13	48.003	47.679	1939	1958	19
14	60.490	60.210	1931	1943	12
			Average difference in years between radii		**7.8**

Table 3-4: The following tables show the results of the calcium assigned year comparisons when using (a) a threshold of > 1.25 st. dev. above the mean to mark annual increments and (b) a threshold of > 1.25 st. dev. above the mean o mark annual increments after a smoothing function has been applied to the data.

(a) **Results for Threshold > 1.25 (No smoothing)**

Comparison No.	2A-R1 Distance from bark (mm)	2A-R2 Distance from bark (mm)	2A-R1 Assigned Ca Year	2A-R2 Assigned Ca Year	Difference between year counts
1	3.291	2.328	2000	2005	5
2	8.976	8.604	1990	1995	5
3 (14C – C)	13.940	10.996	1982	1990	8
4 (14C – B)	19.317	15.176	1973	1985	12
5	21.680	18.679	1966	1981	15
6	23.226	20.309	1965	1978	13
7	27.843	26.898	1957	1966	9
8	28.500	29.644	1956	1965	9
9	32.705	35.397	1948	1964	16
10	35.088	39.474	1945	1956	11
11	39.662	42.215	1939	1951	12
12	42.002	44.552	1935	1947	12
13	48.003	47.679	1927	1945	18
14	60.490	60.210	1913	1921	8
			Average difference in years between radii		**10.9**

(b) Results for Threshold > 1.25 (Smoothed - Moving average)

Comparison No.	2A-R1 Distance from bark (mm)	2A-R2 Distance from bark (mm)	2A-R1 Assigned Ca Year	2A-R2 Assigned Ca Year	Difference between year counts
1	3.291	2.328	2004	2005	1
2	8.976	8.604	1999	1996	3
3 (14C – C)	13.940	10.996	1993	1992	1
4 (14C – B)	19.317	15.176	1986	1989	3
5	21.680	18.679	1980	1986	6
6	23.226	20.309	1980	1983	3
7	27.843	26.898	1973	1979	6
8	28.500	29.644	1972	1978	6
9	32.705	35.397	1966	1978	12
10	35.088	39.474	1963	1975	12
11	39.662	42.215	1960	1974	14
12	42.002	44.552	1958	1974	16
13	48.003	47.679	1953	1974	21
14	60.490	60.210	1946	1964	18
			Average difference in years between radii		**8.7**

Table 3-5: The following tables show the results of the calcium assigned year comparisons when using (a) a threshold of > 1.5 st. dev. above the mean to mark annual increments and (b) a threshold of > 1.5 st. dev. above the mean o mark annual increments after a smoothing function has been applied to the data.

(a) **Results for Threshold > 1.5 (No smoothing)**

Comparison No.	2A-R1 Distance from bark (mm)	2A-R2 Distance from bark (mm)	2A-R1 Assigned Ca Year	2A-R2 Assigned Ca Year	Difference between year counts
1	3.291	2.328	2002	2005	3
2	8.976	8.604	1996	1996	0
3 (14C – C)	13.940	10.996	1989	1992	3
4 (14C – B)	19.317	15.176	1982	1988	6
5	21.680	18.679	1976	1984	8
6	23.226	20.309	1976	1981	5
7	27.843	26.898	1967	1974	7
8	28.500	29.644	1966	1973	7
9	32.705	35.397	1958	1971	13
10	35.088	39.474	1955	1965	10
11	39.662	42.215	1949	1960	11
12	42.002	44.552	1945	1958	13
13	48.003	47.679	1939	1957	18
14	60.490	60.210	1929	1939	10
			Average difference in years between radii		**8.1**

(b) Results for Threshold > 1.5 (Smoothed - Moving average)

Comparison No.	2A-R1 Distance from bark (mm)	2A-R2 Distance from bark (mm)	2A-R1 Assigned Ca Year	2A-R2 Assigned Ca Year	Difference between year counts
1	3.291	2.328	2005	2005	0
2	8.976	8.604	2002	1997	5
3 (14C – C)	13.940	10.996	1996	1996	0
4 (14C – B)	19.317	15.176	1990	1993	3
5	21.680	18.679	1985	1990	5
6	23.226	20.309	1985	1988	3
7	27.843	26.898	1980	1984	4
8	28.500	29.644	1979	1983	4
9	32.705	35.397	1974	1983	9
10	35.088	39.474	1971	1980	9
11	39.662	42.215	1969	1979	10
12	42.002	44.552	1967	1979	12
13	48.003	47.679	1964	1979	15
14	60.490	60.210	1958	1971	13
			Average difference in years between radii		**6.6**

Table 3-6: The following tables show the results of the calcium assigned year comparisons when using (a) a threshold of > 2 st. dev. above the mean to mark annual increments and (b) a threshold of > 2 st. dev. above the mean o mark annual increments after a smoothing function has been applied to the data.

(a) **Results for Threshold > 2 (No smoothing)**

Comparison No.	2A-R1 Distance from bark (mm)	2A-R2 Distance from bark (mm)	2A-R1 Assigned Ca Year	2A-R2 Assigned Ca Year	Difference between year counts
1	3.291	2.328	2005	2005	0
2	8.976	8.604	2002	1998	4
3 (14C – C)	13.940	10.996	1995	1995	0
4 (14C – B)	19.317	15.176	1988	1992	4
5	21.680	18.679	1983	1990	7
6	23.226	20.309	1983	1987	4
7	27.843	26.898	1979	1984	5
8	28.500	29.644	1978	1983	5
9	32.705	35.397	1973	1983	10
10	35.088	39.474	1971	1979	8
11	39.662	42.215	1970	1976	6
12	42.002	44.552	1968	1976	8
13	48.003	47.679	1966	1976	10
14	60.490	60.210	1959	1967	8
			Average difference in years between radii		**5.6**

(b) Results for Threshold > 2 (Smoothed - Moving average)

Comparison No.	2A-R1 Distance from bark (mm)	2A-R2 Distance from bark (mm)	2A-R1 Assigned Ca Year	2A-R2 Assigned Ca Year	Difference between year counts
1	3.291	2.328	2005	2006	1
2	8.976	8.604	2004	1998	6
3 (14C – C)	13.940	10.996	2000	1997	3
4 (14C – B)	19.317	15.176	1997	1994	3
5	21.680	18.679	1996	1993	3
6	23.226	20.309	1996	1992	4
7	27.843	26.898	1994	1991	3
8	28.500	29.644	1993	1991	2
9	32.705	35.397	1991	1991	0
10	35.088	39.474	1989	1991	2
11	39.662	42.215	1988	1990	2
12	42.002	44.552	1987	1990	3
13	48.003	47.679	1986	1990	4
14	60.490	60.210	1983	1984	1
			Average difference in years between radii		**2.6**

3.4.4. Tuning of the Ca Dating Method

The results from the five radiocarbon dates for tree 2A are presented in Table 3-7 and reported at the ±1σ confidence level for conventional radiocarbon years BP[14] (relative to AD 1950), % modern 14C and absolute % modern ^{14}C. These results were corrected to $\delta^{13}C_{VPDB}$‰ using the $\delta^{13}C$ values in the table which represent the $\delta^{13}C$ in the original pre-treated sample material, and measured on a dual inlet stable isotope mass spectrometer at the NERC Radiocarbon Facility (East Kilbride). Only one of the samples was reported with a conventional radiocarbon age (BP) which was the sample taken from the pith of tree 2A (sample identifier 2A-Inner).

The radiocarbon measurements were calibrated using CALIBomb software (Reimer *et al.*, 2013). The summarised results shown in Table 3-8 provide the potential age ranges with the probability value of the sample falling into that range. The output plots for the calibrated age ranges provided by the CALIBomb software (Figure 3-25) illustrate how these age range estimates were calculated. The green curve represents the bomb curve using the Levin dataset (Levin and Kromer, 2004). For each sample which falls within this region, there are two possible age ranges due to the two limbs on either side of the bomb peak.

The age ranges for the sample collected from the pith of the tree (2A-Inner) put the date of this sample as pre-bomb peak age (before AD 1950), however the potential age range is large. Table 3-8 only shows 3 out of the 6 age ranges generated by CALIBomb as the probabilities for the remaining ranges were all ≤ 0.04 therefore these were assumed to be negligible. At the 95% confidence level the sample dates to the periods AD 1636-1691 (0.325), 1726-1813 (0.513) or 1918-1950 (0.151) with the relative likelihood for these individual ranges provided in brackets. This provides several large and quite different potential age ranges for the germination date of the tree. which is not particularly useful for an environmental analysis. The radiocarbon results for 2A-Inner were very similar to that for the explorative date described in Section 3.2.1. Both trees were located within 100m of each other, with 2A located inside the forest transition zone and the other situated further out into the savanna.

[14] Radiocarbon measurements are reported as years before present (BP). For this purpose `present' refers to 1950.

Table 3-7: Results from the radiocarbon dates from tree 2A.

NRCF Allocation Number	Publication code	Sample identifier	$\delta^{13}C_{VPDB}$‰ ± 0.1	Carbon content (% by wt.)	^{14}C Enrichment (% modern)	+/- 1σ (% modern)	^{14}C Enrichment (Absolute % modern)	+/- 1σ (Absolute % modern)	Conventional Radiocarbon Age (years BP)	+/- 1σ (radiocarbon yrs BP)
1562.0411	SUERC-37535	2A - Inner	-24.5	42.2	98.11	0.45	97.40	0.45	153	37
1562.0411.002	SUERC-44294	2A - A	-25.3	33.3	146.04	0.67	144.93	0.67	n/a	n/a
1562.0411	SUERC-37536	2A - B	-25.7	40.7	119.08	0.52	118.22	0.52	n/a	n/a
1562.0411	SUERC-37537	2A - C	-26.2	43.3	115.78	0.53	114.94	0.53	n/a	n/a
1562.0411	SUERC-37540	2A - Bark	-27.5	42.9	106.70	0.46	105.93	0.46	n/a	n/a

Table 3-8: Calibrated radiocarbon dates for each of the samples from tree 2A. Radiocarbon age was calculated using the online CALIBomb calibration software (Reimer *et al.*, 2013) available from http://calib.qub.ac.uk/CALIBomb/. The age ranges with the highest probability is highlighted in yellow.

Publication code (AMS Lab No)	Sample identifier	Absolute % modern	Absolute % modern error	F14C	F14C error	1σ age range	Probability	2σ age range	Probability
SUERC-37535	2A - Inner	97.40	0.45	0.9740	0.0045	1649.00 - 1680.00	0.377	1636.00 - 1691.00	0.325
						1740.00 - 1741.00	0.014	1726.00 - 1813.00	0.513
						1763.00 - 1801.00	0.467	1918.00 - 1950.00	0.151
						1938.00 - 1950.00	0.142	***	
SUERC-44294	2A – A	144.93	0.67	1.4493	0.0067	1962.84 - 1962.89	0.053	1962.64 - 1962.98	0.153
						1972.56 - 1973.03	0.947	1972.37 - 1973.65	0.847
SUERC-37536	2A – B	118.22	0.52	1.1822	0.0052	1957.60 - 1957.98	0.148	1957.26 - 1958.35	0.208
						1986.46 - 1988.25	0.852	1985.92 - 1988.99	0.792
SUERC-37537	2A – C	114.94	0.53	1.1494	0.0053	1956.25 - 1956.86	0.298	1956.01 - 1957.13	0.282
						1990.14 - 1991.51	0.702	1989.75 - 1992.92	0.718
SUERC-37540	2A – Bark	105.93	0.46	1.0593	0.0046	1953.05 - 1953.26	0.073	1952.83 - 1953.49	0.120
						2005.46 - 2007.95	0.927	2004.48 - 2008.29	0.880

***4 other date ranges were produced from CALIBomb for sample 2A-Inner, however these are not included here as probability was less than 0.05. These are shown in Figure 3-25

(a) 2A - Inner

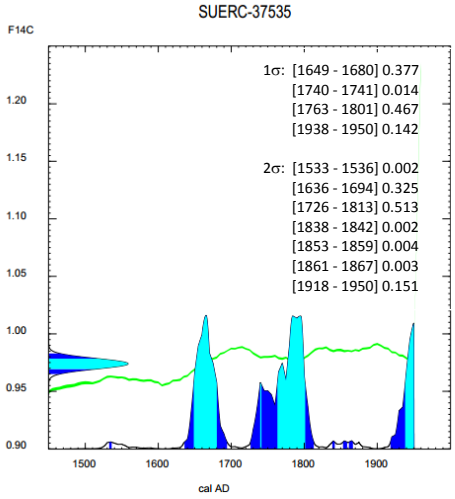

(b) 2A – A

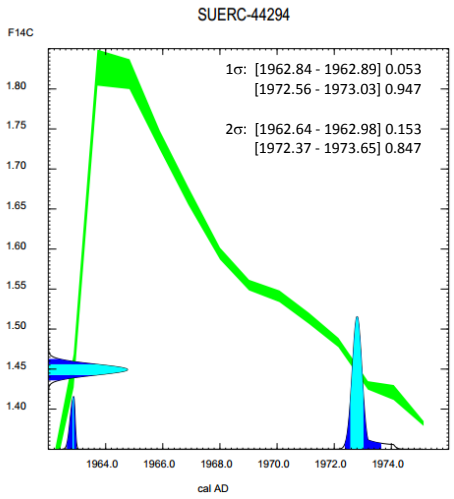

(c) 2A – B

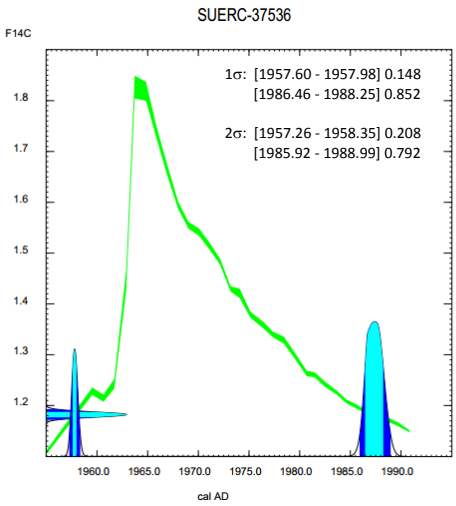

(d) 2A – C

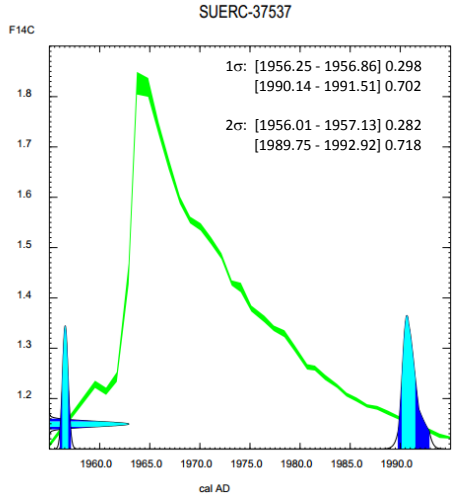

(e) 2A – Bark

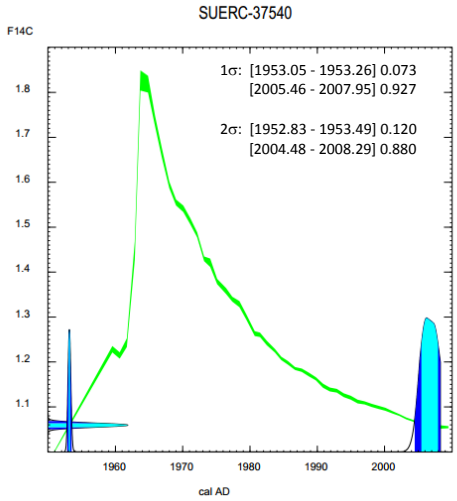

Figure 3-25: The plots (a-e) were produced using the online CALIBomb software which is available from http://calib.qub.ac.uk/CALIBomb/frameset.html. The calibration was carried out using the intcal13 calibration and Levin datasets, using a smoothing factor of 1.0 year.

The sample taken from just under the bark (2A-Bark) of the tree had two potential date ranges at the 95% confidence interval of either 1952-1953 or 2004-2008. The 2004-2008 date range had the high probability of 0.880 which would make this the more likely candidate. In this case, this date can be accepted as it is consistent with the actual known collection date of Nov 2007.

The remaining three ^{14}C dates each have two possible calibrated age ranges. According to the age ranges calculated from CALIBomb, each sample could sit on either limb of the ^{14}C bomb curve (Figure 3-25). In each case the highest probability range is linked to the younger of the possible dates. It is noted however, that the shape of the ^{14}C bomb curve, with the steep ascending limb and shallower descending limb will always produce an age range which is more statistically likely to fall on the descending limb (Moreton, 2012, pers comm.). It is therefore sensible not to automatically rule out the older date ranges based solely on the lower probability. As the sampling locations for 2A-A, 2A-B and 2A-C are known (Figure 3-11), we can therefore use the chronological order of these samples to assess the likelihood of the date ranges for each.

For both 2A-B and 2A-C, the older age ranges (which have lowest probabilities) can be rejected as this would put the samples out of chronological order. Either of the possible date ranges for sample 2A-A would put this sample as younger than the others which is not possible from the location it was taken from. This puts the date ranges of these two samples, at the 95% confidence interval, at 1985.92-1988.99 (0.792) for sample 2A-B and 1989.75-1992.92 (0.718) for sample 2A-C.

For 2A-A, either of the radiocarbon date ranges is theoretically possible as both of these will keep the sample in the correct chronological order with regards to the other samples. The younger of these ^{14}C date ranges (1972.37-1973.65) is statistically more likely, carrying a high probability of 0.847 compared with the much lower probability of 0.153 for the older ^{14}C range (1962.64-1962.98). The growth rates of this species in this location are not known, however a crude calculation of the growth rate based on the accepted ^{14}C dates for samples 2A-B and 2A-C can be done by using the distance from the bark (Table 3-3. Sample 2A-A was collected at approximately 31mm and 35.2mm from the bark edge for radii 1 and 2 respectively. The outcome of this is very much dependant on how the growth rate is calculated. If it is assumed that the growth rate is constant between the 2007 and the mid-point of the 2A-C ^{14}C year range, and using this growth rate to calculate back to 2A-A's sampling location, then the

estimated date would be 1973 on 2A-R1 and 1960 on 2A-R2. On the other hand, if a growth rate is calculated between 2007 and 2A-C, then a separate growth rate calculated between 2A-C and 2A-B, with this one used to calculate back to 2A-A's sampling location, then the estimated dates would be 1974 on 2A-R1 and 1973 on 2A-R2. This may once again suggest that the younger ^{14}C date range is the best 'fit' however it is unfortunately impossible to accurately estimate the growth rate based on such few ^{14}C samples.

3.4.4.1. Comparison of the ^{14}C and Ca Dating Methods

The comparisons made between the 14 points on each radius of sample 2A (Section 3.3.4.1) included the positions where the two radiocarbon samples were taken (2A-B and 2A-C). The results from these two points provided an age range from the calcium record for each threshold, allowing direct comparison with the ^{14}C dates. The calcium age ranges were also calculated for radiocarbon sample 2A-A as the location of sampling could be tracked to both radii. These are all summarised in Table 3-9. Calcium measurements were only available in 2A-R1 for the 2A-Inner sample; therefore only one calcium derived rate (as opposed to a date range) is shown for this sample. Table 3-9 contains all the possible ^{14}C age ranges for each of the radiocarbon dated samples (with exception of 2A-Bark since this date is not in question as the collection date is known. The Ca date range obtained from each threshold is shown in bold, followed by the number of the ^{14}C age range which the Ca age is closest to. The difference (in years) between the radiocarbon and calcium age ranges obtained from these two methods is shown for each comparison. Where no difference is stated, then this means that the age ranges agree or overlap.

The results in Table 3-9 provide an overview of how well each calcium threshold derived date compares with the equivalent ^{14}C age range(s) for the same point. It should be noted that in some cases, the calcium age range may overlap and hence agree with the ^{14}C date, but the within tree error for the calcium date may be quite large at that position.

Table 3-9: Shows a summary of the possible ^{14}C dates obtained for the samples from tree 2A. The calcium date range for each peak threshold was compared to the ^{14}C ranges, and the difference in years between the two ranges were calculated (Figure 3-26). The calcium ranges which agree, or fall within the ^{14}C date range are highlighted in yellow.

Sample	**Potential ^{14}C ranges** (Probability)	**Ca Ranges for all peak thresholds**							
		>1	>1 (smoothed)	>1.25	>1.25 (smoothed)	>1.5	>1.5 (smoothed)	>2	>2 (smoothed)
2A-Inner (pith)	(1) 1636.00 - 1691.00 (0.325) (2) 1726.00 - 1813.00 (0.513) (3) 1918.00 - 1950.00 (0.151)	**1799** (2)	**1875** (3) 43 years	**1837** (2) 24 years	**1898** (3) 20 years	**1862** (2) 49 years	**1924** (3)	**1914** (3) 4 years	**1970** (3) 20 years
2A-A	(1) 1962.64 - 1962.98 (0.153) (2) 1972.37 - 1973.65 (0.847)	**1944-1949** (1) 14 years	**1961-1967** (1) 1 year	**1952-1964** (1)	**1968-1978** (2)	**1961-1971** (1)	**1976-1983** (2) 3 years	**1975-1983** (2) 2 years	**1991-1992** (2) 18 years
2A-B	(1) 1985.92 - 1988.99 (0.792)	**1968-1978** (1) 8 years	**1979-1985** (1)	**1973-1985** (1)	**1986-1989** (1)	**1982-1988** (1)	**1990-1993** (1) 2 years	**1988-1992** (1)	**1994-1997** (1) 5 years
2A-C	(1) 1989.75 - 1992.92 (0.718)	**1977-1986** (1) 3 years	**1987-1990** (1) 2 year	**1982-1990** (1)	**1992-1993** (1)	**1989-1992** (1)	**1996-1996** (1) 4 years	**1995-1995** (1) 3 years	**1997-2000** (1) 5 years

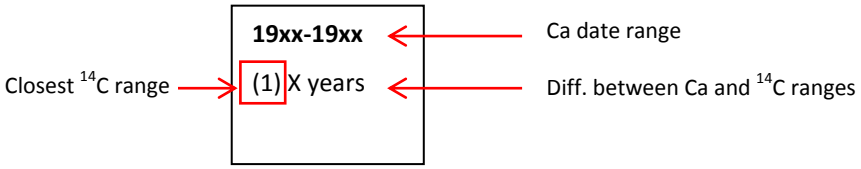

Figure 3-26: Graphical explanation of table layout

The effect of applying the different peak threshold conditions and smoothing the Ca data is clearly observed for sample 2A-Inner (pith date) when comparing the various calcium threshold based ages. A difference of 129 years for the calcium calculated dates was found between the >1 and >2 (non-smoothed) SD thresholds calculated ages. The >1 and >1.5 SD thresholds both resulted in dates which agreed with the radiocarbon ranges despite a 125 year difference in calcium ages. None of the other tested threshold results agreed with any of the radiocarbon ranges. Since it was only possible to measure calcium on one radius as far back as this point, it is not possible to determine whether growth irregularities such as wedging may be impacting the calcium dating. The >1.25 and >1.25 (smoothed) thresholds provide a date which is approximately 20 years out with a radiocarbon range. This could be due to such growth irregularities resulting in missing Ca years, however this conclusion cannot be tested without further experimentation.

For the remaining three samples, the >1.25, >1.25 (smoothed) and >1.5 thresholds all resulted in Ca dates ranges which agreed with radiocarbon date ranges. The >1.25 (smoothed) threshold produced a date which overlapped the highest probability ^{14}C dates, whereas the >1.25 and >1.5 overlapped with the lowest probability ^{14}C range.

From these comparisons, it can be concluded that the >1 SD threshold, which provided the best results on the Scots pine trees in Chapter 2, is not the most suitable for this species. Applying this threshold here resulted in too many calcium peaks being identified as years when compared with the ^{14}C results. The laser ablation settings used a smaller spot size compared with that of the Scots pine, and as *T. macroptera* is a hard wood compared to the softwood pine, the wood will likely abate in a slightly different manner. The vast number of vessels present in *T. macroptera* will be contributing to the nosier manner of the calcium data as the laser moves over these throughout its run. Using the highest and smoothed threshold of >2 SD, however, produced unsatisfactory comparisons with the ^{14}C results as it resulted in too few peaks being identified as calcium years. With the exception of these two, the process of adjusting the threshold for identifying calcium peaks had a minimal effect on the calcium dating for the outer 20-25 years of tree 2A, with most thresholds either resulting in overlapping date ranges, or missing the range by only a few years.

The >1.25 SD (smoothed) threshold provided the overall best fit for the radiocarbon dates as it found agreement with 3 out of 4 of the radiocarbon dates (2A-A, 2A-B and 2A-C). For these three dates, the calcium age ranges overlapped with the highest probability ^{14}C ranges

suggesting that the calcium content in this region may represent an annual signal. The within tree error was calculated at ±8.7 years based on the 14 comparison points in Table 3-4 which, at this threshold, goes back to a calcium age of 1946 for radius 1 or 1964 for radius 2. This is perhaps not a true representation of error however, as the difference between radii year counts doubled between comparison points 8 and 9 then continue to increase with further distance from the bark edge. It is also important to note that this error was based only the measurement and comparison of the 2 radii from 1 tree unlike the presumably more robust error found for the Scots pine in Chapter 2 (Section 2.4.1.1) calculated using 7 trees (9 radii - 2 trees where 2 radii was measured).

It should be noted that an additional threshold approach was investigated for this tropical species which used the troughs in the calcium data to identify for annual boundaries rather than the calcium peaks. Three trough thresholds were tested (<-1 SD, <-0.75 SD and <-0.6 SD) and calcium based age ranges were produced, in the same manner as the peak thresholds but instead using the troughs, for the locations where the ^{14}C samples were taken. The comparison of these trough age ranges with the ^{14}C results for tree 2A are shown in Table 3-10. The <-1 and <-1 smoothed threshold both produced calcium date ranges which found agreement with the radiocarbon dates. The non-smoothed <-1 range agreed with almost all radiocarbon dates, with the exception of 2A-B, however there was only a 5 year difference between the Ca and ^{14}C dates. This particular threshold also agreed with the highest probability ^{14}C ranges for all samples apart from 2A-A where agreement was found with the lower and older date range. The <-1 (smoothed) threshold produced almost identical results to the >1.25 (smoothed) threshold above. The calcium ranges from these two threshold are all within 4 years or less of each other, and agree with the ^{14}C dates in a very similar manner. The <-0.6 and <-0.75 SD thresholds (including the smoothed versions) were unsuitable as these overestimated calcium dates ranges for almost every sample.

Table 3-10: The following table shows a summary of the possible ^{14}C dates obtained for the samples from tree 2A when using the troughs in the calcium data to represent an annual increment. The calcium date range for each threshold was compared to the ^{14}C ranges, and the differences in years between the two ranges were calculated. The calcium ranges which agree, or fall within the ^{14}C date range are highlighted in yellow.

Sample	**Potential ^{14}C ranges** (Probability)	**Ca Ranges for all trough thresholds**					
		<-1	<-1 (smoothed)	<-0.75	<-0.75 (smoothed)	<-0.6	<-0.6 (smoothed)
2A-Inner (pith)	(1) 1636.00 - 1691.00 (0.325) (2) 1726.00 - 1813.00 (0.513) (3) 1918.00 - 1950.00 (0.151)	**1811** (2)	**1900** (3) 18 years	**1775** (2)	**1857** (2) 44 years	**1769** (2)	**1821** (2) 8 years
2A-A	(1) 1962.64 - 1962.98 (0.153) (2) 1972.37 - 1973.65 (0.847)	**1955-1966** (1)	**1972-1981** (2)	**1937-1939** (1) 23 years	**1954-1956** (1) 6 years	**1933-1940** (1) 22years	**1940-1946** (2) 16 years
2A-B	(1) 1985.92 - 1988.99 (0.792)	**1981-1981** (1) 5 years	**1987-1989** (1)	**1968-1973** (1) 13 years	**1978-1980** (1) 6 years	**1967-1974** (1) 22 years	**1974-1974** (1) 12 years
2A-C	(1) 1989.75 - 1992.92 (0.718)	**1988-1989** (1)	**1993-1994** (1) 1 year	**1978-1984** (1) 5 years	**1987-1987** (1) 3 years	**1978-1984** (1) 6 years	**1983-1984** (1) 6 years

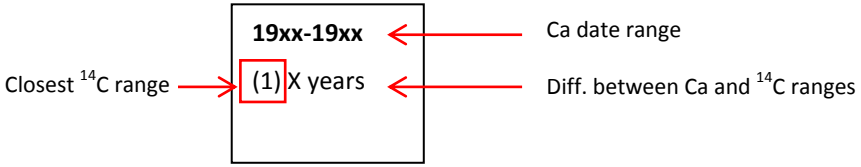

Figure 3-27: Graphical explanation of table layout

Some general observations can be noted which apply to both the peak and trough threshold comparisons. Smoothing the Ca data, even by only a small moving average function (4-point ~ 40µm), reduced the amount of peaks or troughs identified. The purpose of running a smoothing function through the data was to reduce the influence of excess noise in the calcium data therefore this was not unexpected. There is a risk in smoothing out "true" peaks or troughs from the calcium record by treating the data in this way, however it is likely that much of suspected noise is a result of the laser ablating over the small vessels in the wood. The reduction of annual counts with the increasing (for peaks) or decreasing (for troughs) threshold was also expected since this would result in the exclusion of these smaller peaks and troughs.

In summary, the results for this tree suggest that the Ca peaks could be annual in nature, but this can only be verified using the "optimal" thresholds on an independent sample. The peak threshold of >1.25 SD and the trough threshold of <-1, both produced very similar annual calcium counts which agreed with the majority of the radiocarbon dates. Coherence was lost somewhat when considering the inner portion of the radial sequence. Additional radiocarbon dates may improve the results, however it is expected that further dates between samples 2A-Inner and 2A-A would be accompanied with large date ranges (similar to the 2A-Inner date) due to the flattening of the atmospheric carbon curve prior to the bomb peak.

For the remaining *T. macroptera* tree samples, the calcium data has been adjusted following the methods described in this chapter. More detailed plots of the data can be found in Appendix 2. In order to assign dates to these trees, both the >1.25 (smoothed) and <-1 standard deviation thresholds were applied (Threshold plots also in Appendix 2) as these were the two thresholds which resulted in the best matched dates for with the radiocarbon samples.

3.4.5. Validating the "Optimised" Ca Dating Method

The radiocarbon results from the five follow up radiocarbon dates for tree 2Y are given in Table 3-11 and reported at the ±1σ confidence level for conventional radiocarbon years BP (relative to AD 1950), % modern 14C and absolute % modern ^{14}C. As for tree 2A, these results

were corrected to $\delta^{13}C_{VPDB}$‰ using the $\delta^{13}C$ values in the table which represent the $\delta^{13}C$ in the original pre-treated sample material. The radiocarbon measurements were calibrated in the using the online CALIBomb software (Reimer *et al.*, 2013). The summarised results are presented in Table 3-12 and the CALIBomb output plots are presented in Figure 3-28.

The calibrated ^{14}C results for sample 2Y-Bark produced the age ranges of 1951.98 - 1953.17 and 2007.37 - 2008.29 with the probabilities of 0.884 and 0.116 respectively. Since the actual date of collection for the tree sample is known (Nov 2007), it may seem surprising that the probability that fits with this date is so low. This is due to calibration software and the use of the Levin dataset which is less regionally specific than the alternative options. When selecting the Levin dataset, CALIBomb uses data published by Levin and Kromer (2004) appended with data from Levin *et al.* (2008). This dataset was chosen for use with both trees (2A and 2Y) as the alternative calibration dataset which incorporates Cameroon (Northern Hemisphere Zone 3) does not include sufficiently recent measurements to cover all of the samples (Moreton, 2012, pers comm). The CALIBomb software (using these settings) only contains measurements up to the end of 2006 against which it can calibrate the sample, therefore it falls off the end of the calibration curve. This did not affect the 2A-Bark sample as the measured ^{14}C concentration landed just on the end of the distribution (Moreton, 2013, pers comm). A difference of >1.5% modern carbon was found between 2Y-Bark and 2A-Bark. This is itself is a little odd as both trees were sampled at the same time. Both trees appeared to be living when sampled with no signs of internal rot to suggest otherwise, therefore the % modern carbon should be very similar for the portion of wood sampled directly under the bark.

Table 3-11: Results from the radiocarbon dates from tree 2Y.

NRCF Allocation Number	Publication code	Sample identifier	$\delta^{13}C_{VPDB}$‰ ± 0.1	Carbon content (% by wt.)	^{14}C Enrichment (% modern)	+/- 1σ (% modern)	^{14}C Enrichment (Absolute % modern)	+/- 1σ (Absolute % modern)	Conventional Radiocarbon Age (years BP)	+/- 1σ (radiocarbon yrs BP)
1720.0413	SUERC-47603	2Y-Inner	-26.117	41.2	118.9792	0.5339	118.1188	0.5339	n/a	n/a
1720.0413	SUERC-47604	2Y-A	-26.719	41	108.9802	0.5271	108.1921	0.5271	n/a	n/a
1720.0413	SUERC-47605	2Y-B	-27.031	39	108.251	0.5245	107.4682	0.5245	n/a	n/a
1720.0413	SUERC-47606	2Y-C	-27.149	42	107.684	0.5217	106.9053	0.5217	n/a	n/a
1720.0413	SUERC-47607	2Y-Bark	-27.986	15	105.1067	0.5082	104.3466	0.5082	n/a	n/a

Table 3-12: Calibrated radiocarbon dates for each of samples from tree 2Y. Radiocarbon age was calculated using the online CALIBomb calibration software (Reimer *et al.*, 2013) available from http://calib.qub.ac.uk/CALIBomb/. The age ranges with the highest probability is highlighted in yellow.

Publication code (AMS Lab No)	Sample identifier	Absolute % modern	Absolute % modern error	F14C	F14C error	1σ age range	Probability	2σ age range	Probability
SUERC-47603	2Y-Inner	118.12	0.5339	1.1812	0.0053	1957.56 - 1957.94	0.148	1957.22 - 1958.32	0.209
						1986.53 - 1988.38	0.852	1985.99 - 1989.11	0.791
SUERC-47604	2Y-A	108.19	0.5271	1.0819	0.0053	1953.77 - 1954.24	0.187	1953.52 - 1954.52	0.193
						2001.13 - 2003.02	0.813	2000.02 - 2004.08	0.807
SUERC-47605	2Y-B	107.47	0.5245	1.0747	0.0052	1953.51 - 1953.97	0.180	1953.24 - 1954.25	0.185
						2002.34 - 2004.29	0.820	2001.25 - 2005.53	0.815
SUERC-47606	2Y-C	106.91	0.5217	1.0691	0.0052	1953.28 - 1953.77	0.160	1953.10 - 1953.97	0.152
						2003.05 - 2005.45	0.840	2002.46 - 2007.73	0.848
SUERC-47607	2Y-Bark	104.35	0.5082	1.0435	0.0051	1952.28 - 1952.85	1.000	1951.98 - 1953.17	0.884
								2007.37 - 2008.29	0.116

(a) 2Y – Inner

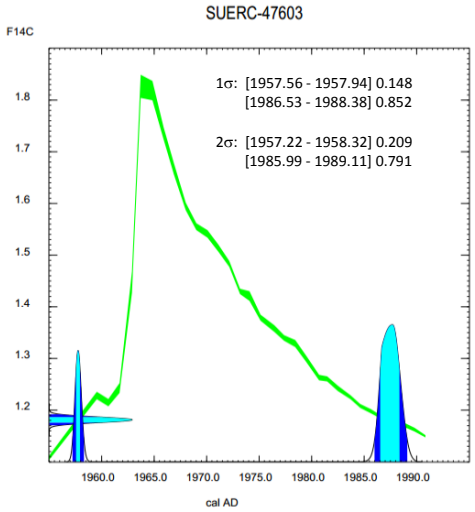

(b) 2Y – A

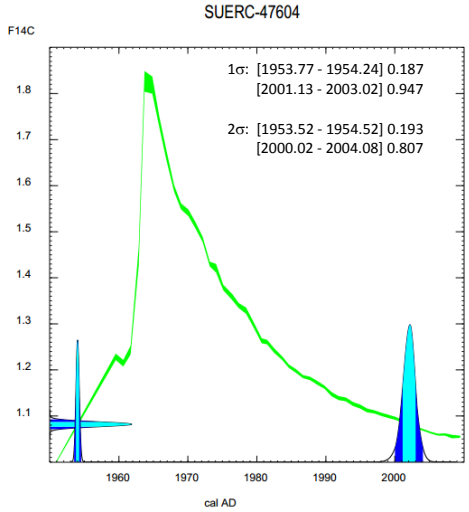

(c) 2Y – B

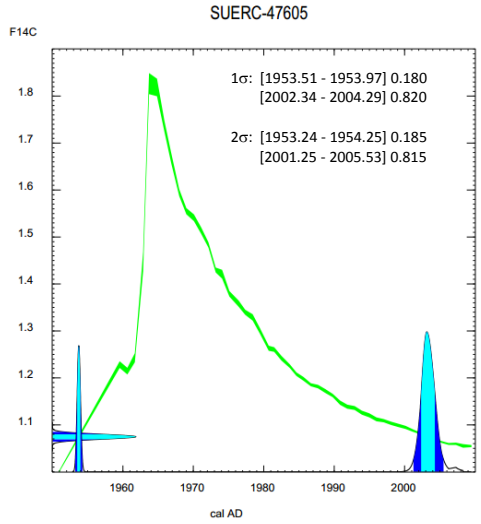

(d) 2Y – C

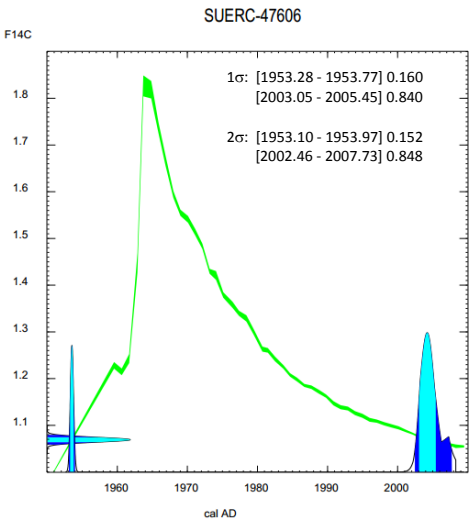

(e) 2Y – Bark

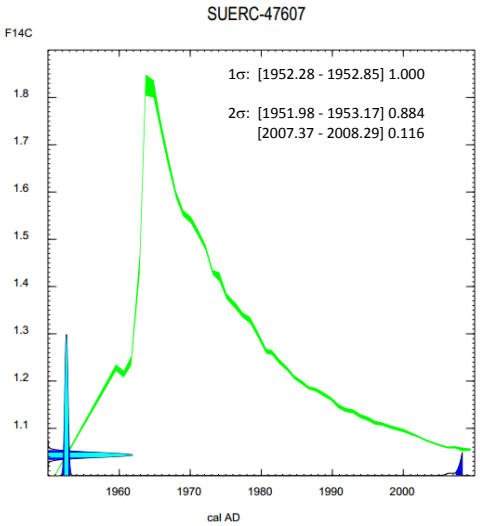

Figure 3-28: The plots (a-e) were produced using the online CALIBomb software which is available from http://calib.qub.ac.uk/CALIBomb/frameset.html. The calibration was carried out using the intcal13 calibration and Levin datasets, using a smoothing factor of 1.0 year.

The calibrated date ranges for samples 2Y-A, 2Y-B and 2Y-C are all very similar. Both sets of ranges (dates from ascending and descending limbs of bomb peak) overlap with each other suggesting that regardless of which date range is correct, the samples are all of very similar ages. As the sampling locations are known it can inferred that for samples 2Y-A, 2Y-B and 2Y-C, that the older date ranges for these three samples can be rejected, as this would put the samples out of chronological order with the 2Y-Inner sample. Finally, both date ranges for the 2Y-Inner sample are feasible since this would not disrupt the chronological order from sampling locations. Unlike with tree 2A, an attempt at a growth rate estimate to determine the likelihood of each of these ranges is not possible due to the very similar results obtained from the samples.

The calcium threshold approach was applied to tree 2Y using the >1.25 peak (smoothed) and <-1 SD trough threshold and results compared to the ^{14}C result (Table 3-13). Unfortunately, the thresholds "tuned" to tree 2A, did not provide dates that were in agreement with the ^{14}C results.

The radiocarbon dates acquired for 2Y are vastly different to that obtained for tree 2A. Both trees were sampled in 2007 and located within 100 metres of each other, although tree 2Y was situated in the savannah whereas 2A was found in the transitional area. It may be expected that both trees would experience similar growth rates but this may be dependant of individual circumstances. It is known that in this location in Cameroon, the forest is expanding out into the savanna (Mitchard *et al.*, 2009a). Evidence confirming this was found near to the field site, where a young forest had established itself in an area where some rotten savanna trees (of this species) remained. The rate of expansion is not known, however the transitional tree almost certainly began its life in a savanna environment, otherwise it could not have survived. Assumptions can me made regarding the effect that a change of environment could have on such a tree. For example, a reduction in growth as the environment becomes less favourable due to decreased light availability. It is therefore not unreasonable to suggest that the growth rates of these trees will have been influenced by the different ecologies in which they were growing. Since both trees would have started life in the savanna, growth rates in the juvenile period would be expected to be more similar, although other sites specific factors could be influential as well.

Although the two trees were of similar DBH[15], tree 2A was much taller than 2Y with the height of the first branch also significantly higher which may indicate an older tree (Table 3-14). Between the 2A-Bark and 2A-A samples, a minimum of 34 years of growth was found to be present in 31-35mm of wood. In comparison, only 7 years of growth were found between sample 2Y-Bark and 2Y-A in 39mm of wood. These vastly different growth rates could be related to faster juvenile growth in 2Y and/or be related to the change of the environment around tree 2A. This tree (2A) was radiocarbon dated at the pith (115.2cm from the bark) with the next closest sample on that radius approximately 8cm closer to the bark (2A-A) therefore the growth rates in the juvenile portion tree 2A are unknown. Further radiocarbon dates would not necessarily help constrain the dating of this younger portion of the tree due to the likelihood of large age uncertainties as a result of the shape of the ^{14}C calibration curve for this period. It is therefore feasible that the juvenile growth for tree 2A was similar to that of 2Y.

Juvenile wood is formed during the early stages of a tree's growth however this juvenile period will vary between tree species. Differences in the physical structure of the wood can exist between juvenile and mature wood such as mature wood exhibiting narrower rings, higher elasticity, higher density and dimensional stability (Medzegue *et al.*, 2007). Brienen and Zuidema (2005) reported that no distinct rings were formed in the juvenile period (up to 10cm of wood) for *Tachigali vasquerzii* trees in Bolivia, despite the trees laying down clear annual rings when mature. Similarly, Dunisch *et al.* (2002) found differences in juvenile ring structures in two plantation grown tropical species in central Amazonia. No obvious structural differences were noted in the *T. macroptera* samples collected for this study, however differences might only be seen at a cellular level and therefore not been observed here.

[15] Diameter at breast height

Table 3-13: Shows a summary of the possible ^{14}C dates obtained for four of the samples from tree 2Y. The calcium date each threshold was compared to the ^{14}C ranges, and the difference in years between the two ranges were calculated (Figure 3-26). The calcium ages which agree, or falls within the ^{14}C date range are highlighted in yellow.

Sample	**Potential ^{14}C ranges** (Probability)	**Ca Ranges – Peak threshold**		**Ca Ranges – Trough threshold**	
		>1	>1 (smoothed)	<-1	<-1 (smoothed)
2Y-Inner	(1) 1957.22 - 1958.32 (0.209) (2) 1985.99 - 1989.11 (0.791)	**1850** (1) 107	**1889** (1) 68 years	**1873** (1) 84 years	**1905** (1) 52 years
2Y-A	(1) 1953.52 - 1954.52 (0.193) (2) 2000.02 - 2004.08 (0.807)	**1943** (1) 10 years	**1954** (1)	**1949** (1) 4 years	**1967** (1) 13 years
2Y-B	(1) 1953.24 - 1954.25 (0.185) (2) 2001.25 - 2005.53 (0.815)	**1952** (1) 1 year	**1963** (1) 9 years	**1959** (1) 5 years	**1975** (1) 21 years
2Y-C	(1) 1951.98 - 1953.17 (0.152) (2) 2002.46 - 2007.73 (0.848)	**1973** (1) 20 years	**1980** (2) 22 year	**1981** (1) 28 years (2) 26 years	**1990** (2) 12 year

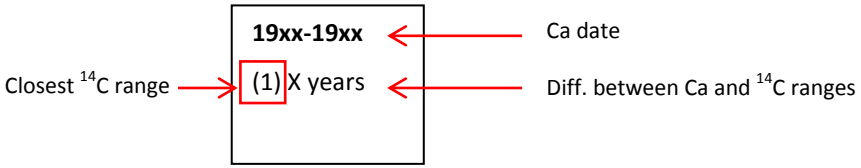

Figure 3-29: Graphical explanation of table layout

Table 3-14: Information collected about physical properties of the two radiocarbon dated trees. Height was estimated using a Laser Vertex Hypsometer (Haglöf, Sweden).

Tree Code	Tree height (m)	1st branch height (m)	Canopy Measurements (m)				DBH (cm)
			N	E	S	W	
2A	24.5	6.6	6.7	3	1	5	28.5
2Y	14.4	1.2	4.8	4.5	5.6	5	25.5

Worbes (2011) warned that care should be taken when utilising juvenile wood as young tropical trees may respond differently to growth limiting factors compared with mature trees. This is echoed in the findings of Priya and Bhat (1999) when they studied growth structure in teak trees in India. Their results showed that during juvenile growth, periods of cambium activity was increased, with shorter dormancy periods, in comparison to the mature trees of more than 20 years old. In addition for the first 3-4 years of growth, the type of wood laid down by the trees was diffuse porous rather than the later ring porous physiology. The radiocarbon results for 2Y-Inner put the most likely age at 1987.55±1.56 suggesting 20 years of growth in approximately 92mm of wood. It is possible that much of this radius is juvenile and on the basis of these previous studies, could therefore be structurally different to the mature wood. Due to the similar DBH of tree 2Y compared with that of 2A, it was not thought at the time of the calcium measurements that this tree would be so young. If the juvenile wood is structurally different as suggested by previous authors, then it is highly likely that the calcium distributions would be different from that of mature wood. Further investigation would be required to confirm whether this species is subject to such a change in wood structure from juvenile to mature wood. The seasonal calcium cycle found in Chapter 2 for the Scots pine trees found the latewood contained low amounts of calcium due to cambium dormancy. However, if dormancy is significantly reduced in juvenile periods as suggested by Medzegue *et al.* (2007), then this may not be well represented in the calcium distributions in this tropical species. It is possible that no annual pattern is present or detectable within this period. This would also help explain the discrepancy between the calcium and radiocarbon dates for the pith of tree 2A.

3.5. Conclusions

Poussart *et al.* (2006) showed that the calcium fluctuation found in the ringless species *Miliusa velutina*, produced a cyclic pattern. They developed an age-growth model for the calcium data which was shown to be annual in nature when compared with radiocarbon dates. This work demonstrated the potential of using dendrochemical techniques to potentially date tropical trees. However Poussart's preliminary work was not followed up. The methods adopted by Poussart *et al.* (2006) used a synchrotron x-ray microprobe to measure the calcium fluctuations which is not a technique readily available to most. LA-ICP-MS systems are frequently used in geological analysis and can be commonly found in many geoscience based laboratories making this a potentially more accessible method of analysis.

As outlined in Chapter 1 (Section 1.4, Figure 1-6), the network of climate stations of the tropics are sparse, and in most cases the data is short-lived. Tree-ring chronologies can potentially be used to study past climatic variability, woodland dynamics and age structure beyond the instrumental record. The lack of dating options for ringless tropical trees or the expense (time and money) of potential methods such as stable isotope analysis has so far halted progress in these areas.

This LA-ICP-MS method of dating using calcium as a tracer was detailed in Chapter 2 and tested using an accurately dated temperate species to validate its potential. This Chapter attempted to validate, and then independently test this threshold Ca dating method on a tropical species which does not contain distinct tree rings. The climate of the local area where the trees were collected experiences one dry season and one wet season per year, therefore it was hypothesised that any cyclic patterns in calcium could be annual in nature. Using this assumption as a basis for the dating, a calcium peak/trough threshold method was tested to attempt to accurately date the trees using these cyclic patterns.

Validation of the method was carried out, using a single sample, by applying various thresholds to the calcium data to test which provided the best agreement with the equivalent radiocarbon dates. Results found that smoothing data then applying either the peak based thresholds of >1.25 SD above the mean or the trough based threshold of <-1 SD below the mean provided the best agreement between the estimated calcium ages and the radiocarbon ages. Both of these thresholds produced almost identical age estimates which suggested that

the calcium annual increments were of a cyclic nature. The calcium distribution was however much noisier than the clear cyclic patterns found for higher latitude Scots pine (Chapter 2).

Despite such promising results from this validation on the initial test sample, application of the same thresholds to an independent tree sample did not confirm these findings. The radiocarbon dates obtained for the tree used in the independent test (2Y) confirmed that the tree was much younger than estimated from the calcium data. Previous authors have found juvenile wood in tropical species to show visual and structural differences compared with the mature wood. Such differences may in turn affect the calcium content and distribution during such a juvenile period resulting in a loss of dateable seasonal pattern. Such a phenomenon would also impact the juvenile portion of tree 2A which could explain the discrepancies between the calcium and radiocarbon pith dates. In addition to this, the different ecologies of the trees at the time of sampling must be considered as an explanation for the different growth rates. Tree 2A was situated in the forest/savanna transitional zone when sampled unlike tree 2Y which was still growing in open savanna. The forest encroachment around tree 2A may have caused reduced growth rates due to the change towards less favourable growing conditions for this species. It is likely that a combination of these two factors may contribute to the growth rates identified in these trees from the radiocarbon dates. However, further samples would need to be analysed in future work order to investigate this fully.

The success of the calcium dating for tree 2A suggests that the calcium signal may still be annual despite the lack of confirmation form tree 2Y. Furthermore, this result could be strengthened if confirmation of juvenile disturbance could be confirmed for the inner pith date. Further work is ultimately required to truly validate using calcium as a tracer to date tropical trees, however the results presented here show potential. To thoroughly assess this calcium based dating method, trees with some degree of dating control are required such as:

- Tropical trees which are known to contain visible annual growth rings allowing traditional dendrochronological methods to date the trees
- Multiple ^{14}C dates (such as outlined in Section 3.3.5) for more than one tree
- Using trees from plantations of known age
- Punched trees or use of dendrometers to assess growth rates (see Section 1.3.1)

Chapter 4: Are Stable Isotopes the Answer to Dating Tropical Trees?

4.1. Introduction

Traditional dendrochronological methods do not work well in the tropics (Section 1.3) due to the lack of distinct annual rings. The previous two chapters concentrated on developing and testing an alternative method for dating tropical trees in situations where traditional methods fail. Fluctuations in calcium concentration identified a promising method for the detection of a seasonal signal using the temperate Scots pine species. Despite showing initial promise when tested on a single sample of the tropical species *Terminalia macroptera*, the method ultimately failed when tested on an independent sample (Chapter 3, Section 3.4.5). Despite this disappointing result, it is felt that further experimentation is needed to test Calcium based dating as it could still be a viable dating method for some tropical tree species.

At this time, stable isotopes are commonly used to identify seasonal trends for some species allowing the dating of some tropical tree species (Evans and Schrag, 2004, Poussart *et al.*, 2004, Poussart and Schrag, 2005, Anchukaitis *et al.*, 2008b, Ohashi *et al.*, 2009, Loader *et al.*, 2011). In addition, stable isotopes may provide further information regarding tree growth and environmental conditions which may not always be obtainable when the ring width climate signal is weak (Loader *et al.*, 2008). Due to the lack of distinct rings, this approach requires high resolution sampling in order to attempt to show seasonality and success is not guaranteed (Poussart and Schrag, 2005). Analyses are expensive in both monetary and labour terms, and validation of the dating is often required from radiocarbon dating, adding to the costs.

As the calcium dating approach failed (Chapter 3), this chapter aims to identify whether a seasonal pattern can be identified from isotopic records measured from *Terminalia macroptera* (tree 2A - which was the focus of Chapter 3). Radiocarbon dates for this tree will be used to calculate growth rates and provide a means to calendar date the isotopic sequences and determine their nature. In addition, the isotopic records, once dated, can be compared with local climate data which may provide insight on the climatic controls of growth.

4.1.1. Isotopic Measurement of Trees

Wood is comprised of several different components including cellulose, lignin and resin. Isotopic analysis can be carried out on either the whole wood or isolated components such as cellulose or lignin. The strength and limitations of the use of each of these materials for isotopic analysis has been discussed by several authors (Wilson and Grinsted, 1977, Barbour *et al.*, 2001, Loader *et al.*, 2003, Cullen and Grierson, 2006). Wilson and Grinsted (1977) demonstrated that not only do the components of wood differ isotopically, but the lignin to cellulose ratio is not constant over a growth ring. This prompted a move towards the isolation and analysis of α-cellulose, which makes up the largest proportion of wood, reducing the potential of associated problems caused by the varying cellulose to lignin ratios.

Cellulose extraction is time consuming and with the constant improvements in instrumentation, has become the limiting factor for throughput of analysis with respect to isotopic analyses in dendrochronology. The need for cellulose extraction has been examined by Borella *et al.* (1998) and Loader *et al.* (2003) concluding that for $\delta^{13}C$ analysis, cellulose extraction provides no significant advantages over the use of whole wood. However, for $\delta^{18}O$, Borella *et al.* (1999) reported significant differences between the wood components and suggested some climatic information may be lost using whole wood over cellulose.

Most stable isotope studies rely on the principle that seasonal changes will be reflected in the tree's stable isotopes. When this principle is applied in the tropics however, the seasonality is more commonly related to precipitation seasonality rather than temperature seasonality which is often the driving force in temperate regions (Worbes, 1999, Evans and Schrag, 2004). Interpretation of the isotopic patterns therefore relies on an understanding the environmental controls influencing the isotopic composition of tropical wood.

4.1.1.1. Oxygen Isotopes

The oxygen found in the wood components of trees comes from soil water. In most tropical environments the soil water originates from precipitation (as opposed to rivers etc.). The following equation, derived by Roden *et al.* (2000) explains how the oxygen isotope

composition of cellulose is dependant of the isotopic composition of the source water and the fractionation from evaporation at the leaf (Roden *et al.*, 2000, Evans and Schrag, 2004):

Equation 2: $\delta^{18}\mathrm{O}_{\mathrm{cx}} = f_o(\delta^{18}O_{wx} + \varepsilon_o) + (1 - f_o)(\delta^{18}O_{wl} + \varepsilon_o)$

$\delta^{18}\mathrm{O}_{\mathrm{cx}}$ - oxygen isotope composition of cellulose

$\delta^{18}O_{wx}$ - oxygen isotope composition of xylem water

$\delta^{18}O_{wl}$ - oxygen isotope composition of leaf water

ε_o - biochemical fractionation factor (+27‰)

f_o - portion of cellulose oxygen which exchanges with stem or leaf water

After water uptake from the soil, the δ^{18}O is fractionated at the leaf via evaporation through the stomata. Modifications of the fractionation model at the leaf were made to account for direct evaporation at leaf surface (Flanagan *et al.*, 1991) with further considerations for backward diffusion of the heavier water molecule at the site of evaporation (Barbour *et al.*, 2004). Further fractionation occurs during sucrose formation (Sternberg *et al.*, 1986) which is required for cellulose formation.

4.1.1.2. Carbon Isotopes

Carbon dioxide is an essential requirement for photosynthesis and thus for tree growth. The following equation summarises the relationship of the carbon isotope composition of cellulose to air (Farquhar *et al.*, 1982, Poussart *et al.*, 2004).

Equation 1: $\delta^{13}\mathrm{C}_{\mathrm{cx}} = \delta^{13}C_a - a - (b - a)(c_i/c_a) + \varepsilon_b$

$\delta^{13}\mathrm{C}_{\mathrm{cx}}$ - carbon isotope composition of cellulose

$\delta^{13}\mathrm{C}_{\mathrm{a}}$ - carbon isotope composition of air

a – discrimination against $^{13}CO_2$ during diffusion through the stomata (≈4.4‰)

b – discrimination against $^{13}CO_2$ during carboxylation (≈27‰)

c_i – intercellular CO_2 concentration

c_a – ambient CO_2 concentration

ε_b – post-photosynthetic fractionation effects

Trees take in CO_2 though the stomata in their leaves which is the first site of fractionation (Section 1.4.1.2) due to the ability of light isotopes to diffuse more easily (Farquhar *et al.*, 1982). Further fractionation occurs due to the isotopic discrimination against $^{13}CO_2$ during carboxylation. The rate of the CO_2 fixation impacts the C_i/C_a ratio, therefore changes in light and moisture availability as well as seasonal variations in the isotopic composition of ambient air will be reflected in $\delta^{13}C_{cx}$.

4.1.1.3. Controls on Isotopic Composition

Seasonality in the tropics is most often reflected with changes in precipitation and relative humidity which can induce periods of cambial dormancy, opposed to temperature which is usually dominant in temperate regions. In the tropics, such dormant periods can result in the formation of a visible annual growth ring (D'Arrigo *et al.*, 1994, Trouet *et al.*, 2001, Therrell *et al.*, 2006, Buckley *et al.*, 2007), but this is more often not the case. With precipitation as the main driver for growth, it may be expected that a seasonal pattern would present itself within the oxygen isotope signal stored within the wood components. Due to the fractionation processes described above, the isotope record is not a direct representation of environmental controls, however these can still heavily influence the records stored within a tree.

A tree growing in a tropical savanna environment has access to light throughout the year and seasonal access to water due to the precipitation seasonality experienced in most tropical regions. In contrast, a tree growing in a forest environment would have less access to light but with increased availability to water (due to reduced evaporation from the soil). The factors controlling the $\delta^{13}C$ and $\delta^{18}O$ values vary depending on the growing conditions. As shown by equation 1 above, for carbon isotopes, fractionation is a function of the C_i/C_a ratio, therefore a measure of the balance between the stomatal conductance and photosynthetic rate (McCarroll and Loader, 2004). Higher $\delta^{13}C$ values therefore reflect a low C_i/C_a ratio which

can indicate low stomatal conductance or a high photosynthetic rate (Gebrekirstos *et al.*, 2009). Reduced stomatal conductance can occur when a tree is moisture stressed such as during drought periods, resulting in increased stomatal closure, subsequently allowing less CO_2 to enter the tree. The overall effect is a reduced C_i/C_a ratio therefore causing an increase in $\delta^{13}C$. If a tree is not moisture stressed then the rate of photosynthesis may be the dominant factor on the $\delta^{13}C$. Photosynthesis is mainly temperature and irradiance controlled, but since temperature in the tropics can be relatively constant, light availability may be of more importance.

The $\delta^{18}O$ values in trees originate from the soil water. This incorporates the $\delta^{18}O$ of precipitation, with fractionation occurring at the leaf through evaporation and the production of sucrose (equation 2). Factors which can affect the $\delta^{18}O$ of leaf water such as temperature and relative humidity therefore influence the signal stored in the wood components, as well as the precipitation signal (from soil water). In tropical climates, during a dry season, relative humidity is reduced. This may result in increased evaporation at the leaf, increasing the loss of the lighter isotope and increasing $\delta^{18}O$. Evaporation at the leaf is likely to be reduced during a rainy season, however during heavy precipitation the $\delta^{18}O$ can be influenced by the "amount effect". This is a process of precipitation which preferentially removes ^{18}O labelled water, reducing the $\delta^{18}O$ of precipitation (Gat, 1996, Evans and Schrag, 2004).

During the rainy season, evaporation at the leaf should be limited which reduces $\delta^{18}O$. The "amount effect" should however dominate, decreasing the $\delta^{18}O$ of precipitation and therefore the $\delta^{18}O$ of water entering the tree (Evans and Schrag, 2004, Pons and Helle, 2011). A decrease in $\delta^{13}C$ would also be expected during the wet season due to increased stomatal conductance (Pons and Helle, 2011). The dry season would likely see increased leaf evaporation, which may be increased with reduced humidity, resulting in an overall increase in $\delta^{18}O$ due to the loss of the light water molecules. An increase in $\delta^{13}C$ values would also be expected in the dry season since increased stomatal closure would be occur when the tree becomes moisture stressed.

4.2. Study Area and Sample Description

The *Terminalia macroptera* Guill. & Perr. (Combretaceae) tree analysed in this chapter was collected in November 2007, as part of the wider TROBIT project, from the same field site as described in Chapter 3 (Section 3.2), located at 5°59'08.33" N, 12°52'12.86" E in Mbam Djerem National Park, Cameroon. This species, *T. macroptera,* is a deciduous hardwood species, commonly found in moist savanna sites in West Africa (Pham *et al.*, 2011), and was the dominant savanna tree species found in this area.

The field area was near to the Djerem River (Figure 4-1 (b)) and was based around a forest-savanna transitional boundary, where past satellite images suggest that the forest is expanding into the savannah (Mitchard *et al.*, 2009b). Evidence supporting this expansion was found at the field site as *T. macroptera* trees were found growing in the transitional area of the forest, and some individuals were located in an area which had been completely overtaken by a young tropical forest trees. The tree which is the focus of this chapter was collected from this transition zone.

(a) (b)

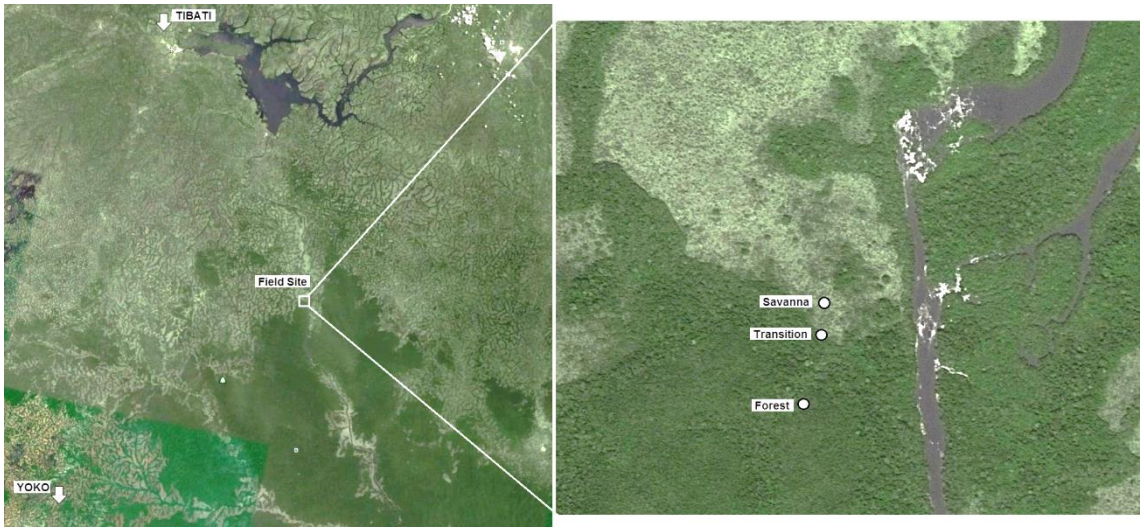

Figure 4-1: Satellite images showing locations of field sampling areas. (a) Positions of the two nearest climate stations to the field area are indicated by white arrows. Image acquired from Google Earth, Image data: Google, Landsat. (b) Shows approximate locations of individual sampling areas. Image acquired from Google Earth, Image data: Google, Cnes/Spot Image.

4.2.1. Field Site Characteristics

The savanna was characterised by tall grasses with frequent *T. macroptera* trees growing throughout. Figure 4-2 shows an example of the savanna environment with photo (a) showing a typical example of a *T. macroptera* tree. The trees appeared to grow in an asymmetrical manner which would likely contribute to the difficulties encountered when assessing the wood for traditional dendrochronological cross-dating and measurement (Section 3.3.1).

Figure 4-2: Photos representative of the savanna in the field site. (a) Shows trunk of *T. macroptera* tree surrounded by tall grasses. (b) General view with *T. macroptera* trees in the background

The forest-savanna boundary in this region represents an abrupt transition from the savanna into the forest. The gallery forest edge was dominated with young trees and saplings with a few savanna trees still present and living inside the forest. The savanna became woodier just before the forest entrance, with young saplings, woodier bushes and shrubs that were not present within the savanna. The remaining living savannah trees which were found inside the forest were found still present up to around 10 metres into the forest zone. Some remaining trees were found a little further away from this transition zone (Figure 4-3), where the forest was dominated by a different species (*Xylopia aethiopica*) which had completely overwhelmed any remaining savanna species.

Figure 4-3 (a) shows the view from the savannah looking towards the forest boundary. In this photo, the woodier bushes can be seen just outside the forest region. Figure 4-3 (b) shows the view of the boundary from just within the forest, looking out to the savanna.

(a) (b)

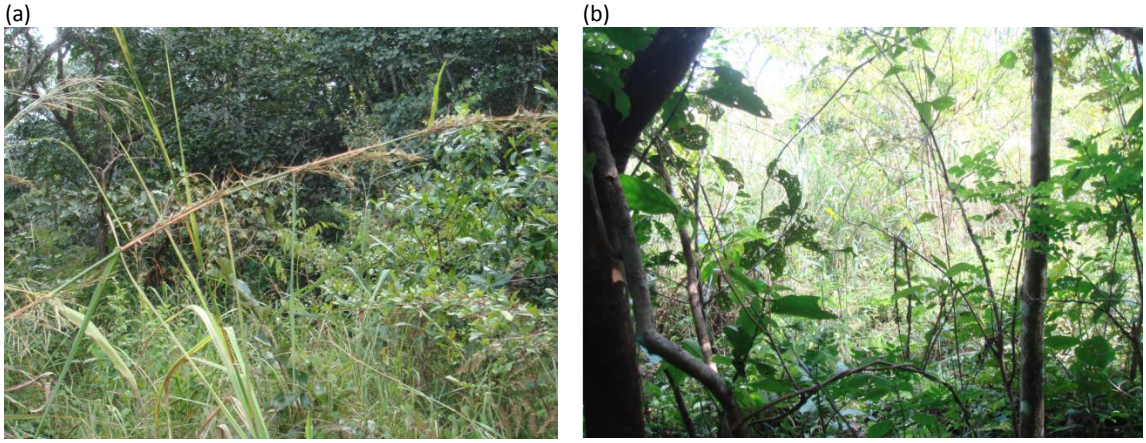

Figure 4-3: Photos show the forest-savanna transitional boundary. (a) Shows the view from the savanna looking towards the forest. (b) shows the view from just inside the forest looking out towards the savanna

4.2.2. Local Climate

The climate station network throughout Africa is sparsely distributed and often incomplete (Section 1.3). The nearest two climate stations to the field site are both situated just outside of Mbam Djerem national park (Section 3.2) near the towns of Tibati and Yoko. Tibati is situated approximately 64Km NNW of the field site, and Yoko is approximately 67Km SW. The data from both these stations are incomplete in places and relatively short. Precipitation records spans from approximately 1940-1994 in both stations however only 9 years of temperature data was available from the Tibati station, and 38 years from Yoko. Figure 4-4 shows the average monthly rainfall recorded for each of these stations. There is a pronounced dry season beginning in November and ending in March, with an average monthly rainfall of 30mm during these months, followed by the wet season from around May to October. The area experiences approximately 1650mm rainfall annually based on this data (Section 3.2). In order to use a more complete data set, precipitation and temperature data from the CRU TS 3.1 dataset (Harris *et al.*, 2014), which covers the period 1901-2009, was used for climate comparisons throughout this chapter. Both of these parameters are also shown in Figure 4-4. The CRU precipitation data is similar to that of the two weather stations and in particular to the Yoko precipitation record. Similarly, the temperature records were also comparable (data not shown here for Yoko and Tibati temperature records).

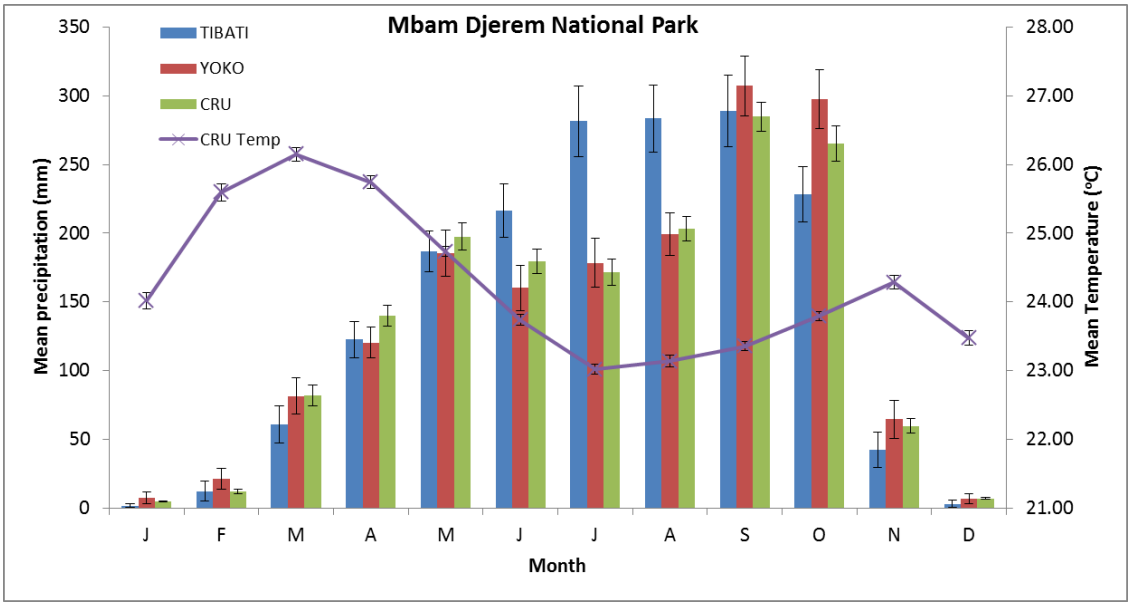

Figure 4-4: Average monthly rainfall data (±2 standard error of the mean (SEM)) from the two closest weather stations to the field site and the gridded CRU TS3.1 ((Mitchell and Jones, 2005, Harris *et al.*, 2014). Precipitation data is shown from the period of 1940-1994 for the two weather stations, and 1901-2009 for CRU dataset. Average monthly temperature data (±2 SEM includes the years 1901-2009 from CRU dataset.

Temperature can remain relatively constant in the tropics. Figure 4-4 shows the mean monthly temperature from the CRU dataset which vary between 22 and 26°C, with an annual average of 24.25°C. The dry season (Nov-Mar) experiences slightly higher mean temperature compared to the rest of the year, and the lowest average temperature fall in the middle of the wet season in July/August.

4.3. Materials and Methods

4.3.1. Sample Preparation

A thorough visual examination of the species was carried out and detailed in Chapter 3 (Section 3.4.1) resulting in the identification of visible ring-like structures in the wood. However both the non-annual nature and irregularity of the structures around the tree prevented traditional dendrochronological dating methods being applied. In species where distinct growth rings are present, sampling for stable isotope analysis can be done by simply splitting the wood into individual rings and analysing either a subsample of the whole rings, or

a particular portion of the ring (such as the latewood). Due to the lack of distinct growth rings in this species this approach was not possible.

Laths, approximately 1cm wide x 0.5cm thick, were cut from the tree wedge sections for each tree using a band saw. A GSL-1 bench top-microtome (Gärtner *et al.*, 2009) was then used to cut incremental slices along the lath at an equal distance of 50µm apart. The resultant small wood slivers could then be easily ground up between gloved fingers into fine shavings for further processing. Each sample was wrapped in tinfoil packets until cellulose extraction was required.

4.3.2. Measuring Isotopic Ratios - Isotope Ratio Mass Spectrometry

Stable isotope ratios are measured as gaseous samples using an isotope ratio mass spectrometer (IRMS). Samples can be converted into gaseous form using either an "off-line" preparation method or an "on-line" or continuous flow (CF) system. A CF-IRMS system interfaces an elemental analyser with an IRMS allowing the analysis of solid samples. Solid samples are combusted or pyrolysed within the elemental analyser where a continuous flow of carrier gas (helium) is introduced, carrying the products into a gas chromatographic separation column (where they are separated by mass). The separated gases are then introduced into the IRMS system via the helium flow. A visual representation of these on-line processes is shown in Figure 4-5 (a) which represents this process using a High Temperature Conversion Elemental Analyser (TC/EA) for the analysis of stable oxygen isotopes and an Elemental Analyser for carbon isotope measurements in Figure 4-5(b). On entering the mass spectrometer, the sample gas is ionised and the resultant charged particles are accelerated by high voltage passing down a flight tube. The charged particles are deflected, according to their mass, to Faraday cup detectors. This is illustrated in Figure 4-6.

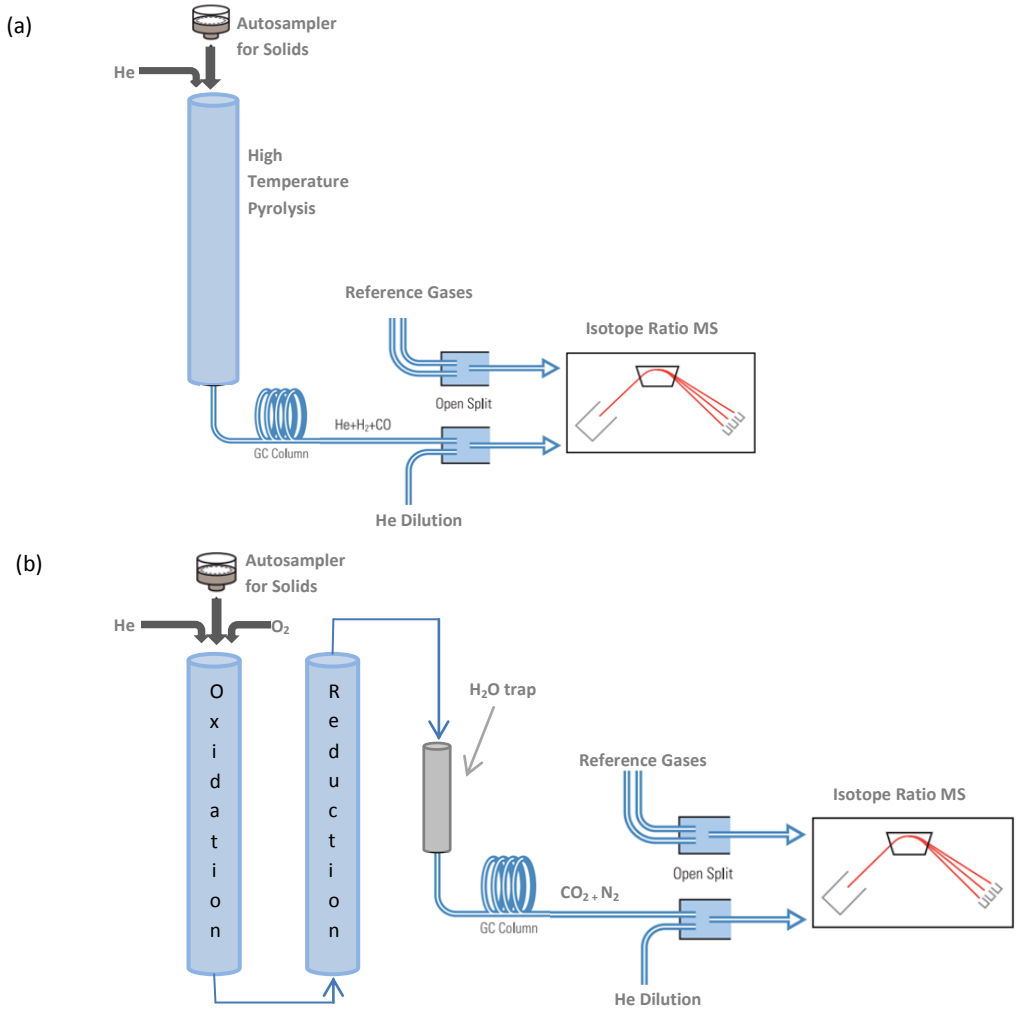

Figure 4-5: Schematic representation of an (a) on-line TC/EA system for $\delta^{18}O$ measurements (b) on-line EA system for $\delta^{13}C$ measurements. Images modified from (Scinco.com)

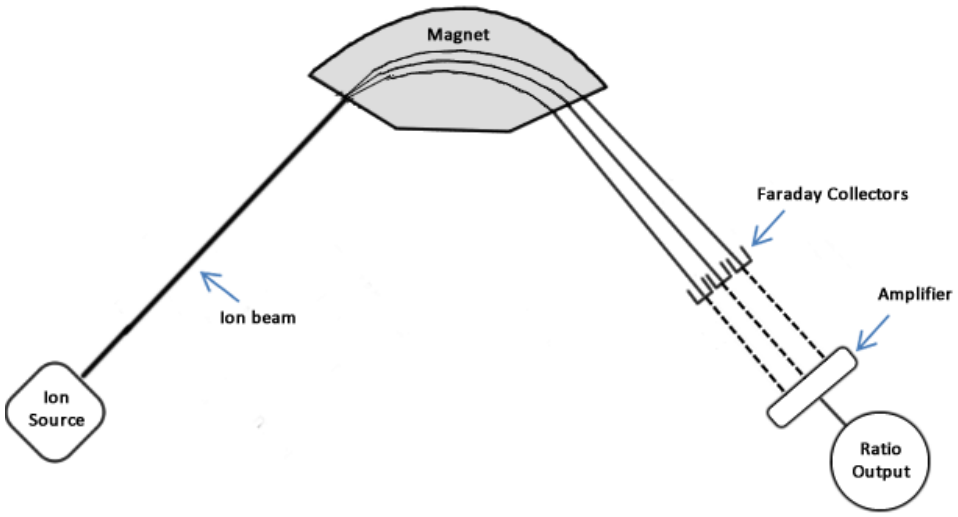

Figure 4-6: Schematic representation of an Isotope Ratio Mass Spectrometer

Although samples were cut into 50µm slices, samples were prepared and measured at 200µm increments due to the high analysis costs. Samples were prepared for isotopic measurements using the following protocols.

4.3.2.1. Cellulose Extraction

There are a variety of different cellulose extraction methods available. The Brendel method (Brendel *et al.*, 2000) was originally developed to process samples of 10-100mg of α-cellulose. Evans and Schrag (2004) adopted the Brendel method for analysis of tropical wood samples. The protocol was adapted to allow for analysis of smaller samples (0.2mg – 2mg) and to significantly increase the overall speed of the procedure. In order to ensure this modified procedure was to the highest accuracy, the modified and un-modified Brendel methods were tested alongside another cellulose extraction procedure (Jayme-Wise) at the University of Utah (Evans and Schrag, 2004). No significant differences were found in the % yield between the original and modified Brendel methods, and similarly no significant difference between the Brendel and Jayme-Wise methods.

The Brendel method (Brendel *et al.*, 2000) as modified by Evans and Schrag (2004) used here was chosen partly for practical reasons, since general purpose laboratory equipment could be used rather than expensive specialised glassware, but more importantly, the modified version allowed the extraction from small samples. This extraction procedure is summarised below.

The fine wood shavings for a sample which had been prepared previously, were removed from the tinfoil packet and emptied into a 1.5mL micro-centrifuge tube. Previous experimentation confirmed that the weight of a single ground up 50µm slice, fell within the recommended weight requirement of 500-2000µg. 120µL of 80% acetic acid (reagent grade) was carefully pipetted into the tube, followed by 12µL of 69% nitric acid (reagent grade). The cap was securely closed and the tube placed in a pre-heated dry bath at 120^{o}C for 30 minutes. After 30 minutes, the tube was removed from the dry bath and allowed to cool inside the fume hood for a few minutes. 400µL of 100% ethanol was added to the tube, the cap securely closed, and shaken thoroughly to mix the sample before being centrifuged for 20 minutes. The

supernatant was carefully removed and discarded. The remaining "wash" steps rinsed the resultant cellulose free from acid and involved adding the rinsing agent, capping the tube, mixing the sample, centrifuging for 15 minutes and finally removing the supernatant. The first rinse was done using 300µL of distilled deionised water (DDW), followed by a second rinse of 150µL of 100% ethanol, and finally 150 µL of acetone. The tube was then placed in a 40^{o}C drying oven for 30 minutes then freeze dried overnight. Batches of 20 samples were processed at one time. The procedure produced α-cellulose which was white and cottony in appearance.

4.3.2.2. Oxygen Isotope Analysis

For oxygen isotope analysis, 150-200µg of α-cellulose for each sample was weighed into a small pressed silver capsule. Each capsule was careful compressed to remove air from the sample and placed into a loading tray then freeze dried overnight prior to analysis. Samples were loaded into a zero-blank autosampler and residual air inside the autosampler was purged out with a helium flow. On-line pyrolysis was carried out using a Thermo Scientific High Temperature Conversion Elemental Analyser (TC/EA) by individually dropping each sample into the glassy carbon pyrolysis tube packed with glassy carbon chips at 1350^{o}C. The resultant gases (H_2 and CO) were carried by a helium flow through the GC separation column where they were separated by mass, into a Thermo Delta Plus XP isotope ratio mass spectrometer (IRMS) via a ConFlo III interface. The samples were measured and compared with reference gases of known composition. Two standard materials (an in-house cellulose standard and the standard reference material IAEA-601) of known isotopic composition were measured and distributed evenly though each run sequence. Results were exported into Microsoft Excel where data was corrected to the standards and also corrected for drift and linearity effects[16] within each run. The oxygen isotope ratios are reported in relation to VSMOW.

[16] A drift or a slight change in the results can be observed as a function of time (drift) or as a function of sample size (linearity). Including a sufficient number of identical standards distributed evenly through a run can allow these issues to be corrected for. Drift corrections require a sufficient standards number of identical standards to be distributed within the data, whilst linearity corrections require standards of varying weights.

4.3.2.3. Carbon Isotope Analysis

For carbon isotope analysis, 100-150µg of α-cellulose for each sample was weighed into a small pressed tin capsule. Each capsule was carefully compressed removing air from the sample and loaded into a Costech zero-blank autosampler before residual air inside the autosampler was purged out with a helium flow. On-line combustion of the samples was carried out using a Costech Elemental Analyser (EA), converting the carbon present in the sample to CO_2. Each sample was individually dropped into a quartz tube heated to 1000^{o}C where a volume of oxygen was introduced. The tin capsule reacted with the oxygen and combusted the sample at a temperature of around 1700^{o}C. The sample was then oxidised as it passed through chromium oxide and silvered cobaltous-cobaltic oxide. The combustion products, which include CO_2 and H_2O, were carried by a helium flow through a reduction reagent (copper wires) which removed excess oxygen before passing through a water trap. The gases were passed through a packed gas chromatography column where they were separated by mass before entering the Thermo Delta Plus XP IRMS via a ConFlo III interface. Reference gases of known composition were measured and compared with each sample. Results were recorded using the mass spectrometer software (Isodat), and the raw data was exported into Microsoft Excel for further processing. Samples of two standard materials of known isotopic composition (standard reference material B2155 and an in-house sugar based standard (Tesco)) were distributed evenly throughout each run sequence allowing data corrections to the standards and results to be reported in relation to VPDB. The standards also allowed each run sequence to be corrected for linearity and drift.

4.3.3. Calendar Dating the Isotopic Series

The samples selected for isotopic analysis were analysed at intervals of 200µm. Plotting the data on a distance scale may not therefore provide a true representation of the signal along the tree's radius as it is very unlikely that the tree grew at the same constant rate throughout its lifetime. Since growth rates are not known, the radiocarbon dates which were obtained for this tree (2A - see Chapter 3, Section 3.4.4) were utilised to place the isotope data for this tree on a calendar time-scale. Average growth rates were calculated based upon the mid-points of

each radiocarbon date range. Using these mid-points as tie points, an average rate of growth was assumed and the distance between the points was simply divided by the number of years to produce an average growth rate for that period. Each growth rate was then translated to the isotopic series for tree 2A. Since the isotopic sampling was originally done using equal distanced increments, more than one sequential value would equate to one year growth and the number of data points per year was dependant on the growth rate which was applied. Since average growth rates were assumed, each year was therefore equally split between the number of data points. For example, if 4 data points were allocated to the year 2000 to 2001, then these would be divided equally to 2000.25, 2000.50, 2000.75 and 2001. This was applied to both the $\delta^{18}O$ and $\delta^{13}C$ series.

Once the $\delta^{13}C$ series was translated to a calendar year scale, a further correction was applied to the data. This addresses the changes in atmospheric CO_2 which are not related to changes in climate, such as that caused by the burning of fossil fuels which preferentially releases isotopically lighter carbon (known as Suess effect) as well as the increasing atmospheric CO_2 concentration. For each $\delta^{13}C$ value, an appropriate correction factor was added. The correction factor was based on the values published in McCarroll and Loader (2004).

4.3.4. Climate Comparisons

With the isotopic data converted to a calendar scale, comparisons with precipitation and temperature data were possible. However, as multiple measures had been taken for some years in the earlier sections of the sample, it was possible to split the isotope data into "seasons". As outlined above, the portion of the year that each isotope point relates to was artificially generated by the equal sub-division of the year. To split the data further, a linear interpolation was performed on the data to produce four (quarterly) artificial seasons, allowing the relationship between each to be compared with seasonalised climate data.

Both the precipitation and temperature data (CRU dataset) was available with monthly values. The monthly climate variables were split into four quarterly seasons with the first season incorporating the dry season (Dec-Feb). Season 2 (Mar-May) represented "spring" which covers the start of the wet period, season 3 (Jun-Aug) included the central wet season month, and season 4 (Sep-Nov) consisted of the remaining three months (see Figure 4-4).

Correlations were performed between each quarterly isotopic series and seasonal values of precipitation and temperature to examine potential relationships between each variable. In addition, to remove influences of trend, correlations were performed using first differenced transformations of each series ($\delta^{18}O$ and $\delta^{13}C$, precipitation and temperature). Note however, that this analysis is performed in the knowledge that (1) the dating error of the isotopic series is ≥ ±1.6 years (Section 3.4.4) and (2) this transformation may lead to spurious correlations so any identified relationship ideally needs to be backed up with some biological theory.

4.4. Results

4.4.1. Standards

For oxygen and carbon isotope analysis, two standards (one international standard plus an in-house standard) were measured during each run sequence to monitor the accuracy and precision of the instrument and measurements. The precision (standard deviation) for each standard is given in Table 4-1. The precisions quoted here are representative for the entire run sequences carried out during the analysis in this study. The errors bars shown on the graphs in this chapter are reported as the precision of the standards as measured in each sequence.

Table 4-1: Precision is based on the average standard deviations for each standard analysed throughout all runs.

Oxygen		**Carbon**	
Standard	Precision (‰)	Standard	Precision (‰)
Cellulose (in-house)	0.1	B2155 (International)	0.04
IAEA 601 (international)	0.13	Tesco (in-house)	0.1

4.4.2. Isotope Records

The oxygen and carbon isotope ratios, measured at 200µm intervals along the tree radius from the outer bark end, towards the pith are presented in Figure 4-7 and Figure 4-8 respectively. Tabulated data can be found in Appendix 3 for each.

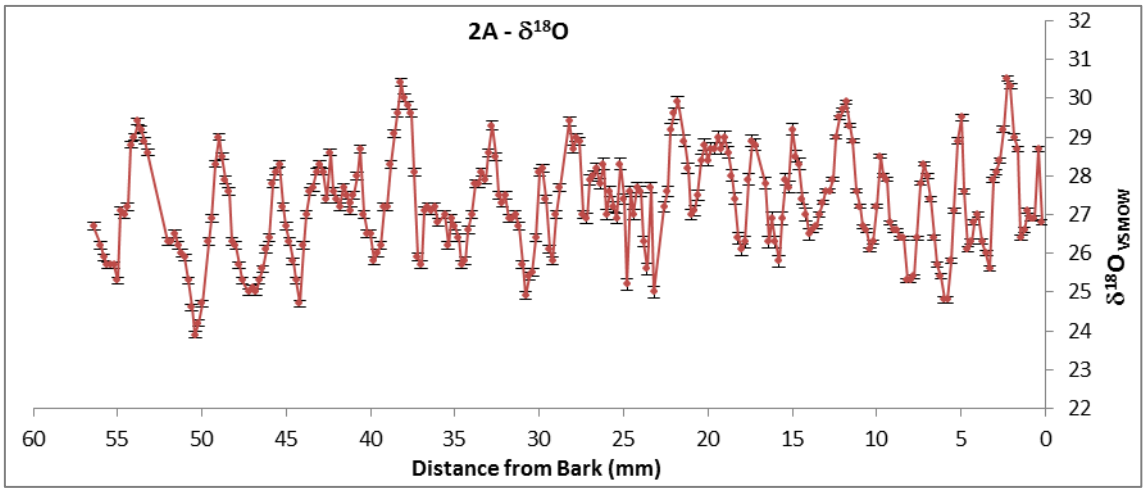

Figure 4-7: Oxygen isotope series for tree 2A, plotted by distance sampled along the tree's radius.

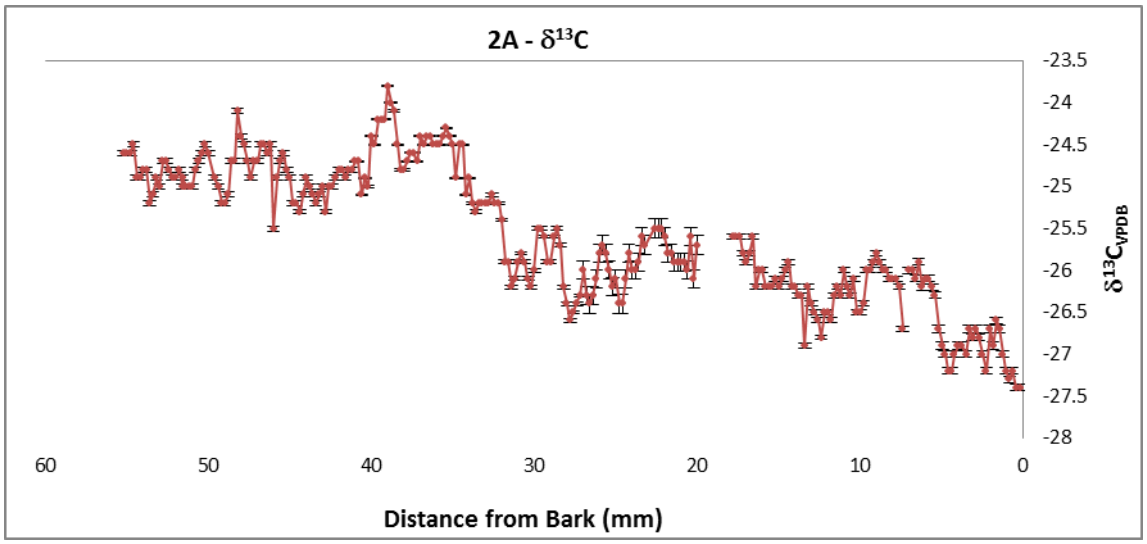

Figure 4-8: Carbon isotope series for tree 2A, plotted by distance sampled along the tree's radius. Data is uncorrected for Suess effect.

Initial observations show that the $\delta^{18}O$ record appears to show a clear cyclic pattern over the measurement period. There is an overall variation in the $\delta^{18}O$ record of 6.6‰, ranging from approximately 24‰ to 30.5‰, with the variation in most of the individual isotopic cycles of around 3-4‰.

The $\delta^{13}C$ record shows a declining trend across the tree's radius. This trend is commonly observed in carbon isotopic tree ring records measured over the industrial period (post AD 1950) and is thought to be influenced by the burning of fossil fuels which preferentially

releases isotopically lighter carbon (known as Suess effect) as well as the increasing atmospheric CO_2 concentration (McCarroll *et al.*, 2009). The overall variation in $\delta^{13}C$ values across the record was 3.6‰, which ranged from approximately -23‰ to -28‰. This range is accounted for mostly by the decreasing trend in carbon values. The isotopic 'cycles' in the $\delta^{13}C$ record are much less pronounced than seen with the oxygen isotopes averaging around 0.5‰ in amplitude.

4.4.3. Calendar Dating the Isotopic Series

The radiocarbon dates obtained for tree 2A (Chapter 3, Section 3.4.4) are summarised in Table 4-2. The sub-sampling of the wood for isotopic analysis (Section 4.3.1) was performed on the same area of the tree as where the radiocarbon samples were taken. This allowed growth rates to be calculated and applied to the isotopic series.

Table 4-2: Summary of ^{14}C dates which were obtained for tree 2A (NERC allocation number 1562.0411). The ^{14}C age ranges which have the highested probability are highlighted in yellow.

Sample identifier	Distance from Bark (mm)	^{14}C age range (2σ)	Probability
2A - Inner	115.00	1636.00 - 1691.00	0.325
		1726.00 - 1813.00	0.513
		1918.00 - 1950.00	0.151
2A – A	35.50	1962.64 - 1962.98	0.153
		1972.37 - 1973.65	0.847
2A – B	15.18	1957.26 - 1958.35	0.208
		1985.92 - 1988.99	0.792
2A – C	10.97	1956.01 - 1957.13	0.282
		1989.75 - 1992.92	0.718
2A – Bark	0	1952.83 - 1953.49	0.120
		2004.48 - 2008.29	0.880

The ^{14}C date ranges with the highest probability were used to calculate the growth rates. The three resultant growth rates (Table 4-3) were used to identify the positions of 'annual' boundaries in the isotope series. As would expected on most trees, growth rates are greater during the earlier years and the decrease from 1.36 to 0.7 is likely simply related to the

biological age trend. The 2A-Inner ^{14}C date was not included in the growth calculations as the uncertainty surrounding each of the possible age ranges was too large (Table 4-2).

Table 4-3: Growth rates used to date the isotopic series. These were calculated based on ^{14}C dates for the tree

Between ^{14}C Samples	Period	No of years	Distance between (mm)	Growth Rate
2A-A & 2A-B	1972.51 - 1987.46	14.96	20.32	1.360 mm/year
2A-B & 2A-C	1987.46 - 1991.34	3.88	4.21	1.085 mm/year
2A-C & 2A-Bark	1991.34 - 2007	15.67	10.97	0.7 mm/year

Figure 4-9 shows the oxygen isotope data after transforming to a calendar dated scale. The series is plotted from 1972-2007 which equates to the outer 35.5mm of growth (Figure 4-7). The clear cyclic pattern is still present in the data, with the outer ≈20 years producing much wider $\delta^{18}O$ cycles opposed to the narrower tighter cycles in the ten years preceding (1977-1987). It is apparent however, that each oscillation does not represent an annual cycle. In the period 1990-2007 (17 years), only 8-9 cycles are present within the data which is approximately half of what would be expected if the if the $\delta^{18}O$ expressed annual cycles.

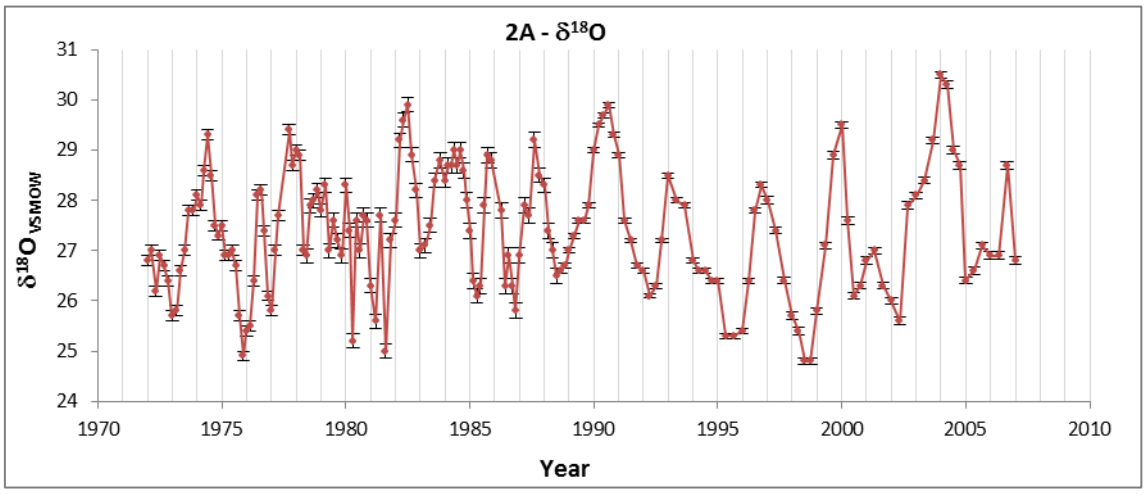

Figure 4-9: Oxygen isotope series for tree 2A. Data is plotted on calendar scale using growth rates calculated from the ^{14}C results.

In addition to assigning calendar years to both series, the $\delta^{13}C$ values were corrected (as outlined in Section 4.3.3) for changes related to atmospheric CO_2 (Suess effect and increasing

atmospheric CO_2 concentration). The result of this, as well as the translation of the data series to a calendar dated series, is shown in Figure 4-10. The data are similarly limited to 1972-2007 due to the radiocarbon dates. The data correction reduced the overall variation in the data range by approximately 1‰ for this region. The declining trend has been reduced. There is still a decline in values in the inner few years, and a drop in values after 1999. The series appears to flatten out in the middle section (1975-1998). No obvious annual patterns present themselves within this series.

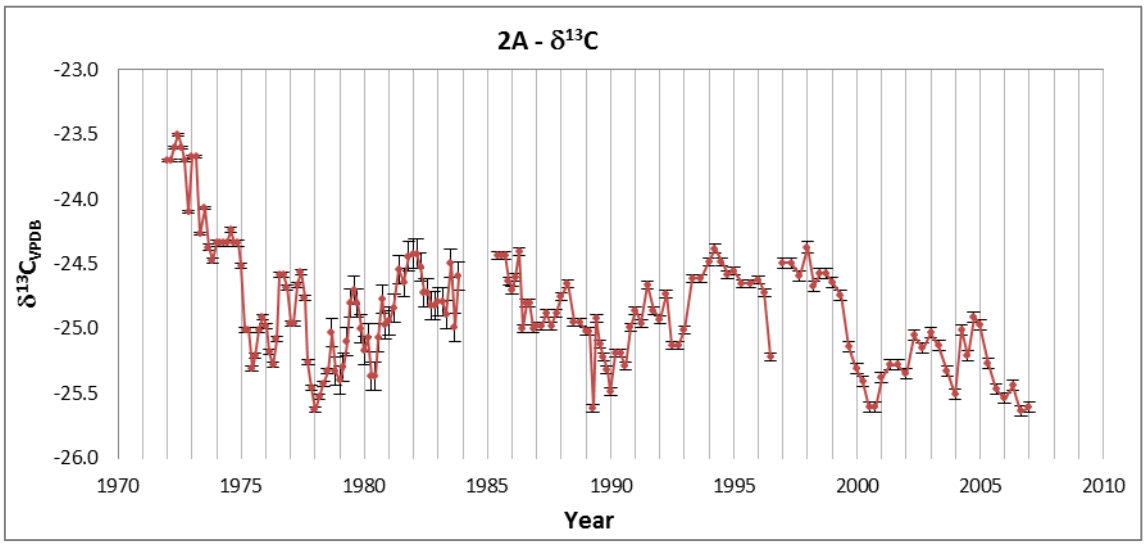

Figure 4-10: Carbon isotope series for tree 2A. Data is plotted on calendar scale using growth rates calculated from the ^{14}C results. $\delta^{13}C$ has been corrected for Suess effect based on (McCarroll and Loader, 2004)

4.4.4. Climate Comparisons

The results of separating the isotopic sequences into "seasonal" series, by linear interpolation of each data series, are shown in Figure 4-11 ($\delta^{18}O$) and Figure 4-12 ($\delta^{13}C$). In both figures, the original isotopic series is shown in the upper plot, as dated from ^{14}C derived growth rates, with four "quarterly" seasonal plots displayed below. The linear interpolations were performed in the same way for both isotopic series resulting in Season 1 representing the 1st quarter of the year, Season 2 as the 2nd quarter and so on. The correlations between each "season" are shown in the table within each figure which provides an indication of how each season relates or differs from the next.

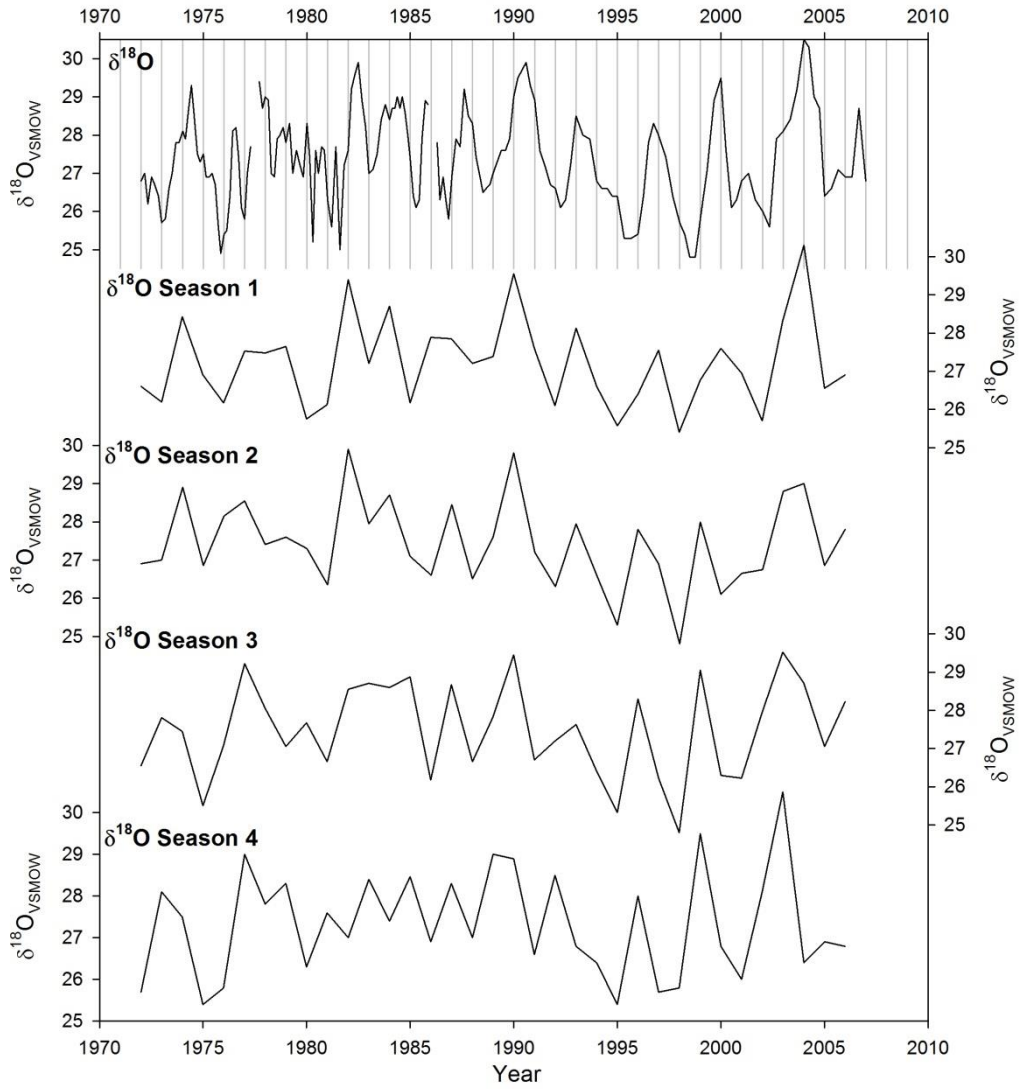

Correlations

		δ18O S1	δ18O S2	δ18O S3	δ18O S4
δ18O S1	Pearson Correlation	1	.758**	.460**	.198
	Sig. (2-tailed)		.000	.005	.255
δ18O S2	Pearson Correlation	.758**	1	.806**	.442**
	Sig. (2-tailed)	.000		.000	.008
δ18O S3	Pearson Correlation	.460**	.806**	1	.760**
	Sig. (2-tailed)	.005	.000		.000
δ18O S4	Pearson Correlation	.198	.442**	.760**	1
	Sig. (2-tailed)	.255	.008	.000	

**. Correlation is significant at the 0.01 level (2-tailed).

*. Correlation is significant at the 0.05 level (2-tailed).

Figure 4-11: The five plot show the original $\delta^{18}O$ data for tree 2A, followed by 'seasonal quaterly' $\delta^{18}O$ series generated by the linear interpolation of the orginal series. The correlations between each 'season' are shown as a representation of how this data relates to each other.

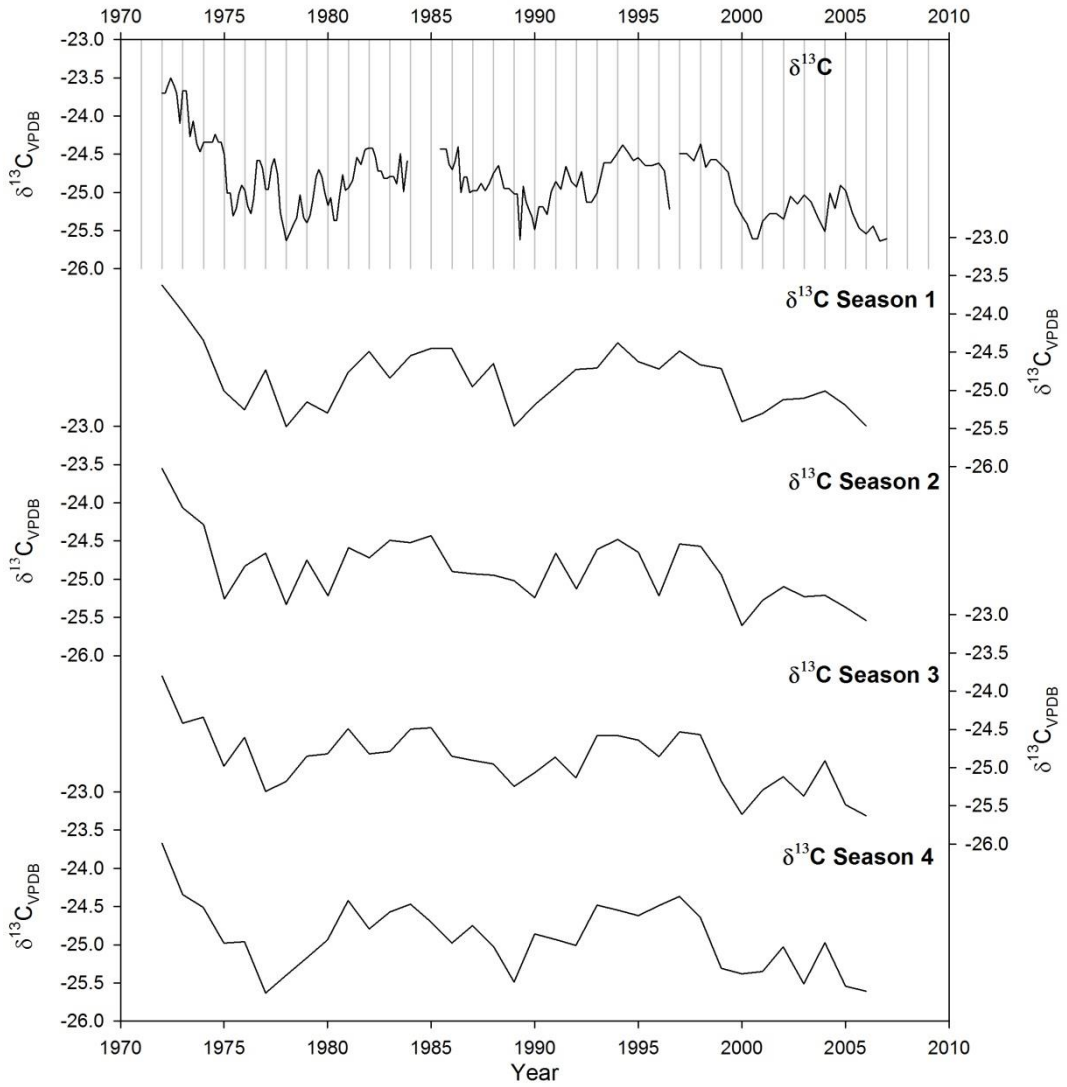

Correlations

		δ^{13}C S1	δ^{13}C S2	δ^{13}C S3	δ^{13}C S4
δ^{13}C S1	Pearson Correlation	1	.852**	.780**	.777**
	Sig. (2-tailed)		.000	.000	.000
δ^{13}C S2	Pearson Correlation	.852**	1	.877**	.775**
	Sig. (2-tailed)	.000		.000	.000
δ^{13}C S3	Pearson Correlation	.780**	.877**	1	.923**
	Sig. (2-tailed)	.000	.000		.000
δ^{13}C S4	Pearson Correlation	.777**	.775**	.923**	1
	Sig. (2-tailed)	.000	.000	.000	

**. Correlation is significant at the 0.01 level (2-tailed).

*. Correlation is significant at the 0.05 level (2-tailed).

Figure 4-12: The five plot show the original δ^{13}C data for tree 2A, followed by the 'seasonal quaterly' δ^{13}C series generated by the linear interpolation of the orginal series. The correlations between each 'season' are shown as a representation of how this data relates to each other.

For each parameter, the correlations are strong between each adjacent season, but become weaker when compared with the data from the other seasons. This is particularly marked for the $\delta^{18}O$ data compared to the $\delta^{13}C$ series which suggests much stronger autocorrelation in the original isotopic $\delta^{13}C$ data compared to $\delta^{18}O$. Similar seasonal plots are shown in Figure 4-13 for precipitation and Figure 4-14 for temperature. The study area features one dry season, starting during November and ending in March, and one wet season for the remaining months. The 1st quarterly "season" was chosen to cover the main dry season (Dec-Feb) since during this time there is almost no rainfall (Section 4.2.2, Figure 4-4), with each of the other seasons containing 3 months, following directly on from this. The same season periods were defined for the temperature data.

There were no significant correlations between each of the four precipitation seasons which is not surprising when comparing the distributions of monthly rainfall (Section 4.2.2, Figure 4-4) again highlighting the distinct hydroclimatic seasonality in the region. Since temperature remains relatively stable throughout the year, it is unsurprising that there is a marked about of coherence between the different temperature seasons.

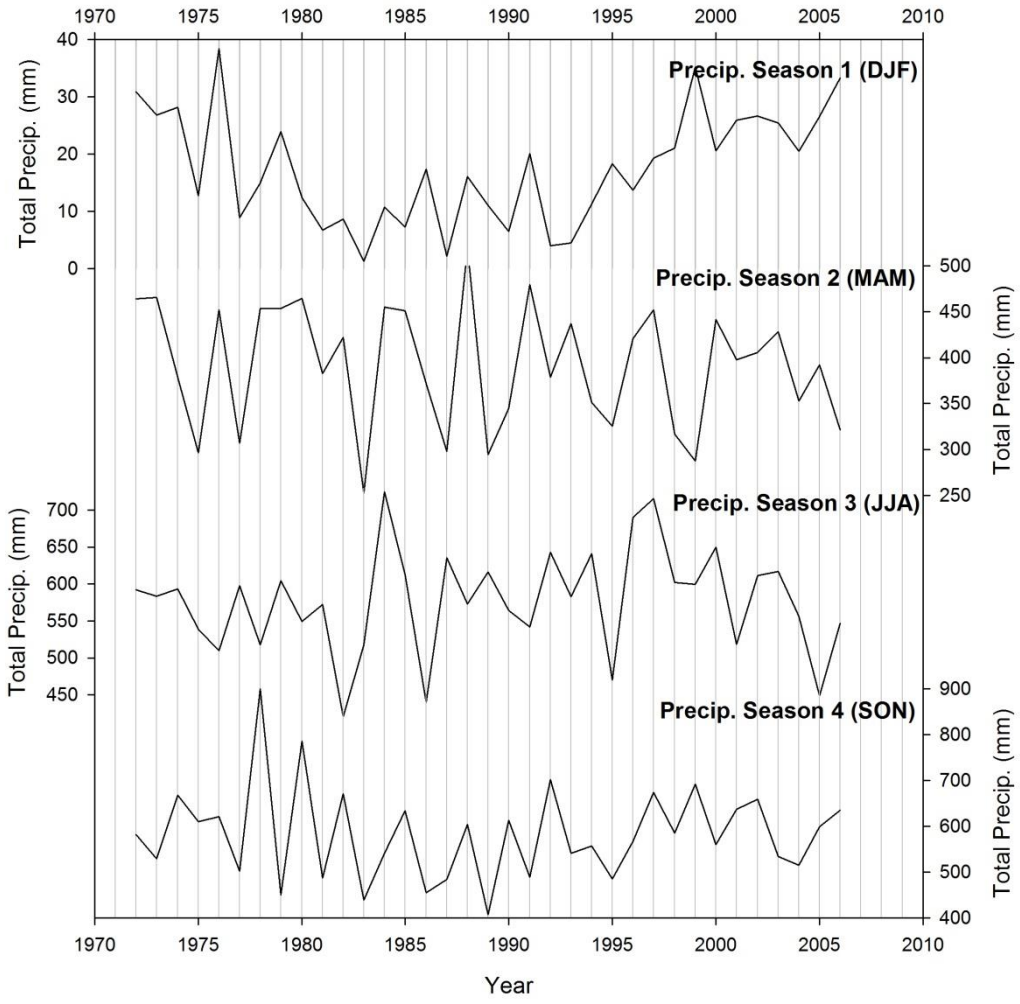

Correlations

		Precip S1	Precip S2	Precip S3	Precip S4
Precip S1	Pearson Correlation	1	.201	-.126	.179
	Sig. (2-tailed)		.248	.469	.302
Precip S2	Pearson Correlation	.201	1	.121	.292
	Sig. (2-tailed)	.248		.487	.089
Precip S3	Pearson Correlation	-.126	.121	1	-.043
	Sig. (2-tailed)	.469	.487		.806
Precip S4	Pearson Correlation	.179	.292	-.043	1
	Sig. (2-tailed)	.302	.089	.806	

**. Correlation is significant at the 0.01 level (2-tailed).

*. Correlation is significant at the 0.05 level (2-tailed).

Figure 4-13: The four plots represent the seasonal precipitation (data from CRU TS 3.1 (Mitchell and Jones, 2005, Harris *et al.*, 2014)) for 4 periods of the year. The correlations between each season show the relationship between the data for each season.

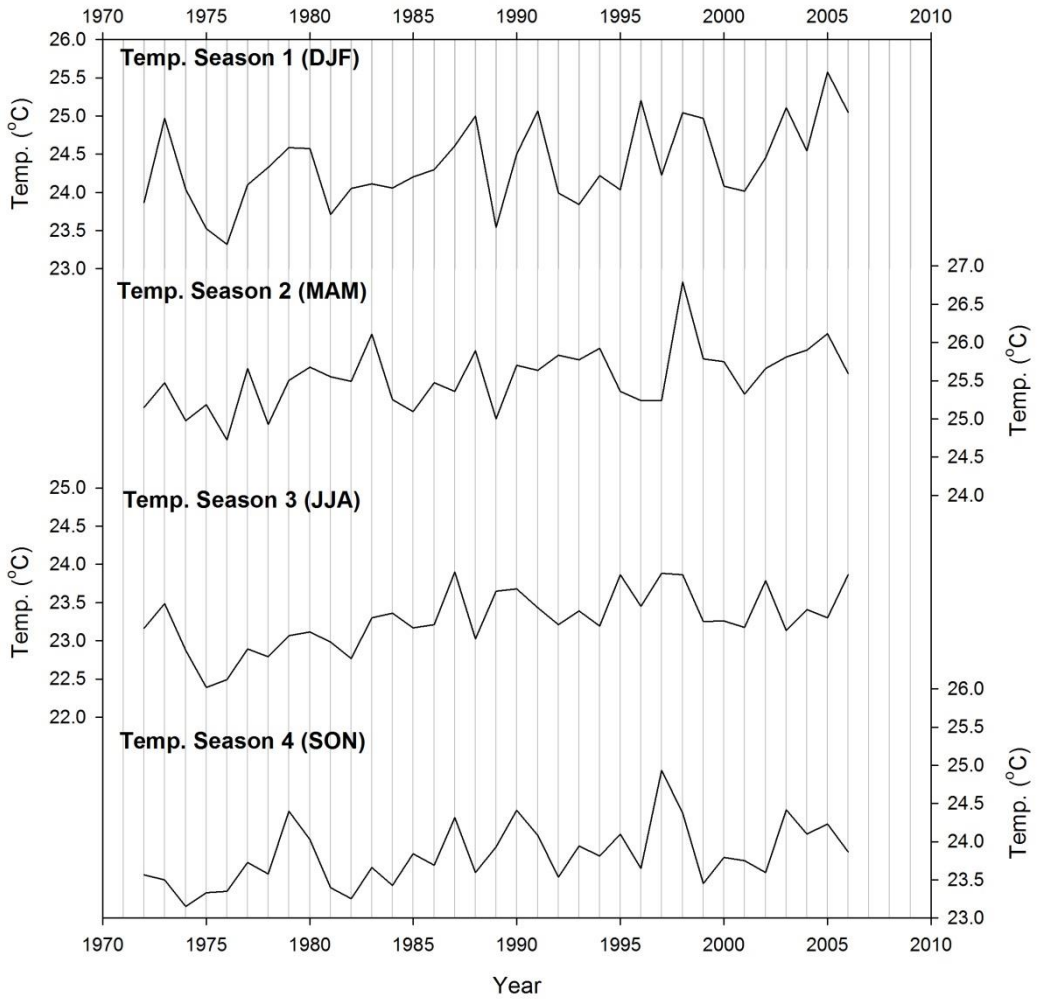

Correlations

		Temp S1	Temp S2	Temp S3	Temp S4
Temp S1	Pearson Correlation	1	.517**	.395*	.390*
	Sig. (2-tailed)		.001	.019	.021
Temp S2	Pearson Correlation	.517**	1	.322	.331
	Sig. (2-tailed)	.001		.060	.052
Temp S3	Pearson Correlation	.395*	.322	1	.604**
	Sig. (2-tailed)	.019	.060		.000
Temp S4	Pearson Correlation	.390*	.331	.604**	1
	Sig. (2-tailed)	.021	.052	.000	

**. Correlation is significant at the 0.01 level (2-tailed).

*. Correlation is significant at the 0.05 level (2-tailed).

Figure 4-14: The four plots represent the seasonal temperature (data from CRU TS 3.1 (Mitchell and Jones, 2005, Harris *et al.*, 2014)) for 4 periods of the year. The correlations between each season show the relationship between the data for each season.

Correlations were performed between each of the $\delta^{18}O$ and $\delta^{13}C$ quarterly series and seasonal records of precipitation and temperature. A first differenced transform was also performed on each of these datasets which removed any longer-term trends in the data by calculating the differences between each consecutive observation. Only the significant relationships are discussed here. Full correlation matrices for each of isotopic series with the seasonal precipitation and temperature data can be found in Appendix 3 (including the first differenced correlations).

Significant correlations were only found using the first differenced datasets for both the $\delta^{18}O$ and $\delta^{13}C$ series. Three significant correlations were found for the $\delta^{18}O$ records (Table 4-4), two of which related to the precipitation record, and one with temperature. For each of the parameters where significant correlations were found, their time-series are shown in Figure 4-15 ($\delta^{18}O$ S2 and Temp. S2), Figure 4-16 ($\delta^{18}O$ S3 and Precip. S3), and Figure 4-17 ($\delta^{18}O$ S4 and Precip. S3) - both for none and first differenced transformed versions.

Table 4-4: Significant correlations found between the $\delta^{18}O$ data with relevant climate records.

CORRELATIONS		**Precip. Season 3 (JJA) (1st Diff)**	**Temp. Season 2 (MAM) (1st Diff)**
$\delta^{18}O$ Season 2 (1st Diff)	Pearson Correlation Sig. (2-tailed) N	N/A	-0.342* 0.048 34
$\delta^{18}O$ Season 3 (1st Diff)	Pearson Correlation Sig. (2-tailed) N	0.370* 0.031 34	N/A
$\delta^{18}O$ Season 4 (1st Diff)	Pearson Correlation Sig. (2-tailed) N	0.405* 0.018 34	N/A

The correlation between the $\delta^{18}O$ (S2) and temperature (Mar, Apr, May) relates to a period of higher temperature which coincides with the start of the wet season (Figure 4-4). The highest average temperature is found in March, which then decreases to the mean annual low in July. Both of the significant correlations found between $\delta^{18}O$ (S3 & S4) and precipitation, are linked to the quarterly period of June, July and August (JJA). The monthly averages for precipitation show this period to be in the middle of the wet season. However, during these months, the

precipitation appears to be of similar amounts and has not yet reached its peak (higher amounts are found Sept/Oct).

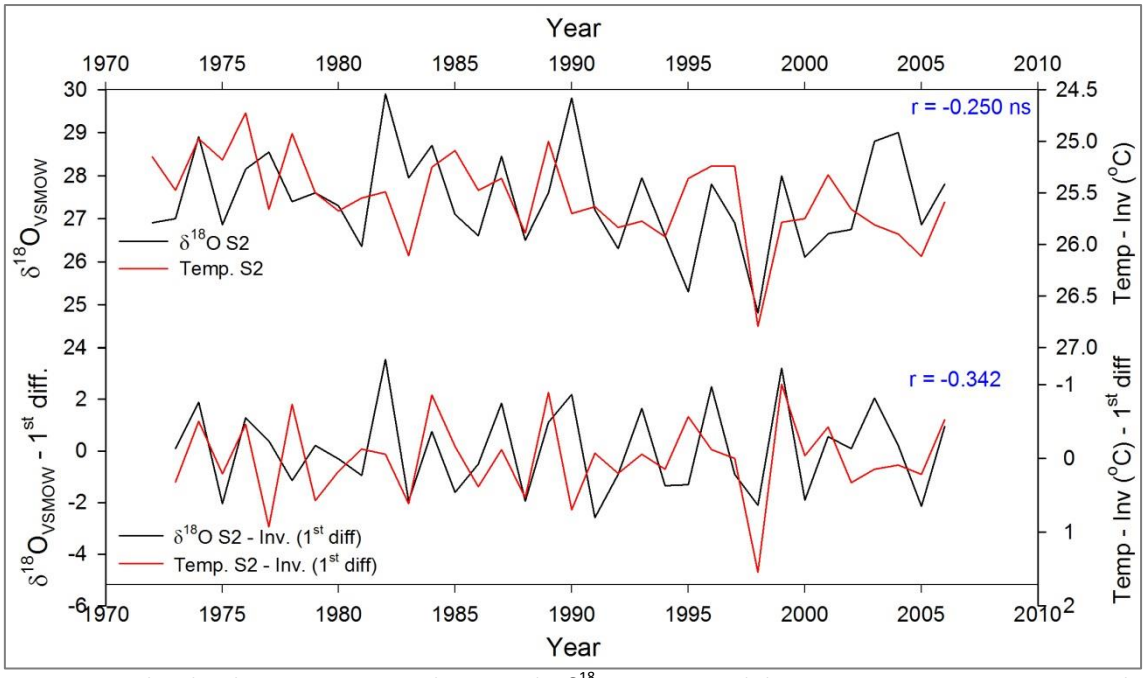

Figure 4-15: The plot shows a comparison between the $\delta^{18}O$ season 2 and the temperature season 2 series, with the first differenced versions of the same series (inverted for visual comparison). A significant negative correlation was found only between the 1st diff. series (r=-0.342).

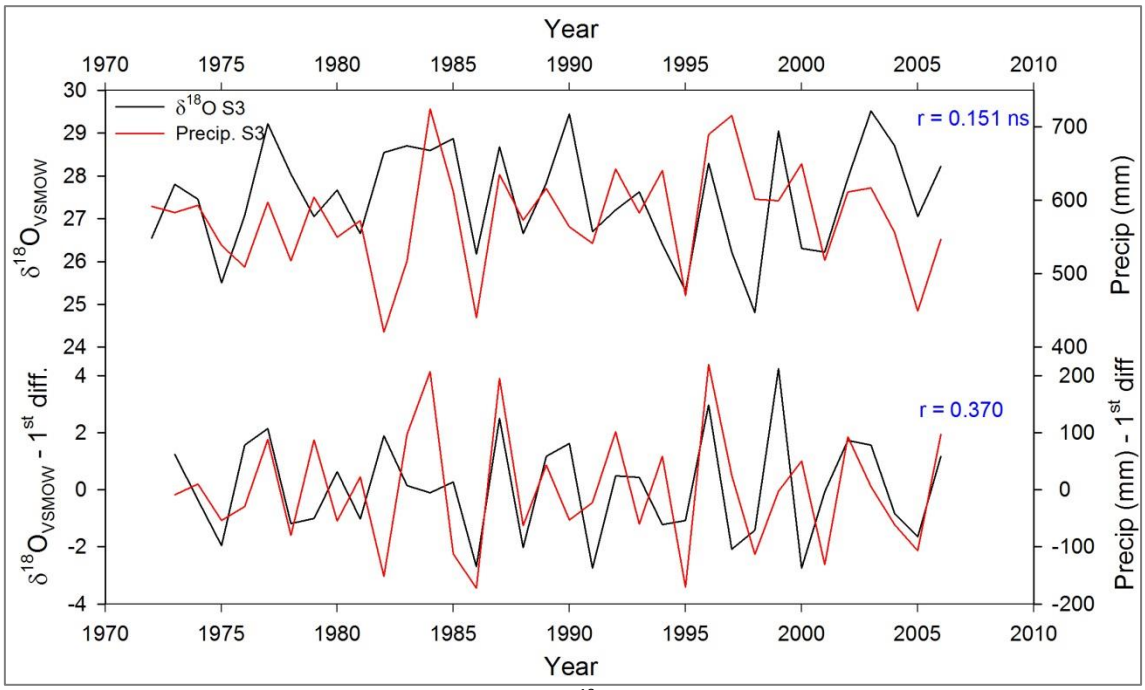

Figure 4-16: The plot shows a comparison between the $\delta^{18}O$ season 3 and the precipitation season 3 series, with the first differenced versions of the same series. A significant correlation was found only between the 1st diff. series (r=0.370)

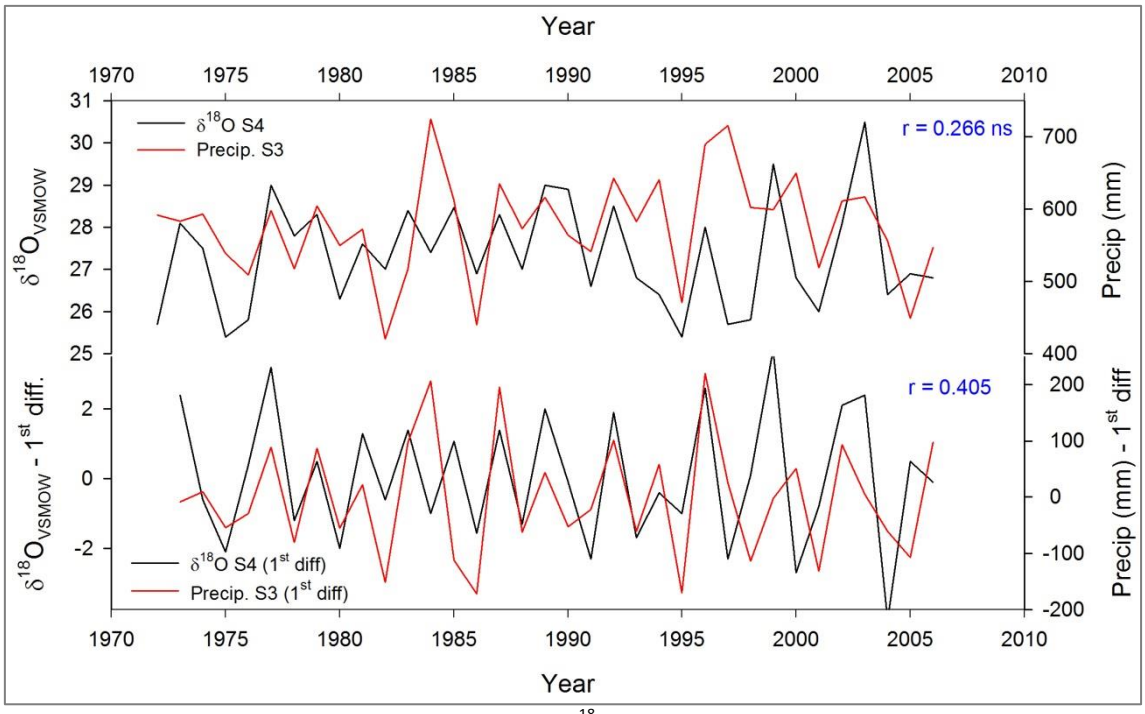

Figure 4-17: The plot shows a comparison between the $\delta^{18}O$ season 4 and the precipitation season 3 series, with the first differenced versions of the same series. A significant correlation was found only between the 1st diff. series (r=0.405)

For the $\delta^{13}C$ series, two significant correlations were found between the first differenced datasets (Table 4-5), both related to the precipitation record. Comparisons between the data before and after the first difference values are shown in Figure 4-18 ($\delta^{13}C$ S2 and Precip. S4), and Figure 4-19 ($\delta^{13}C$ S3 and Precip. S1).

Table 4-5: Significant correlations found between the $\delta^{13}C$ data with relevant climate records.

CORRELATIONS		**Precip. Season 4 (SON) (1st Diff)**	**Precip. Season 1 (DJF) (1st Diff)**
$\delta^{13}C$ Season 2 (1st Diff)	Pearson Correlation Sig. (2-tailed) N	0.371 0.031 34	N/A
$\delta^{13}C$ Season 3 (1st Diff)	Pearson Correlation Sig. (2-tailed) N	N/A	-0.417 0.0014 34

The quarterly periods for precipitation which correlated with the $\delta^{13}C$ series include the driest season (S1) and the wettest season (S4). The two "seasonal" $\delta^{13}C$ series which were involved were from 'neighbouring' seasons (S2 and S3) which correlated highly with each other (Figure 4-12) therefore it may be expected that the correlations for both of these $\delta^{13}C$ would be similar to each other with respect to the precipitation of S1 and S4. Although not significant, this was the case for correlations with precipitation S1 (dry season), although not for the S4 (wet season).

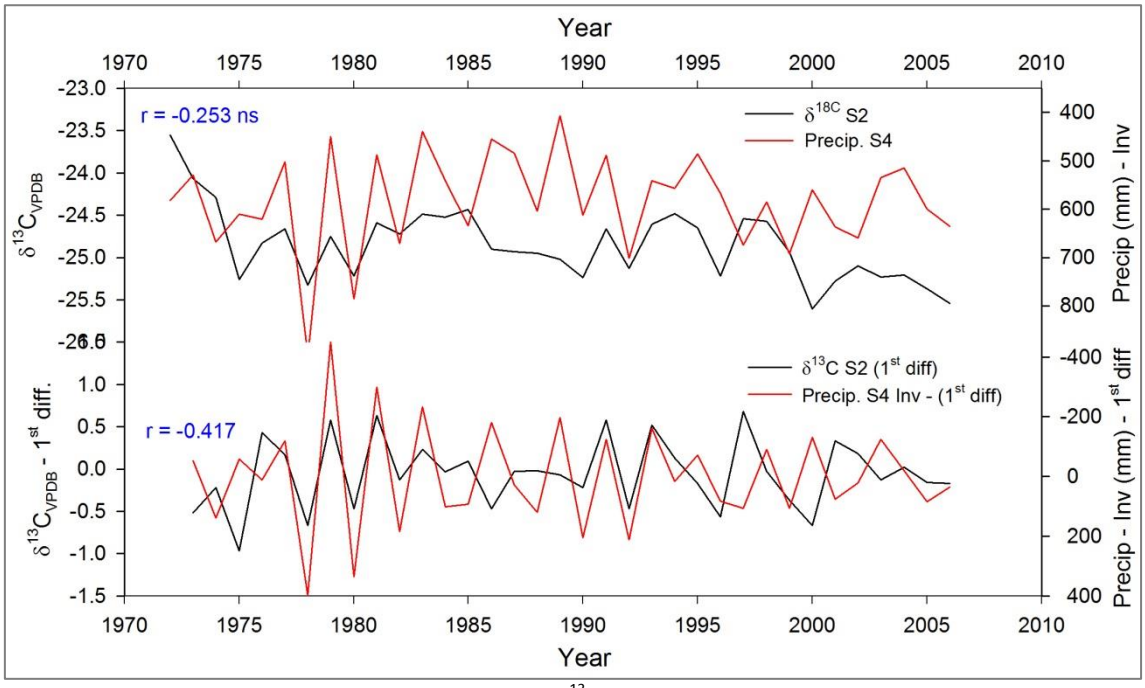

Figure 4-18: The plot shows a comparison between the $\delta^{13}C$ season 2 and the precipitation season 4, with the first differenced versions of the same series (series inverted for visual comparison). A significant negative correlation was found only between the 1st diff. series (r=-0.417).

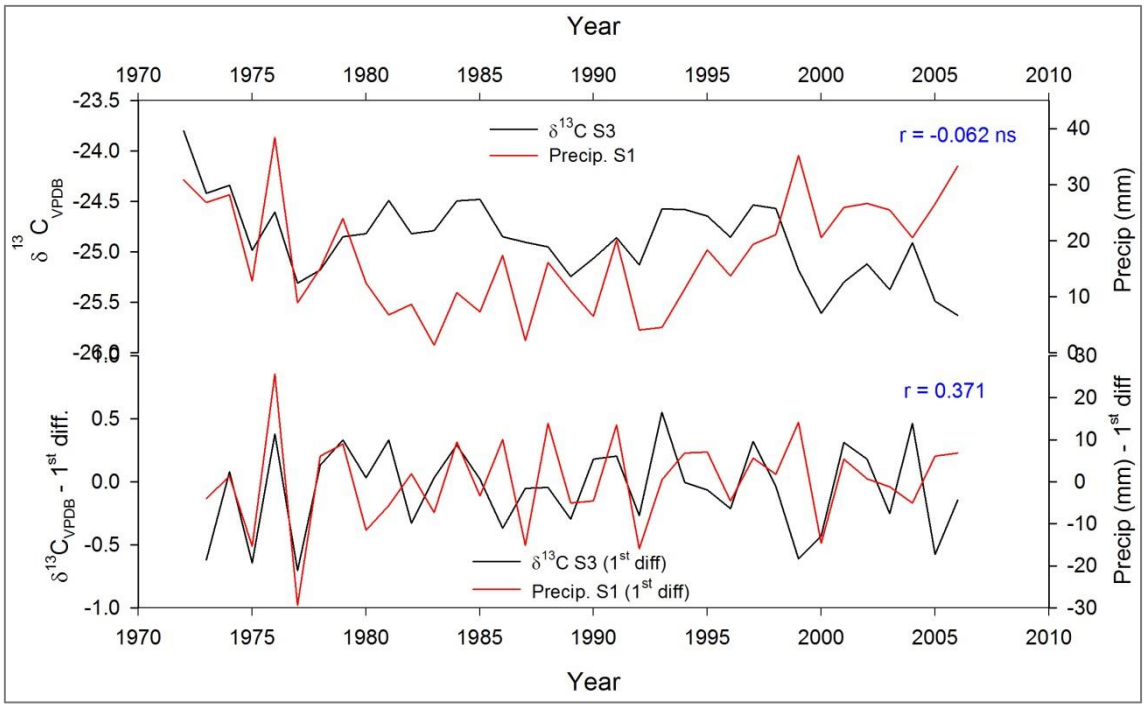

Figure 4-19: The plot shows a comparison between the $\delta^{13}C$ season 3 and the precipitation season 1 series, with the first differenced versions of the same series. A significant correlation was found only between the 1st diff. series (r=0.371)

4.5. Discussion

4.5.1. The $\delta^{18}O$ and $\delta^{13}C$ records

Tropical regions can experience significant precipitation seasonality, where prolonged monthly dry periods can induce cambial dormancy in the trees (Worbes, 1995). Annual and inter-annual variation in the isotopic records may be recorded in accordance with this seasonal environment. At the start of the wet (growing) season low $\delta^{13}C$ can be expected, due to the low rate of CO_2 fixation, with high inter-cellular CO_2 concentrations and increased discrimination against $^{13}CO_2$ during carboxylation. As growth continues, the inter-cellular CO_2 concentrations relative to ambient CO_2, result in increased $\delta^{13}C$ values (Poussart *et al.*, 2004). During the dry season, trees will have access to less water which directly affects the stomatal conductance (McCarroll and Loader, 2004). Source water (usually precipitation) has a large effect on the $\delta^{18}O$ in cellulose/wood. Evaporation in the leaf (a site of fractionation) is minimal during the wet season therefore the $\delta^{18}O$ of the precipitation has a large influence.

Evaporation in the soil before entering the tree can influence dry season signals as well as the evaporation at leaf (Farquhar and Gan, 2003).

The undated $\delta^{18}O$ series (Figure 4-7) presented a clear repeating cyclic pattern throughout the whole period of measurement, which exhibited a slight upward trend from pith to bark. The $\delta^{13}C$ record showed an expected decreasing which is common in trees and usually attributed to the Suess effect and increasing atmospheric CO_2 levels (McCarroll *et al.*, 2009). Without correcting for this, this strong declining trend in the data would likely mask any shorter term trends which may be present in the isotopic record.

Dating the isotopic series using the radiocarbon dates required the assumption of equal growth rates between each radiocarbon date (which has an error of ±1.6 years). Tree growth is heavily linked to the changing environmental conditions in which it grows, therefore although growth rates in a radial section may be similar in places, they would vary at least slightly depending of the conditions of growth at different times. As the relative dating uncertainty was small for the outer three ^{14}C dates (±1.6 years), all analysis in this chapter focused on the outer 35mm of the sample representing 1970-2007. Data prior to this period was ignored as the dating error was well in excess of 300 years (Table 4-2). The growth rates calculated over the period of measurement (Table 4-3) reduced in amount in direction of pith to bark. Growth generally decreases as a function of tree age resulting in smaller increments being laid as roughly the same amount of wood is laid down around an ever expanding girth. This observation is therefore not unexpected. The implication of applying fixed growth rates to each dataset are that series may become offset between each radiocarbon date which could result in the peaks/troughs in the series being slightly misaligned in time with respect to the exactly dated climate records. This may introduce addition errors or uncertainties to the data, which already have an error of ±1.6 years from the radiocarbon dates. If more trees were measured and dated in a similar manner, the effects of this could be minimised.

Poussart and Schrag (2005) used a similar approach to date two species (*Miliusa velutina* and *Quercus kerrii*) with multiple ^{14}C dates through the periods of 1950–2000 (nine ^{14}C dates) and 1980–2000 (five ^{14}C dates) respectively. Using the ^{14}C dates, it was confirmed that both $\delta^{13}C$ and $\delta^{18}O$ for these trees represented annual cycles with an error of ≤3 years. The Poussart study was based on one sample of each of the two species.

The dated $\delta^{18}O$ series (Figure 4-9) retained the cyclicity in the record. Applying the three calculated growth rates to the data resulted in wider peaks in the outer 20 years of the record compared with much narrower and noisier peaks in the inner period. It is clear from the dated series that the peaks and troughs in the $\delta^{18}O$ do not represent an annual signal.

The dating of the isotopic series using the radiocarbon dates allowed the decreasing trend in the $\delta^{13}C$ series to be addressed. A correction was applied to the data to assist in the removal of the decreasing trend related to the Suess effect. There are several proposed methods for handling the declining trend, which essentially involve adding an appropriate $\delta^{13}C$ correction factor to each year's value (Feng and Epstein, 1995, Treydte *et al.*, 2001, McCarroll and Loader, 2004) which was the method employed here. It is argued however, that such approach may not fully take into account the physiological responses of trees to the increasing atmospheric CO_2 (McCarroll *et al.*, 2009). McCarroll *et al.* (2009) developed a correction procedure which attempts to account for such responses. However, such an approach was deemed impractical for this study due to the slight dating uncertainties. To overcome this potential trend bias, correlations were performed between series after the data had been transformed to first differences. The $\delta^{13}C$ record does show some cyclic patterns within the records although these are much less pronounced than those in the $\delta^{18}O$ records.

Tree 2A was situated in the forest/savanna transition zone, therefore it is possible that this change in isotopic frequency may be related to a change in circumstances which accompanied the forest encroachment. However, it is not possible to make any definitive conclusion from the data of only one tree from the transition zone. Comparison of similar data from multiple trees situated from the savannah, transition and forest zones would provide a good methodological design for assessing the physiological changes (and resultant influence on isotopic series) for such a transition change.

4.5.2. Climate Comparisons

Visual comparisons between the $\delta^{18}O$ and the $\delta^{13}C$ records initially suggest that the oxygen record may reflect seasonal changes more clearly compared to carbon due to the more obvious cycles present in the data. The variability in the carbon records is much smaller in terms of overall variation and the amplitude of the peaks. This is in agreement to findings

from other tropical studies who reported the variability of $\delta^{18}O$ to be several times higher than of $\delta^{13}C$ (Poussart *et al.*, 2004, Pons and Helle, 2011). In addition, previous authors have suggested that an agreement between the $\delta^{13}C$ and $\delta^{18}O$ should be expected. This is due to both having an inverse relationship to precipitation amount and reliance on stomatal conductance (Poussart *et al.*, 2004, Verheyden *et al.*, 2004, Gebrekirstos *et al.*, 2009, Pons and Helle, 2011). However, as the isotopic series of some species have been found to lack any detectible seasonality signal, it would seem logical to assess the relationships of the isotope records separately.

Since this tree species analysed here (*T. macroptera*) lacked distinct tree rings, samples for isotopic analysis were cut from the tree lath in incremental 50µm slices, with isotopic analysis carried out at 200µm intervals. Subsequent conversion of the isotopic series on to a calendar scale using growth rates derived from ^{14}C dates, stretched and squeezed the dataset as required to fit the calendar dated scale. When making comparisons with monthly climate data, it was necessary to create so-called "quarterly season" time-series for each of the isotopic data-sets as there were multiple measurements for some years in the earlier sections due to the higher growth rates. This was done by a simple linear interpolation of the data which split each allocated year into four equal segments. It should be noted, that this artificial method of determining seasons within the record may not be truly representative of the actual seasonal periods due to the dating error of the radiocarbon dates. A similar approach for assessing relationships between tropical isotopic series with climate parameters was applied by Poussart and Schrag (2005) who used radiocarbon dates to produce growth rates for dating a tropical species with indistinct rings. Rather than applying a linear interpolation function to the series to produces seasonal values, they instead created three seasons using the maximum and minimum δ^{18} values, plus the maximum δ^{18} minus the minimum δ^{18}. Significant correlations were found between $\delta^{18}_{max\text{-}min}$ with dry season precipitation for some trees, as well as a negative correlation between δ^{18}_{min} and wet season precipitation which they suggest was linked to the "amount effect" (Section 4.1.1.3).

The correlation analysis between the isotopic series and climate variables produced some intriguing observations. Comparisons between the $\delta^{18}O$ and the $\delta^{13}C$ quarterly series, with either climate variable, produced no significant results without utilising the first differenced transform. When comparing the first differenced versions, three significant correlations were observed using the $\delta^{18}O$ series, and two from the $\delta^{13}C$ series (Table 4-4 and Table 4-5). All

significant correlations except one were with precipitation, which is the dominating factor is defining seasons in the tropics. The study area contains one wet and one dry season (Figure 4-4).

The two $\delta^{18}O$ (1st diff.) significant correlations with precipitation occur within adjacent $\delta^{18}O$ seasons (S3 and S4), and both correlate with summer (JJA) precipitation in both cases. This particular period is wet and slightly cooler than other season, however neither of these $\delta^{18}O$ seasons significantly correlate with temperature. Season 2 of the $\delta^{18}O$ (1st diff.) series correlated negatively with spring (MAM) temperature, which incorporates the highest temperatures of the year. For the $\delta^{13}C$ records, the two adjacent seasons (S2 and S3) produced significant correlations with precipitation seasons. However, one of these is the wettest season, and one is the driest.

For each of the correlations, it should be stressed that the so-called isotopic quarterly "seasonal" series may not be truly representative of their respective defined portion of the year due to ^{14}C dating uncertainties so the correlations noted herein should be interpreted very cautiously, especially as the results come from only a single tree. However, similar correlations have been previously reported between wet season rainfall and $\delta^{18}O$ series; these were inverse correlations which have been attributed to the "amount effect" (see Section 4.1.1.1) (Poussart and Schrag, 2005, Brienen *et al.*, 2011). Poussart and Schrag (2005) also reported a positive correlation between $\delta^{18}O$ and dry season precipitation, which showed no significance here. With regards to the temperature correlation with $\delta^{18}O$, a scan of the tropical isotope literature did not identify any temperature related relationships with $\delta^{18}O$ series from other studies. This is not to say that such a relationship is not possible, but the variability of the oxygen isotope signal is likely mainly controlled by hydroclimatic variability (i.e. water source). Temperatures may also have an effect on the fractionation of the lighter oxygen isotope at the leaf so a physiological explanation of the identified correlations may also be plausible as reduced temperatures may lead to less evaporation which in turn influences the isotopic values.

As mentioned above, one of the $\delta^{13}C$ (1st diff) seasons significantly correlated with the precipitation dry season (S1 - DJF), and the other is negatively correlated with the wettest season (S4 - SON). Although the carbon in a tree comes from atmospheric CO_2, the fractionation processes (Section 1.4.1.2) are also influenced by precipitation. During wet

periods, stomatal conductance will increase which in turn will decrease the $\delta^{13}C$ (Pons and Helle, 2011), and the opposite occurs during dry periods. Most authors have found negative correlation between $\delta^{13}C$ with precipitation (Gebrekirstos *et al.*, 2009, Ohashi *et al.*, 2009) which agrees with the wet season correlations presented here.

Isotopes have been measured in the tropics with mixed success. Verheyden *et al.* (2004) reported very similar and clear annual patterns between $\delta^{13}C$ and $\delta^{18}O$ on a mangrove species lacking distinct rings (*Rhizophora mucronata*, Kenya) reporting correlations with October relative humidity and a single, but extreme, El-Niño event in 1997. Gebrekirstos *et al.* (2009) found the $\delta^{13}C$ records with 4 tropical African species correlated highly with precipitation records for the region. They suggested this relationship was a direct result of moisture stress on the stomatal conductance rather than being influenced by photosynthetic rate. In contrast, when Pons and Helle (2011) studied two tropical species in Central Guyana (*Carapa guianensis* and *Goupia glabra*), they found no significant trends within the $\delta^{13}C$ record and reported that $\delta^{13}C$ was an unsuitable parameter for the detections of ring identification due to the small radial variations.

In a study of tropical trees from Indonesia and Thailand, Poussart *et al.* (2004) found the behaviour of these stable isotopes to be very different. In the ringed *Tectona grandis*, they found $\delta^{18}O$ records showed variations of 2-3 times greater (~7‰) than the $\delta^{13}C$, however the $\delta^{13}C$ was much better defined with clear seasonality. Records from the ringless *Samenea samen* species, had variations of 4‰ in the seasonal $\delta^{18}O$ records while the $\delta^{13}C$ was inconsistent, and a third species, *Podocarpus neriifolius* (no clear rings), produced a seasonal cycle but with variations of up to 18‰ for $\delta^{18}O$. This large range in variation both within and between species makes it difficult to predict or assess whether the observations noted herein for *T. macroptera* can be generalised at all across the tropics. In a related study, Poussart and Schrag (2005) measured $\delta^{18}O$ and $\delta^{13}C$ on nine different species. Six of the species showed seasonal patterns in both the $\delta^{13}C$ and $\delta^{18}O$ records, while the other three did not produce coherent $\delta^{18}O$ series. These studies highlight the inconsistency and vast differences between the species and the level of variation that may be experienced. Compared with traditional dendrochronology and dendroclimatology (Section 1.3), there is a general lack of knowledge regarding the suitability of species and their locations, yet without this information it is difficult to see how the science can advance.

While several significant correlations were found between the isotopic series and climate signals, no definitive conclusions can be made from these observations. The analysis and correlations here are only based on a single tree with a dating error of ±1.6 years at best. Therefore, it would be unwise to over interpret the observed relationships between the isotopic records and climate. In addition, the transform to 1st differences may also lead to spurious correlations.

4.6. Conclusions

Dendrochronological and dendrochemical studies involving tropical trees are rare in comparison to work carried out in temperate regions. This is mainly due to the problems associated with accurately dating tropical trees. The lack of dating control has resulted in far less tropical dendro-based studies compared to higher latitudes, therefore information regarding what species may be suitable or problematic, is sparse at best.

Many studies have hailed the use of stable isotopes to successfully identify seasonal patterns in the records allowing the dating of the trees (Evans and Schrag, 2004, Poussart *et al.*, 2004, Poussart and Schrag, 2005, Pons and Helle, 2011). Analysis of both $\delta^{18}O$ and $\delta^{13}C$ isotopes for this tropical species has shown that stable isotopes do not necessarily assist in dating the wood. In particular, the $\delta^{18}O$ series measured from tree 2A in this study, although portraying a clear cyclic pattern, was shown using radiocarbon dating, that this cyclic pattern does not relate to an annual signal. This important observation highlights the ongoing problems with dendrochronological and dendrochemical studies in the tropics and that stable isotopes cannot be assumed to provide a robust measure of the annual cycle.

The significant correlations noted between the isotopic series and climate data provide an intriguing hint that some useful information could be extant in these data. However, the fact remains that no real conclusions can be realistically made at this time while utilising data from only a single tree. Although these series have been placed on a calendar scale using growth rates derived from ^{14}C dates, the potential error from assuming average growth rates between these periods remains unknown (i.e. it is ca. ±1.6 years around the ^{14}C dates themselves but would be worse between them) and remains an issue with regards to any comparisons with

climate data. With more isotopic and better dated trees, more robust climate analyses could be made.

This chapter (and thesis as a whole) adds to the ever expanding range of ambiguous studies hinting at possibilities within the Tropics but not actually providing clear results. Dating tropical trees remains a difficult and costly problem. Even with reduced analytical costs, currently the easiest way to verify isotope based dating of topical tree species lacking distinct rings requires multiple ^{14}C dates. This is a valid approach in the 20th century around the "bomb peak" but prior to this period ^{14}C dates can come with large margins of error.

Chapter 5: Discussion and Conclusions

5.1. Introduction

Traditional dendrochronological methods have restricted use in the tropics due to many tree species lacking distinct or visible annual rings. Dendrochronology has a rich heritage for providing information over a range of disciplines (e.g. palaeoclimatology, ecology, geomorphology etc.) but has so far had minimal success in the Tropics (Speer, 2010). An understanding of the tropical biome coupled with a means by which to gauge environmental change and ecosystem response is integral to a whole host of disciplines, ranging from climatology through to ecology. Long term assessment of both past climate and ecosystem change is hampered by a paucity of instrumental or observational records. Therefore, with few records relating to tropical regions, the scope for assessing past changes in forest dynamics or studying past climates is limited. The importance of developing new methods to extract environmental information from tropical trees cannot be understated. Other methods can be used to measure tree growth rates such as dendrometer bands (Worbes, 1999, da Silva *et al.*, 2002, Ohashi *et al.*, 2009) or cambial wounding (Mariaux, 1967, Sass *et al.*, 1995, Ohashi *et al.*, 2009). Whilst they are certainly useful for studies focusing on only a few years, these methods can only provide information over short periods. Analytical methods such as stable isotope analysis can detect seasonal cycles in isotopic records measured from tropical trees (Poussart *et al.*, 2004, Verheyden *et al.*, 2004, Norström *et al.*, 2008, Gebrekirstos *et al.*, 2009). High resolution measurements are however needed, which makes this a potentially expensive process with no guarantee of success (Poussart and Schrag, 2005, Pons and Helle, 2011). Radiocarbon analyses can assist with dating (Poussart and Schrag, 2005, Norström *et al.*, 2008, Wils *et al.*, 2009) but multiple dates are usually required, and dating for recent centuries prior to ca. 1950 have large errors depending on the age of the trees and their position on the ^{14}C curve. Radiocarbon analysis therefore is most useful in confirming chronologies established by other methods.

This thesis set out to develop and test a novel dendrochemical based method using calcium as a tracer for detecting seasonal growth in tropical trees. Calcium is a critical component in the structure and regulation of cells (White and Broadley, 2003, Maathuis, 2009, Lautner and Fromm, 2010) and plays an important role in wood formation (Lautner and Fromm, 2010)

indicating its potential for dendrochemical studies. A main driving force behind the development of the calcium dating approach explored in this thesis is the encouraging results from Poussart *et al.* (2006), which demonstrated the seasonal and annual nature of the calcium record in a ringless tropical species.

The three preceding chapters describe (1) the development of the calcium threshold based dating method using Scots pine, (2) the application and performance of this technique on a tropical tree species from Cameroon with indistinct rings, (3) determination and assessment of the isotopic signal from a single tropical tree from Cameroon.

This chapter will first summarises each of these main chapters (2-4), followed by an assessment of their overall conclusions. Potential improvements to the methods are suggested and recommendations for future work then made.

5.2. Calcium Tracers and the Dating of Scots Pine

A method was developed using calcium as a tracer to detect seasonality in trees using Laser Ablation-Inductively Coupled-Mass Spectrometry (LA-ICP-MS). This was developed and tested using a temperate species with well-defined annual rings *Pinus sylvestris* (Scots pine) with the premise of applying the same methods to a ringless tropical species. Results were based on measurements from 9 tree laths (7 separate trees, with 2 radii each from 2 trees).

Continuous LA-ICP-MS measurements resulted in a clear and reproducible cyclic seasonal pattern in the calcium measurements which coincided with the physical positions of the annual tree-rings. Each calcium cycle was represented by a sharp increase at the onset of the earlywood, followed by a decreasing trend over the ring, until a minimum value was reached in the latewood; a finding which agreed with previous observations made for calcium in other temperature tree species (*Fagus sylvatica* and *Populus trichocarpa*) (Follet-Gueye *et al.*, 1998, Arend and Fromm, 2000).

An objective statistical approach was developed to utilise the calcium data to estimate the age of the samples, essentially by counting the calcium peaks, a method which was hypothesised to be applicable to other species, including ringless tropical species. Three different thresholds were tested to determine the calcium “peak” count that best represented the actual annual

ring count based on how many standard deviations (SD) they were above the mean. The results showed the >1 SD threshold provided the closest date with an average error of ±6 years, which, if could be applied to tropical tree species, would be a vast improvement for dating ringless tropical trees where traditional dendrochronological methods generally do not work.

The results from this chapter demonstrated the potential for the measurement and analysis of calcium fluctuations to independently date (±6 years) a clearly ringed temperature conifer tree species. LA-ICP-MS also allowed the continuous measurement of a track along the tree lath which allowed the visualisation of intra-annual variation throughout the pine rings. Although beyond the scope of this thesis, the inter-annual variability of the peaks (earlywood) and troughs (latewood) may provide useful environmental information and should be a focus of future work.

5.3. Calcium Tracers and the Dating of Tropical Trees

Tropical trees play a critical role in modulating climate and carbon cycling at local, regional and global scales. However, few species are amenable to analysis by conventional dendrochronological methods. The development of both the methodological and analytical dating methods from Chapter 2 which, although not as accurate as traditional cross-dating methods, could prove vital in providing a new method in which ringless tropical trees could be dated more accurately than is currently possible.

The calcium threshold dating method, which was developed in Chapter 2, was applied to a tropical species from Cameroon (*T. macroptera*) which presented no distinct datable tree rings. The data, measured from multiple tracks, appeared much noisier compared to Scots pine with more densely packed calcium peaks and troughs. Further methodological "tuning" was required to accommodate this hardwood species and therefore an additional peak threshold was tested as well as trough thresholds. Validation of the "optimal" threshold method was made through radiocarbon dating which identified an optimal peak (>1.25 SD) and trough (<-1 SD) threshold, producing almost identical date estimates.

An attempt to validate these "optimal" thresholds was sought on a second radiocarbon dated *T. macroptera* sample using the same "tuned" approach derived from the first sample. Unfortunately, validation of the dating method failed for the second tree. Possible explanations for this result may be linked to the effect of juvenile tree growth in the second sample as ^{14}C dates showed this tree to be much younger than the first sample. Alternatively, the different ecologies from which the two samples were located may have influenced results. However, further work is required to investigate the matter further before true explanations can be provided. Calcium still holds promise for dating some tropical species, but significant challenges exist due to the "unknown" growth rates of the trees being analysed and possible changes of tree physiology as the trees age.

5.4. Are Stable Isotopes the Answer to Dating Tropical Trees?

The problems associated with dating tropical trees restrict the potential for understanding the environmental forces controlling growth. Once dating control is in place, the possibilities for dendrochronological based tropical research are massive. With the failure of validating the calcium dating method in Chapter 3, this chapter focussed on stable isotope analysis to ascertain whether seasonal trends within the oxygen or carbon isotope series for a single *T. macroptera* sample could be identified, and whether any trends represented an annual signal.

Since no distinct tree rings were visible in this species, high resolution incremental sampling and isotopic analysis was performed on the same tree which was used in Chapter 3 (2A). Results produced a very clear and cyclic pattern of $\delta^{18}O$ across the radial section of the tree, but no obvious cyclic or seasonal pattern in the $\delta^{13}C$ series. Radiocarbon dates provided the means to date the isotopic series by the calculation and application of growth rates to each isotopic series.

The interpretation of the isotope records to a calendar scale produced an important result which showed that the clear cyclicity in the $\delta^{18}O$ did not represent an annual signal. With the large associated costs of high resolution isotope studies as well as supplementary radiocarbon dates (to date the isotopic series), this key finding highlights the ongoing problems with dendrochronological and dendrochemical studies in the tropics.

In addition, the dated isotopic series were compared with regional gridded precipitation and temperature records to investigate possible climatic controls on the stable isotopes. Significant correlations were identified between the $\delta^{18}O$ series (both season 2 and 3) and the summer precipitation (season 3 – JJA) and between $\delta^{18}O$ (season 2) with an inverse correlation with spring temperature (Season 2 – MAM). For $\delta^{13}C$, significant correlations were identified between $\delta^{13}C$ (season 2) with spring precipitation (MAM), and $\delta^{13}C$ (season 3) correlated inversely with dry season precipitation (DJF). However, no real conclusion could be drawn from these results based on only one single tree. These results did however provide an intriguing suggestion that useful climatic information could be gleamed from the isotope records if the dating issues can be resolved.

5.5. General Overview

The original scope of this PhD had an altogether different purpose. It was initially set out to develop oxygen and carbon isotope records from trees situated in a forest/savanna transition zone where the forest is encroaching into the savanna. It was hypothesised that

1. the large changes in soil moisture, relative humidity, temperature and light availability that will accompany such a transition change will induce a readily detectable isotope response in tree-ring cellulose, and therefore
2. isotope time-series developed from trees close to the modern boundary will contain a detailed record of shifts in the boundary over the life of the tree.

It became apparent that without dating control, the information which may be interpreted from isotope records is ultimately meaningless. The scope of the PhD project therefore took a dramatic shift to focus on developing a potential dating method for tropical tree species.

Unfortunately, the calcium dating method which initially showed such promise for temperate Scots pine, could not be validated as a dating method for a single tropical tree species (*T. mactroptera* - Chapter 3) in the thesis. Further work is intended to pursue this as a dating method however. Details of methodological improvements and a summary of proposed future work is outlined in the next section.

Chapter 4 also highlighted the risks of stable isotope analysis as a dating tool for tropical species. Although this analytical method has had proven success in the tropics (Evans and Schrag, 2004, Poussart *et al.*, 2004, Poussart and Schrag, 2005, Pons and Helle, 2011), it is clear that this is not guaranteed. Without radiocarbon dating, it may have been tempting to hypothesise that the cyclicity seen in the oxygen isotope data of tree 2A (Figure 4-7) was annual in nature.

5.6. An "Ideal" Approach

Regardless of the success of an experiment, improvements or alternative approaches should always be sought. The development of a new experimental method, such as the calcium based dating described in this thesis, can be thought of as a multi-step process which likely involves multiple iterations of change to procedures and instrumentation.

This section therefore reviews the methods and approaches within this PhD and provides recommendations for future improvements.

5.6.1. Species Choice

Scots pine is a temperate softwood (gymnosperm) species while *T. macroptera* is a tropical diffuse porous hardwood (angiosperm) species and they therefore contain different anatomical cell features. The main difference between the species, except for the vastly different growing environments, is the presence of vessels in *T. macroptera.* Scots pine tree-rings do not contain vessels but do contain resin ducts which were the cause of the large calcium spikes observed in the laser data (Chapter 2, Section 2.3.4.2). Vessels are used for water transport within a tree (Speer, 2010) and therefore are unlikely to contain mineral residue in the same manner as resin ducts in conifers. Scots pine was chosen as a testing species due to the nature of its well defined rings and ease of access.

On reflection, the use of a temperate diffuse porous tree species (e.g. poplar) should have been considered as this could potentially have reduced the differences in ablation and allowed easier comparison of calcium signals between temperate regions and the tropics. However,

there is scope for additional improvements regarding species selection. The tropical species targeted for this PhD (*T. macroptera*) was selected based on the fieldwork related to the TROBIT project, the general location of which was determined prior to the start of this PhD project. The specific site used was selected on arrival, based on the existence of savanna trees within the forest boundary, confirming the forest had encroached into the savanna. *T. macroptera* was the dominant species at this location and the only species of savanna tree found apparently alive within the forest regions. However, it was not an ideal choice for this study. Ideally, the target trees should have had some degree of dating control thus allowing an assessment of the calcium and isotopic data and the associated dating methods. Consequently, tropical species and woodland environments which fall into the following categories would be recommended for future work:

- Trees from plantations – i.e. known planting/germination age
- Tropical trees with annual rings that have been cross-dated using traditional methods (e.g. *Pterocarpus angolensis* – Zimbabwe (Stahle *et al.*, 1999, Fichtler *et al.*, 2004), *Tectona grandis* - Indonesian Teak) (D'Arrigo *et al.*, 1994), *Piranhea trifoliate*- Amazon basin (Schongart *et al.*, 2004))
- Ringless species with dating control
    - Dendrometer bands to measure short term growth rates (several years)
    - Cambial wounded
    - Ringless species which are known to experience seasonality as confirmed by peer reviewed papers (*Samanea saman* – Bali, *Podocarpus neriifolius* – Thailand (Poussart *et al.*, 2004), *Miliusa velutina* – Thailand (Poussart *et al.*, 2006))

There are some issues to consider from the above list. Plantation trees could either be ringed or ringless. Ideally two species, one of each type, would be preferred. An annually ringed species would allow testing and optimisation of the method whilst also allowing direct comparison to the ringless species from the same location. Another concern would be the age of the trees being analysed and how tree-growth may vary over time. Brienen and Zuidema (2005) studied tropical tree species in the Bolivian Amazon where they reported that while the Brevi-deciduous[17] species *Tachigali vasquezii* produced distinct annual rings, the species did not develop annual rings during its juvenile phase due to it physiologically acting as an

[17] Experiences a brief loss of leaves prior to flowering

evergreen species at that period of its life cycle. A similar effect was noted in a recent undergraduate dissertation which reported differences between the nature of the rings from heartwood to sapwood in Zambezi Teak, where cross-dating was only successful in the heartwood region of the trees (Dickenson, 2012). Dendrometer bands and cambial wounding (Section 1.3.1) could provide annual and potentially intra-annual growth rate information although this is limited to the period of time they are in-situ and gives only a snapshot of the actual tree lifetime. Care would need to be taken with cambial wounding as Sass *et al.* (1995) used this technique on Malaysian *Dryobalanops sumatrensis* and *Shorea leprosula* species and reported that relatively large areas of callus tissue formed around the wounded areas which would likely interfere with the calcium signal as well as growth rates. A final alternative would be to identify suitable species based on previous studies which have successfully identified annual rings or seasonality through traditional dendrochronological cross-dating methods. As tropical forests are often incredibly diverse, an additional consideration would be to compare the Ca series from different tree types in the same region - evergreen, diffuse porous, ring porous etc. - and assess the trends in their calcium records.

Multiple radiocarbon dates could provide a method to assess growth rates. Multiple dates obtained throughout the 20th century would help to assess the dating around the bomb peak, proving a robust estimate of dates, from which dating could be inferred. This would be an expensive method requiring funding, but could be applied to all species and locations. The limitation of radiocarbon dating is that any dates prior to the nuclear testing (1950's) often have very large errors, making them ultimately useless for climate or ecology based studies (see Section 3.2.1).

Analysing a combination of species from the above groups would allow the refinement of the LA-ICP-MS calcium dating method in terms of instrumental settings and the threshold method for seasonality detection.

5.6.2. Analytical Sampling Strategy

The analytical sampling strategy could also be improved. Ideally, 3-5 tracks per radius should be measured with at least 2 radii per tree. Increasing the number of radii per tree would provide a more robust measure of the within tree error from the comparisons of the calcium

threshold dating method. A more thorough investigation of the appropriate threshold to use to determine seasonal peak counts could be performed for several different species and thus used to test whether a single threshold is appropriate for multiple species.

5.7. Future Work

The calcium based dating method shows some potential but much more experimentation is needed. The use of tropical species from the categories outline above, would aid the development and tuning of this method to establish a more robust methodology. Samples have already been acquired from multiple tropical species from collaborative partners for such future work.

The work on Scots pine was initially intended as a test bed for applying the LA-ICP-MS Ca dating method and refining it for tropical species. However, the results from the analysis were so reproducible, without the need for laborious sample preparation methods, that it is now the intention to take this work further. Although robust temperature reconstructions can be derived using both ring-width and maximum density parameters (Luckman and Wilson, 2005), other parameters may provide new measures of environmental forcing. Stable isotopes can, in some cases, provide such additional climate information or can be used as an alternative where ring-width signals are weak (Loader *et al.*, 2008). However, as discussed this can be expensive (in both a monetary and labour intensive manner) without necessarily wielding viable results. Calcium measurements in temperate clearly show a distinct seasonal pattern (Chapter 2). Since LA-ICP-MS analyses the wood in terms of distance along the tree core, this provides a simple method of examining the intra-annual calcium fluctuations for each individual ring. What the peaks and troughs in the calcium represent with respect to environmental forcing is not yet known but does provide an exciting new area of research. The continuous measurement approach of the LA-ICP-MS allows the opportunity to investigate the relationship between different statistical parameters from the continuous measurements of each ring (e.g. maxima, minima, mean, median, 10^{th} and 90^{th} percentiles) and compare the relationships between radii (i.e. within tree signal) and between trees. If common variability from any of these parameters can be detected between trees then there is potential to

investigate potential relationships with climate. If such an approach was successful using well dated temperate tree samples, then this could be applied to the tropical records.

In summary, the results in this thesis may not have provided the ideal solution for dating ringless trees in the tropics, but they have provided many intriguing and exciting observations, and directions for future work. With calcium being such an important mineral in trees (Section 1.4.5), which clearly shows a seasonal cycle, there is the opportunity to investigate what such stores may represent with respect to environmental forcing. Most tree parameters measured from temperate trees such as ring-width, stable isotopes and density, express growing season (i.e. spring/summer) environmental information. The peak of calcium during the beginning of the earlywood may well represent the influence of winter conditions on early year tree-growth and could represent an important new proxy for cold season conditions and how they influence the onset of growth. Accurate dating of tropical trees, without relying on expensive radiocarbon methods, still remains elusive and although the results from this thesis have been disappointing, the calcium threshold approach still needs to be tested further on many more species. Currently, there is an assumption that stable isotopes provide the best means for dating tropical trees, but the results herein clearly show that this assumption may not always hold. Although some statistical relationships were identified between $\delta^{18}O$ and $\delta^{13}C$ isotopes and climate, these observations need to be replicated using data from other trees before robust physiological assessment of the correlations can be made. But for this to be successful, the tree parameters (Ca, $\delta^{18}O$ and $\delta^{13}C$) need to be calendar dated. It all comes down to accurate dating of the tree parameter time-series - something that still remains rare in the tropics.

References

Aberg, G. (1995). The use of natural strontium isotopes as tracers in environmental studies. *Water, Air, & Soil Pollution*, 79 (1-4), 309-322.

Alloway, B. J. (2013). Bioavailability of Elements in Soil. *In* O. Selinus ed. *Essentials of Medical Geology*. Springer Netherlands. 351-373.

Anchukaitis, K. J.*, et al.* (2008a). Consequences of a rapid cellulose extraction technique for oxygen isotope and radiocarbon analyses. *Analytical Chemistry*, 80 (6), 2035-2041.

Anchukaitis, K. J.*, et al.* (2008b). Stable isotope chronology and climate signal calibration in neotropical montane cloud forest trees. *Journal of Geophysical Research: Biogeosciences*, 113 (G3), G03030.

Andrews, J. A., T. G. Siccama and K. A. Vogt (1999). The effect of soil nutrient availability on retranslocation of Ca, Mg and K from senescing sapwood in Atlantic white cedar. *Plant and Soil*, 208 (1), 117-123.

Arbonnier, M. (2004). *Trees, shrubs and lianas of West Africa dry zones*. Weikersheim Margraf Publishers.

Arend, M. and J. Fromm (2000). *Seasonal variation in the K, Ca and P content and distribution of plasma membrane H+-ATPase in the cambium of Populus trichocarpa*. Oxford: Bios Scientific Publishers Ltd.

Austin, C.*, et al.* (2011). Factors affecting internal standard selection for quantitative elemental bio-imaging of soft tissues by LA-ICP-MS. *Journal of Analytical Atomic Spectrometry*, 26 (7), 1494-1501.

Baes, C. F. and S. B. McLaughlin (1984). Trace-elements in tree rings - evidence of recent and historical air-pollution. *Science*, 224 (4648), 494-497.

Baillie, M. G. L. (1995). *A Slice Through Time: Dendrochronology and Precision Dating*: Routledge.

Barbour, M. M., T. J. Andrews and G. D. Farquhar (2001). Correlations between oxygen isotope ratios of wood constituents of *Quercus* and *Pinus* samples from around the world. *Australian Journal of Plant Physiology*, 28 (5), 335-348.

Barbour, M. M.*, et al.* (2004). Expressing leaf water and cellulose oxygen isotope ratios as enrichment above source water reveals evidence of a Peclet effect. *Oecologia*, 138 (3), 426-435.

Bennett, K. D. (1984). The post-glacial history of *Pinus sylvestris* in the British Isles. *Quaternary Science Reviews*, 3 (2-3), 133-155.

Berger, T., G. Köllensperger and R. Wimmer (2004). Plant-soil feedback in spruce (*Picea abies*) and mixed spruce-beech (*Fagus sylvatica*) stands as indicated by dendrochemistry. *Plant and Soil*, 264 (1), 69-83.

Berlage, H. P. (1931). Over het verband tusschen de dikte der jaarringen van djatiboomen (*Tectona grandis* L. f.) en den regenval op Java. *Tectona*, 24, 939-953.

Biondi, F. (2001). A 400-year tree-ring chronology from the tropical treeline of North America. *Ambio*, 30 (3), 162-166.

Bondietti, E. A.*, et al.* (1990). A historical perspective on divalent cation trends in red spruce stemwood and the hypothetical relationship to acidic deposition. *Canadian Journal of Forest Research-Revue Canadienne De Recherche Forestiere*, 20 (12), 1850-1858.

Borella, S., M. Leuenberger and M. Saurer (1999). Analysis of $\delta^{18}O$ in tree rings: Wood-cellulose comparison and method dependent sensitivity. *Journal of Geophysical Research: Atmospheres*, 104 (D16), 19267-19273.

Borella, S.*, et al.* (1998). Reducing uncertainties in $\delta^{13}C$ analysis of tree rings: Pooling, milling, and cellulose extraction. *Journal of Geophysical Research: Atmospheres*, 103 (D16), 19519-19526.

Brendel, O., P. P. M. Iannetta and D. Stewart (2000). A rapid and simple method to isolate pure alpha-cellulose. *Phytochemical Analysis*, 11 (1), 7-10.

Brienen, R., W. Wanek and P. Hietz (2011). Stable carbon isotopes in tree rings indicate improved water use efficiency and drought responses of a tropical dry forest tree species. *Trees - Structure and Function*, 25 (1), 103-113.

Brienen, R. J. W. and P. A. Zuidema (2005). Relating tree growth to rainfall in bolivian rain forests: A test for six species using tree ring analysis. *Oecologia*, 146 (1), 1-12.

Brown, P. M. (2013). *Rocky Mountain Tree-Ring Research* [*online*]: Rocky Mountain Tree-Ring Research. Available at: http://www.rmtrr.org/basics.html [Accessed 1 May 2013].

Buckley, B. M.*, et al.* (2007). Analyses of growth rings of *Pinus merkusii* from Lao P.D.R. *Forest Ecology and Management*, 253 (1–3), 120-127.

Buntgen, U.*, et al.* (2005). A 1052-year tree-ring proxy for Alpine summer temperatures. *Climate Dynamics*, 25 (2-3), 141-153.

Cook, E. R.*, et al.* (1995). The 'segment length curse' in long tree-ring chronology development for palaeoclimatic studies. *The Holocene*, 5 (2), 229-237.

Cook, E. R.*, et al.* (2004). Long-term aridity changes in the western United States. *Science*, 306 (5698), 1015-1018.

Coplen, T. B. (1995). Discontinuance of SMOW and PDB. *Nature*, 375 (6529), 285-285.

Cullen, L. E. and P. F. Grierson (2006). Is cellulose extraction necessary for developing stable carbon and oxygen isotopes chronologies from *Callitris glaucophylla*? *Palaeogeography, Palaeoclimatology, Palaeoecology*, 236 (3-4), 206-216.

Currie, K.*, et al.* (2006). $^{14}CO_2$ in the Southern Hemisphere atmosphere – the rise and the fall. *Chemistry in New Zealand*, 70 (1), 20-22.

Cutter, B. E. and R. P. Guyette (1993). Anatomical, chemical, and ecological factors affecting tree species choice in dendrochemistry studies. *Journal of Environmental Quality*, 22 (3), 611-619.

D'Arrigo, R., R. Wilson and G. Jacoby (2006a). On the long-term context for late twentieth century warming. *Journal of Geophysical Research: Atmospheres*, 111 (D3), D03103.

D'Arrigo, R.*, et al.* (2006b). Monsoon drought over Java, Indonesia, during the past two centuries. *Geophys. Res. Lett.*, 33 (4), L04709.

D'Arrigo, R. D., G. C. Jacoby and P. J. Krusic (1994). Progress in dendroclimatic studies in Indonesia. *Terrestrial, Atmospheric and Oceanic Sciences* (5), 349-363.

da Silva, R. P.*, et al.* (2002). Diameter increment and growth patterns for individual tree growing in Central Amazon, Brazil. *Forest Ecology and Management*, 166 (1–3), 295-301.

De Ridder, F.*, et al.* (2002). An improved multiple internal standard normalisation for drift in LA-ICP-MS measurements. *Journal of Analytical Atomic Spectrometry*, 17 (11), 1461-1470.

de Vives, A. E. S.*, et al.* (2006). Monitoring of the environmental pollution by trace element analysis in tree-rings using synchrotron radiation total reflection X-ray fluorescence. *Spectrochimica Acta Part B: Atomic Spectroscopy*, 61 (10–11), 1170-1174.

Dickenson, J. (2012). *An investigation of the dendrochronological potential of Zambezi Teak.* Thesis, (BSc (Hons)). University of St. Andrews

DoITPoMS. (2008). *The structure and mechanical behaviour of wood* [*online*]. University of Cambridge: University of Cambridge. Available at: http://www.doitpoms.ac.uk/tlplib/wood/structure_wood_pt2.php [Accessed 25th March 2014].

Douglass, A. E. (1941). Crossdating in Dendrochronology. *Journal of Forestry*, 39 (10), 825-831.

Drew, D. M. and G. M. Downes (2009). The use of precision dendrometers in research on daily stem size and wood property variation: A review. *Dendrochronologia*, 27 (2), 159-U157.

Drouet, T., J. Herbauts and D. Demaiffe (2005). Long-term records of strontium isotopic composition in tree rings suggest changes in forest calcium sources in the early 20th century. *Global Change Biology*, 11 (11), 1926-1940.

Dunisch, O., J. Bauch and L. Gasparotto (2002). Formation of increment zones and intraannual growth dynamics in the xylem of *Swietenia macrophylla, Carapa guianensis*, and *Cedrela odorata* (Meliaceae). *IAWA Journal*, 23 (2), 101-119.

Durrant, S., F. (1999). Laser ablation inductively coupled plasma mass spectrometry: achievements, problems, prospects. *Journal of Analytical Atomic Spectrometry*, 14 (9), 1385-1403.

Eklund, L. and L. Eliasson (1990). Effects of calcium ion concentration on cell wall synthesis. *Journal of Experimental Botany*, 41 (7), 863-867.

Eronen, M.*, et al.* (2002). The supra-long Scots pine tree-ring record for Finnish Lapland: Part 1, chronology construction and initial inferences. *Holocene*, 12 (6), 673-680.

Esper, J.*, et al.* (2007). Long-term drought severity variations in Morocco. *Geophysical Research Letters*, 34 (17), L17702.

Evans, M. N. and D. P. Schrag (2004). A stable isotope-based approach to tropical dendroclimatology. *Geochimica Et Cosmochimica Acta*, 68 (16), 3295-3305.

Farquhar, G. D. and K. S. Gan (2003). On the progressive enrichment of the oxygen isotopic composition of water along a leaf (Reprinted from Plant, Cell and Environment, vol 26, pg 801-819, 2003). *Plant Cell and Environment*, 26 (9), 1579-1597.

Farquhar, G. D., M. H. Oleary and J. A. Berry (1982). On the relationship between carbon isotope discrimination and the inter-cellular carbon-dioxide concentration in leaves. *Australian Journal of Plant Physiology*, 9 (2), 121-137.

Feng, X. and S. Epstein (1995). Carbon isotopes of trees from arid environments and implications for reconstructing atmospheric CO_2 concentration. *Geochimica Et Cosmochimica Acta*, 59 (12), 2599-2608.

Ferretti, M.*, et al.* (2002). Air pollution and environmental chemistry - what role for tree-ring studies? *Dendrochronologia*, 20 (1-2), 159-174.

Fichtler, E., D. A. Clark and M. Worbes (2003). Age and long-term growth of grees in an old-growth tropical rain forest, based on analyses of tree rings and ^{14}C. *Biotropica*, 35 (3), 306-317.

Fichtler, E*., et al.* (2004). Climatic signals in tree rings of *Burkea africana* and *Pterocarpus angolensis* from semiarid forests in Namibia. *Trees - Structure and Function*, 18 (4), 442-451.

Fink, S. (1991). The micromorphological distribution of bound calcium in needles of Norway spruce [*Picea abies* (L.) Karst.]. *New Phytologist*, 119 (1), 33-40.

Fish, T*., et al.* (2010). Exploring for senescence signals in native scots pine (*Pinus sylvestris* L.) in the Scottish Highlands. *Forest Ecology and Management*, 260 (3), 321-330.

Flanagan, L. B., J. P. Comstock and J. R. Ehleringer (1991). Comparison of modeled and observed environmental-influences on the stable oxygen and hydrogen isotope composition of leaf water in *Phaseolus vulgaris* L. *Plant Physiology*, 96 (2), 588-596.

Follet-Gueye, M.-L*., et al.* (1998). Cambium pre-activation in beech correlates with a strong temporary increase of calcium in cambium and phloem but not in xylem cells. *Cell Calcium*, 24 (3), 205-211.

Franceschi, V. R. and P. A. Nakata (2005). Calcium oxalate in plants: Formation and function. *Annual Review of Plant Biology*. 41-71.

Fritter, A. H. and R. K. M. Hay (2002). *Environmental Physiology of Plants*. Third ed. London: Academic Press Ltd.

Fritts, H. C. (1976). *Tree Rings and Climate*. New York: Academic Press.

Fritts, H. C. and T. W. Swetnam (1989). Dendroecology - a tool for evaluating variations in past and present forest environments. *Advances in Ecological Research*, 19, 111-188.

Funada, R. and A. M. Catesson (1991). Partial cell-wall lysis and the resumption of meristematic activity in *Fraxinus excelsior* cambium. *IAWA Bulletin*, 12 (4), 439-444.

Gagen, M., *et al.* (2007). Exorcising the 'segment length curse': Summer temperature reconstruction since AD 1640 using non-detrended stable carbon isotope ratios from pine trees in northern Finland. *Holocene*, 17 (4), 435-446.

Gagen, M., *et al.* (2011). Cloud response to summer temperatures in Fennoscandia over the last thousand years. *Geophysical Research Letters*, 38.

Garbe-Schonberg, C. D., C. Reimann and V. A. Pavlov (1997). Laser ablation ICP-MS analyses of tree-ring profiles in pine and birch from N Norway and NW Russia - a reliable record of the pollution history of the area? *Environmental Geology*, 32 (1), 9-16.

Gärtner, H., F. H. Schweingruber and S. Luccinetti. (2009). *GSL Microtomes* [*online*]. Available at: http://www.woodecology.ch/willyjoomla/index.php?option=com_content&view=article&id=136&Itemid=179 [Accessed 10 September 2012].

Gat, J. R. (1996). Oxygen and hydrogen isotopes in the hydrologic cycle. *Annual Review of Earth and Planetary Sciences*, 24, 225-262.

Gebrekirstos, A., *et al.* (2009). Stable carbon isotope ratios in tree rings of co-occurring species from semi-arid tropics in Africa: Patterns and climatic signals. *Global and Planetary Change*, 66 (3-4), 253-260.

Gilliham, M., *et al.* (2011). Calcium delivery and storage in plant leaves: exploring the link with water flow. *Journal of Experimental Botany*, 62 (7), 2233-2250.

Goslar, T., *et al.* (2005). Radiocarbon dating of modern peat profiles: Pre- and post-bomb ^{14}C variations in the construction of age-depth models. *Radiocarbon*, 47 (1), 115-134.

Gourlay, I. D. (1995). Growth ring characteristics of some African *Acacia* species. *Journal of Tropical Ecology*, 11, 121-140.

Grudd, H., *et al.* (2002). A 7400-year tree-ring chronology in northern Swedish Lapland: natural climatic variability expressed on annual to millennial timescales. *Holocene*, 12 (6), 657-665.

Guillong, M. (2007) LA-ICP-MS and ICP-MS. Available at: http://www.eurispet.eu/docs/paris/downloads/Eurispet-Guillong.pdf [Accessed 3 September 2012].

Hagemeyer, J.*, et al.* (1992). Are there seasonal variations of trace element concentrations (Cd, Pb, Zn) in wood of *Fagus* trees in Germany? *Vegetatio*, 101 (1), 55-63.

Hagemeyer, J. and H. Schäfer (1995). Seasonal variations in concentrations and radial distribution patterns of Cd, Pb and Zn in stem wood of beech trees (*Fagus sylvatica* L.). *Science of The Total Environment*, 166 (1–3), 77-87.

Harris, I.*, et al.* (2014). Updated high-resolution grids of monthly climatic observations – the CRU TS3.10 Dataset. *International Journal of Climatology*, 34 (3), 623-642.

Helama, S.*, et al.* (2002). The supra-long Scots pine tree-ring record for Finnish Lapland: Part 2, interannual to centennial variability in summer temperatures for 7500 years. *Holocene*, 12 (6), 681-687.

Helama, S.*, et al.* (2008). Finnish supra-long tree-ring chronology extended to 5634 BC. *Norsk Geografisk Tidsskrift-Norwegian Journal of Geography*, 62 (4), 271-277.

Hepler, P. K. (2005). Calcium: A central regulator of plant growth and development. *Plant Cell*, 17 (8), 2142-2155.

Hindshaw, R. S.*, et al.* (2013). Calcium isotope fractionation in alpine plants. *Biogeochemistry*, 112 (1-3), 373-388.

Hirano, Y. and I. Brunner (2006). Quantitative determination of callose in tree roots. *Journal of Plant Physiology*, 163 (12), 1333-1336.

Hirano, Y.*, et al.* (2004). Induction of callose in roots of Norway spruce seedlings after short-term exposure to aluminum. *Tree Physiology*, 24 (11), 1279-1283.

Hirschi, K. (2001). Vacuolar H^+/Ca^{2+} transport: who's directing the traffic? *Trends in Plant Science*, 6 (3), 100-104.

Hirschi, K. D. (2004). The calcium conundrum. Both versatile nutrient and specific signal. *Plant Physiology*, 136 (1), 2438-2442.

Hoffmann, E.*, et al.* (1994). Analytical investigations of tree-rings by laser-ablation ICP-MS. *Fresenius Journal of Analytical Chemistry*, 350 (4-5), 253-259.

Hoffmann, E.*, et al.* (2002). New methodical and instrumental developments in laser ablation inductively coupled plasma mass spectrometry. *Spectrochimica Acta Part B-Atomic Spectroscopy*, 57 (10), 1535-1545.

Hoffmann, E., H. Stephanowitz and J. Skole (1996). Investigations of the migration of elements in tree rings by Laser-ICP-MS. *Fresenius' Journal of Analytical Chemistry*, 355 (5), 690-693.

Hopkins, W. G. (1995). *Introduction to Plant Physiology*. U.S.A.: John Wiley & Sons, Inc.

Hristovski, S. and L. Melovski (2010). Radial patterns of 13 elements in the tree rings of beech trees from Mavrovo National Park, Fyrom. *Archives of Biological Sciences*, 62 (2), 351-361.

Hudgins, J. W., T. Krekling and V. R. Franceschi (2003). Distribution of calcium oxalate crystals in the secondary phloem of conifers: a constitutive defense mechanism? *New Phytologist*, 159 (3), 677-690.

ITRDB. (2012). *IGBP PAGES/World Data Center for Paleoclimatology* [*online*]. Boulder, Colorado, USA: NOAA/NCDC Paleoclimatology Program. Available at: http://www.ncdc.noaa.gov/paleo/treering.html [Accessed 6 April 2012.

Jansen, E.*, et al.* (2007). Palaeoclimate. *In* S. Solomon *et al.* eds. *Climate Change 2007: The Physical Science Basis. Contribution of Working Group I to the Fourth Assessment Report of the Intergovernmental Panel on Climate Change*. Cambridge, United Kingdom and New York, N.Y., Cambridge University Press.

Jones, P. D.*, et al.* (2009). High-resolution palaeoclimatology of the last millennium: a review of current status and future prospects. *The Holocene*, 19 (1), 3-49.

Kaennel, M. and F. H. Schweingruber (1996). *A multilingual glossary of dendrochronology: Terms and definitions in English, German, French, Spanish, Italian, Portuguese and Russian*. Bern: Paul Haupt.

Karley, A. J. and P. J. White (2009). Moving cationic minerals to edible tissues: potassium, magnesium, calcium. *Current Opinion in Plant Biology*, 12 (3), 291-298.

Kimball, J. W. (2013). *Transport of Water and Minerals in Plants* [*online*]. Available at: http://users.rcn.com/jkimball.ma.ultranet/BiologyPages/X/Xylem.html [Accessed 10 November 2013.

Kirchner, P.*, et al.* (2008). Variability of trace metal concentrations in Jeffrey pine (*Pinus jeffreyi*) tree rings from the Tahoe Basin, California, USA. *Journal of Forest Research*, 13 (6), 347-356.

Kirkby, E. (2012). Introduction, Definition and Classification of Nutrients. *In* P. Marschner ed. *Marschner's Mineral Nutrition of Higher Plants (Third Edition)*. San Diego, Academic Press. 3-5.

Knoke, T. (2003). Predicting red heartwood formation in beech trees (*Fagus sylvatica* L.). *Ecological Modelling*, 169 (2–3), 295-312.

Kwak, J.-H.*, et al.* (2009). Relating tree ring chemistry of *Pinus densiflora* to precipitation acidity in an industrial area of South Korea. *Water, Air, & Soil Pollution*, 199 (1), 95-106.

Lambers, H., F. S. Chapin III and T. L. Pons (1998). *Plant Physiological Ecology*. New York: Springer-Verlag New York Inc.

Larcher, W. (2003). *Physiological Plant Ecology*. Forth ed. Berlin: Springer-Verlag.

Lautner, S.*, et al.* (2007). Calcium nutrition has a significant influence on wood formation in poplar. *New Phytologist*, 173 (4), 743-752.

Lautner, S. and J. Fromm (2010). Calcium-dependent physiological processes in trees. *Plant Biology*, 12 (2), 268-274.

Levin, I.*, et al.* (2008). Radiocarbon observations in atmospheric CO_2: Determining fossil fuel CO_2 over Europe using Jungfraujoch observations as background. *Science of The Total Environment*, 391 (2–3), 211-216.

Levin, I. and B. Kromer (2004). The tropospheric $^{14}CO_2$ level in mid-latitudes of the Northern Hemisphere (1959-2003). *Radiocarbon*, 46 (3), 1261-1272.

Lévy, G., C. Bréchet and M. Becker (1996). Element analysis of tree rings in pedunculate oak heartwood: an indicator of historical trends in the soil chemistry, related to atmospheric deposition. *Annals of Forest Science*, 53 (2-3), 685-696.

Lieberman, D.*, et al.* (1985). Growth rates and age-size relationships of tropical wet forest trees in Costa Rica. *Journal of Tropical Ecology*, 1 (2), 97-109.

Liu, Y.*, et al.* (2009). Trace elements in tree rings and their environmental effects: A case study in Xi'an City. *Science in China Series D: Earth Sciences*, 52 (4), 504-510.

Loader, N.*, et al.* (2013). Quantifying uncertainty in isotope dendroclimatology. *The Holocene*, 23 (9), 1221-1226.

Loader, N. J.*, et al.* (2010). Twentieth-century summer temperature variability in the southern Altai Mountains: A carbon and oxygen isotope study of tree-rings. *The Holocene*, 20 (7), 1149-1156.

Loader, N. J.*, et al.* (2007). Extracting climatic information from stable isotopes in tree rings. *In* E. D. Todd and T. W. S. Rolf eds. *Terrestrial Ecology*. Elsevier. 25-48.

Loader, N. J., I. Robertson and D. McCarroll (2003). Comparison of stable carbon isotope ratios in the whole wood, cellulose and lignin of oak tree-rings. *Palaeogeography Palaeoclimatology Palaeoecology*, 196 (3-4), 395-407.

Loader, N. J.*, et al.* (2008). Multiple stable isotopes from oak trees in southwestern Scotland and the potential for stable isotope dendroclimatology in maritime climatic regions. *Chemical Geology*, 252 (1-2), 62-71.

Loader, N. J.*, et al.* (2011). Recent trends in the intrinsic water-use efficiency of ringless rainforest trees in Borneo. *Philosophical Transactions of the Royal Society B: Biological Sciences*, 366 (1582), 3330-3339.

Luckman, B. H. and R. J. S. Wilson (2005). Summer temperatures in the Canadian Rockies during the last millennium: a revised record. *Climate Dynamics*, 24 (2), 131-144.

Maathuis, F. J. M. (2009). Physiological functions of mineral macronutrients. *Current Opinion in Plant Biology*, 12 (3), 250-258.

Mariaux, A. (1967). Les cernes dans les bois tropicaux africains, nature et periodicite. *Bois et Forets des Tropiques* (113-114), 3-14, 23-37.

Marschner, H. (1995). *Mineral Nutrition of Higher Plants*. Second ed. London: Academic Press Limited.

Martin, R. R.*, et al.* (2003). Micro-synchrotron x-ray fluorescence of the metal distribution in a black spruce tree stem: evidence for radial mobility. *X-Ray Spectrometry*, 32 (5), 402-407.

Martin, R. R.*, et al.* (2001). Synchrotron x-ray fluorescence and secondary ion mass spectrometry in tree ring microanalysis: applications to dendroanalysis. *X-Ray Spectrometry*, 30 (5), 338-341.

McCarroll, D.*, et al.* (2009). Correction of tree ring stable carbon isotope chronologies for changes in the carbon dioxide content of the atmosphere. *Geochimica Et Cosmochimica Acta*, 73 (6), 1539-1547.

McCarroll, D. and N. J. Loader (2004). Stable isotopes in tree rings. *Quaternary Science Reviews*, 23 (7-8), 771-801.

McLaughlin, S. B. and R. Wimmer (1999). Tansley Review No. 104 - Calcium physiology and terrestrial ecosystem processes. *New Phytologist*, 142 (3), 373-417.

Medzegue, M.*, et al.* (2007). Radial growth and characterization of juvenile and adult wood in plantation grown okoumé (*Aucoumea klaineana* Pierre) from Gabon. *Annals of Forest Science*, 64 (8), 815-824.

Meerts, P. (2002). Mineral nutrient concentrations in sapwood and heartwood: a literature review. *Annals of Forest Science*, 59 (7), 713-722.

Mihaljevič, M.*, et al.* (2011). Lead isotopic and metallic pollution record in tree rings from the Copperbelt mining-smelting area, Zambia. *Water, Air, & Soil Pollution*, 216 (1-4), 657-668.

Mihaljevič, M.*, et al.* (2008). A comparison of tree rings and peat deposit geochemical archives in the vicinity of a lead smelter. *Water, Air, & Soil Pollution*, 188 (1), 311-321.

Mitchard, E. T. A*., et al.* (2009a). Measuring woody encroachment along a forest–savanna boundary in Central Africa. *Earth Interactions*, 13 (8), 1-29.

Mitchard, E. T. A*., et al.* (2009b). Using satellite radar backscatter to predict above-ground woody biomass: A consistent relationship across four different African landscapes. *Geophys. Res. Lett.*, 36 (23), L23401.

Mitchell, T. D. and P. D. Jones (2005). An improved method of constructing a database of monthly climate observations and associated high-resolution grids. *International Journal of Climatology*, 25 (6), 693-712.

Momoshima, N. and E. A. Bondietti (1990). Cation binding in wood: applications to understanding historical changes in divalent cation availability to red spruce. *Canadian Journal of Forest Research*, 20 (12), 1840-1849.

Monticelli, D*., et al.* (2009). Tree ring microanalysis by LA–ICP–MS for environmental monitoring: validation or refutation? Two case histories. *Microchimica Acta*, 164 (1), 139-148.

Moreton, S. (2012). Radiocabon Analysis Allocation Number 1562.0411. East Kilbride, NERC Radiocarbon Facility.

Moreton, S. (2013). Radiocabon Analysis Allocation Number 1720.0413. East Kilbride, NERC Radiocarbon Facility.

Nabais, C., H. Freitas and J. Hagemeyer (1999). Dendroanalysis: a tool for biomonitoring environmental pollution? *Science of The Total Environment*, 232 (1-2), 33-37.

Nagy, N. E., P. Krokene and H. Solheim (2006). Anatomical-based defense responses of Scots pine (*Pinus sylvestris*) stems to two fungal pathogens. *Tree Physiology*, 26 (2), 159-167.

NOAA. (2012). *Fingerprints of emissions and the carbon cycle: Stable and radiocarbon isotopes of carbon dioxide* [*online*]: National Oceanic and Atmospheric Administration. Available at: http://www.esrl.noaa.gov/gmd/outreach/isotopes/bombspike.html [Accessed 22 August 2012.

Norström, E., K. Holmgren and C.-M. Mörth (2008). A 600-year-long $\delta^{18}O$ record from cellulose of *Breonadia salicina* trees, South Africa. *Dendrochronologia*, 26 (1), 21-33.

Ohashi, S*., et al.* (2009). Detecting invisible growth rings of trees in seasonally dry forests in Thailand: isotopic and wood anatomical approaches. *Trees - Structure and Function*, 23 (4), 813-822.

Padilla, K. L. and K. A. Anderson (2002). Trace element concentration in tree-rings biomonitoring centuries of environmental change. *Chemosphere*, 49 (6), 575-585.

Parn, H. (2001). Variations of element concentrations in tree rings of Scots pine (*Pinus sylvestris* L.) in the vicinity of an oil shale-fired power plant. *Oil Shale*, 18 (1), 57-71.

Pearson, C*., et al.* (2005). Can tree-ring chemistry reveal absolute dates for past volcanic eruptions? *Journal of Archaeological Science*, 32 (8), 1265-1274.

Pearson, C. L*., et al.* (2009). Dendrochemical analysis of a tree-ring growth anomaly associated with the Late Bronze Age eruption of Thera. *Journal of Archaeological Science*, 36 (6), 1206-1214.

Penninckx, V*., et al.* (2001). Radial variations in wood mineral element concentrations: a comparison of beech and pedunculate oak from the Belgian Ardennes. *Annals of Forest Science*, 58 (3), 253-260.

Penninckx, V*., et al.* (1999). Ring width and element concentrations in beech (*Fagus sylvatica* L.) from a periurban forest in central Belgium. *Forest Ecology and Management*, 113 (1), 23-33.

Pham, A. T*., et al.* (2011). *Terminalia macroptera*, its current medicinal use and future perspectives. *Journal of Ethnopharmacology*, 137 (3), 1486-1491.

Plomion, C., G. Leprovost and A. Stokes (2001). Wood formation in trees. *Plant Physiology*, 127 (4), 1513-1523.

Pons, T. and G. Helle (2011). Identification of anatomically non-distinct annual rings in tropical trees using stable isotopes. *Trees - Structure and Function*, 25 (1), 83-93.

Poszwa, A., *et al.* (2003). A retrospective isotopic study of spruce decline in the Vosges Mountains (France). *Water, Air, & Soil Pollution: Focus*, 3 (1), 201-222.

Pouomegne, J. B. (2008) Final Report: RarePride Campaign. Mbam and Djerem National Park, Cameroon. Available at: http://www.rareplanet.org/sites/rareplanet.org/files/Bosco-Final.pdf [Accessed 4 april 2010].

Poussart, P. F., M. N. Evans and D. P. Schrag (2004). Resolving seasonality in tropical trees: multi-decade, high-resolution oxygen and carbon isotope records from Indonesia and Thailand. *Earth and Planetary Science Letters*, 218 (3-4), 301-316.

Poussart, P. F. and D. P. Schrag (2005). Seasonally resolved stable isotope chronologies from northern Thailand deciduous trees. *Earth and Planetary Science Letters*, 235 (3-4), 752-765.

Poussart, P. M., S. C. B. Myneni and A. Lanzirotti (2006). Tropical dendrochemistry: A novel approach to estimate age and growth from ringless trees. *Geophysical Research Letters*, 33 (17).

Priya, P. B. and K. M. Bhat (1999). Influence of rainfall, irrigation and age on the growth periodicity and wood structure in teak (*Tectona grandis*). *IAWA Journal*, 20 (2), 181-192.

Prohaska, T., *et al.* (1998). Investigation of element variability in tree rings of young Norway spruce by laser-ablation-ICPMS. *The Science of The Total Environment*, 219 (1), 29-39.

Reimer, P. J., *et al.* (2013). IntCal13 and Marine13 Radiocarbon Age Calibration Curves 0–50,000 Years cal BP. *Radiocarbon*, 55 (4), 1869-1887.

Roden, J. S., G. G. Lin and J. R. Ehleringer (2000). A mechanistic model for interpretation of hydrogen and oxygen isotope ratios in tree-ring cellulose. *Geochimica Et Cosmochimica Acta*, 64 (1), 21-35.

Saint-Laurent, D., *et al.* (2011). Reconstructing contamination events on riverbanks in southern Québec using dendrochronology and dendrochemical methods. *Dendrochronologia*, 29 (1), 31-40.

Sampling Technologies Pty Ltd (2013) What is XRF Technology. Available at: http://www.sampletech.com.au/content/what-xrf-technology [Accessed11 November 2013].

Sass, U., W. Killmann and D. Eckstein (1995). Wood formation in two species of dipterocarpaceae in Peninsular Malaysia. *IAWA Journal*, 16 (4), 371-384.

Sattelmacher, B. (2001). The apoplast and its significance for plant mineral nutrition. *New Phytologist*, 149 (2), 167-192.

Schongart, J.*, et al.* (2004). Teleconnection between tree growth in the Amazonian floodplains and the El Nino-Southern Oscillation effect. *Global Change Biology*, 10 (5), 683-692.

Schongart, J.*, et al.* (2006). Climate-growth relationships of tropical tree species in West Africa and their potential for climate reconstruction. *Global Change Biology*, 12 (7), 1139-1150.

Schongart, J.*, et al.* (2005). Wood growth patterns of *Macrolobium acaciifolium* (Benth.) Benth. (Fabaceae) in Amazonian black-water and white-water floodplain forests. *Oecologia*, 145 (3), 454-461.

Schweingruber, F. (2006). Modification of Organs. *Atlas of Woody Plant Stems*. Springer Berlin Heidelberg. 117-129.

Scinco.com. *Newsletter Vol. 44* [*online*]: SCINCO Co. Ltd. Available at: http://www.scinco.com/kor/letter/news_100531/sub09_2.html [Accessed 10 August 2012].

Shigo, A. L. and W. E. Hillis (1973). Heartwood, discoloured wood, and microorganisms in living trees. *Annual Review of Phytopathology*, 11, 197-222.

Silva, O.*, et al.* (2010). LC-UV-MS characterization of *Terminalia macroptera* leaf. *Planta Medica*, 76 (12), 1311-1311.

Silva, O.*, et al.* (1997). Antimicrobial activity of *Terminalia macroptera* root. *Journal of Ethnopharmacology*, 57 (3), 203-207.

Sitbon, F.*, et al.* (1993). Patterns of protein-synthesis in the cambial regions of Scots pine shoots during reactivation. *Physiologia Plantarum*, 87 (4), 601-608.

Smith, K. T. and W. C. Shortle (1996). *Tree biology and dendrochemistry*. Tucson: Radiocarbon.

Speer, J. H. (2010). *Fundamentals of Tree-Ring Research*: University of Arizona Press.

Speer, J. H.*, et al.* (2001). Changes in pandora moth outbreak dynamics during the past 622 years. *Ecology*, 82 (3), 679-697.

St George, S., P. M. Outridge and E. Nielsen (2006). High-resolution dendrochemical analysis of flood-affected oaks using laser ablation ICP-mass spectrometry. *IAWA Journal*, 27 (1), 19-31.

Stahle, D. W. (1999). Useful strategies for the development of tropical tree-ring chronologies. *IAWA Journal*, 20 (3), 249-253.

Stahle, D. W.*, et al.* (1999). Management implications of annual growth rings in *Pterocarpus angolensis* from Zimbabwe. *Forest Ecology and Management*, 124 (2-3), 217-229.

Sternberg, L. and P. F. V. Ellsworth (2011). Divergent biochemical fractionation, not convergent temperature, explains cellulose oxygen isotope enrichment across latitudes. *Plos One*, 6 (11).

Sternberg, L.*, et al.* (2006). Variation in oxygen isotope fractionation during cellulose synthesis: intramolecular and biosynthetic effects. *Plant Cell and Environment*, 29 (10), 1881-1889.

Sternberg, L. D. L., M. J. Deniro and R. A. Savidge (1986). Oxygen isotope exchange between metabolites and water during biochemical reactions leading to cellulose synthesis. *Plant Physiology*, 82 (2), 423-427.

Stokes, M. A. and T. L. Smiley (1996). *An Introduction to Tree-Ring Dating*: University of Arizona Press.

Taiz, L. and E. Zeiger (2010). *Plant Physiology*. Fifth ed. U.S.A. : Sinauer Associates, Inc.

Tarhule, A. and M. K. Hughes (2002). Tree-ring research in semi-arid west Africa: Need and potential. *Tree-Ring Research* (58 (1/2)), 31-46.

Tarhule, A. and S. W. Leavitt (2004). Comparison of stable-carbon isotope composition in the growth rings of *Isorberlinia doka*, *Daniella oliveri*, and *Tamarindus indica* and West African climate. *Dendrochronologia*, 22 (1), 61-70.

Taylor, A. M., B. L. Gartner and J. J. Morrell (2002). Heartwood formation and natural durability - A review. *Wood and Fiber Science*, 34 (4), 587-611.

Thermo Electron Corporation (2002) X Series ICP-MS Training Course Lectures.

Thermo Electron Corporation (2005) X Series II ICP-MS: Extraction – Designed to meet the most demanding applications for both conventional and collision cell ICP-MS. Available at: http://www.thermo.com/eThermo/CMA/PDFs/Articles/articlesFile_24979.pdf [Accessed 5 June 2012].

Therrell, M.*, et al.* (2006). Tree-ring reconstructed rainfall variability in Zimbabwe. *Climate Dynamics*, 26 (7), 677-685.

Touchan, R.*, et al.* (2011). Spatiotemporal drought variability in northwestern Africa over the last nine centuries. *Climate Dynamics*, 37 (1-2), 237-252.

Treydte, K.*, et al.* (2001). The climatic significance of delta ^{13}C in subalpine spruces (Lotschental, Swiss Alps) - A case study with respect to altitude, exposure and soil moisture. *Tellus Series B-Chemical and Physical Meteorology*, 53 (5), 593-611.

Treydte, K. S.*, et al.* (2009). Impact of climate and CO_2 on a millennium-long tree-ring carbon isotope record. *Geochimica Et Cosmochimica Acta*, 73 (16), 4635-4647.

Treydte, K. S.*, et al.* (2006). The twentieth century was the wettest period in northern Pakistan over the past millennium. *Nature*, 440 (7088), 1179-1182.

Trouet, V.*, et al.* (2001). Tree ring analysis of *Brachystegia spiciformis* and *Isoberlinia tomentosa*: Evaluation of the ENSO-signal in the miombo woodland of eastern Africa. *IAWA Journal*, 22 (4), 385-399.

Ursprung, A. (1900). Beitrage zur Anatomie und Jahresringbildung tropischer Holzarten. *Diss. Basel*, 81.

Vaganov, E., M. K. Hughen and A. V. Shashkin (2006). Growth Dynamics of Conifer Tree Rings. Springer Berlin Heidelberg. 183.

Verheyden, A*., et al.* (2004). Annual cyclicity in high-resolution stable carbon and oxygen isotope ratios in the wood of the mangrove tree Rhizophora mucronata. *Plant Cell and Environment*, 27 (12), 1525-1536.

Visit Scotland. (2012). Visit Scotland. Available at: http://www.visitscotland.com/info/towns-villages/abernethy-forest-and-dell-woods-p249201 [Accessed 28 July 2012].

W. H. Freeman & Co. (No Date). *Life. The Science of Biology* [*online*]: Sinauer Associates, Inc. Available at: http://bcs.whfreeman.com/thelifewire8e/pages/bcs-main_body.asp?v=chapter&s=36000&n=00010&i=36010.01&o=%7C00010%7C&ns=0 [Accessed 20 October 2013.

Waterhouse, J. S*., et al.* (2002). Oxygen and hydrogen isotope ratios in tree rings: how well do models predict observed values? *Earth and Planetary Science Letters*, 201 (2), 421-430.

Watmough, S. A. (1997). An evaluation of the use of dendrochemical analyses in environmental monitoring. *Environmental Reviews*, 5 (3-4), 181-201.

Watmough, S. A. (1999). Monitoring historical changes in soil and atmospheric trace metal levels by dendrochemical analysis. *Environmental Pollution*, 106 (3), 391-403.

Watmough, S. A. and T. C. Hutchinson (2002). Historical changes in lead concentrations in tree-rings of sycamore, oak and Scots pine in north-west England. *The Science of The Total Environment*, 293 (1-3), 85-96.

Watmough, S. A., T. C. Hutchinson and R. D. Evans (1996). Application of laser ablation inductively coupled plasma-mass spectrometry in dendrochemical analysis. *Environmental Science & Technology*, 31 (1), 114-118.

Watmough, S. A., T. C. Hutchinson and R. D. Evans (1998). Development of solid calibration standards for trace elemental analyses of tree rings by laser ablation inductively

coupled plasma-mass spectrometry. *Environmental Science & Technology*, 32 (14), 2185-2190.

Watt, S. F. L*., et al.* (2007). The use of tree-rings and foliage as an archive of volcanogenic cation deposition. *Environmental Pollution*, 148 (1), 48-61.

White, P. J. (2000). Calcium channels in higher plants. *Biochimica et Biophysica Acta (BBA) - Biomembranes*, 1465 (1–2), 171-189.

White, P. J. (2001). The pathways of calcium movement to the xylem. *Journal of Experimental Botany*, 52 (358), 891-899.

White, P. J. (2012). Ion Uptake Mechanisms of Individual Cells and Roots: Short-distance Transport. *In* P. Marschner ed. *Marschner's Mineral Nutrition of Higher Plants (Third Edition)*. San Diego, Academic Press. 7-47.

White, P. J. and M. R. Broadley (2003). Calcium in plants. *Annals of Botany*, 92 (4), 487-511.

Whitmore, T. C. (1998). *An introduction to tropical rain forests*. 2nd ed: Oxford.

Wills, J*., et al.* (2007) Improved time resolved analysis (TRA) Software for LA-ICP-MS. Available at: http://www.analiticaweb.com.br/newsletter/06/AN30114-XSERIES_2_TRA_Analysis.pdf [Accessed 12 October 2013].

Wils, T. H. G*., et al.* (2009). Periodicity of growth rings in *Juniperus procera* from Ethiopia inferred from crossdating and radiocarbon dating. *Dendrochronologia*, 27 (1), 45-58.

Wilson, A. T. and M. J. Grinsted (1977). $^{12}C/^{13}C$ in cellulose and lignin as palaeothermometers. *Nature*, 265 (5590), 133-135.

Wilson, R*., et al.* (2012). Reconstructing Holocene climate from tree rings: The potential for a long chronology from the Scottish Highlands. *Holocene*, 22 (1), 3-11.

Wilson, R*., et al.* (2007). Cycles and shifts: 1,300 years of multi-decadal temperature variability in the Gulf of Alaska. *Climate Dynamics*, 28 (4), 425-440.

Wilson, R. J. S., J. Esper and B. H. Luckman (2004). Utilising historical tree-ring data for dendroclimatology: A case study from the Bavarian Forest, Germany. *Dendrochronologia*, 21 (2), 53-68.

Worbes, M. (1992). Occurrence of seasonal climate and tree ring research in the tropics. *Lundqua Report*, 34, 338-342.

Worbes, M. (1995). How to measure growth dynamics in tropical trees - A review. *IAWA Journal*, 16 (4), 337-351.

Worbes, M. (1999). Annual growth rings, rainfall-dependent growth and long-term growth patterns of tropical trees from the Caparo Forest Reserve in Venezuela. *Journal of Ecology*, 87 (3), 391-403.

Worbes, M. (2002). One hundred years of tree-ring research in the tropics - a brief history and an outlook to future challenges. *Dendrochronologia*, 20 (1-2), 217-231.

Worbes, M. (2011). Wood Anatomy and Tree-Ring Structure and Their Importance for Tropical Dendrochronology. *In* W. J. Junk *et al.* eds. *Amazonian Floodplain Forests*. Springer Netherlands. 329-346.

Young, G. H. F*., et al.* (2011). Age trends in tree ring growth and isotopic archives: A case study of Pinus sylvestris L. from northwestern Norway. *Global Biogeochemical Cycles*, 25 (2), GB2020.

Young, G. H. F*., et al.* (2012). Changes in atmospheric circulation and the Arctic Oscillation preserved within a millennial length reconstruction of summer cloud cover from northern Fennoscandia. *Climate Dynamics*, 39 (1-2), 495-507.

Yu, K.-F*., et al.* (2007). High-precision analysis on annual variations of heavy metals, lead isotopes and rare earth elements in mangrove tree rings by inductively coupled plasma mass spectrometry. *Nuclear Instruments and Methods in Physics Research Section B: Beam Interactions with Materials and Atoms*, 255 (2), 399-408.

Appendices

Appendix 1: Additional Data for Chapter 2

The following graphs show the raw data from the LA-ICP-MS analysis of calcium in Scots Pine, followed by the final dataset after detrending, conversion to z-scores, and the splicing into one single dataset for each tree. The results of the ring identification using the >1 SD threshold method are also shown for each tree.

The following graphs show the raw $^{44}Ca/^{13}C$ data (with overlay of the low pass Gaussian filter used for detending), followed by the final adjusted calcium data for tree 05129.

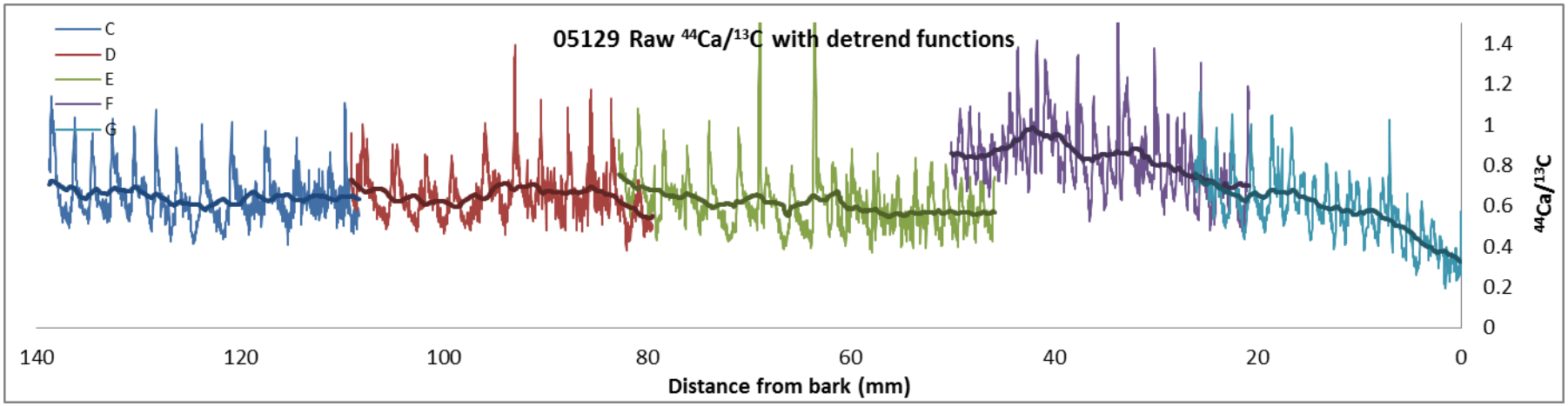

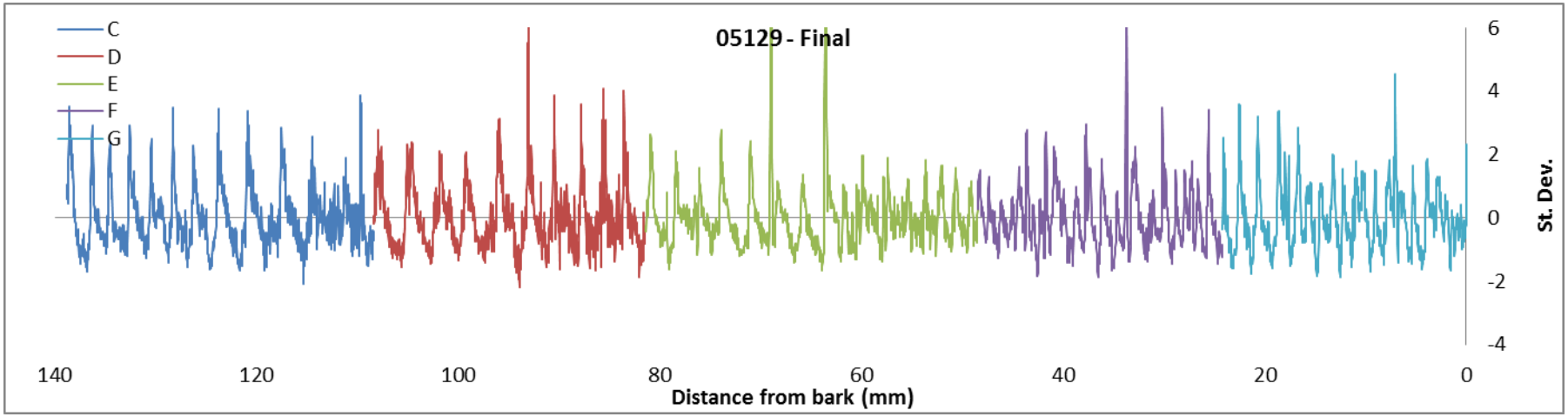

The following graphs illustrate results from assigning calcium ages to the data using the >1 and >2 threshold limits for tree 05129

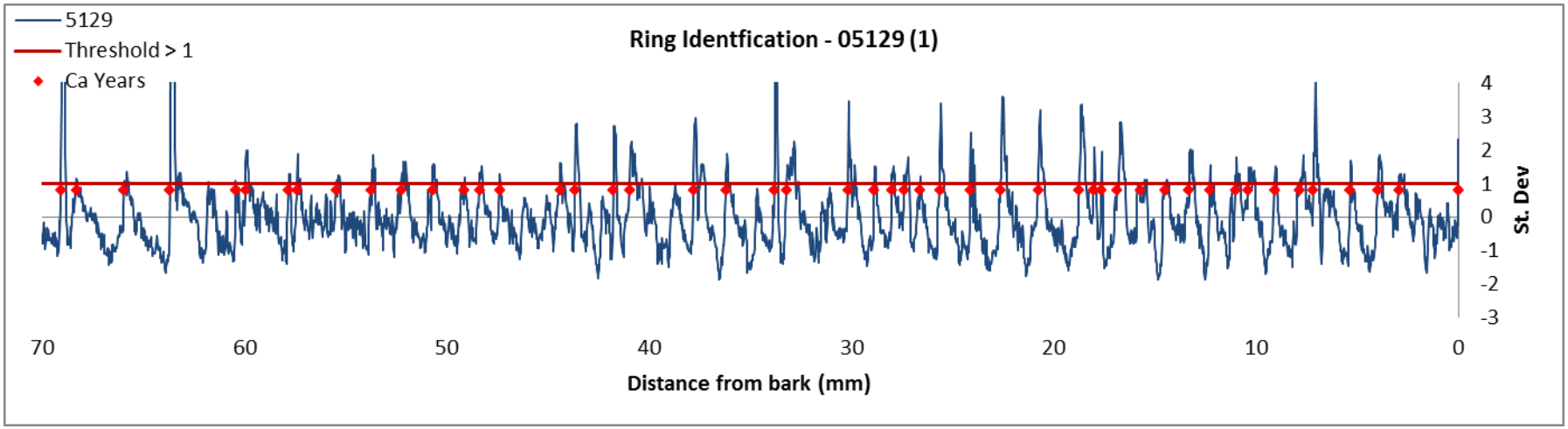

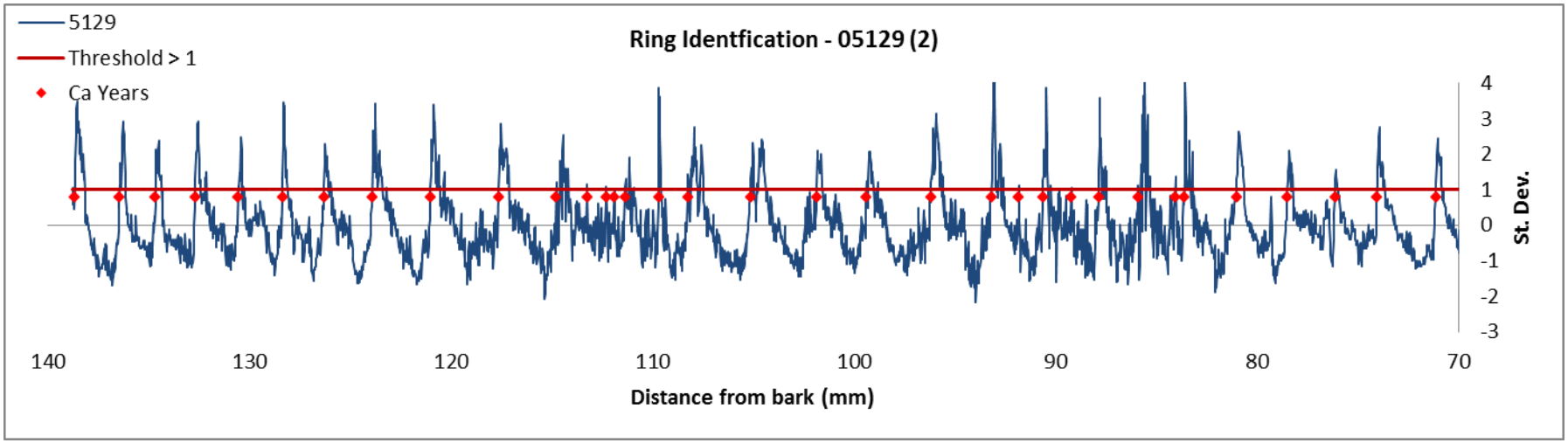

The following graphs show the raw $^{44}Ca/^{13}C$ data (with overlay of the low pass Gaussian filter used for detending), followed by the final adjusted calcium data for tree 05130.

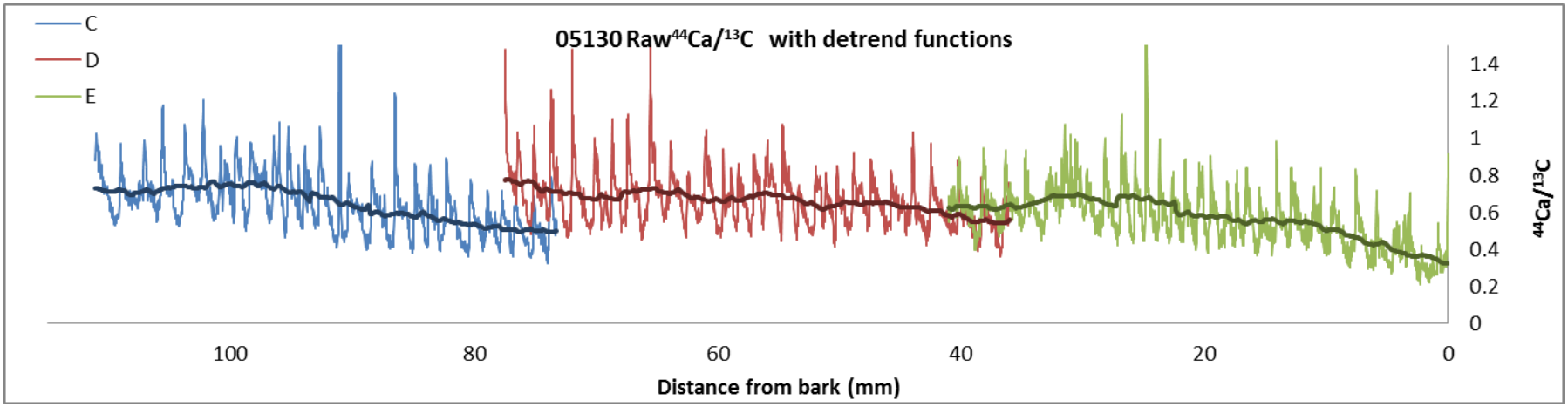

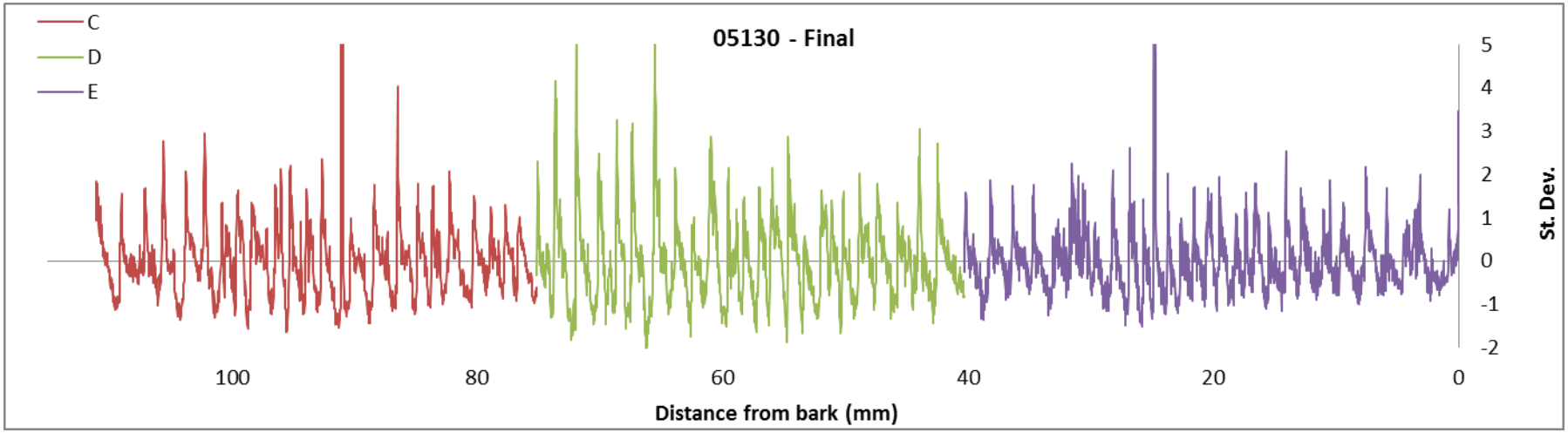

The following graphs illustrate results from assigning calcium ages to the data using the >1 and >2 threshold limits for tree 05130.

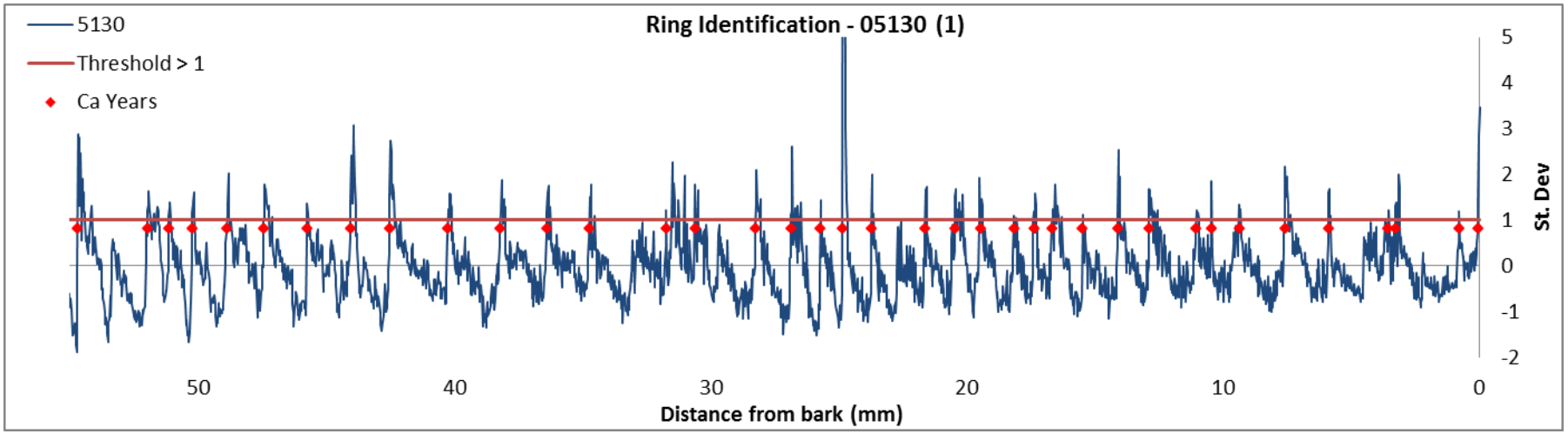

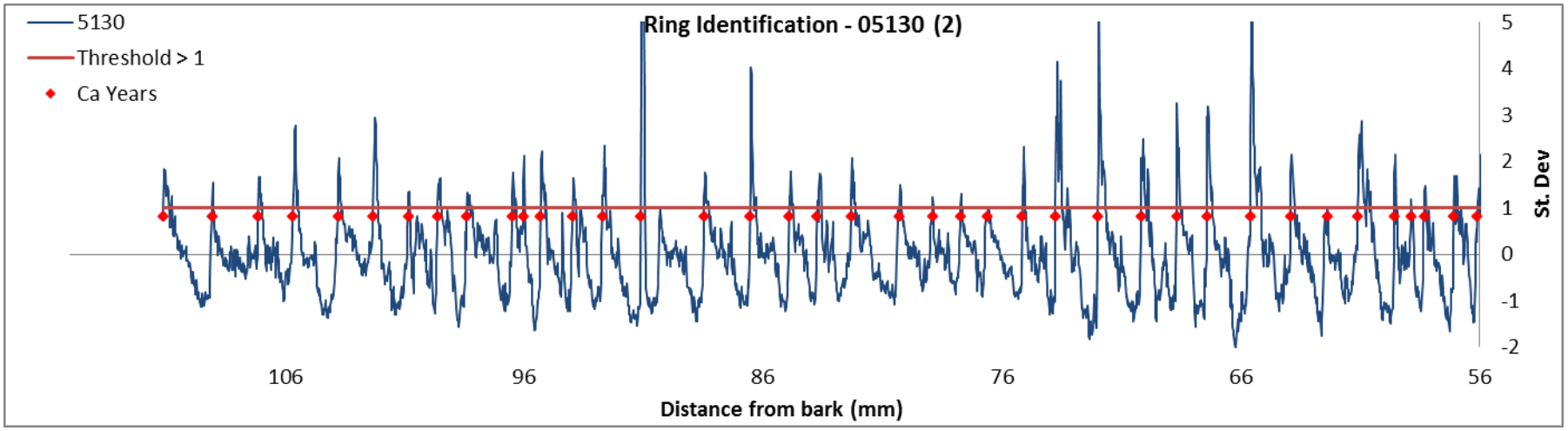

The following graphs show the raw $^{44}Ca/^{13}C$ data (with overlay of the low pass Gaussian filter used for detending), followed by the final adjusted calcium data for tree 05134 R1.

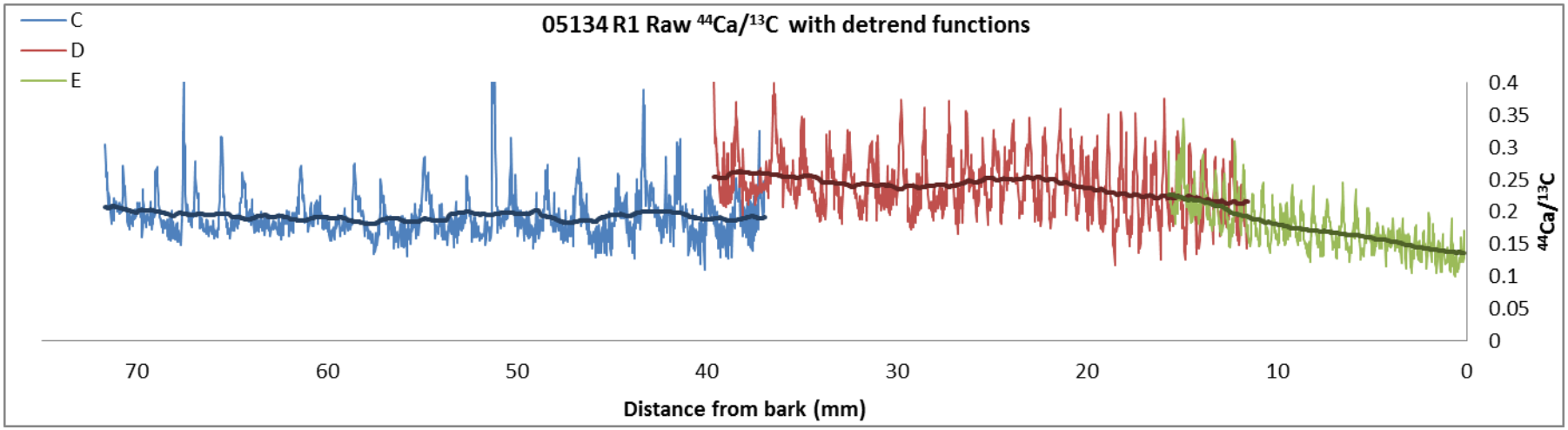

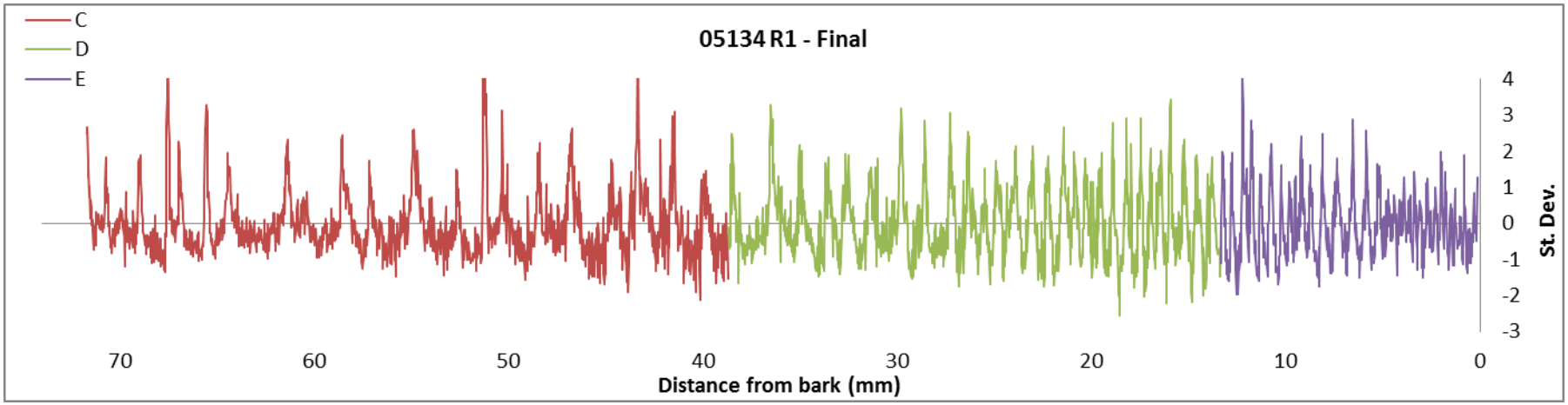

The following graphs illustrate results from assigning calcium ages to the data using the >1 and >2 threshold limits for tree 05134 R1.

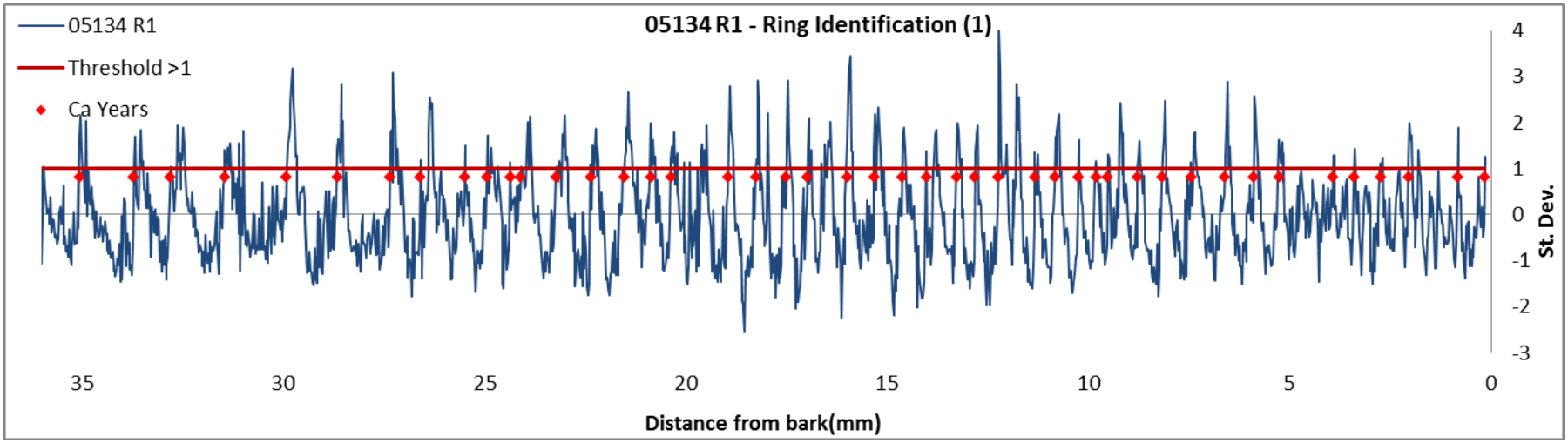

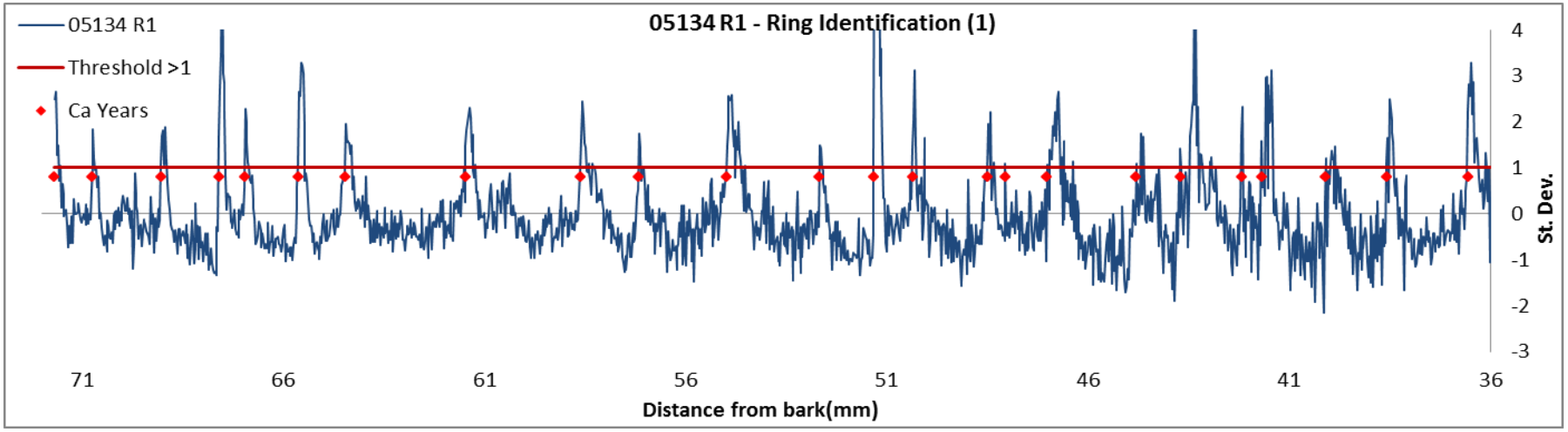

The following graphs show the raw $^{44}Ca/^{13}C$ data (with overlay of the low pass Gaussian filter used for detending), followed by the final adjusted calcium data for tree 05134 R2.

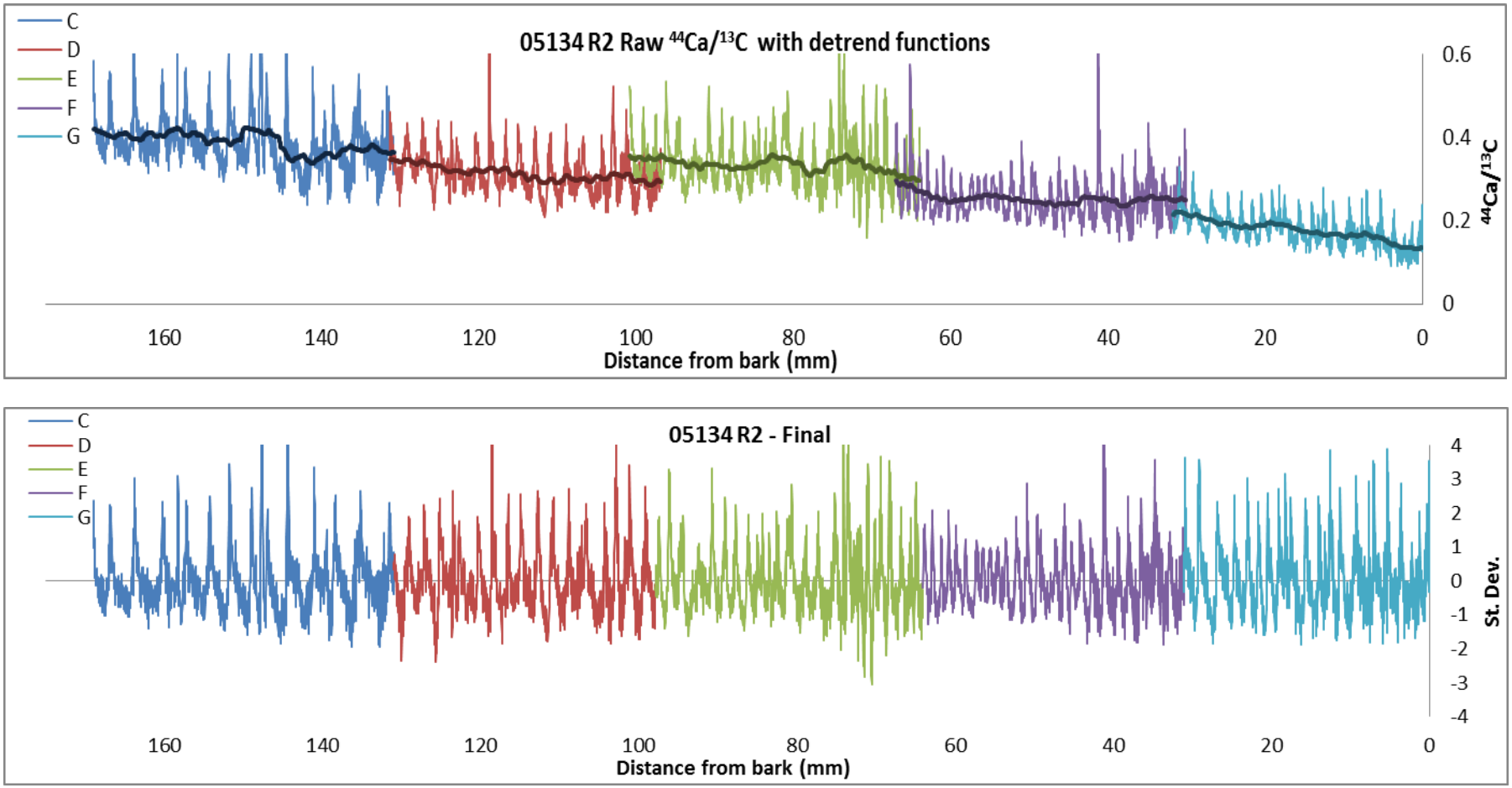

The following graphs illustrate results from assigning calcium ages to the data using the >1 and >2 threshold limits for tree 05134 R2.

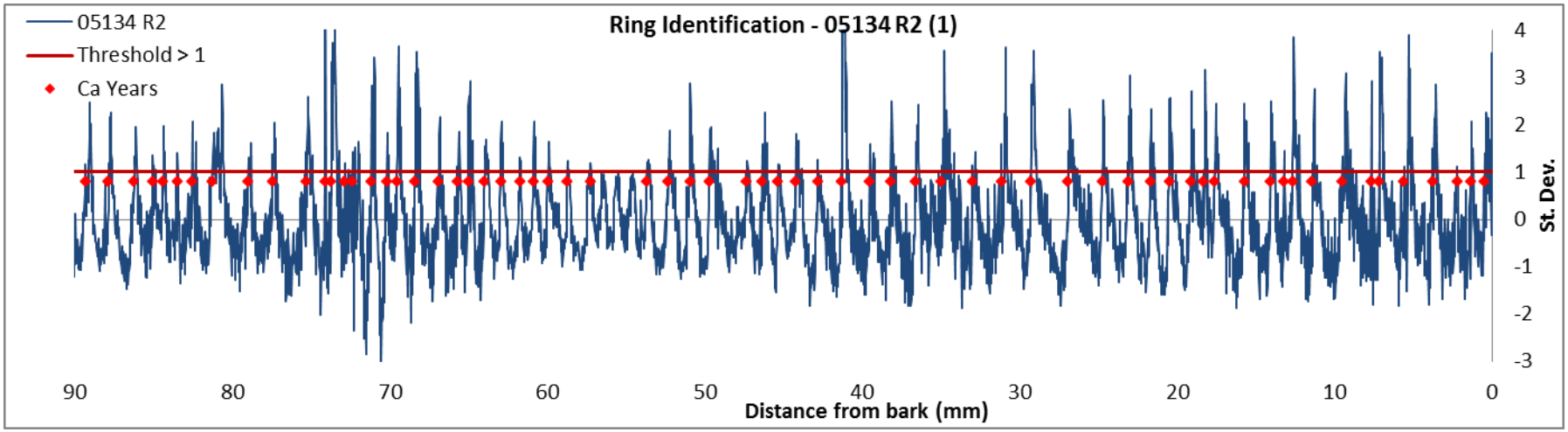

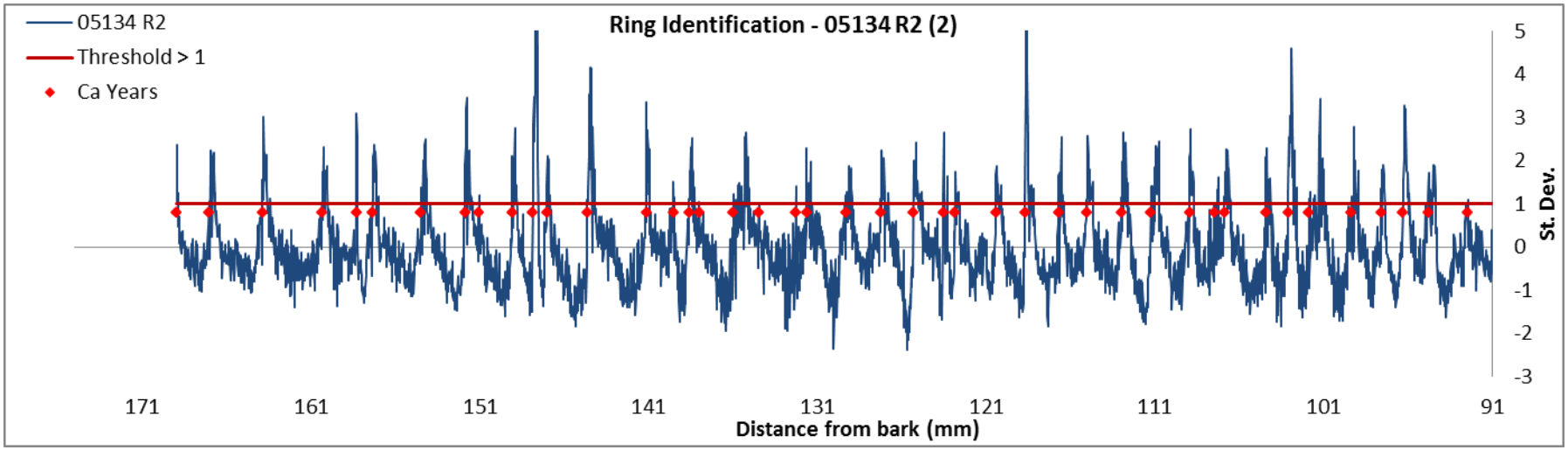

The following graphs show the raw $^{44}Ca/^{13}C$ data (with overlay of the low pass Gaussian filter used for detending), followed by the final adjusted calcium data for tree 05135 R1.

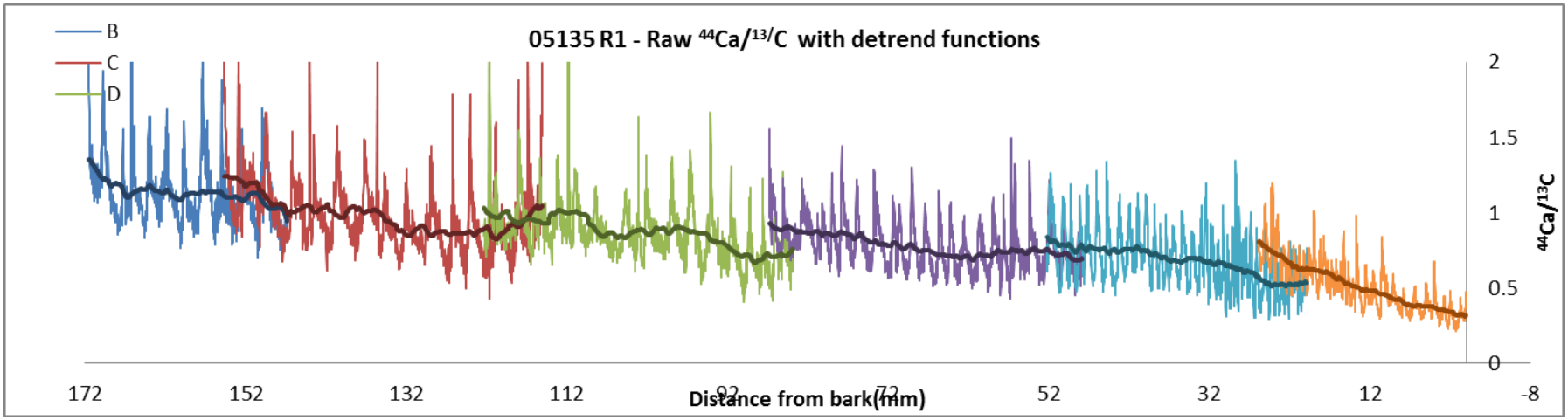

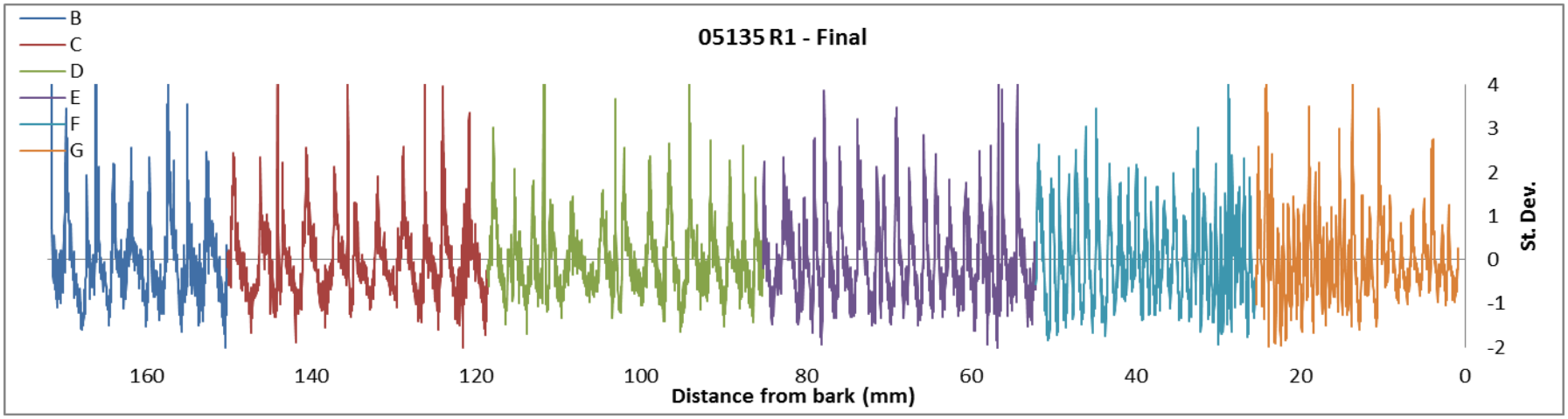

The following graphs illustrate results from assigning calcium ages to the data using the >1 and >2 threshold limits for tree 05135 R1.

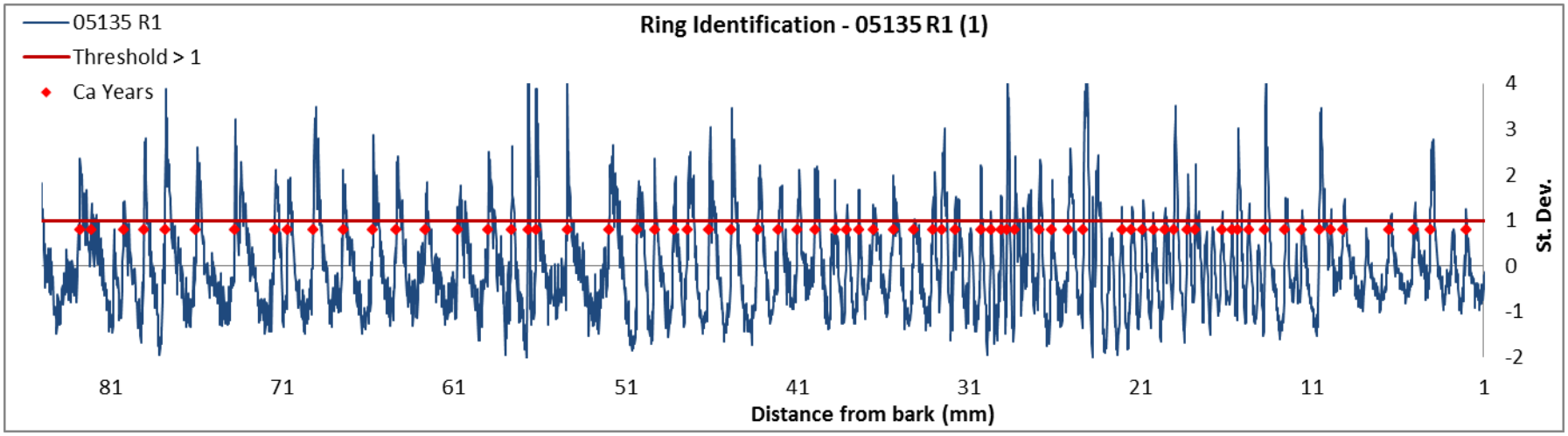

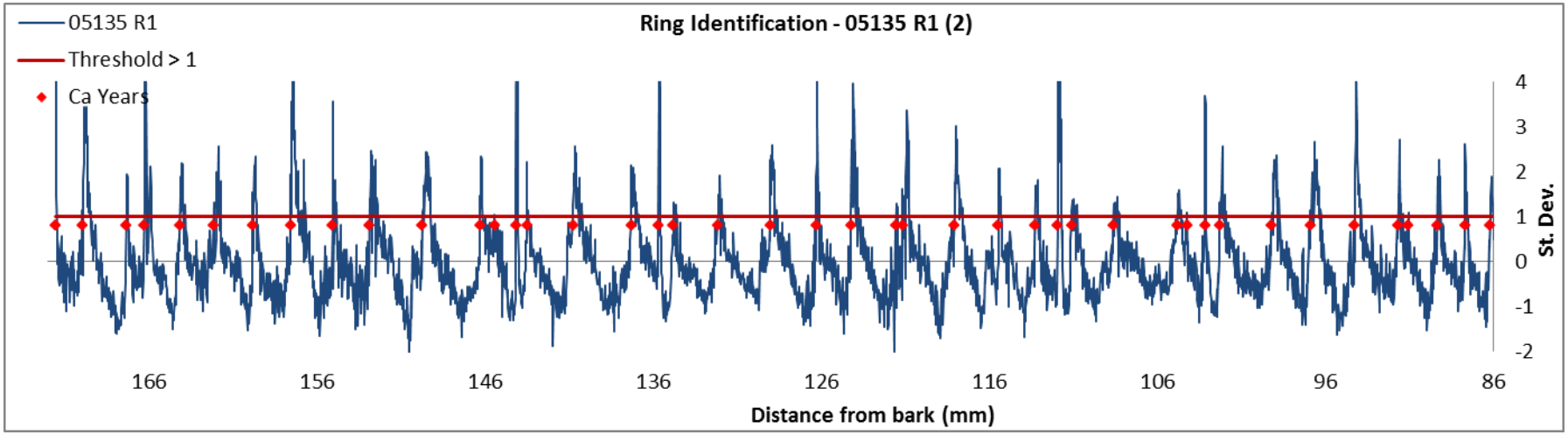

The following graphs show the raw $^{44}Ca/^{13}C$ data (with overlay of the low pass Gaussian filter used for detending), followed by the final adjusted calcium data for tree 05135 R2

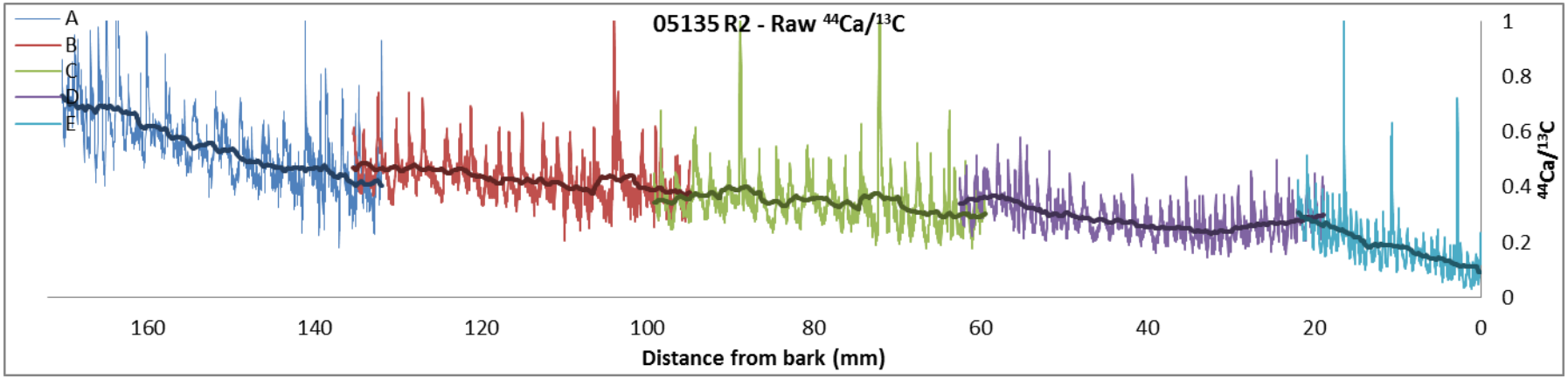

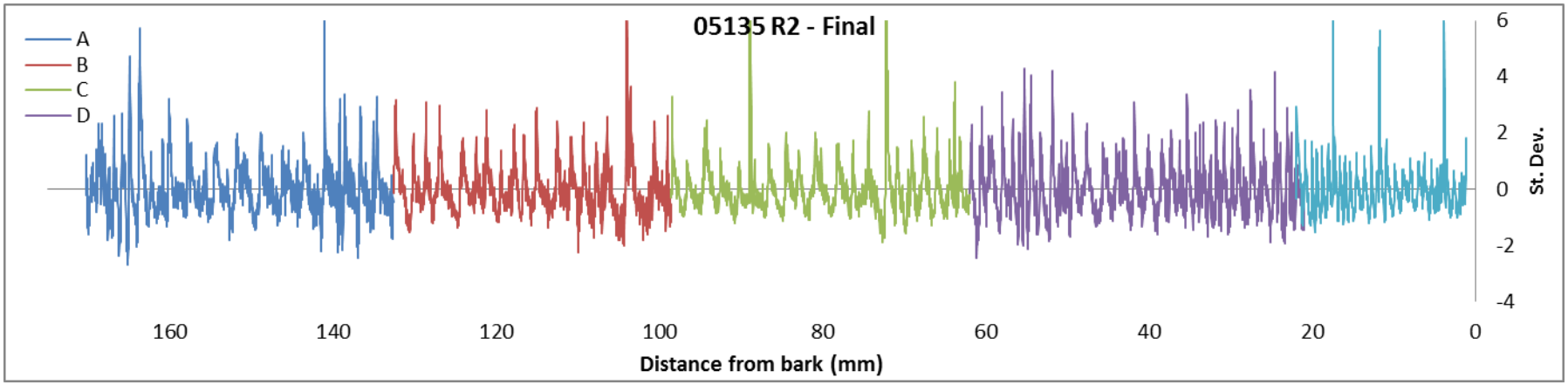

The following graphs illustrate results from assigning calcium ages to the data using the >1 and >2 threshold limits for tree 05135 R2.

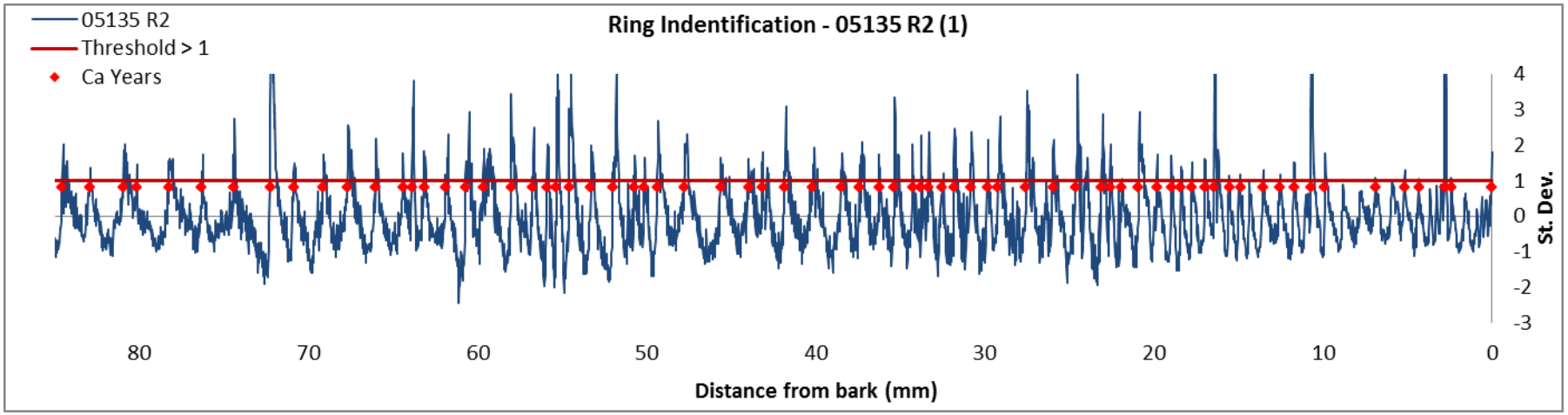

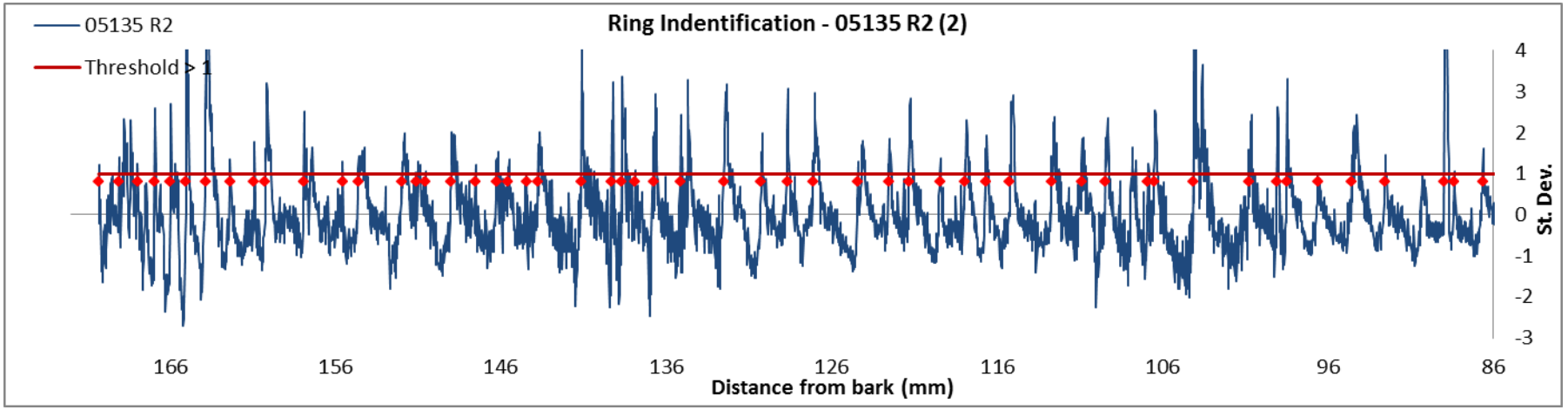

The following graphs show the raw $^{44}Ca/^{13}C$ data (with overlay of the low pass Gaussian filter used for detending), followed by the final adjusted calcium data for tree 05142.

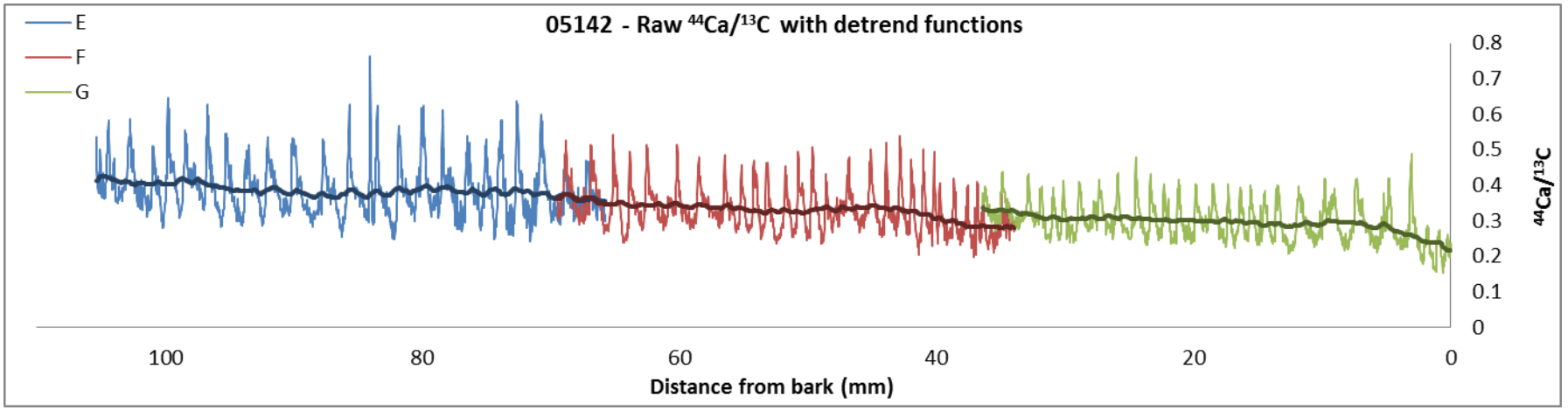

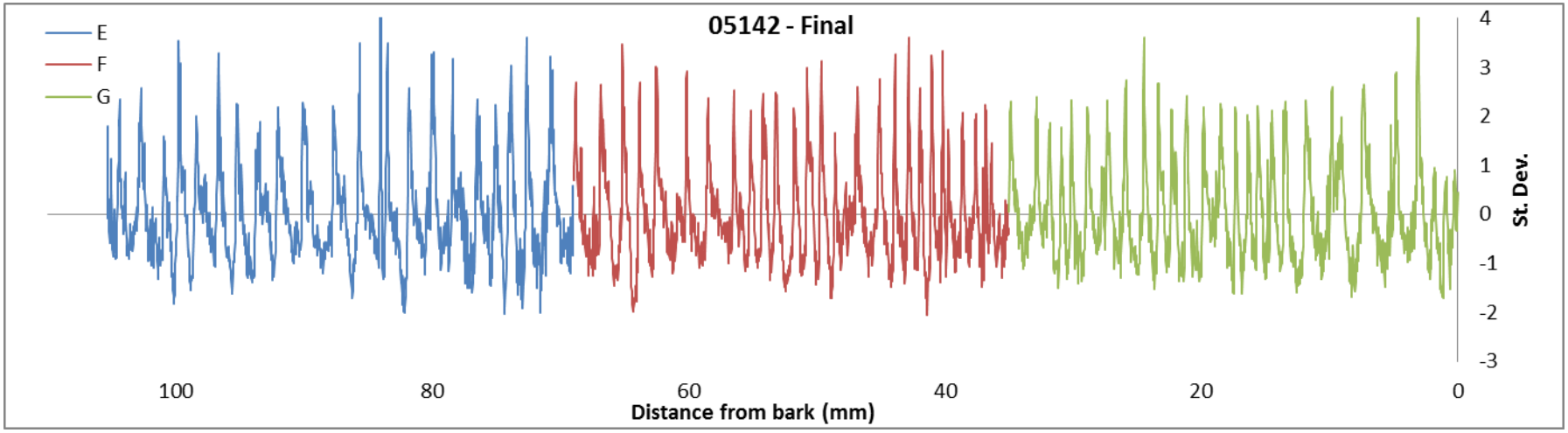

The following graphs illustrate results from assigning calcium ages to the data using the >1 and >2 threshold limits for tree 05142

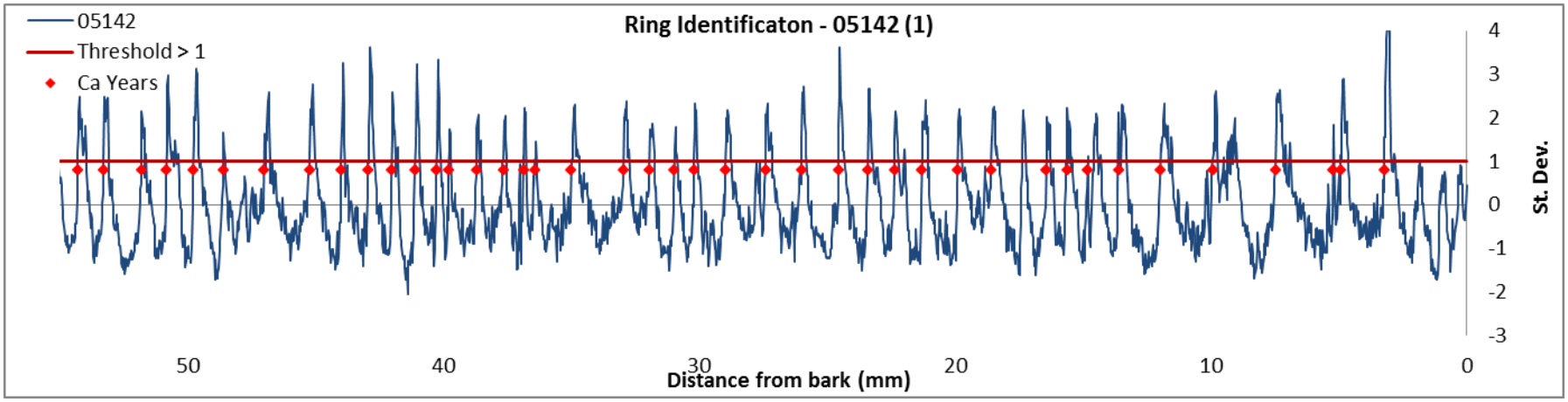

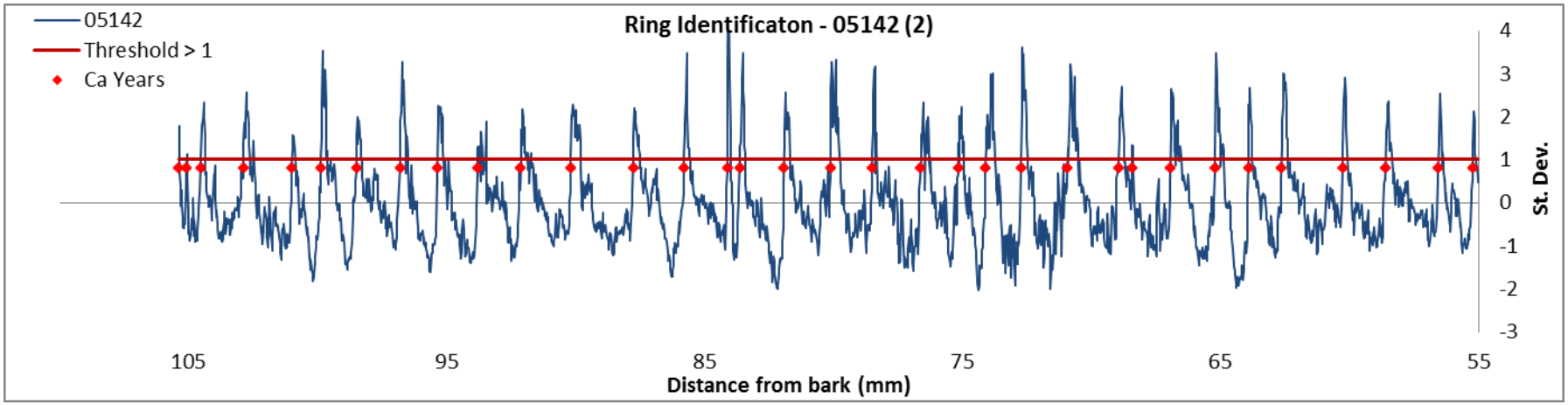

The following graphs show the raw $^{44}Ca/^{13}C$ data (with overlay of the low pass Gaussian filter used for detending), followed by the final adjusted calcium data for tree 05144.

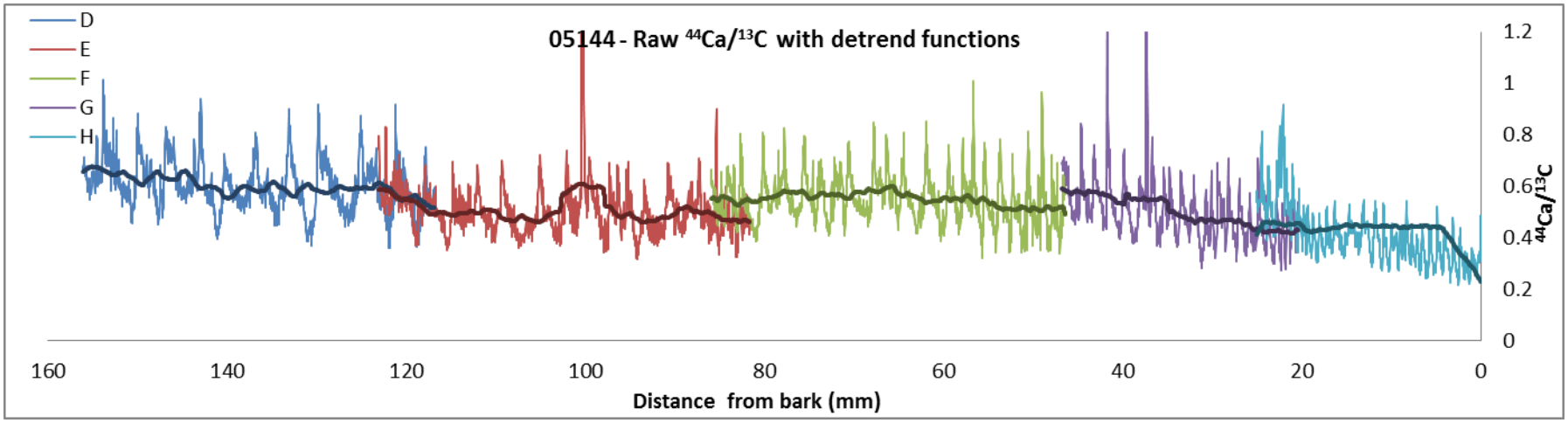

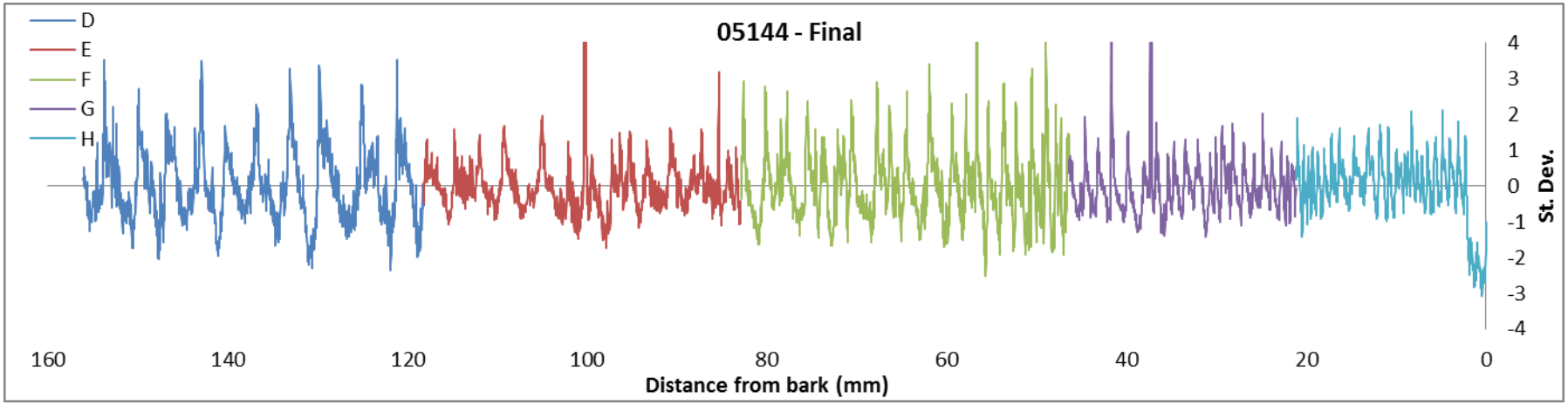

The following graphs illustrate results from assigning calcium ages to the data using the >1 and >2 threshold limits for tree 05144.

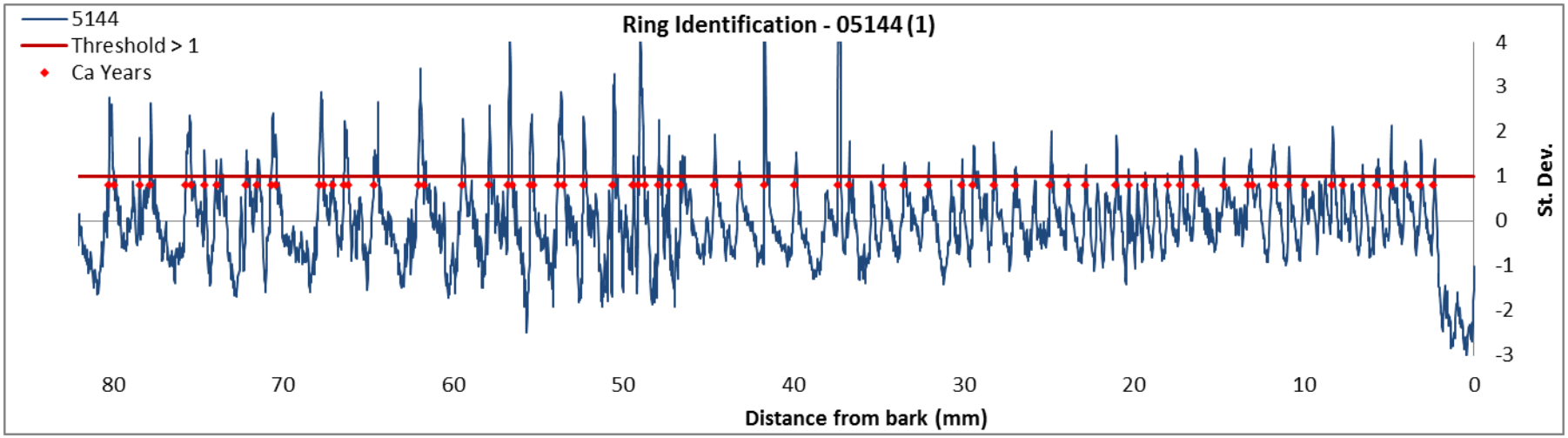

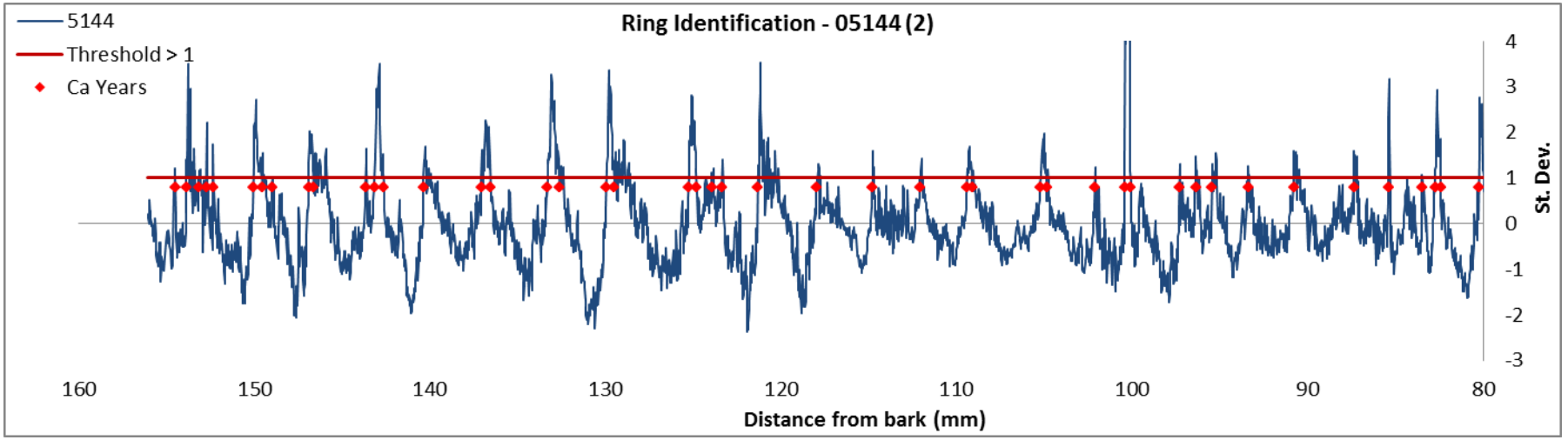

The following graphs show the raw $^{44}Ca/^{13}C$ data (with overlay of the low pass Gaussian filter used for detending), followed by the final adjusted calcium data for tree 05147.

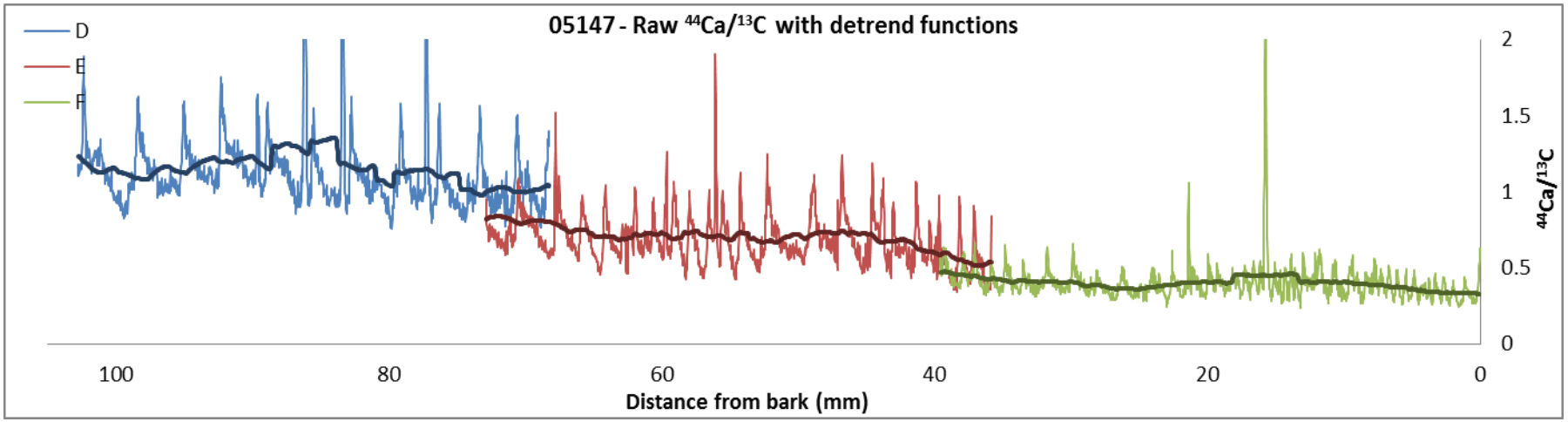

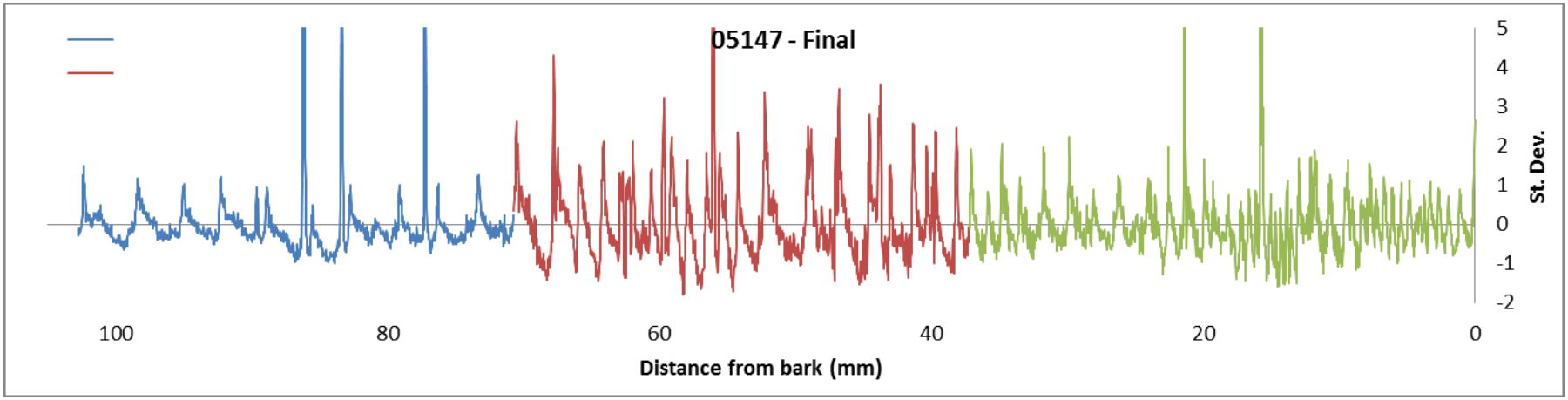

The following graphs illustrate results from assigning calcium ages to the data using the >1 and >2 threshold limits for tree 05147.

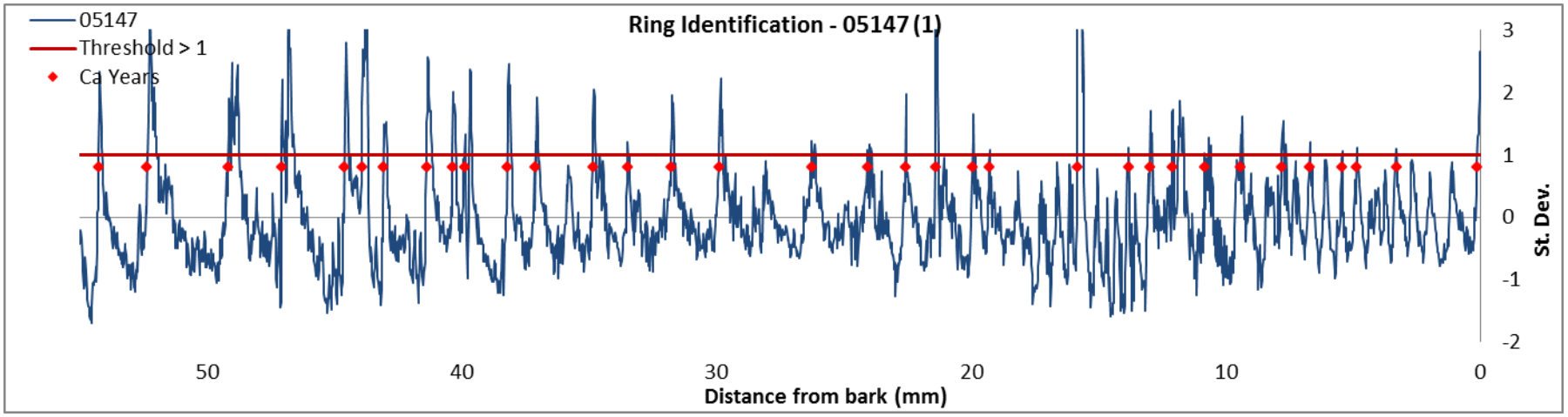

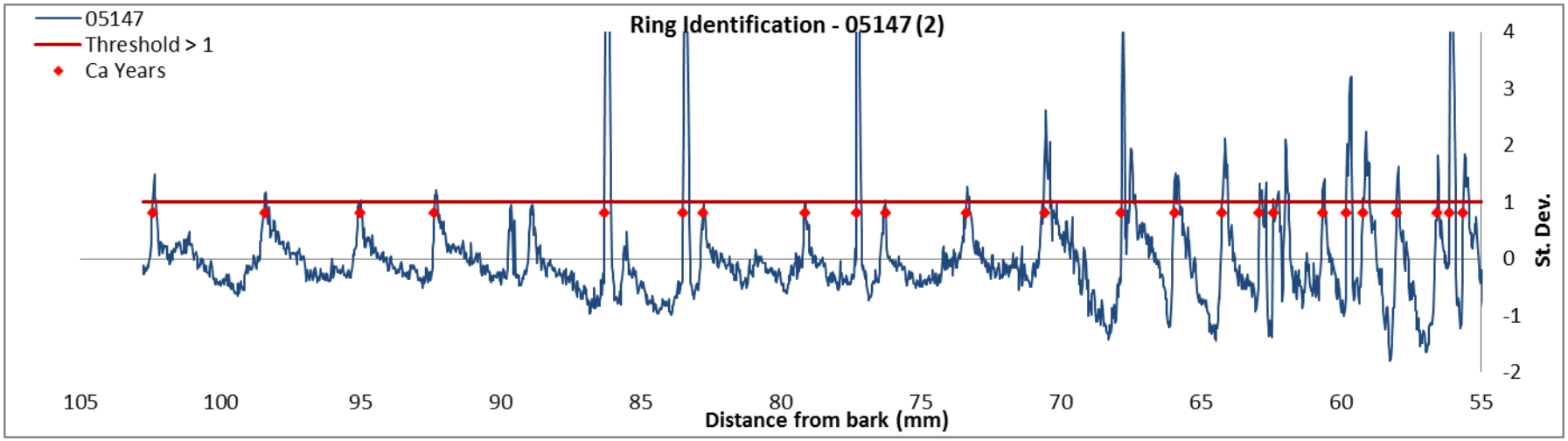

Appendix 2: Additional Data for Chapter 3

The following graphs show the raw data from the LA-ICP-MS analysis of calcium in *Terminalia macroptera*, followed by the final dataset after detrending, conversion to z-scores, and the splicing into one single dataset for each tree. The results of using the >1 SD and >2 SD thresholds to determine annual cycles within the calcium data are also shown for each tree.

The following graphs illustrate results from assigning calcium ages to the data using the >1.25 (smoothed) threshold limits for tree 2A-R1.

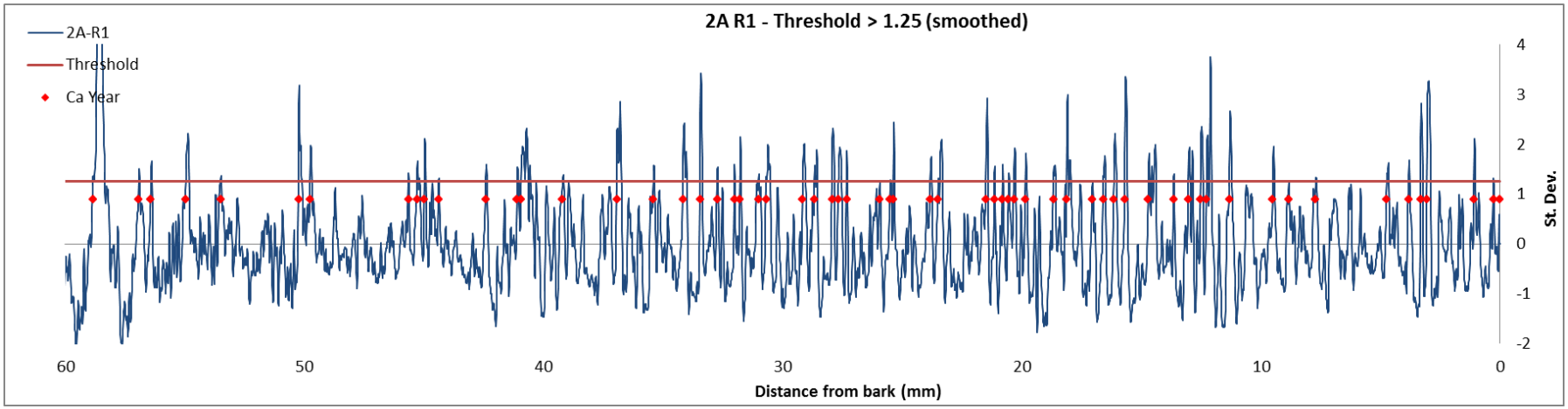

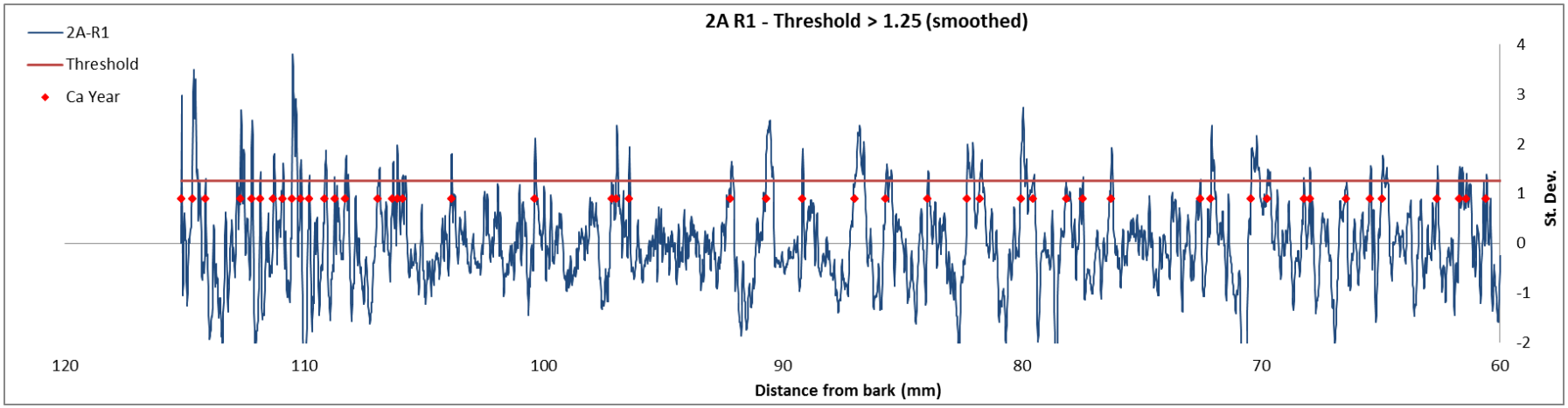

The following graphs illustrate results from assigning calcium ages to the data using the <-1 (smoothed) threshold limit for tree 2A-R1 (two parts).

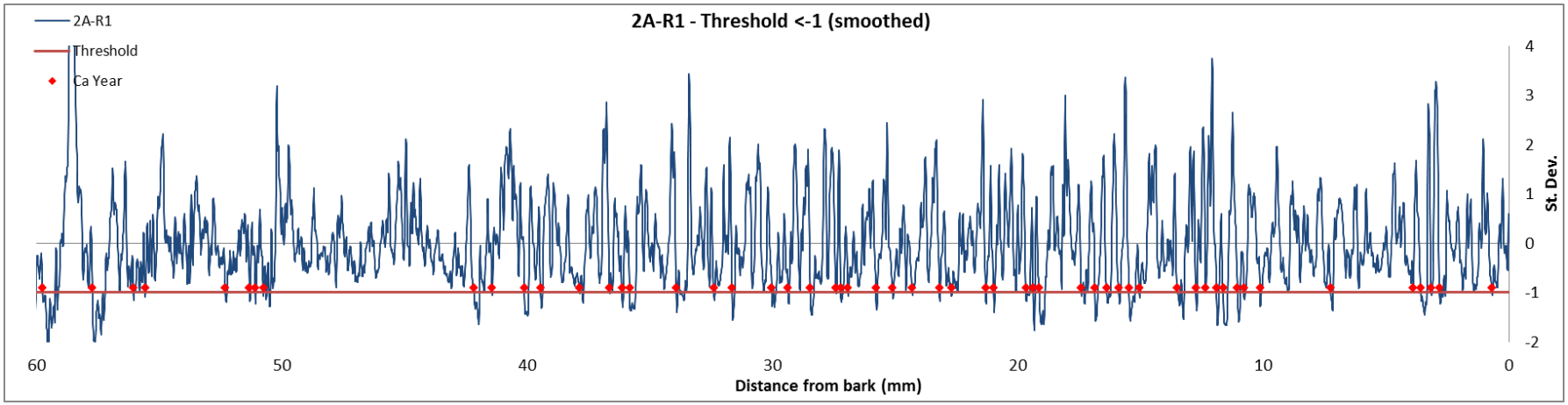

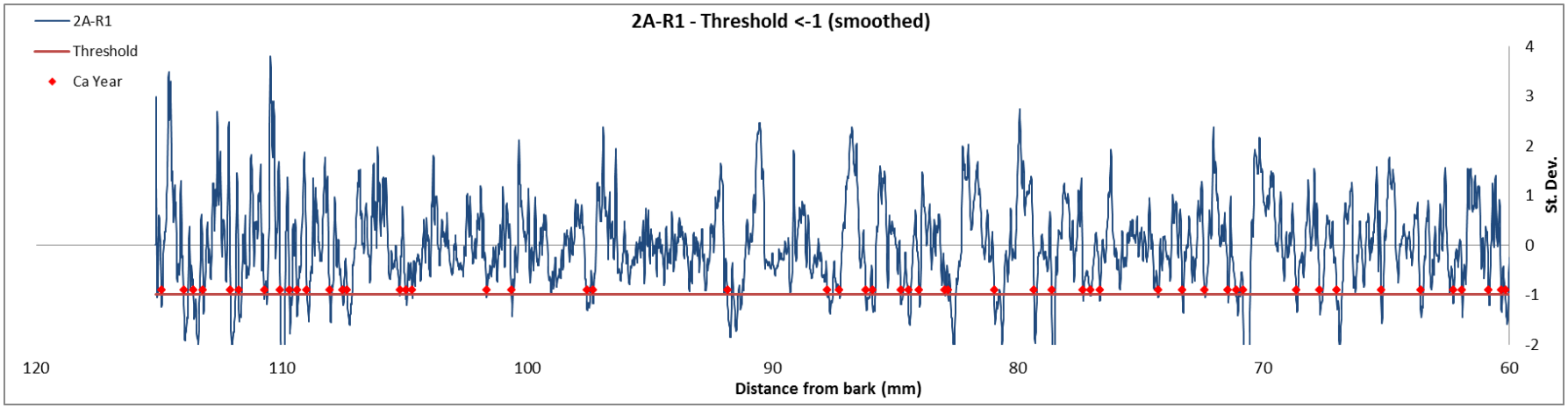

The following graphs illustrate results from assigning calcium ages to the data using the >1.25 (smoothed) and <-1 (smoothed) threshold limits for tree 2A-R2.

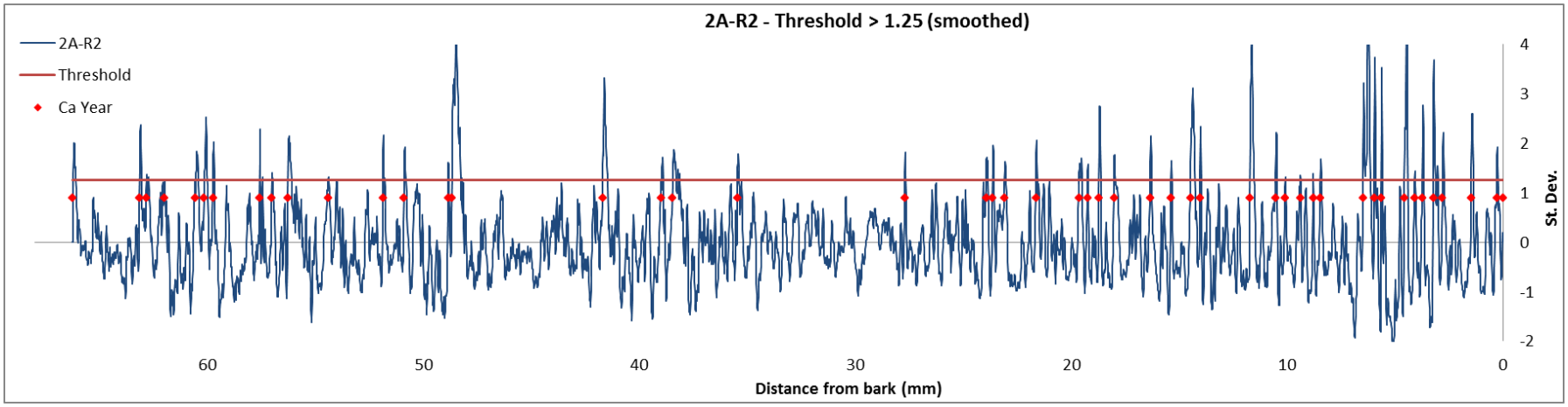

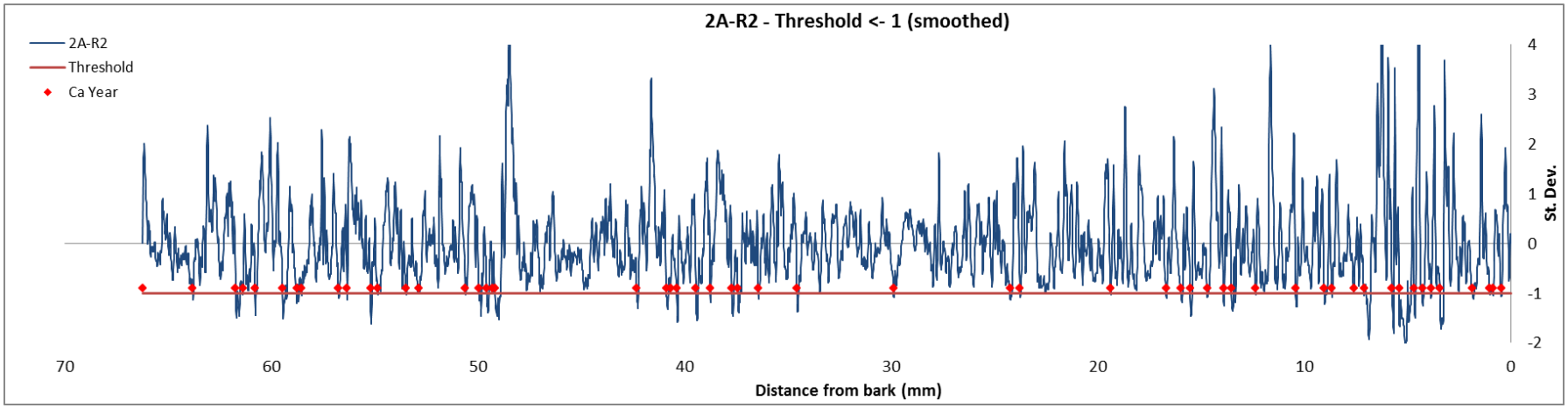

The following graphs show the raw $^{44}Ca/^{13}C$ data (with overlay of the low pass Gaussian filter used for detending), followed by the final adjusted calcium data for tree 2T.

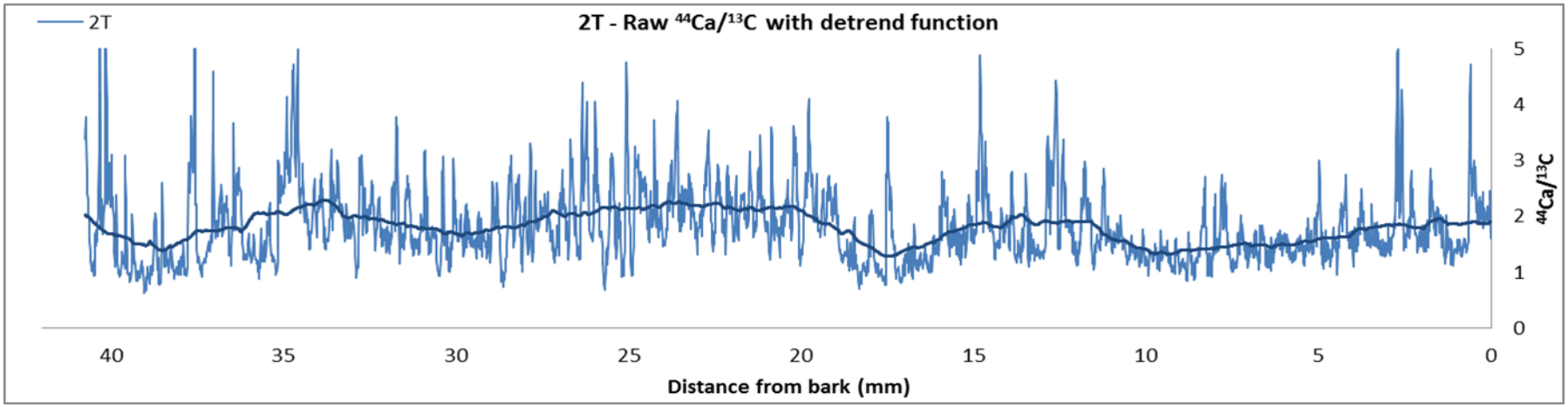

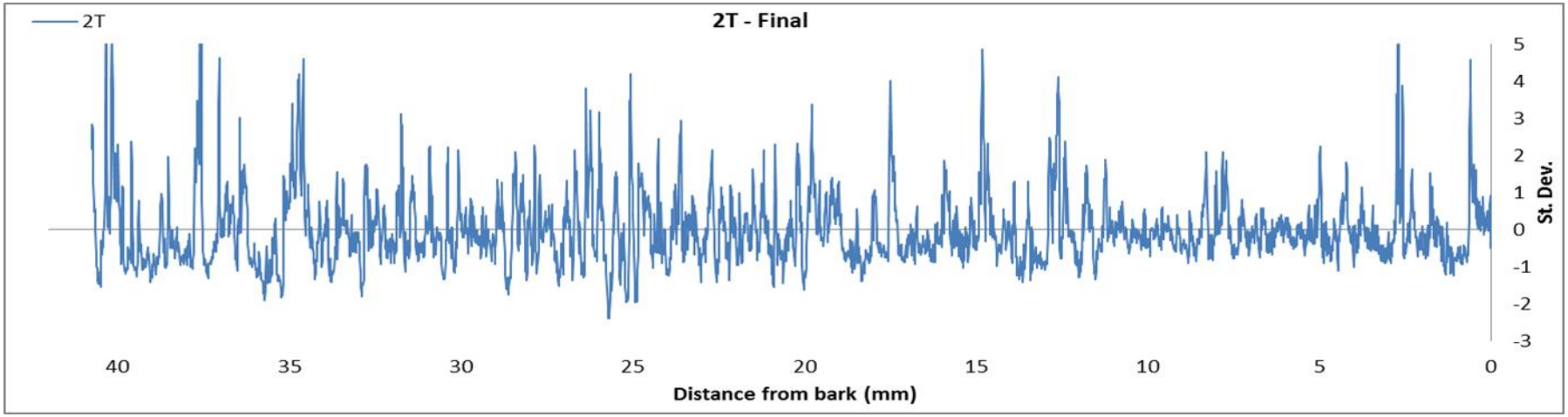

The following graphs illustrate results from assigning calcium ages to the data using the >1.25 (smoothed) and <-1 (smoothed) threshold limits for tree 2T.

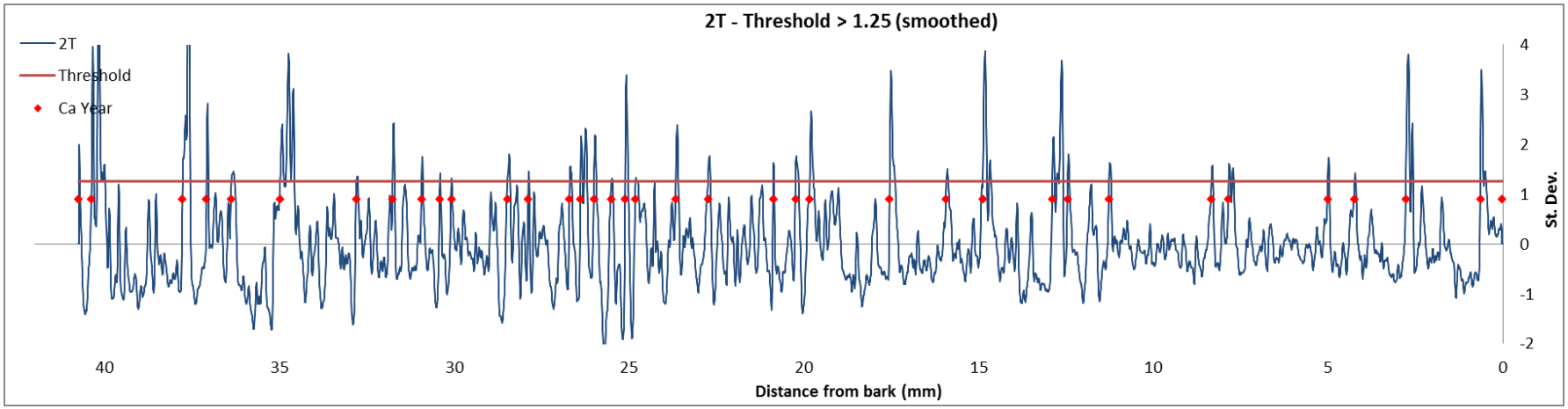

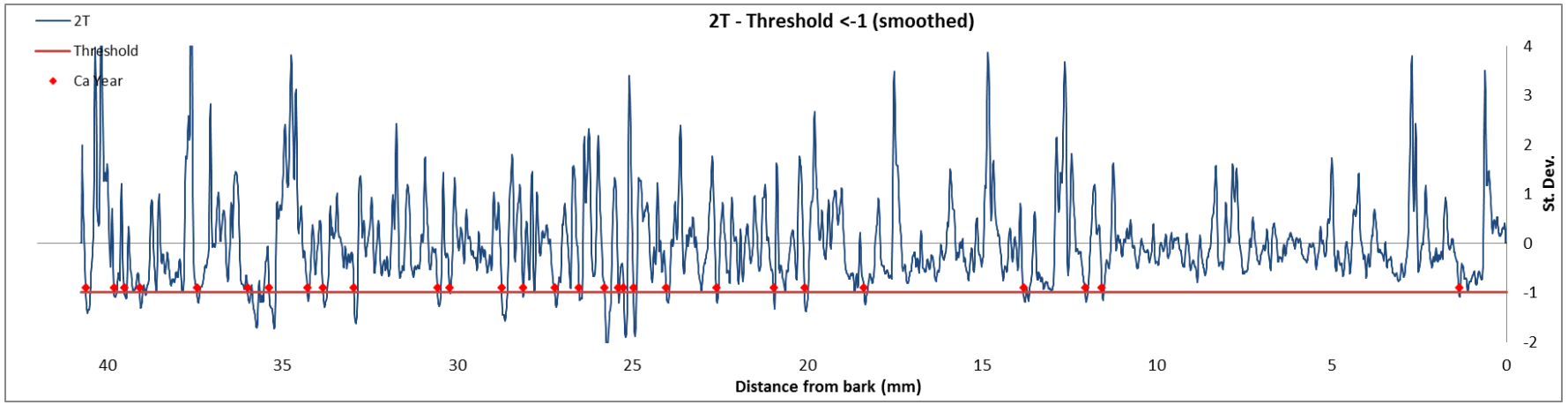

The following graphs show the raw $^{44}Ca/^{13}C$ data (with overlay of the low pass Gaussian filter used for detending), followed by the final adjusted calcium data for tree 2Y.

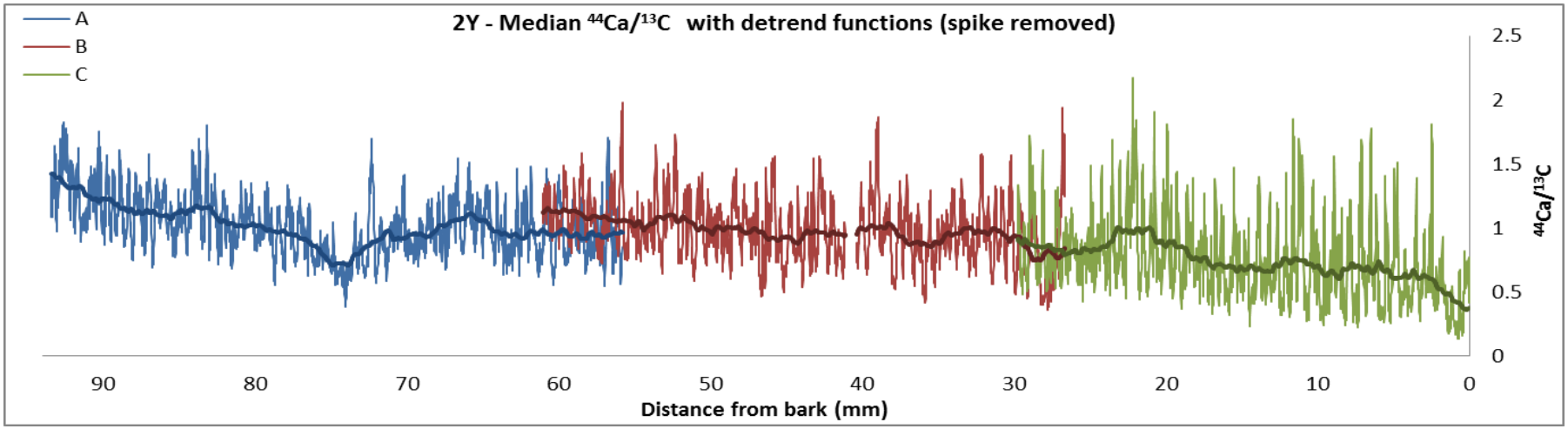

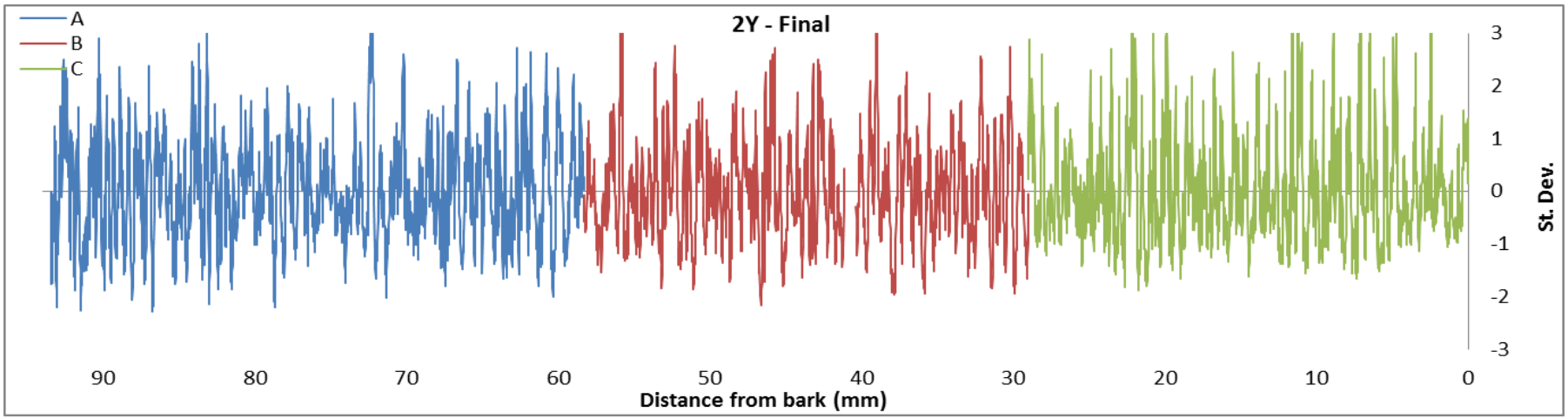

The following graphs illustrate results from assigning calcium ages to the data using the >1.25 (smoothed) threshold limits for tree 2Y (split into 2 sections).

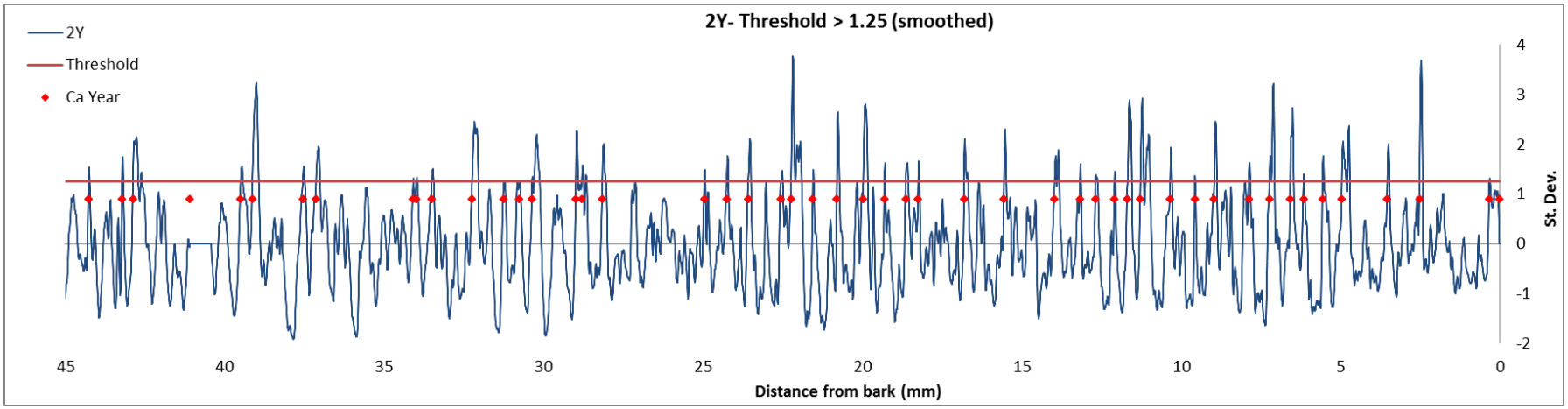

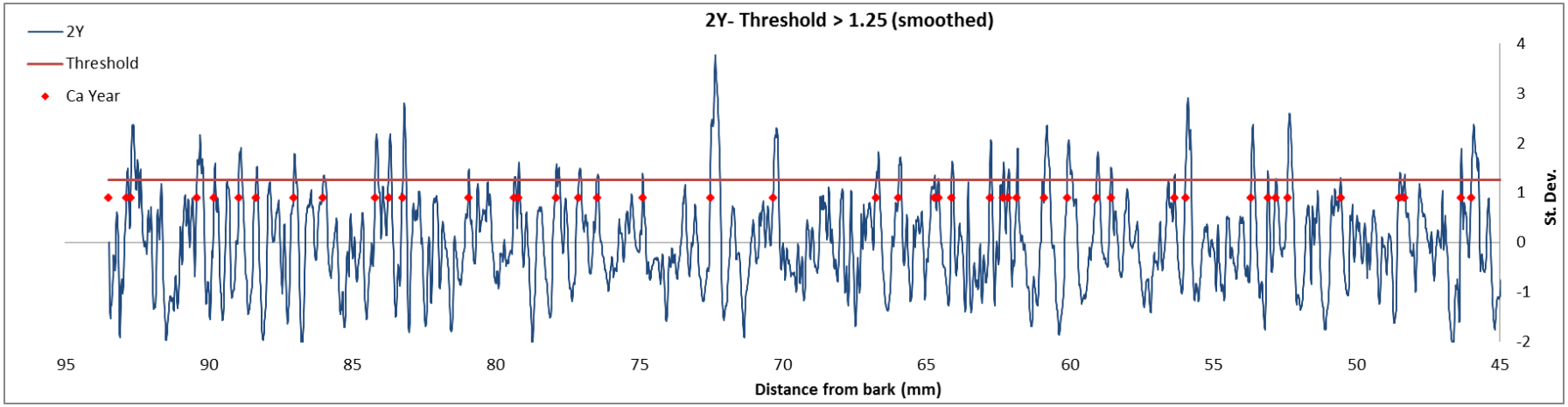

The following graphs illustrate results from assigning calcium ages to the data using the <-1 (smoothed) threshold limits for tree 2Y (split into 2 sections).

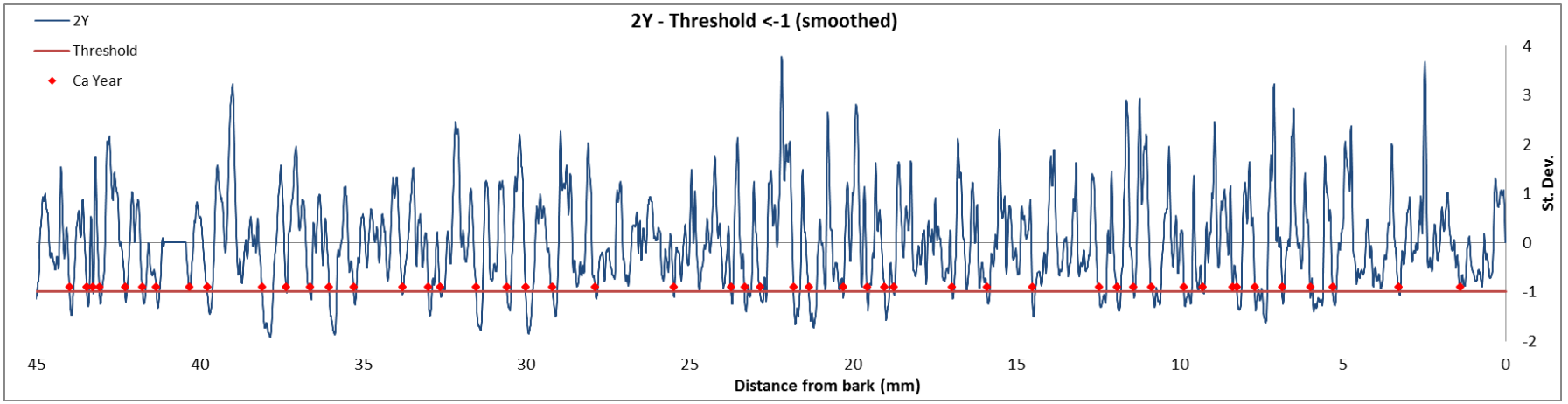

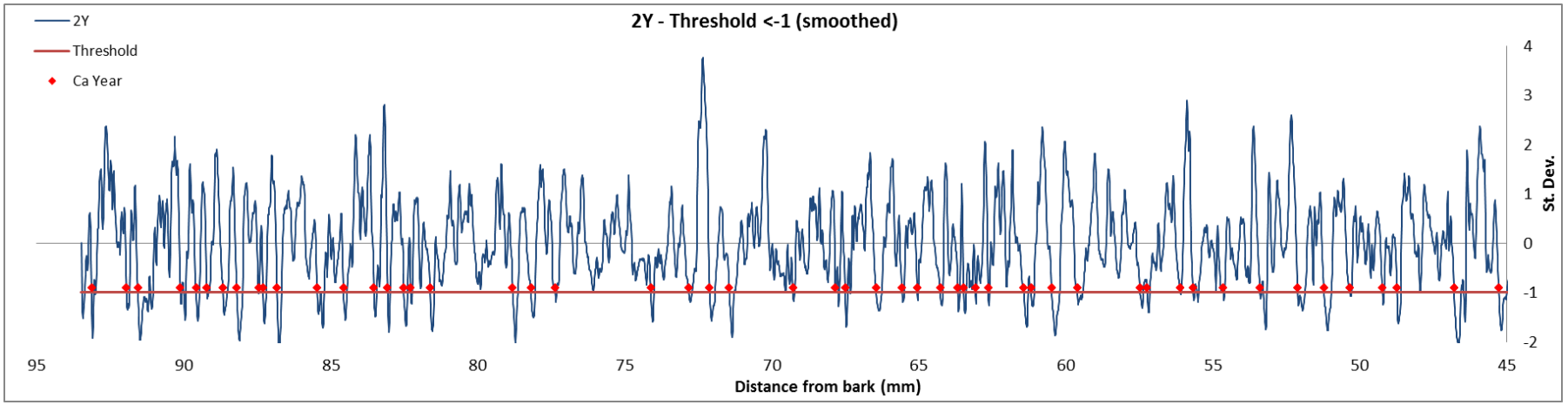

The following graphs show the raw $^{44}Ca/^{13}C$ data (with overlay of the low pass Gaussian filter used for detending), followed by the final adjusted calcium data for tree 4P.

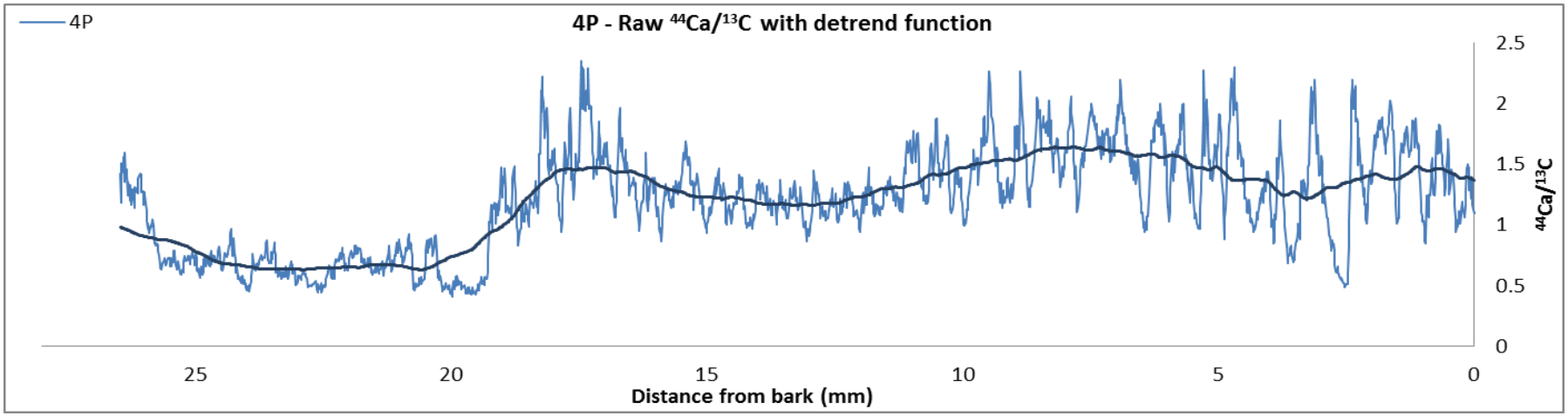

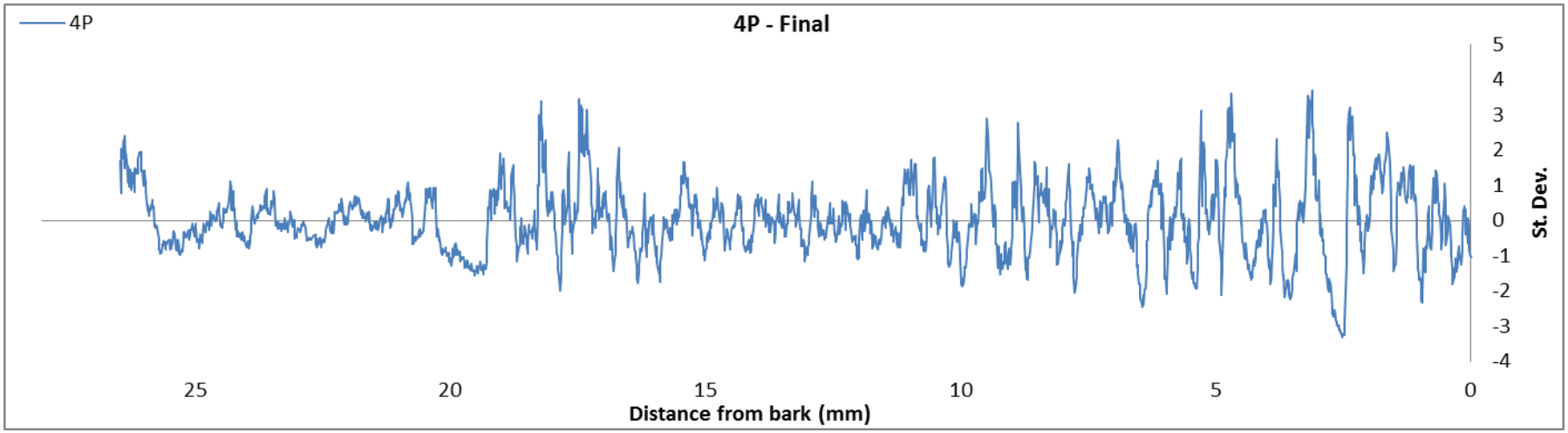

The following graphs illustrate results from assigning calcium ages to the data using the >1.25 (smoothed) threshold limits for tree 4P

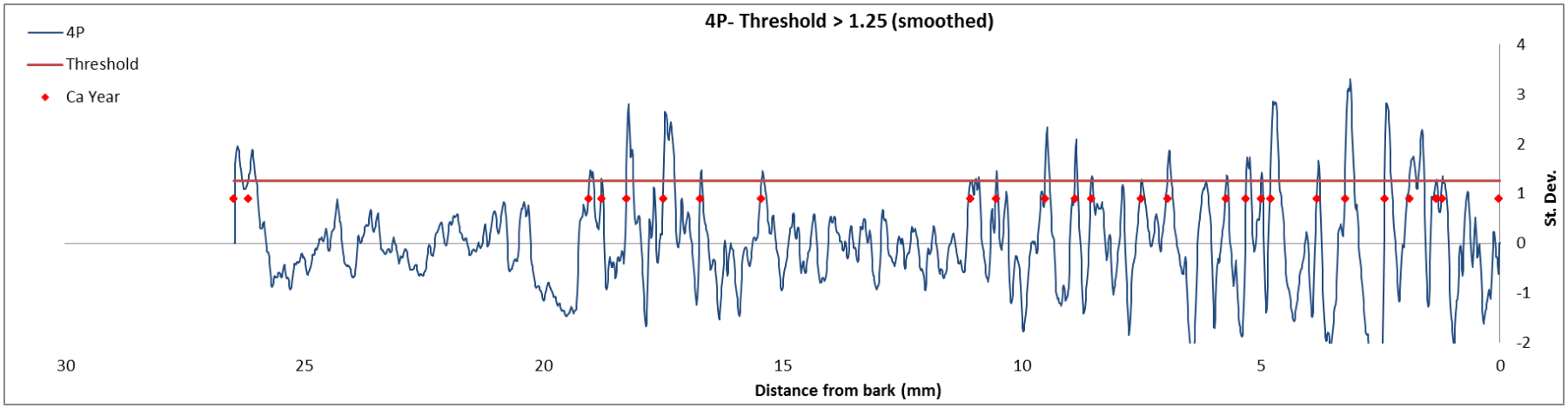

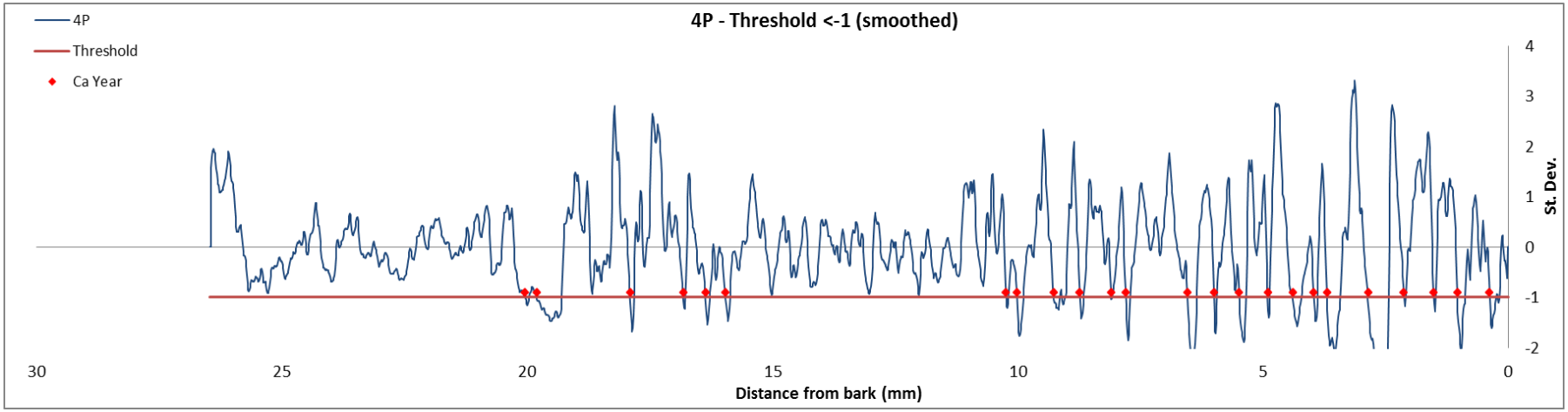

The following graphs show the raw $^{44}Ca/^{13}C$ data (with overlay of the low pass Gaussian filter used for detending), followed by the final adjusted calcium data for tree 4Q.

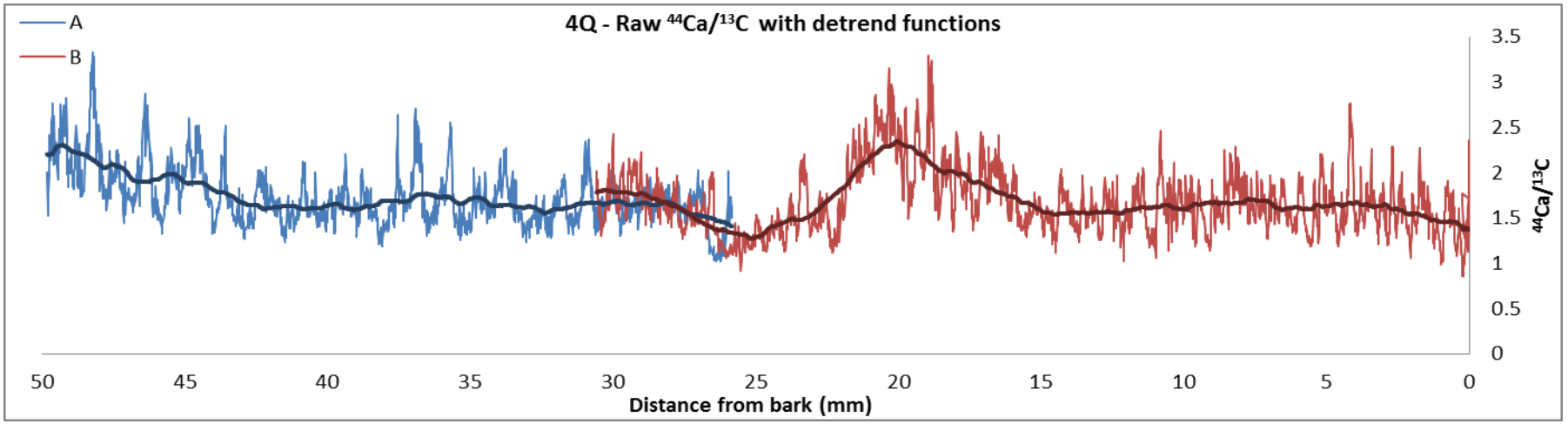

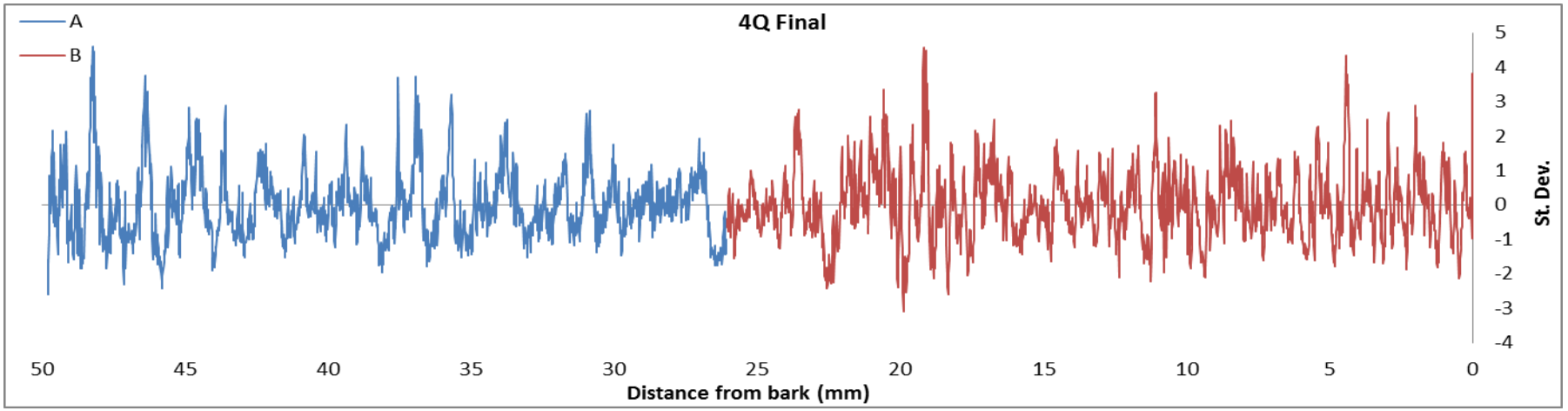

The following graphs illustrate results from assigning calcium ages to the data using the >1.25 (smoothed) threshold limits for tree 4Q.

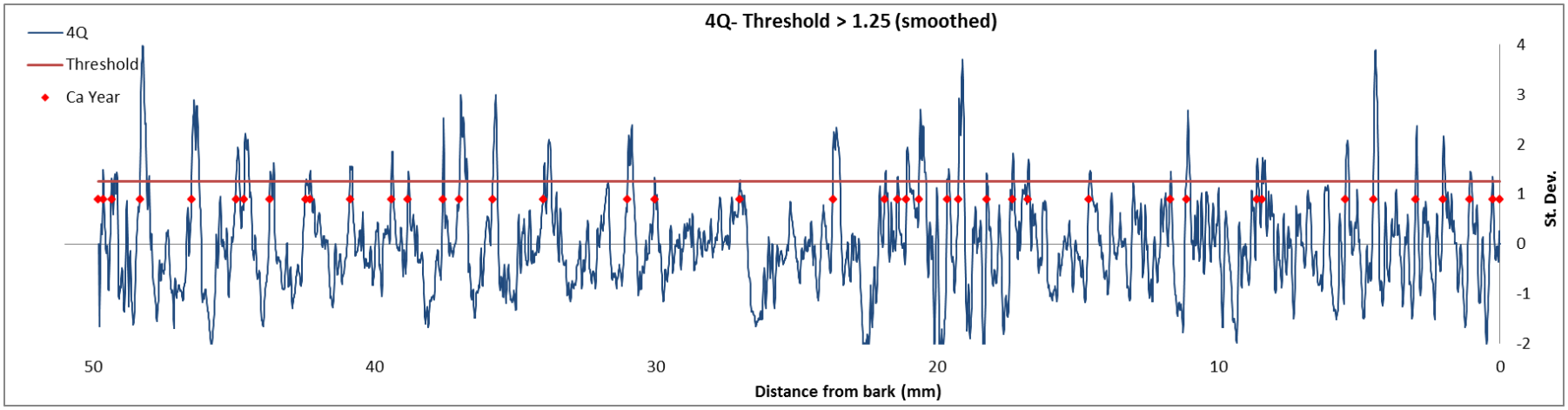

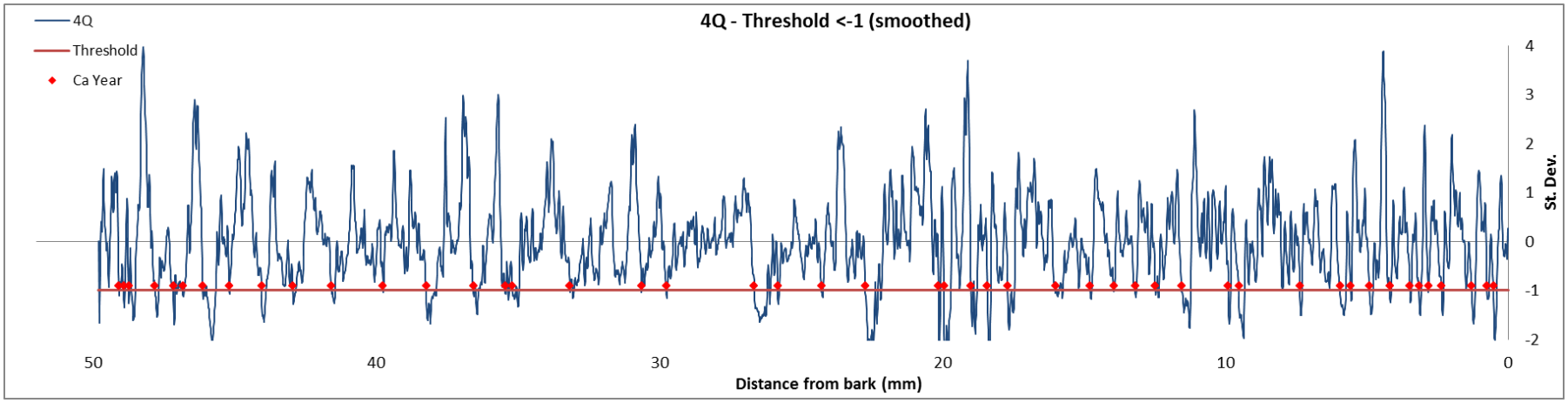

Appendix 3: Additional Data for Chapter 4

The following tables provide the isotopic values for all of $\delta^{18}O$ and $\delta^{18}C$ measured for tree 2A:

Oxygen Isotope Data: Tree 2A

Slice #	$\delta^{18}O$	Slice #	$\delta^{18}O$	Slice #	$\delta^{18}O$	Slice #	$\delta^{18}O$
4	26.8	164	25.3	320	26.3	492	27.6
8	28.7	168	26.4	324	26.9	496	25.2
13	26.9	172	26.4	328	26.3	500	27.4
17	26.9	176	26.6	332	27.8	504	28.3
21	27.1	180	26.6	344	28.8	508	26.9
25	26.6	184	26.8	348	28.9	512	27.2
29	26.4	188	27.9	352	27.9	516	27.6
33	28.7	192	28.0	356	26.3	520	27.0
37	29.0	196	28.5	360	26.1	524	28.3
41	30.3	200	27.2	364	26.4	528	27.8
45	30.5	204	26.3	368	27.4	532	28.2
50	29.2	208	26.1	372	28.0	536	28.0
54	28.4	212	26.6	376	28.6	540	27.9
58	28.1	216	26.7	380	29.0	544	26.9
62	27.9	220	27.2	384	28.7	548	27.0
66	25.6	224	27.6	388	29.0	552	28.9
70	26.0	228	28.9	392	28.7	556	29.0
75	26.3	232	29.3	396	28.7	560	28.7
80	27.0	236	29.9	400	28.4	564	29.4
85	26.8	240	29.7	404	28.8	576	27.7
88	26.3	244	29.5	408	28.4	580	27.0
92	26.1	248	29.0	408	28.6	584	25.8
96	27.6	252	27.9	412	27.5	588	26.1
99	29.5	256	27.6	416	27.1	592	27.4
104	28.9	260	27.6	420	27.0	596	28.2
108	27.1	264	27.3	424	28.2	600	28.1
112	25.8	268	27.0	428	28.9	604	26.4
116	24.8	272	26.7	436	29.9	608	25.5
120	24.8	276	26.6	440	29.6	612	25.4
124	25.4	280	26.5	444	29.2	616	24.9
128	25.7	284	27.0	448	27.6	620	25.7
132	26.4	288	27.4	452	27.2	624	26.7
136	27.4	292	28.3	464	25.0	628	27.0
140	28.0	296	28.5	468	27.7	632	26.9
144	28.3	300	29.2	472	25.6	636	26.9
148	27.8	304	27.7	476	26.3	640	27.5
152	26.4	308	27.9	480	27.6	644	27.3
156	25.4	312	26.9	484	27.7	648	27.5
160	25.3	316	25.8	488	27.0	652	28.5

Oxygen Isotope Data: Tree 2A - Continued

Slice #	$\delta^{18}O$	Slice #	$\delta^{18}O$	Slice #	$\delta^{18}O$
656	29.3	816	28.0	968	27.6
660	28.6	820	27.5	972	27.9
664	27.9	824	27.3	976	28.5
668	28.1	824	27.1	980	29.0
672	27.8	828	27.5	984	28.3
676	27.8	832	27.7	988	26.9
680	27.0	836	27.2	992	26.3
684	26.6	840	27.4	1000	24.7
688	25.8	844	27.6	1004	24.2
692	25.7	848	28.6	1008	23.9
696	26.4	852	27.4	1012	24.6
700	26.7	856	28.1	1016	25.3
704	26.9	860	28.3	1020	25.9
708	26.2	864	28.1	1024	26.0
712	27.0	868	27.7	1028	26.2
720	26.8	872	27.6	1032	26.5
724	27.2	876	27.0	1036	26.3
728	27.1	880	26.2	1040	26.3
732	27.2	884	24.7	1064	28.6
736	27.1	888	25.3	1068	28.9
740	25.7	892	25.8	1072	29.2
744	25.9	896	26.3	1076	29.4
748	28.1	900	26.7	1080	29.0
752	29.6	904	27.2	1084	28.8
756	29.8	908	28.3	1088	27.2
760	30.0	912	28.1	1092	27.0
764	30.4	916	27.8	1096	27.1
768	29.6	920	26.4	1100	25.3
772	29.1	924	26.1	1104	25.7
776	28.3	928	25.6	1108	25.7
780	27.2	932	25.3	1112	25.7
784	27.2	936	25.0	1116	25.9
788	26.2	940	25.1	1120	26.2
792	26.0	944	25.0	1128	26.7
796	25.8	952	25.3		
800	26.5	956	25.7		
804	26.5	960	26.2		
808	27.0	960R	25.7		
812	28.7	964	26.3		

Carbon Isotope Data: Tree 2A

Slice #	$\delta^{13}C$	Slice #	$\delta^{13}C$	Slice #	$\delta^{13}C$	Slice #	$\delta^{13}C$
4	-27.4	168	-26	324	-26	528	-26.3
8	-27.4	172	-26	328	-26.2	532	-26.4
13	-27.2	176	-25.9	332	-25.6	536	-26.3
17	-27.3	180	-25.8	336	-25.8	540	-26
21	-27.2	184	-25.9	340	-25.9	544	-26.3
25	-27	188	-26	344	-25.8	548	-26.4
29	-26.7	192	-26	348	-25.6	552	-26.5
33	-26.6	196	-26.4	352	-25.6	556	-26.6
37	-26.9	200	-26.5	356	-25.6	560	-26.4
41	-26.7	204	-26.5	400	-25.7	564	-26.2
45	-27.2	208	-26.1	404	-26.1	568	-25.7
50	-27	212	-26.3	408	-25.6	572	-25.5
54	-26.8	216	-26.2	412	-26	576	-25.6
58	-26.7	220	-26	416	-25.9	580	-25.9
62	-26.8	224	-26.3	420	-25.9	584	-25.9
66	-26.7	228	-26.2	424	-25.9	588	-25.6
70	-27	232	-26.3	428	-25.9	592	-25.5
75	-26.9	236	-26.6	432	-25.8	596	-25.5
80	-26.9	240	-26.5	436	-25.8	600	-26
85	-27	244	-26.5	440	-25.6	604	-26.2
88	-27.2	248	-26.8	444	-25.5	608	-26.1
92	-27.2	252	-26.6	448	-25.5	612	-25.9
96	-27	256	-26.5	452	-25.5	616	-25.8
99	-26.9	260	-26.4	464	-25.7	620	-25.9
104	-26.7	264	-26.2	468	-25.6	624	-26.1
108	-26.3	268	-26.9	472	-25.9	628	-26.2
112	-26.2	272	-26.3	476	-26	632	-25.9
116	-26.1	276	-26.3	480	-26	636	-25.9
120	-26.1	280	-26.2	484	-25.8	640	-25.4
124	-26.2	284	-26.2	488	-26.1	644	-25.2
128	-25.9	288	-25.9	492	-26.4	648	-25.2
132	-26.1	292	-26	496	-26.4	652	-25.1
136	-26	296	-26.1	500	-26.1	656	-25.2
140	-26	300	-26.2	504	-26.2	660	-25.2
148	-26.7	304	-26.1	508	-26	664	-25.2
152	-26.2	308	-26.2	512	-25.8	668	-25.2
156	-26.1	312	-26.2	516	-25.7	672	-25.3
160	-26.1	316	-26.2	520	-25.8	676	-25.2
164	-26.1	320	-26	524	-26.1	680	-24.9

Carbon Isotope Data: Tree 2A - Continued

Slice #	$\delta^{13}C$	Slice #	$\delta^{13}C$	Slice #	$\delta^{13}C$
684	-25.1	840	-24.8	992	-24.9
688	-24.5	844	-24.9	1000	-24.6
692	-24.5	848	-25	1004	-24.5
696	-24.9	852	-25	1008	-24.6
700	-24.5	856	-25.3	1012	-24.7
704	-24.4	860	-25	1016	-24.8
708	-24.3	864	-25.1	1020	-25
712	-24.4	868	-25.2	1024	-25
716	-24.5	872	-25.1	1028	-25
720	-24.5	876	-25	1032	-24.9
724	-24.5	880	-24.9	1032R	-25
728	-24.4	884	-25.1	1036	-24.8
732	-24.4	888	-25.3	1040	-24.9
736	-24.5	892	-25.2	1044	-24.9
740	-24.4	896	-25.2	1048	-24.8
744	-24.7	900	-24.9	1052	-24.7
748	-24.6	904	-24.8	1056	-24.7
752	-24.6	908	-24.6	1060	-25
756	-24.7	912	-24.7	1064	-24.9
760	-24.8	916	-24.9	1068	-25.1
764	-24.8	920	-25.5	1072	-25.2
768	-24.5	924	-24.5	1076	-24.8
772	-24.1	928	-24.6	1080	-24.8
776	-24	932	-24.5	1084	-24.9
780	-23.8	936	-24.5	1088	-24.9
784	-24.2	940	-24.7	1092	-24.5
788	-24.2	944	-24.7	1096	-24.6
792	-24.2	948	-24.9	1100	-24.6
796	-24.5	952	-24.7	1104	-24.6
800	-24.4	956	-24.5		
804	-25	960	-24.4		
808	-24.9	960R	-24.4		
812	-25.1	964	-24.1		
816	-24.7	968	-24.7		
820	-24.7	972	-24.7		
824	-24.8	976	-25.1		
828	-24.8	980	-25.2		
832	-24.9	984	-25.2		
836	-24.8	988	-25		

The following tables show the correlation matrices between the $\delta^{18}O$ "seasonal" data series and the seasonal precipitation and temperature data.

Correlations: $\delta^{18}O$ – Precipitation (p)

		$\delta^{18}O$ S1	$\delta^{18}O$ S2	$\delta^{18}O$ S3	$\delta^{18}O$ S4	pS1	pS2	pS3	pS4
$\delta^{18}O$ S1	Pearson Correlation	1	.758**	.460**	.198	-.189	-.002	-.030	-.145
	Sig. (2-tailed)		.000	.005	.255	.278	.990	.862	.407
	N	35	35	35	35	35	35	35	35
$\delta^{18}O$ S2	Pearson Correlation	.758**	1	.806**	.442**	-.109	-0.05683	-.010	.022
	Sig. (2-tailed)	.000		.000	.008	.534	.746	.955	.902
	N	35	35	35	35	35	35	35	35
$\delta^{18}O$ S3	Pearson Correlation	.460**	.806**	1	.760**	-.186	-.097	.151	.061
	Sig. (2-tailed)	.005	.000		.000	.284	.581	.387	.728
	N	35	35	35	35	35	35	35	35
$\delta^{18}O$ S4	Pearson Correlation	.198	.442**	.760**	1	-.203	-.176	.266	-.118
	Sig. (2-tailed)	.255	.008	.000		.243	.312	.122	.500
	N	35	35	35	35	35	35	35	35
pS1	Pearson Correlation	-.189	-.109	-.186	-.203	1	0.200554	-.126	.179
	Sig. (2-tailed)	.278	.534	.284	.243		.248	.469	.302
	N	35	35	35	35	35	35	35	35
pS2	Pearson Correlation	-.002	-0.05683	-.097	-.176	0.200554	1	.121	.292
	Sig. (2-tailed)	.990	.746	.581	.312	.248		.487	.089
	N	35	35	35	35	35	35	35	35
pS3	Pearson Correlation	-.030	-.010	.151	.266	-.126	.121	1	-0.04307
	Sig. (2-tailed)	.862	.955	.387	.122	.469	.487		.806
	N	35	35	35	35	35	35	35	35
pS4	Pearson Correlation	-.145	.022	.061	-.118	.179	.292	-0.04307	1
	Sig. (2-tailed)	.407	.902	.728	.500	.302	.089	.806	
	N	35	35	35	35	35	35	35	35

**. Correlation is significant at the 0.01 level (2-tailed).

Correlations: $\delta^{18}O$ – Temperature (t)

		$\delta^{18}O$ S1	$\delta^{18}O$ S2	$\delta^{18}O$ S3	$\delta^{18}O$ S4	tS1	tS2	tS3	tS4
$\delta^{18}O$ S1	Pearson Correlation	1	.758**	.460**	.198	-.037	-.063	-.081	.110
	Sig. (2-tailed)		.000	.005	.255	.833	.717	.644	.530
	N	35	35	35	35	35	35	35	35
$\delta^{18}O$ S2	Pearson Correlation	.758**	1	.806**	.442**	-.022	-0.24972	-.194	-.090
	Sig. (2-tailed)	.000		.000	.008	.898	.148	.263	.607
	N	35	35	35	35	35	35	35	35
$\delta^{18}O$ S3	Pearson Correlation	.460**	.806**	1	.760**	.189	-.086	.010	-.048
	Sig. (2-tailed)	.005	.000		.000	.276	.622	.953	.785
	N	35	35	35	35	35	35	35	35
$\delta^{18}O$ S4	Pearson Correlation	.198	.442**	.760**	1	.236	.051	.044	.004
	Sig. (2-tailed)	.255	.008	.000		.172	.771	.801	.982
	N	35	35	35	35	35	35	35	35
tS1	Pearson Correlation	-.037	-.022	.189	.236	1	.517**	.395*	.390*
	Sig. (2-tailed)	.833	.898	.276	.172		.001	.019	.021
	N	35	35	35	35	35	35	35	35
tS2	Pearson Correlation	-.063	-0.24972	-.086	.051	.517**	1	.322	.331
	Sig. (2-tailed)	.717	.148	.622	.771	.001		.060	.052
	N	35	35	35	35	35	35	35	35
tS3	Pearson Correlation	-.081	-.194	.010	.044	.395*	.322	1	.604**
	Sig. (2-tailed)	.644	.263	.953	.801	.019	.060		.000
	N	35	35	35	35	35	35	35	35
tS4	Pearson Correlation	.110	-.090	-.048	.004	.390*	.331	.604**	1
	Sig. (2-tailed)	.530	.607	.785	.982	.021	.052	.000	
	N	35	35	35	35	35	35	35	35

**. Correlation is significant at the 0.01 level (2-tailed).

*. Correlation is significant at the 0.05 level (2-tailed).

Correlations: $\delta^{18}O$ – Precipitation (p) – First Differenced

		$\delta^{18}O$ S1	$\delta^{18}O$ S2	$\delta^{18}O$ S3	$\delta^{18}O$ S4	pS1	pS2	pS3	pS4
$\delta^{18}O$ S1	Pearson Correlation	1	.725**	.295	-.052	-.027	.097	.093	-.023
	Sig. (2-tailed)		.000	.091	.771	.881	.585	.600	.899
	N	34	34	34	34	34	34	34	34
$\delta^{18}O$ S2	Pearson Correlation	.725**	1	.794**	.362*	.040	-0.00645	.219	.166
	Sig. (2-tailed)	.000		.000	.036	.821	.971	.212	.349
	N	34	34	34	34	34	34	34	34
$\delta^{18}O$ S3	Pearson Correlation	.295	.794**	1	.716**	-.171	-.154	.370*	.211
	Sig. (2-tailed)	.091	.000		.000	.333	.385	.031	.230
	N	34	34	34	34	34	34	34	34
$\delta^{18}O$ S4	Pearson Correlation	-.052	.362*	.716**	1	-.186	-.320	.405*	-.126
	Sig. (2-tailed)	.771	.036	.000		.291	.065	.018	.478
	N	34	34	34	34	34	34	34	34
pS1	Pearson Correlation	-.027	.040	-.171	-.186	1	.454**	-.289	.045
	Sig. (2-tailed)	.881	.821	.333	.291		.007	.097	.801
	N	34	34	34	34	34	34	34	34
pS2	Pearson Correlation	.097	-0.00645	-.154	-.320	.454**	1	-.022	.334
	Sig. (2-tailed)	.585	.971	.385	.065	.007		.901	.053
	N	34	34	34	34	34	34	34	34
pS3	Pearson Correlation	.093	.219	.370*	.405*	-.289	-.022	1	-0.12366
	Sig. (2-tailed)	.600	.212	.031	.018	.097	.901		.486
	N	34	34	34	34	34	34	34	34
pS4	Pearson Correlation	-.023	.166	.211	-.126	.045	.334	-0.12366	1
	Sig. (2-tailed)	.899	.349	.230	.478	.801	.053	.486	
	N	34	34	34	34	34	34	34	34

**. Correlation is significant at the 0.01 level (2-tailed).

*. Correlation is significant at the 0.05 level (2-tailed).

Correlations: $\delta^{18}O$ – Temperature (t) – First differenced

		$\delta^{18}O$ S1	$\delta^{18}O$ S2	$\delta^{18}O$ S3	$\delta^{18}O$ S4	tS1	tS2	tS3	tS4
$\delta^{18}O$ S1	Pearson Correlation	1	.725**	.295	-.052	-.142	-.207	-.088	.117
	Sig. (2-tailed)		.000	.091	.771	.424	.240	.621	.511
	N	34	34	34	34	34	34	34	34
$\delta^{18}O$ S2	Pearson Correlation	.725**	1	.794**	.362*	.057	-.342*	-.030	.004
	Sig. (2-tailed)	.000		.000	.036	.747	.048	.867	.982
	N	34	34	34	34	34	34	34	34
$\delta^{18}O$ S3	Pearson Correlation	.295	.794**	1	.716**	.218	-.208	.099	-.070
	Sig. (2-tailed)	.091	.000		.000	.216	.238	.579	.694
	N	34	34	34	34	34	34	34	34
$\delta^{18}O$ S4	Pearson Correlation	-.052	.362*	.716**	1	.289	.027	.028	-.041
	Sig. (2-tailed)	.771	.036	.000		.097	.881	.873	.818
	N	34	34	34	34	34	34	34	34
tS1	Pearson Correlation	-.142	.057	.218	.289	1	.472**	-.133	-.017
	Sig. (2-tailed)	.424	.747	.216	.097		.005	.454	.926
	N	34	34	34	34	34	34	34	34
tS2	Pearson Correlation	-.207	-.342*	-.208	.027	.472**	1	.023	.127
	Sig. (2-tailed)	.240	.048	.238	.881	.005		.896	.473
	N	34	34	34	34	34	34	34	34
tS3	Pearson Correlation	-.088	-.030	.099	.028	-.133	.023	1	.432*
	Sig. (2-tailed)	.621	.867	.579	.873	.454	.896		.011
	N	34	34	34	34	34	34	34	34
tS4	Pearson Correlation	.117	.004	-.070	-.041	-.017	.127	.432*	1
	Sig. (2-tailed)	.511	.982	.694	.818	.926	.473	.011	
	N	34	34	34	34	34	34	34	34

**. Correlation is significant at the 0.01 level (2-tailed).

*. Correlation is significant at the 0.05 level (2-tailed).

The following tables show the correlation matrices between the $\delta^{13}C$ "seasonal" data series and the seasonal precipitation and temperature data.

Correlations: $\delta^{13}C$ – Precipitation (p)

		$\delta^{13}C$ S1	$\delta^{13}C$ S2	$\delta^{13}C$ S3	$\delta^{13}C$ S4	pS1	pS2	pS3	pS4
$\delta^{13}C$ S1	Pearson Correlation	1	.852**	.780**	.777**	-.033	.161	.148	-.141
	Sig. (2-tailed)		.000	.000	.000	.849	.356	.398	.419
	N	35	35	35	35	35	35	35	35
$\delta^{13}C$ S2	Pearson Correlation	.852**	1	.877**	.775**	-.014	0.149484	.133	-.253
	Sig. (2-tailed)	.000		.000	.000	.937	.391	.446	.143
	N	35	35	35	35	35	35	35	35
$\delta^{13}C$ S3	Pearson Correlation	.780**	.877**	1	.923**	-.062	.266	.139	-.098
	Sig. (2-tailed)	.000	.000		.000	.722	.123	.425	.577
	N	35	35	35	35	35	35	35	35
$\delta^{13}C$ S4	Pearson Correlation	.777**	.775**	.923**	1	-.174	.211	.229	-.111
	Sig. (2-tailed)	.000	.000	.000		.319	.225	.185	.524
	N	35	35	35	35	35	35	35	35
pS1	Pearson Correlation	-.033	-.014	-.062	-.174	1	0.200554	-.126	.179
	Sig. (2-tailed)	.849	.937	.722	.319		.248	.469	.302
	N	35	35	35	35	35	35	35	35
pS2	Pearson Correlation	.161	0.149484	.266	.211	0.200554	1	.121	.292
	Sig. (2-tailed)	.356	.391	.123	.225	.248		.487	.089
	N	35	35	35	35	35	35	35	35
pS3	Pearson Correlation	.148	.133	.139	.229	-.126	.121	1	-0.04307
	Sig. (2-tailed)	.398	.446	.425	.185	.469	.487		.806
	N	35	35	35	35	35	35	35	35
pS4	Pearson Correlation	-.141	-.253	-.098	-.111	.179	.292	-0.04307	1
	Sig. (2-tailed)	.419	.143	.577	.524	.302	.089	.806	
	N	35	35	35	35	35	35	35	35

**. Correlation is significant at the 0.01 level (2-tailed).

Correlations: $\delta^{13}C$ – Temperature (t)

		$\delta^{13}C$ S1	$\delta^{13}C$ S2	$\delta^{13}C$ S3	$\delta^{13}C$ S4	tQ1	tQ2	tQ3	tQ4
$\delta^{13}C$ S1	Pearson Correlation	1	.852**	.780**	.777**	-.062	-.020	-.011	-.235
	Sig. (2-tailed)		.000	.000	.000	.725	.909	.950	.174
	N	35	35	35	35	35	35	35	35
$\delta^{13}C$ S2	Pearson Correlation	.852**	1	.877**	.775**	-.242	-0.12918	-.016	-.162
	Sig. (2-tailed)	.000		.000	.000	.162	.460	.926	.353
	N	35	35	35	35	35	35	35	35
$\delta^{13}C$ S3	Pearson Correlation	.780**	.877**	1	.923**	-.308	-.231	-.064	-.162
	Sig. (2-tailed)	.000	.000		.000	.071	.182	.716	.354
	N	35	35	35	35	35	35	35	35
$\delta^{13}C$ S4	Pearson Correlation	.777**	.775**	.923**	1	-.230	-.119	.112	-.118
	Sig. (2-tailed)	.000	.000	.000		.184	.496	.522	.500
	N	35	35	35	35	35	35	35	35
tQ1	Pearson Correlation	-.062	-.242	-.308	-.230	1	.517**	.395*	.390*
	Sig. (2-tailed)	.725	.162	.071	.184		.001	.019	.021
	N	35	35	35	35	35	35	35	35
tQ2	Pearson Correlation	-.020	-0.12918	-.231	-.119	.517**	1	.322	.331
	Sig. (2-tailed)	.909	.460	.182	.496	.001		.060	.052
	N	35	35	35	35	35	35	35	35
tQ3	Pearson Correlation	-.011	-.016	-.064	.112	.395*	.322	1	.604**
	Sig. (2-tailed)	.950	.926	.716	.522	.019	.060		.000
	N	35	35	35	35	35	35	35	35
tQ4	Pearson Correlation	-.235	-.162	-.162	-.118	.390*	.331	.604**	1
	Sig. (2-tailed)	.174	.353	.354	.500	.021	.052	.000	
	N	35	35	35	35	35	35	35	35

**. Correlation is significant at the 0.01 level (2-tailed).

*. Correlation is significant at the 0.05 level (2-tailed).

Correlations: $\delta^{13}C$ – Precipitation (p) – First Differenced

		$\delta^{13}C$ S1	$\delta^{13}C$ S2	$\delta^{13}C$ S3	$\delta^{13}C$ S4	pS1	pS2	pS3	pS4
$\delta^{13}C$ S1	Pearson Correlation	1	.557**		.193	.117	.118	.032	-.074
	Sig. (2-tailed)		.001	.089	.275	.510	.507	.856	.676
	N	34	34	34	34	34	34	34	34
$\delta^{13}C$ S2	Pearson Correlation	.557**	1	.652**	.355*	.312	-0.01218	.062	-.417*
	Sig. (2-tailed)	.001		.000	.039	.072	.945	.727	.014
	N	34	34	34	34	34	34	34	34
$\delta^{13}C$ S3	Pearson Correlation	.296	.652**	1	.826**	.371*	.246	.015	-.027
	Sig. (2-tailed)	.089	.000		.000	.031	.160	.931	.879
	N	34	34	34	34	34	34	34	34
$\delta^{13}C$ S4	Pearson Correlation	.193	.355*	.826**	1	.015	.173	.179	.025
	Sig. (2-tailed)	.275	.039	.000		.935	.328	.312	.888
	N	34	34	34	34	34	34	34	34
pS1	Pearson Correlation	.117	.312	.371*	.015	1	.454**	-.289	.045
	Sig. (2-tailed)	.510	.072	.031	.935		.007	.097	.801
	N	34	34	34	34	34	34	34	34
pS2	Pearson Correlation	.118	-0.01218	.246	.173	.454**	1	-.022	.334
	Sig. (2-tailed)	.507	.945	.160	.328	.007		.901	.053
	N	34	34	34	34	34	34	34	34
pS3	Pearson Correlation	.032	.062	.015	.179	-.289	-.022	1	-0.12366
	Sig. (2-tailed)	.856	.727	.931	.312	.097	.901		.486
	N	34	34	34	34	34	34	34	34
pS4	Pearson Correlation	-.074	-.417*	-.027	.025	.045	.334	-0.12366	1
	Sig. (2-tailed)	.676	.014	.879	.888	.801	.053	.486	
	N	34	34	34	34	34	34	34	34

**. Correlation is significant at the 0.01 level (2-tailed).

*. Correlation is significant at the 0.05 level (2-tailed).

Correlations: $\delta^{13}C$ – Temperature (t) – First Differenced

		$\delta^{13}C$ S1	$\delta^{13}C$ S2	$\delta^{13}C$ S3	$\delta^{13}C$ S4	tQ1	tQ2	tQ3	tQ4
$\delta^{13}C$ S1	Pearson Correlation	1	.557**	.296	.193	.243	.309	-.166	-.100
	Sig. (2-tailed)		.001	.089	.275	.165	.075	.349	.575
	N	34	34	34	34	34	34	34	34
$\delta^{13}C$ S2	Pearson Correlation	.557**	1	.652**	.355*	-.055	0.081346	.275	.276
	Sig. (2-tailed)	.001		.000	.039	.758	.647	.115	.115
	N	34	34	34	34	34	34	34	34
$\delta^{13}C$ S3	Pearson Correlation	.296	.652**	1	.826**	-.193	-.112	.177	.096
	Sig. (2-tailed)	.089	.000		.000	.275	.529	.318	.587
	N	34	34	34	34	34	34	34	34
$\delta^{13}C$ S4	Pearson Correlation	.193	.355*	.826**	1	-.151	.000	.286	.088
	Sig. (2-tailed)	.275	.039	.000		.393	.999	.101	.621
	N	34	34	34	34	34	34	34	34
tQ1	Pearson Correlation	.243	-.055	-.193	-.151	1	.472**	-.133	-.017
	Sig. (2-tailed)	.165	.758	.275	.393		.005	.454	.926
	N	34	34	34	34	34	34	34	34
tQ2	Pearson Correlation	.309	0.081346	-.112	.000	.472**	1	.023	.127
	Sig. (2-tailed)	.075	.647	.529	.999	.005		.896	.473
	N	34	34	34	34	34	34	34	34
tQ3	Pearson Correlation	-.166	.275	.177	.286	-.133	.023	1	.432*
	Sig. (2-tailed)	.349	.115	.318	.101	.454	.896		.011
	N	34	34	34	34	34	34	34	34
tQ4	Pearson Correlation	-.100	.276	.096	.088	-.017	.127	.432*	1
	Sig. (2-tailed)	.575	.115	.587	.621	.926	.473	.011	
	N	34	34	34	34	34	34	34	34

**. Correlation is significant at the 0.01 level (2-tailed).

*. Correlation is significant at the 0.05 level (2-tailed).

Appendix 4: Additional Data

The original proposed PhD project aimed to identify a forest/savanna boundary shift using stable isotope data from savanna trees which had survived a forest encroachment into the savanna. Due to the lack of traditional dendrochronological dating control, the calcium threshold method was proposed and tested with the intent of applying this to the isotope data measured from the savannah and transition trees. However, since the calcium data could not be validated, the isotope data remains undated and therefore unusable to address the original aim of this study. However, for completeness, these data are presented here.

Oxygen Isotope Ratios

Oxygen isotope ratios were measured at approximately 200µm apart along each tree radius, with results plotted in Figure A4-1 (Tabulated data not provided), with the record plotted relative to distance along the x-axis. Initial observations show that the oxygen isotope records for all the trees show a degree of cyclicity. This is more pronounced in tree 2A (see Chapter 4) where the amplitude of the cycles is greater compared to the other trees. Trees 2T and 2Q contain some similar sized peaks to these in 2A, however these are interspersed with peaks of much lower amplitudes. The overall $\delta^{18}O$ variation across all of the measured trees is approximately 7‰, ranging from approximately 24‰ to 31‰. Variation of the isotopic cycles within the trees was around 1-3‰ in all trees with the exception of 2A which exhibited consistently larger cycles of around 3-4‰. The $\delta^{18}O$ record for tree 2Q appears to contain a single analytical outlier at around 46mm from the bark, with a value that is approximately 5‰ lower than the mean for that tree. It is possible that this value represents a true event, however no other surrounding points indicate this to be the case despite the high resolution of the measurements. Similarly tree 4P contains a possible analytical outlier at ~13mm.

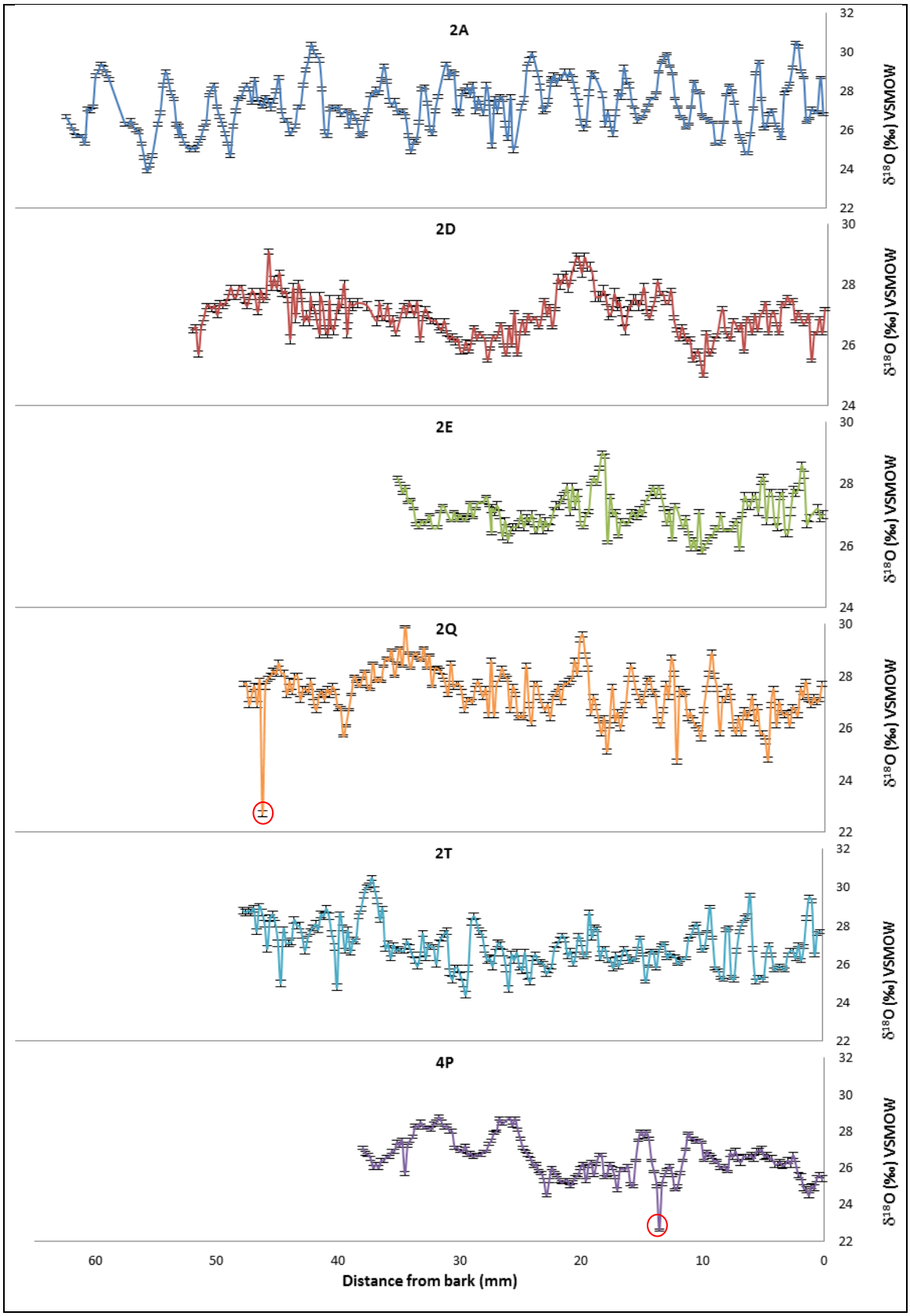

Figure A4-1: Oxygen isotope data for all measured trees. Data is plotted as a function of distance. Error bars represent the precision as per the measurements from the standards. N.B. the y-axis are not all at same scale. Potential outliers are highlighted with red circles.

There are no immediately obvious trends or common signals between trees from the individual plots for oxygen isotope data shown in Figure A4-1. Trees 2D, 2E and 2Q however do present a common pattern which is clearer when plotted on the same graph (Figure A4-2). Each tree contains narrow peaks and troughs throughout, but also appear to follow an overall longer term trend with common areas of elevated and lower values over the measured period. These common lower sections occur at ~25mm, 16mm and 10mm, and increased regions at ~14mm and 16mm. Additionally a further low point occurs at ~40 mm for 2D and 2Q. If the growth rates of these trees were similar then the distance from the bark could potentially equate to the same relative time. However, chapter 3 clearly showed that trees of the same species growing in slightly different environmental could have profoundly different growth rates. Therefore, without any form of dating control, these data cannot be used at this time.

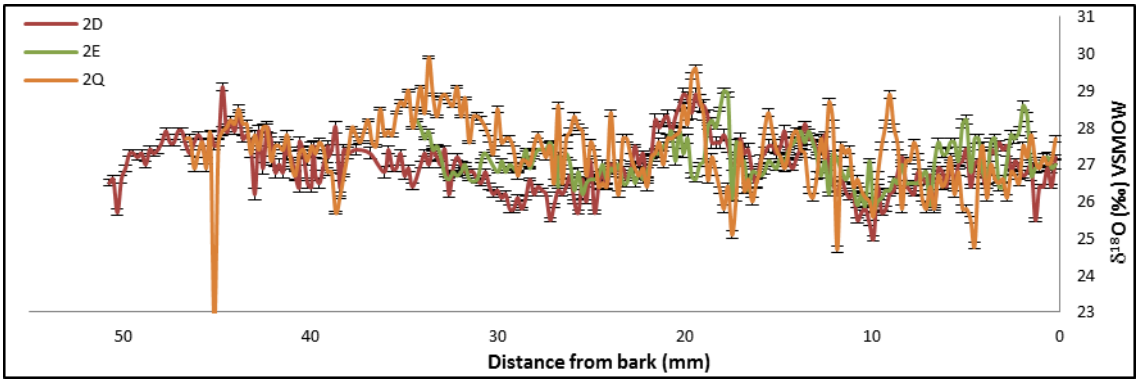

Figure A4-2: Oxygen isotope data from trees 2D, 2E and 2Q. This is the same data which is found in Figure A4-1, but plotted on same graph for comparison purposes.

Carbon Isotope Ratios

The carbon isotope ratios are plotted in Figure A4-3 with distance along the x-axis (tabulated data is not provided). The first graph in Figure A4-3 shows all 4 of the measured trees plotted together which illustrates the common declining trend in $\delta^{13}C$ values for all trees which is almost certainly related to the Suess effect and increasing atmospheric CO_2 concentration (McCarroll *et al.*, 2009). The overall variation in $\delta^{13}C$ values across all trees is approximately 8‰, ranging from 23‰ to 31‰. This large range is accounted mostly by the decreasing trend in carbon values. The isotopic cycles in the $\delta^{13}C$ record are less pronounced than seen with the oxygen isotopes averaging around 0.5‰. All trees also contain a steeper decline in values in

the region closest to the bark which could be related to increasing atmospheric CO_2. Tree 4P appears to contain one outlier at approximately 22mm from the bark. This single value does not fit with surround measurements resulting in a value with is higher than any other in the entire record.

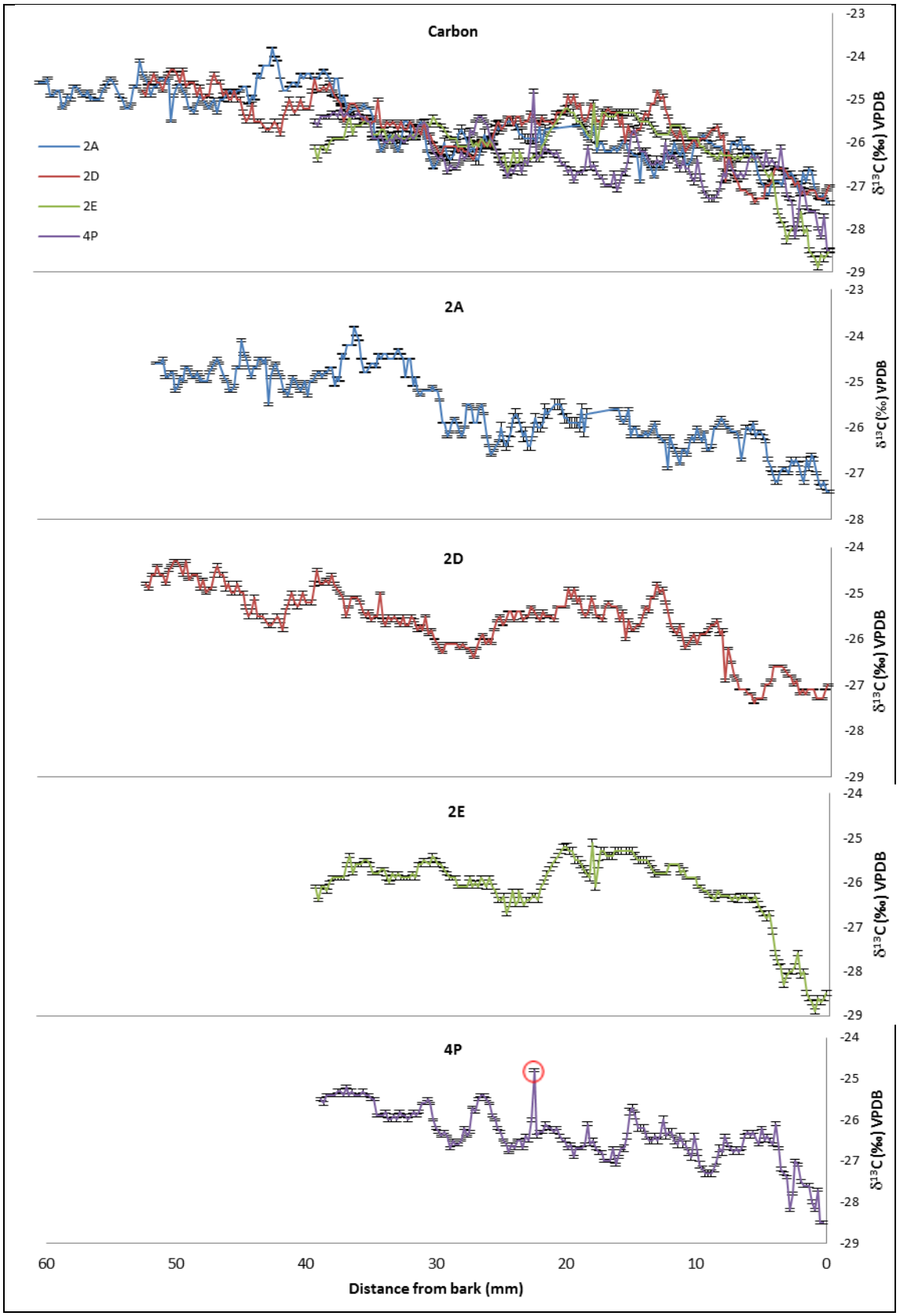

Figure A4-3: Carbon isotope data from all measured trees plotted as a function of distance. Each record shows a declining trend and all appear to feature a common dip in a similar position across the record. Potential outlier is highlighted with a red circle

Comparison of $\delta^{18}O$ and $\delta^{13}C$ Records

Carbon and oxygen use in trees are closely related. Changes in the supply and demand of CO_2 at the photosynthetic site has a direct effect of stomatal conductance and the photosynthetic rate (main controls on $\delta^{13}C$) (Loader *et al.*, 2007), which in turn influences $\delta^{18}O$ since water molecules are lost via the stomata by evaporation. Photosynthesis requires water which comes from soil moisture therefore water availability will affect the photosynthetic rate therefore influencing both $\delta^{18}O$ and $\delta^{13}C$. Although these relationships exist, neither carbon or oxygen isotopes in trees are controlled by one factor therefore the dominant control changes with regards to the growing conditions (McCarroll and Loader, 2004).

Direct comparisons of each of the $\delta^{18}O$ and $\delta^{13}C$ records for each tree (with exception of 2T and 2Q where only the $\delta^{18}O$ records are available) are shown in Figure A4-4. Tree 2A does not appear to show agreement between the two records. The slight increasing trend in the $\delta^{18}O$ record contradicts the trends in the other trees and the large cyclic pattern is not replicated in the equivalent $\delta^{13}C$ record. Even without addressing the declining carbon trend, some similarities in the patterns between the carbon and oxygen isotope data are clear. Trees 2D and 4P show an overall similar general trend throughout the records which show correlations of 0.366 and 0.463 respectively. The coherence is lost at the bark end of the tree. This is more apparent in tree 2D where the two records drift apart around 10mm from the bark. Comparison of the two isotope records in tree 2E show some agreement in the general trend, particularly between the distances of 10mm and 32mm. Both records also highlight a sharp spike in the records at 18mm. The carbon record for this tree is less variable than in the other trees.

The steep decline which occurs in the most recent period (approximately between 0-10mm from bark) will compromise the correlations between data. To gain a better understanding of the relationship between the $\delta^{18}O$ and $\delta^{13}C$ series for each tree, the data would need to be dated and corrected for Suess effect and increasing atmospheric CO_2. As it stands in this form, the two series from 4P correlate reasonably well as does 2D. It is likely however that the drop in $\delta^{13}C$ in the 0-9mm will have impacted this value, but little correlation is currently found between 2A and 2E. The difference in the variations of the $\delta^{18}O$ and $\delta^{13}C$ isotopic cycles, with the $\delta^{18}O$ being around 3-4 times greater than that of $\delta^{13}C$, coupled with the declining trend in the carbon records makes it more difficult to compare the records visually.

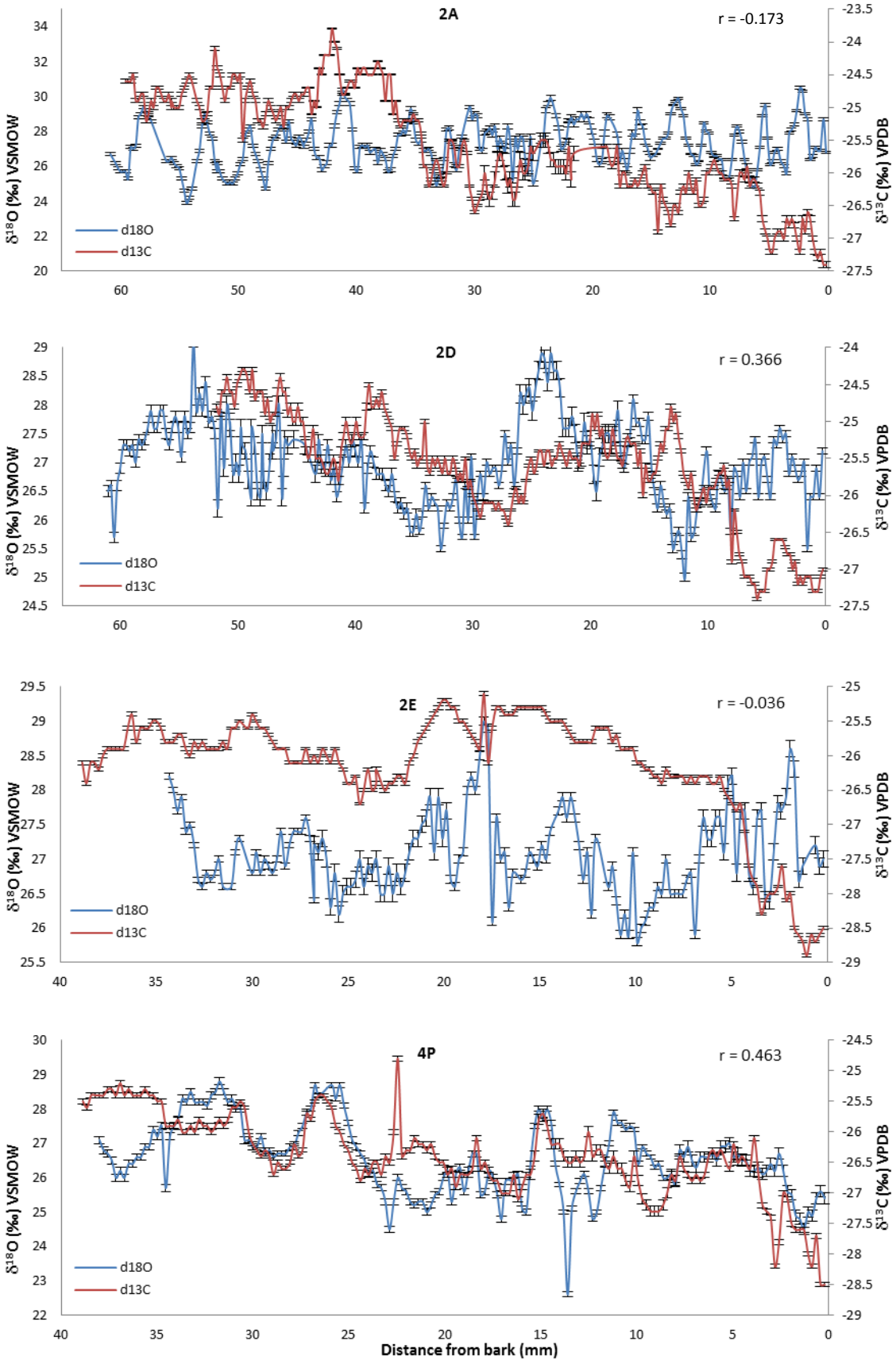

Figure A4-4: Comparison of the $\delta^{18}O$ and $\delta^{13}C$ records for the trees where both isotopes were measured.